



DISSERTATION

**Uranium and Plutonium Isotopic Fingerprinting of
Single Particles by
Laser Ablation – Multi Collector –
Inductively Coupled Plasma Mass Spectrometry**

ausgeführt zum Zwecke der Erlangung des akademischen Grades
Doctor rerum naturalium technicarum unter der Leitung von

Ao.Univ.Prof. Dipl.-Ing. Dr.techn. Thomas Prohaska
Department für Chemie, Abteilung für Analytische Chemie,
Universität für Bodenkultur Wien

und

PD Dr. Sergei Boulyga
Safeguards Analytical Services, Department of Safeguards,
International Atomic Energy Agency

eingereicht

an der Universität für Bodenkultur Wien

von

Dipl.-Ing. Stefanie Kappel, Bakk.techn.

Wien, im November 2012

Acknowledgements

This scientific work could not have been accomplished without the help of many people. I want to thank...

...Thomas Prohaska and Sergei Boulyga for supervising this work, giving me the opportunity to work in such an intriguing scientific field and sharing their comprehensive scientific knowledge with me.

...Dave Donohue, Jane Poths and Gabi Voigt for giving me the opportunity to work in such a great international and extraordinary environment and supporting this work.

...Stefan Bürger for his advices and help in particular with respect to the calculation of total combined uncertainty budgets and TIMS measurements.

... Andreas Köpf and Alan Cunningham for their support regarding TIMS measurements.

...Detlef Günther and Bodo Hattendorf for supervising this work during my stay at the ETH Zurich. Thanks also go to Ladina Dorta for her support during the measurements and all colleagues at the ETH Zurich for the warm welcome.

...Gregor Laaha, Friedrich Leisch and Daniel Koffler from the Institute of Applied Statistics and Computing at the BOKU for the positive collaboration considering the finite mixture model, which represented an important milestone.

...all my (present and past) colleagues from the VIRIS group, whereupon I want to highlight the tireless support from Johanna Irrgeher and Monika Horsky during this thesis. Christopher Weiß is acknowledged for his helping hand in the laboratory.

...all my colleagues from the IAEA Safeguards Analytical Laboratory in Seibersdorf for the positive working environment.

... Gerhard Stingeder, Stephan Hann, Gunda Köllensperger and Hedda Drexler for their support when working in the "Muthgasse" labs.

... Ulla Deinbacher, Luzia Kneisz and Sonja Ringhofer for their help regarding administrative questions.

... my friends for having a great leisure time.

...my cousin Claudia for always giving me an accommodation and the awesome time in Zurich.

The International Atomic Energy Agency and the Austrian Science Fund are acknowledged for financial support.

Exceptional thanks go to the most important people in my life: Thomas and my parents, Christina and Heinz, for their everlasting support and faith in my skills. This work is dedicated to you.

Abstract

One of the objectives of nuclear safeguards is the prevention of the non-peaceful use of nuclear material, the handling of which typically goes along with the release of radioactive single particles. As the isotopic signature of both uranium (U) and plutonium (Pu) directly reflects the origin and the intended use of nuclear material, its knowledge is of particular relevance for fulfilling the aforementioned objective. The strength of particle analysis is that it allows detecting even small amounts of nuclear material exhibiting an undeclared isotopic signature in the presence of an entity of particles having a declared or known natural composition. Even though most reliable and state-of-the-art analytical techniques are currently applied for determining the isotopic signatures of particles, it is important to look into complementary techniques as well in order to extend the amount of safeguards-relevant information that can be gained from the analysis of swipe and/or environmental samples. Thus, in this work the applicability of laser ablation – multi collector – inductively coupled plasma mass spectrometry (LA-MC-ICPMS) was evaluated for the U and Pu isotopic analysis of single particles. Introductorily, general information about the international safeguards system of the International Atomic Energy Agency, the isotopic systems of interest, radioactive particles as well as analytical techniques currently applied in nuclear safeguards are given. Special emphasis was put on the description of basic principles of LA-MC-ICPMS. The first part of the accomplished scientific work addressed method development and validation, whereupon the use of certified reference materials (CRMs) allowed demonstrating the reliability and robustness of LA-MC-ICPMS for single particle analysis. Another study focused on the evaluation of different data processing strategies for the computation of isotope ratios from short transient signals. The ‘fitness for purpose’ of a so called ‘finite mixture model’ for the computation of an unknown number of different isotopic compositions of an entity of particles present on the same substrate could be demonstrated using particle CRMs, as well. In the third study micro-samples of the Chernobyl fallout were analyzed for their Pu isotopic compositions, giving new insight into the variation of the Pu isotopic distribution within the Chernobyl reactor. The analyses of these samples enabled to demonstrate the usefulness of LA-MC-ICPMS for determining radioactive contamination sources in environmental matrices. The scientific work was performed at the VIRIS laboratory at the University of Natural Resources and Life Sciences, Vienna in collaboration with the International Atomic Energy Agency.

Kurzfassung

Ein Ziel der „Nuclear Safeguards“ ist die Verhinderung des nicht-friedlichen Gebrauchs von nuklearem Material, dessen Handhabung üblicherweise mit der Freisetzung von radioaktiven Einzelpartikeln einhergeht. Da die Isotopensignatur sowohl von Uran (U) als auch von Plutonium (Pu) die Herkunft sowie die beabsichtigte Verwendung des nuklearen Materials direkt widerspiegelt, hat deren Kenntnis besondere Bedeutung für die Erreichung des zuvor erwähnten Ziels. Die Stärke der Partikelanalyse liegt darin, dass sogar kleine Mengen nuklearen Materials, welches eine nicht deklarierte oder unbekannte Isotopensignatur aufweist, in Gegenwart einer größeren Anzahl an Partikeln mit einer deklarierten oder bekannten (natürlichen) Zusammensetzung, nachgewiesen werden können. Obwohl gegenwärtig zuverlässige und hochmoderne analytische Techniken für die Bestimmung von Partikel-Isotopensignaturen eingesetzt werden, ist es wichtig, auch die Anwendbarkeit komplementärer Techniken zu untersuchen. Hierdurch kann der Umfang von „International Safeguards“ relevanter Information aus der Analyse von Wisch- und/oder Umweltproben erweitert werden. In dieser Arbeit wurde die Anwendbarkeit von Laser Ablation – Multi Kollektor – Induktiv gekoppelter Plasma Massenspektrometrie (LA-MC-ICPMS) für die U- und Pu-Isotopenanalyse von Einzelpartikeln untersucht. Einleitend findet man allgemeine Informationen über das „International Safeguards“-System der Internationalen Atomenergiebehörde, über relevante Isotopensysteme, über radioaktive Partikel als auch Informationen über analytische Techniken, die momentan in den „Nuclear Safeguards“ eingesetzt werden. Ein besonderer Schwerpunkt wurde auf die Beschreibung der grundlegenden Prinzipien von LA-MC-ICPMS gelegt. Die durchgeführte wissenschaftliche Arbeit befasste sich mit Methodenentwicklung und Validierung, wobei die Verwendung von zertifizierten Referenzmaterialien (RM) erlaubte, die Zuverlässigkeit und Robustheit von LA-MC-ICPMS für die Einzelpartikelanalyse zu veranschaulichen. Eine weitere Studie konzentrierte sich auf die Evaluierung von verschiedenen Datenauswertungsstrategien für die Berechnung von Isotopenverhältnissen aus kurzen transienten Signalen. Die Anwendbarkeit eines sogenannten „Finite Mixture“-Modells für die Berechnung einer unbekannt Anzahl von verschiedenen Isotopenverhältnissen von einer Gesamtheit an Partikeln, die auf demselben Substrat abgeschieden waren, konnte anhand zertifizierter Partikel-RM gezeigt werden. In der dritten Studie wurden Mikro-Proben vom

Tschernobyl-Fallout bezüglich ihrer Pu-Isotopenzusammensetzung analysiert, wodurch neue Erkenntnisse über die Pu-Isotopenverteilung im Tschernobyl-Reaktorkern gewonnen wurden. Die Analyse dieser Proben ermöglichte es, das Potential von LA-MC-ICPMS für die Bestimmung von radioaktiven Kontaminationsquellen in Umweltmatrices zu zeigen. Die wissenschaftliche Arbeit wurde an der Universität für Bodenkultur Wien in Kollaboration mit der Internationalen Atomenergiebehörde durchgeführt.

Table of contents

1 Introduction	9
1.1 International safeguards system of the International Atomic Energy Agency	9
1.1.1 Strengthened nuclear safeguards and environmental sampling.....	10
1.1.1.1 Swipe sampling.....	11
1.2 Isotopic systems of interest in this study	14
1.2.1 Uranium	14
1.2.2 Plutonium.....	19
1.2.3 Isotopic signatures of U and Pu.....	22
1.3 Radioactive particles.....	26
1.4 Analytical techniques currently applied in international safeguards for the determination of U and Pu isotopic signatures of single particles collected by swipe sampling	28
1.4.1 Particle identification and localization	29
1.4.1.1 Fission track.....	29
1.4.1.2 Scanning electron microscopy combined with energy-dispersive x-ray spectrometry	31
1.4.2 U and Pu isotopic analysis of single particles	32
1.4.2.1 Thermal ionization mass spectrometry.....	32
1.4.2.2 Secondary ion mass spectrometry.....	32
1.5 Laser ablation – (multi collector) – inductively coupled plasma mass spectrometry.....	35
1.5.1 Basic concepts of laser ablation	38
1.5.1.1 Laser ablation fundamentals	38
1.5.1.2 Elemental fractionation during laser ablation.....	39

1.5.2	Basic principles of (multi collector) – inductively coupled plasma mass spectrometry	52
1.5.2.1	ICPMS fundamentals	52
1.5.2.2	Multi collector – ICPMS	55
1.5.2.3	Detectors typically used in a multi collector array	57
1.5.2.4	Multi collector configurations for the simultaneous analysis of U and Pu in ICPMS	71
1.5.3	Application of LA-ICPMS for the analysis of single particles – literature review	76
1.5.3.1	Analysis of airborne particulate matter and fly ash	76
1.5.3.2	Analysis of particles containing platinum group elements	78
1.5.3.3	Analysis of crime scene evidence	79
1.5.3.4	Application of LA-ICPMS for single particle analysis in nuclear forensics	79
2	Applications	83
2.1	Application I	85
2.2	Application II	105
2.3	Application III	127
3	Summary and conclusions	141
4	References	143
5	Appendices	159
5.1	Supplementary information	159
5.1.1	Particle sampling for subsequent LA-MC-ICPMS analysis	159
5.1.2	Dead time determination and linearity studies of secondary electron multipliers installed in the ‘Nu Plasma HR’ MC-ICPMS at BOKU, Vienna	162
5.2	List of Tables	168
5.3	List of Figures	169
5.4	List of Abbreviations	171
5.5	Curriculum Vitae	175

1 Introduction

1.1 International safeguards system of the International Atomic Energy Agency

The need for a nuclear safeguards system became evident in the aftermath of the nuclear bombing of Hiroshima and Nagasaki in 1945, when fear about uncontrolled spreading of nuclear weapons technology arose (Goldschmidt, 1999). A milestone was the proposal of Dwight D. Eisenhower, President of the United States of America, in December 1953 at the General Assembly of the United Nations to create an organization promoting the peaceful use of nuclear energy and to seeking to ensure that nuclear energy would not serve any military purpose (Fisher, 1997).

In 1957 the international atomic energy agency (IAEA), which headquarters are situated in Vienna, Austria, was created as an autonomous intergovernmental organization in the United Nations family, and was assigned dual responsibilities: 1) promoting the safe and peaceful use of nuclear energy and 2) providing assurances that nuclear energy is not being misused for non-peaceful purposes (Goldschmidt, 1999). The IAEA's principal objective is "to accelerate and enlarge the contribution of atomic energy to peace, health and prosperity throughout the world" (IAEA, 2002).

A major step towards a global international safeguards system was the Treaty on the Non-Proliferation of Nuclear weapons (NPT) which entered into force in 1970. As of 2010 more than 190 countries have signed the Treaty (Zendel et al., 2011), and have committed to three objectives: 1) preventing the proliferation of nuclear weapons, 2) pursuing nuclear disarmament and 3) promoting the peaceful uses of nuclear energy. With signing this Treaty non-nuclear weapon States (NNWS) are pledging to not develop or otherwise acquire nuclear weapons (IAEA, 2001). Moreover, the NPT makes it mandatory for all NNWS to conclude comprehensive safeguards agreements (CSAs) with the IAEA, and thus to allow for the application of safeguards to all their nuclear material. Hence, the international community is assured that no nuclear material is diverted to nuclear weapons or other nuclear explosive

devices (IAEA, 2011) and that all nuclear materials and activities under safeguards are used exclusively for peaceful purposes (Zendel et al., 2011).

Traditional safeguards focused on the verification of the correctness of declared nuclear materials and activities. Within comprehensive safeguards agreements, a State is obliged to declare all nuclear material and facilities subject to safeguards under the agreement to the IAEA. In addition, the State has the obligation to update the declared information.

The basic measure used by the IAEA for safeguarding declared material is nuclear material accountancy, which monitors the quantities of nuclear material present in a nuclear facility and the changes in these quantities that take place over time to ensure consistency with a State's declarations (IAEA, 2001), and to verify that nuclear material had not been diverted for non-peaceful purposes (Zendel et al., 2011). However, the capability to detect undeclared activities is limited under such a safeguards system as inspectors just have access to specified points during routine inspections (Goldschmidt, 1999; IAEA, 2001).

1.1.1 Strengthened nuclear safeguards and environmental sampling

The discovery of Iraq's clandestine nuclear weapon program in the early 1990s as well as the discovery of undeclared nuclear material in the Democratic People's Republic of Korea (DPRK) demonstrated the need for strengthening traditional safeguards measures. The key to the strengthened safeguards system is the Model Additional Protocol (AP), which measures helped to improve the IAEA's capability to detect undeclared nuclear material or activities, and thus to verify that State's declarations are both correct and complete.

The AP includes the following specific measures: 1) information about, and access to, all aspects of State's nuclear fuel cycle, from uranium mines to nuclear waste and any other locations where nuclear material intended for non-nuclear uses is present, 2) short-notice inspector access to all buildings on a nuclear site, 3) access to other nuclear-related locations and 4) collection of environmental samples beyond declared locations (IAEA, 2001).

Especially environmental sampling (ES) is a powerful tool for detecting undeclared nuclear material and activities. Every nuclear process emits small amounts of process material to the environment. The emitted material can settle on equipment and surfaces within buildings but it can also be transported away from the facility where it can deposit on vegetation or soil or it can be carried into water systems. Worth mentioning is that the quantities of the emitted nuclear material are below concern from a health physics and safety standpoint. However, analytical

techniques have to be capable to detect these low amounts in order to gain information about the process from which the emitted nuclear material originated (IAEA, 2005).

The strength of environmental sampling was demonstrated through a series of field trials during the so called 'Program 93+2', which aimed at the systematical evaluation of a strengthened and more cost-effective safeguards regime. The IAEA conducted twelve environmental sampling field trials in and around various nuclear facilities from September 1993 to March 1995. The purpose of these field trials was the evaluation of sampling methods as well as of analytical techniques, which results help to detect and identify nuclear activities. During these field trials it was demonstrated that swipe sampling is the preferred sampling method as a variety of nuclear signatures can be detected by means of this sampling material. In addition, sampling and transport are easy. An environmental sample is a sample that is taken in the environment of the nuclear facility for the purpose of assisting the IAEA to verify the absence of undeclared nuclear materials or activities (IAEA, 2005).

Environmental sampling was approved as a new safeguards measure by the IAEA's Board of Governors (BOG) in 1995 and the first environmental samples were taken in 1996 (IAEA, 2005).

1.1.1.1 Swipe sampling

Swipe sampling is the standard sampling method for environmental sampling. However, in special cases sampling of vegetation, biota, soil or water is accomplished (IAEA, 2005) as well. Such sampling is not performed on a routine basis as large dilution and mixing effects of the isotopic signatures of interest were observed during the field trials under 'Program 93+2'. Nonetheless, nuclear materials were detectable 10-20 km away from the facilities by use of water, sediment, biota and vegetation samples (Zendel et al., 2011), which demonstrates the usefulness of such samples in special cases.

In general, swipe samples can either be collected at a selected point or as a composite of several sampling points. Point samples are usually taken at a specific location in the facility such as a glove box or a fume hood. On the other hand, composite samples involve the collection of replicate swipes at multiple locations over a wider area than a point sample (IAEA, 2005).

Two different types of sampling kits were developed for swipe sampling: the 1) cotton swipe sampling kit and the 2) hot cell swipe sampling kit. The cotton swipe sampling kit (Fig. 1.1-1) is the most common and versatile sampling kit, and contains, amongst other things, a piece of cloth — the cotton swipe (~ 10 x 10 cm) — that is used for swipe sampling at

all areas other than inside a hot cell or a glove box. For the latter the hot cell swipe sampling kit, which contains a cellulose paper disc with folded tab, is applied. Usually, sampling kits consist of several replicate swipes for taking sub-samples that are simultaneously analyzed by different laboratories (see below) (IAEA, 2005). Typically, 300 – 700 swipe samples are collected each year. Each sample is subject to screening and further isotopic and elemental analysis at two separate laboratories in order to obtain cross confirmation about the presence of undeclared nuclear material (Zendel et al., 2011).



Fig. 1.1-1: Cotton swipe sampling kit (adopted from (Zendel et al., 2011)).

Analyses (see 1.4) of environmental samples are accomplished at the IAEA Clean Laboratory (CL) for Safeguards and by Network Analytical Laboratories (NWAL) that are located in IAEA Member States. In general Network Analytical Laboratories are a group of laboratories that were approved by the IAEA to analyze safeguards samples (IAEA, 2002). In Table 1.1-1 the member laboratories for environmental sample analysis are given.

The Clean Laboratory is a unit of the Safeguards Analytical Laboratory (SAL), which is located in Seibersdorf, Lower Austria, and is responsible for the provision and certification of sampling kits and for the receipt, screening and distribution of environmental samples taken by IAEA

inspectors. In order to reduce the risk of cross-contamination, part of its laboratory space is at 'Class 100' cleanliness level (IAEA, 2002). Moreover, cross-contamination is also checked at the sampling site as the inspection team has to collect swipe samples from the surface of their hands before entering the facility of interest (IAEA, 2005).

Table 1.1-1: Member laboratories of the IAEA NWAL for environmental sample analysis (adopted from (Zendel et al., 2011)).

Laboratory	Particle analysis	Bulk analysis
U.K. Atomic Energy Authority – Aldermaston, U.K.	FT-TIMS	
QinetiQ – Malvern, U.K.	SIMS	
Australian Nuclear Science and Technology Organization, Lucas Heights, Australia		AMS
Air Force Technical Applications Center – Patrick Air Force Base, Florida, U.S.A	FT-TIMS	
U.S. Department of Energy – Oak Ridge National Laboratory, Los Alamos National Laboratory, Pacific Northwest National Laboratory, Lawrence Livermore National Laboratory		HRGS, TIMS and ICPMS
Commissariat à l'Énergie Atomique, Bruyères-le Chatel, France	FT-TIMS	
European Commission Joint Research Centre Institute for Transuranium Elements, Karlsruhe, Germany	SIMS	HRGS, TIMS and ICPMS
Khlopin Radium Institute, St. Petersburg, Russian Federation		HRGS, TIMS
Laboratory for Microparticle Analysis, Moscow, Russian Federation	SIMS	
Japan Atomic Energy Research Institute, Tokai-mura, Japan	SIMS, SEM, FT-TIMS	HRGS, TIMS

(FT –)TIMS : (Fission-track) thermal ionization mass spectrometry

SIMS: secondary ion mass spectrometry

SEM: scanning electron microscopy

HRGS: high-resolution gamma spectrometry

ICPMS: inductively coupled plasma mass spectrometry

1.2 Isotopic systems of interest in this study

1.2.1 Uranium

Uranium (U) has the atomic number 92 and is a naturally occurring radioactive element (Melo and Burkart, 2004). U was discovered in 1789 by the German chemist Martin Klaproth, who extracted uranium oxide from pitchblende, a black mineral (Goldschmidt, 1989). U is a heavy (i.e. density of $\sim 18.9 \text{ g/cm}^3$) (Melo and Burkart, 2004), silvery-white, ductile and slightly paramagnetic and pyrophoric —when finely divided — element (Bleise et al., 2003), with a melting point of 1132°C and a boiling point of 3818°C (Melo and Burkart, 2004).

The International Atomic Energy Agency defines U as Low Specific Activity material (IAEA. Features: Depleted Uranium). Natural U consists of three isotopes, which are given in Table 1.2-1. ^{238}U has the lowest specific activity as the radioactivity depends on the half-life of the radionuclide. Even though ^{234}U is the less abundant U isotope, it contributes to the same extent as ^{238}U to the radioactivity of natural U due to its rather short half-life. However, natural U is considered as a weakly radioactive element (Bleise et al., 2003). ^{235}U is the fissile isotope as its atoms have a high probability of undergoing fission after capturing a thermal neutron (Nuclear Fuel Cycle Information System, 2009). Moreover, ^{236}U may additionally be present in tiny amounts (i.e. $^{236}\text{U}/^{238}\text{U} \leq 10^{-10}$) in natural U ores (Hotchkis et al., 2000; Richter et al., 1999; Sahoo, 2009; Zhao et al., 1994). Is it generated by neutron capture in ^{235}U . which is also the dominant path for its anthropogenic generation in a nuclear reactor (Hotchkis et al., 2000).

Table 1.2-1: Properties of natural U isotopes.

Isotope	Representative isotopic composition (mole fraction) ¹	Half-life years ²	/ Specific activity / Bq mg ⁻¹ ²
^{234}U	0.000 054(5)	2.47×10^5	231000
^{235}U	0.007 204(6)	7.1×10^8	80
^{238}U	0.992 742(10)	4.51×10^9	12.4

¹ (Berglund and Wieser, 2011)

² (IAEA. Features: Depleted Uranium)

^{235}U and ^{238}U are the starting points for two different decay chains, which are shown in Fig. 1.2-1 and Fig. 1.2-2. Both isotopes decay to a stable lead (Pb) isotope; ^{238}U finally decays to ^{206}Pb and ^{235}U decays to ^{207}Pb .

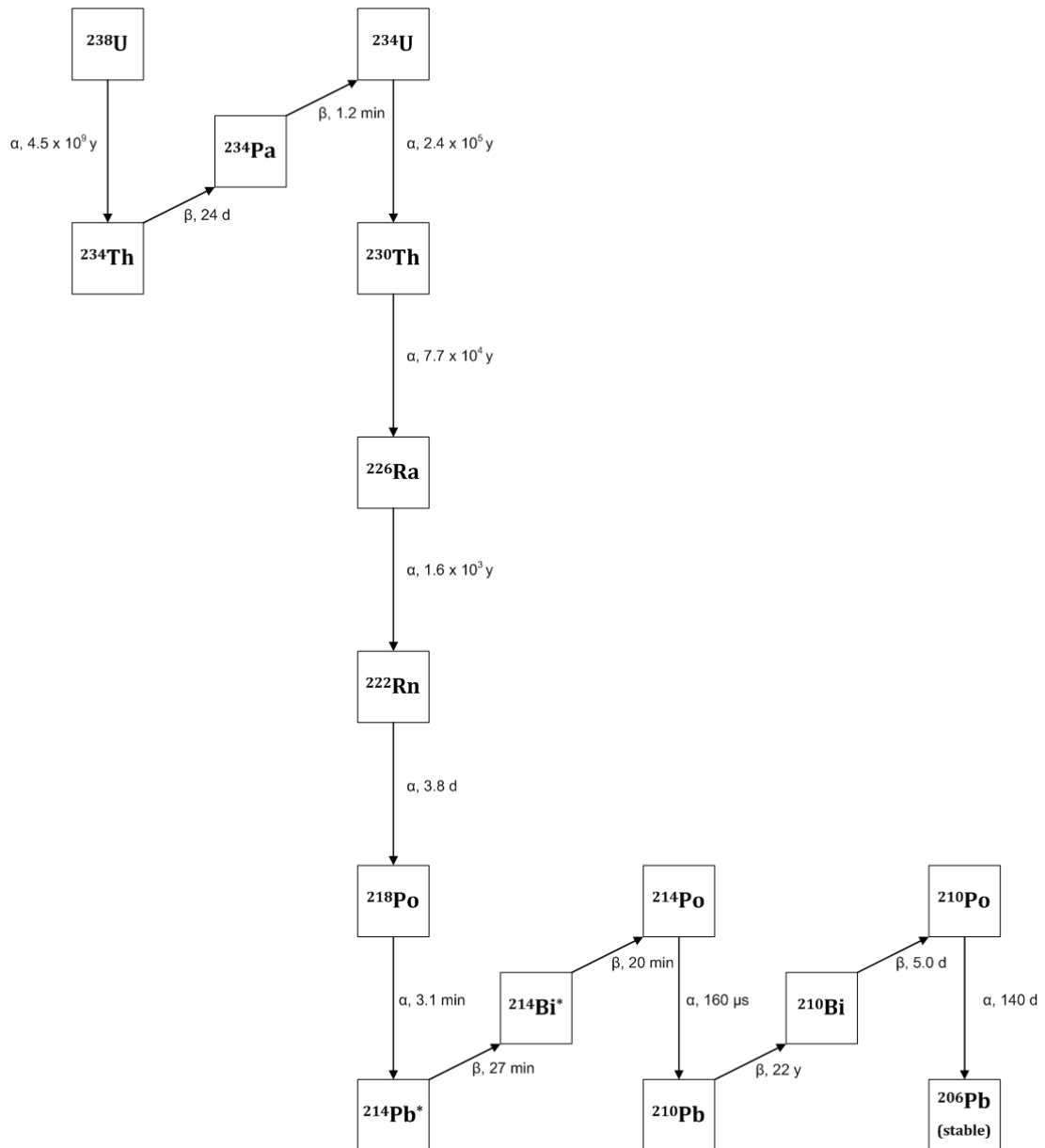


Fig. 1.2-1: Natural decay series of ^{238}U (Natural Decay Series: Uranium, Radium, and Thorium). The symbols α and β are indicating alpha and beta decay, whereas the times are presenting the half-lives. The * symbol indicates isotopes that are also a gamma (γ) emitter (Argonne National Laboratory, 2005).

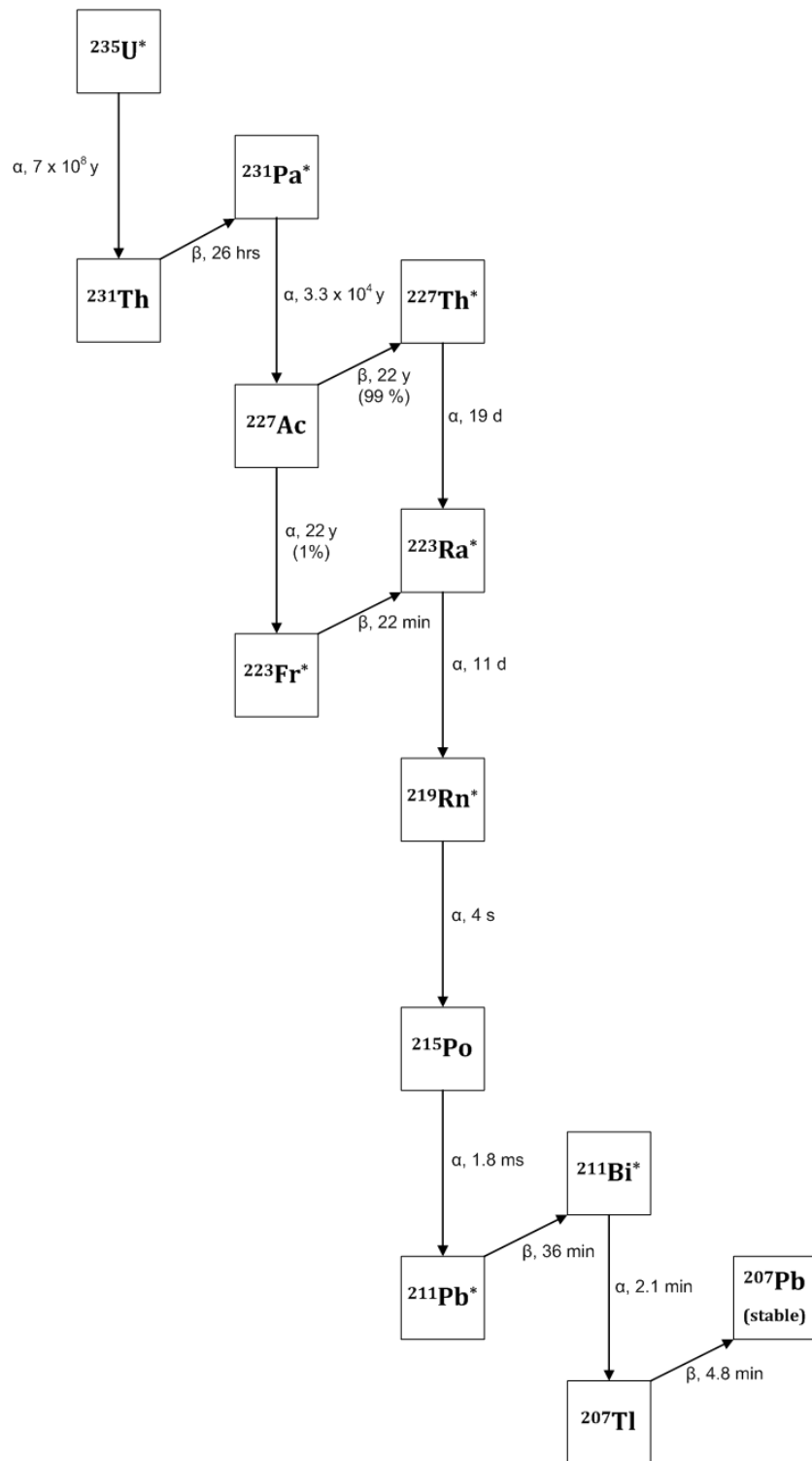


Fig. 1.2-2: Natural decay series of ^{235}U (Natural Decay Series: Uranium, Radium, and Thorium). The symbols α and β are indicating alpha and beta decay, whereas the times are presenting the half-lives. The * symbol indicates isotopes that are also a gamma (γ) emitter (Argonne National Laboratory, 2005).

Natural occurrence

U can be found in trace amounts in the Earth's crust ($\sim 2.4 \mu\text{g g}^{-1}$) and in seawater ($\sim 1\text{-}3 \text{ ng g}^{-1}$) (Melo and Burkart, 2004). Typical U concentrations in granite range from $2 \mu\text{g g}^{-1}$ to $20 \mu\text{g g}^{-1}$, whereas higher concentrations (i.e. $50 \mu\text{g g}^{-1}$ to $1000 \mu\text{g g}^{-1}$) can be found in soils associated with phosphates (IAEA. Features: Depleted Uranium). U is also present in surface and ground water, in which the U concentrations range from $3 \times 10^{-2} \mu\text{g L}^{-1}$ to $2.1 \mu\text{g L}^{-1}$. Typical concentrations in air range from $2.5 \times 10^{-8} \text{ mg m}^{-3}$ to $10^{-7} \text{ mg m}^{-3}$. As a consequence U is also present in plants, animals, food and drinking water. The daily intake is estimated to be $1\text{-}2 \mu\text{g}$ from food and $1.5 \mu\text{g}$ from water. The U content of the human body is approximately $56 \mu\text{g}$, whereas 56 % are stored in the skeleton (Bleise et al., 2003).

Uranium mainly occurs in oxidized form, e.g. as uranite (UO_2^{2+}), pitchblende (UO_3^{2+}) or as secondary minerals (complex oxides, silicates, phosphates, vanadates) (Bleise et al., 2003). The solubility in water and hence the migration behavior of U depends on the oxidation state and the presence of organic chelators. E.g. U present in the +4 oxidation state under anoxic conditions has a much lower solubility than U present in the +6 oxidation state (Melo and Burkart, 2004). Because of U's solubility chemical toxicity may under some circumstances surpass radiotoxic effects. Mostly, U is present in the form of the uranyl ion (UO_2^{2+}) in the mammalian body (Domingo, 2001).

Nuclear fuel cycle

Uranium's principle use is as primary fuel for nuclear power reactors. The following fuel types can be distinguished: natural U (NU, 0.7 %), low enriched U (LEU, 3 – 5% ^{235}U), high enriched U (HEU, > 90% ^{235}U), mixtures of U and plutonium (Pu) and mixtures of U and thorium (Th) (Lieser, 2008).

The set of processes and operations needed to manufacture nuclear fuel, its irradiation in nuclear power reactors and storage, reprocessing, recycling or disposal of the irradiated fuel is defined as nuclear fuel cycle. It starts with the U exploration and ends with the disposal of the materials used and generated during the cycle. The nuclear fuel cycle is subdivided into a front-end and a back-end stage. The front-end stage includes the stages before irradiation and the back-end begins with the discharge of spent fuel from the reactor (Nuclear Fuel Cycle Information System, 2009).

The first steps of the front-end stage are uranium ore exploration and uranium ore mining. Uranium ores typically contain 0.1 % to 0.5 % of U. After U was extracted by e.g. underground-

mining, open-pit mining or in situ leaching, it is processed in a mill, where it is leached from the ore by means of an acid or alkaline leaching solution. Afterwards ion exchange or solvent extraction is used to recover U from the leaching solution. The mill product is a uranium ore concentrate. Because of its color it is named yellowcake. Typically, the yellowcake is heated to remove impurities, thereby increasing the U_3O_8 concentration. Afterwards the yellowcake is converted to either uranium hexafluoride (UF_6) for the production of enriched fuel or natural U oxide (UO_2) for fuel for pressurized heavy water reactors or metal U for fuel based on metallic U alloy. Enrichment of U (i.e. increasing the concentration of ^{235}U) is usually accomplished by means of gaseous diffusion or centrifugal enrichment of UF_6 . Finally, fuel fabrication takes place with fuel assemblies as end-products (Nuclear Fuel Cycle Information System, 2009).

The back-end stage involves the at-reactor spent fuel storage, the away from reactor spent fuel storage, spent fuel reprocessing and recycling, spent fuel conditioning (i.e. production of spent fuel packages suitable for handling, transport, storage and/or disposal) and disposal of spent fuel. The insertion of fuel into the reactor and the irradiation is considered as a step in between the front- and the back-end stage (Nuclear Fuel Cycle Information System, 2009).

The main steps of the nuclear fuel cycle are schematically shown in Fig. 1.2-3.

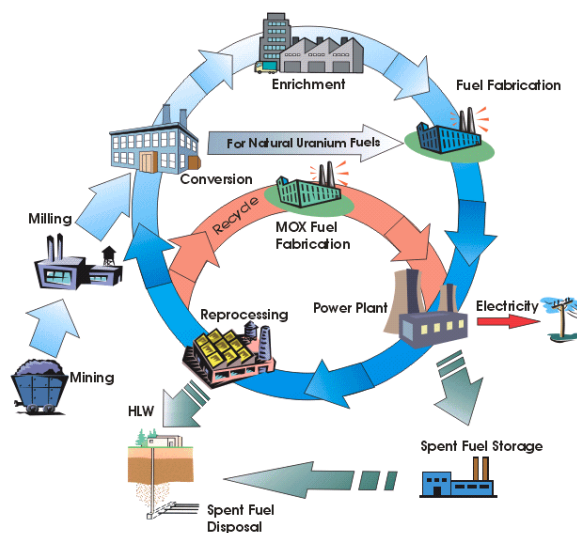


Fig. 1.2-3: Schematic illustration of the nuclear fuel cycle (adopted from (IAEA NFCIS. Nuclear Fuel Cycle)).

Generally, there are two fuel cycle options: 1) open and 2) closed fuel cycle. In the open (or once-through) fuel cycle the nuclear material is not reused. After irradiation the spent fuel is sent away for storage. This strategy is applied for pressurized heavy water reactors (PHWR) and graphite moderated light water cooled reactors (RBMK). In the closed fuel cycle spent fuel is reprocessed to extract the remaining U and Pu from the fission products and other actinides. Reprocessed fuel is mainly reused in light water reactors (LWR) in the form of mixed oxide fuel (MOX). However, the closed fuel cycle is also used with respect to fast reactors, which can produce more fissile Pu than it consumes.

Further details on the nuclear fuel cycle can be found in the IAEA-TECDOC document 'Nuclear Fuel Cycle Information System' (Nuclear Fuel Cycle Information System, 2009).

Depleted uranium

Depleted uranium (DU) is a by-product of the enrichment step in the nuclear fuel cycle, having a lower relative concentration of ^{235}U (< 0.7 %) and ^{234}U than natural U. The ^{235}U concentration of DU is typically ranging from 0.2 % to 0.3 %, whereas the radioactivity is about 60 % of the activity of natural U (Bleise et al., 2003). Besides its use for military purposes (i.e. kinetic energy penetrators or tank armor), DU is also applied for civilian applications such as counterweights or ballasts in aircraft, radiation shields in medical equipment, containers for the transport of radioactive material or as chemical catalyst (Betti, 2003).

1.2.2 Plutonium

Plutonium (Pu), which has the atomic number 94, was a primeval element (Taylor, 2011). It was named after the planet Pluto (Clark et al., 2006) and is because of its high alpha particles emission rate a very radiotoxic element. In biological systems it predominantly exists predominantly in the +4 oxidation state (Wallenius, 2001).

Giga tons of ^{239}Pu and ^{244}Pu were produced during the creation of the universe and at the genesis of the earth by supernova explosions. Since all Pu isotopes are radioactive, all cosmogenic Pu has been lost due to radioactive decay. Natural ^{239}Pu is produced by nuclear processes occurring in uranium ore bodies, whereas minute traces of ^{244}Pu exist as a consequence of primordial stellar nucleosynthesis (Clark et al., 2006). It is estimated that about $2 \times 10^{-17} \text{ g g}^{-1}$ natural ^{239}Pu are present in the Earth's crust due to spontaneous neutron capture in ^{238}U (Taylor, 2011).

Pu (i.e. ^{238}Pu) was first artificially produced in 1940 by Seaborg, McMillian, Kennedy and Wahl by bombarding ^{238}U with deuterons. ^{239}Pu was discovered in 1941 by bombardment of ^{238}U with neutrons, which produced ^{239}U that decayed to ^{239}Np and finally to ^{239}Pu (Fig. 1.2-4). Since then numerous Pu isotopes (i.e. ^{228}Pu - ^{247}Pu) have been produced (Clark et al., 2006).

Pu that is present in today's Earth's surface environment principally consists of five isotopes: ^{238}Pu ($t_{1/2} = 87.74$ y), ^{239}Pu ($t_{1/2} = 24110$ y), ^{240}Pu ($t_{1/2} = 6563$ y), ^{241}Pu ($t_{1/2} = 14.4$ y) and ^{242}Pu ($t_{1/2} = 373000$ y). While ^{238}Pu , ^{239}Pu , ^{240}Pu and ^{242}Pu decay by the emission of α particles, ^{241}Pu decays by β decay, thereby producing ^{241}Am (Ketterer and Szechenyi, 2008). Abundances of these isotopes cannot be stated as Pu isotopes are virtually of anthropogenic origin. However, ^{239}Pu and ^{240}Pu are the isotopes with the highest abundance. The major pathways of Pu formation using ^{235}U and ^{238}U , respectively, as starting materials are given in Fig. 1.2-4.

'Man-made' Pu is produced in nuclear reactors by irradiation of U fuel with any type of neutron spectrum (i.e. thermal or fast). The main isotopes that are produced are ^{238}Pu - ^{242}Pu . Reactors with fast spectrum predominantly yield ^{239}Pu , whereas heavier Pu isotopes are more abundant in the spent fuel of thermal reactors. Besides the neutron spectrum, burn-up, neutron flux and the initial ^{235}U enrichment of the U fuel are additional reactor-type specific parameters influencing the generation of different Pu isotopes. Highly ^{235}U enriched nuclear fuel, for example, results in a build-up of ^{238}Pu , whereas high neutron fluxes result in larger amounts of Pu isotopes heavier than ^{239}Pu (Wallenius, 2001). Thus, the Pu isotopic composition is highly dependent on nuclear reactor properties.

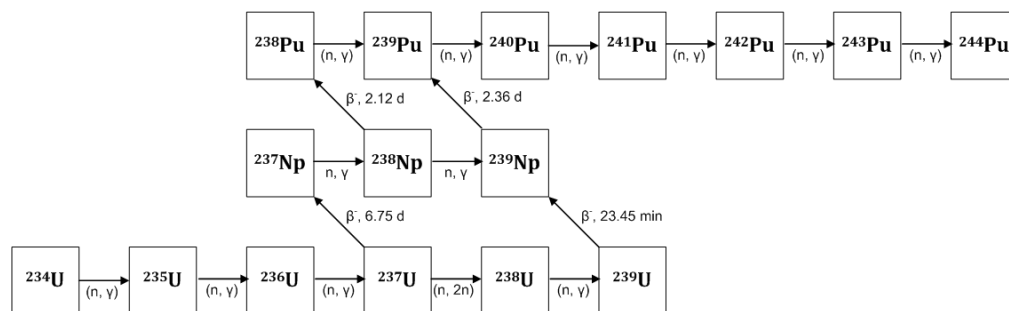


Fig. 1.2-4: Major pathways for the formation of Pu isotopes in uranium fuels (Clark et al., 2006).

Pu is very valuable in nuclear reactors and nuclear weapons as neutrons of all energies are inducing fission in ^{239}Pu (Wallenius, 2001), which yields about the same energy as fission in ^{235}U . More than half of the Pu created in the reactor core is 'burned' in situ (World Nuclear

Association. Plutonium). In general, it has to be distinguished between reactor-grade and weapons-grade Pu. Reactor-grade Pu is a by-product of spent fuel, which has been irradiated for about three years. On the other hand, weapons-grade Pu is produced by irradiating fuel for only 2-3 months in a Pu production reactor (World Nuclear Association. Plutonium). The short irradiation time for producing weapons-grade Pu is a prerequisite in order to circumvent the generation of Pu isotopes heavier than ^{239}Pu . Especially ^{240}Pu is regarded as a contaminant due to its relatively high rate of spontaneous fission and subsequent neutron emission and higher heat production (World Nuclear Association. Plutonium). Pu is used in mixed oxide (MOX) fuel after reprocessing of spent nuclear fuel (World Nuclear Association. Mixed Oxide (MOX) Fuel).

Today, the main amounts of Pu found in the environment mainly results from stratospheric nuclear weapons tests that took place between 1945 and 1975 (Carter and Moghissi, 1977). The Pu input into the ecosystem due to atmospheric weapons tests is known as 'global fallout' that reached its maximum around 1963 (Ketterer and Szechenyi, 2008). The Pu isotopic signature of this global fallout is well known as regional Pu isotopic baselines have been established for recognizing further Pu inputs into the ecosystem. Kelley et al. (Kelley et al., 1999), for example, monitored 54 locations around the world with regard to the Pu isotopic signatures present at these locations. The mean ^{239}Pu concentration for the surface soil level is approximately $10^{-13} \text{ g g}^{-1}$. However, Pu concentrations of $\geq 10^{-12} \text{ g g}^{-1}$ are regarded as hazardous level when accumulated in the human body (Perelygin and Chuburkov, 1997).

Anthropogenic sources other than atmospheric weapons tests are nuclear power production, fuel processing, nuclear waste disposal and nuclear accidents (Taylor, 2011). Considering nuclear accidents, about 1-2 % of the total Pu content in the environment was emitted during the accident at the 4th unit of the Chernobyl nuclear power plant (ChNPP-4) on the 26th of April 1986 (Perelygin and Chuburkov, 1997). Accidental Pu releases into the environment (e.g. aircraft accidents above Palomares and Thule) are summarized in Taylor (Taylor, 2011).

Because of Pu's high specific activities (e.g. $634 \text{ kBq } \mu\text{g}^{-1}$ for ^{238}Pu and $2.3 \text{ kBq } \mu\text{g}^{-1}$ for ^{239}Pu) radiotoxic effects are predominating over chemical toxicity. Generally, Pu is entering the human body by inhalation of contaminated air or by ingestion of food and drinking water (Taylor, 1995). However, as the fractional absorption of Pu from the gastrointestinal tract is rather low (i.e. $\sim (1-10) \times 10^{-4}$ of the ingested activity), inhalation is regarded as the major route of Pu intake. Less than 0.1 % of ingested Pu is absorbed into the bloodstream from where it will be deposited predominantly in the liver and the skeleton. Inhaled Pu will, depending on its chemical form, penetrate deep into the lung from where it is absorbed into the blood, whereas another fraction will migrate into the alveolar macrophages. It is assumed that 30 % of the Pu

that enters the bloodstream will be deposited in the liver, where it will be retained with a half-time of 20 years. Another 50 % will be deposited in the skeleton with a half-time of 50 years. The remaining amount will be deposited in other tissues or will be excreted (Taylor, 2011).

1.2.3 Isotopic signatures of U and Pu

The knowledge of uranium's and plutonium's isotopic signature is of special importance for international safeguards (see 1.1), which aim to provide assurance to the international community that nuclear energy is not misused for non-peaceful purposes (Goldschmidt, 1999). Furthermore, the knowledge of these signatures is also of particular interest for nuclear forensic investigations (Mayer et al., 2007; Mayer et al., 2005; Wallenius et al., 2007; Wallenius et al., 2006), which address questions related to the intended use of illicitly trafficked nuclear material, its origin and its last legal owner (Wallenius et al., 2007). Conclusions on the origin and on the last legal owner of nuclear material helps to improve physical protection measures (Mayer et al., 2005) in order to prevent future diversions from poorly guarded sites, which is of particular importance with respect to radiological hazards arising from inappropriate handling, transport or storage (Wallenius et al., 2007).

Nuclear material e.g. useable for nuclear explosion devices can be either produced in a reactor (weapons-grade Pu) or via enrichment of U. The nature of the production process is thereby reflected inter alia in the elemental and isotopic composition of the nuclear material (Wallenius et al., 2007). Thus, the identification of both U's and Pu's isotopic signatures helps for instance to determine the origin of nuclear material or to detect undeclared nuclear materials or activities.

The classification of nuclear material is based on the element that is contained and on the purity of the fissile isotope. The following six classes are defined: Pu, high enriched U (HEU), ^{233}U , depleted U (DU), natural U (NU), low enriched uranium (LEU) and Th (Zendel et al., 2011). The IAEA uses so called significant quantities (SQ) (Table 1.2-2) as estimates of the amount of material that would be sufficient to manufacture a nuclear explosive device (Zendel et al., 2011).

Table 1.2-2: IAEA Significant Quantities (SQ).

Material type	Isotopic composition	Significant Quantities
HEU	$^{235}\text{U} > 20\%$	25 kg ^{235}U
LEU	$^{235}\text{U} < 20\%$	75 kg ^{235}U
Natural U (NU)	$^{235}\text{U} = 0.7\%$	10 t NU
Depleted U	$^{235}\text{U} < 0.7\%$	20 t DU
	^{233}U	8 kg ^{233}U
Plutonium	$< 80\% \text{ } ^{238}\text{Pu}$	8 kg Pu
Thorium		20 t Th

The uranium types shown in Table 1.2-2 are categorized according to the enrichment or depletion of ^{235}U compared to the ^{235}U abundance found in natural U (see Table 1.2-3) (IAEA, 2005).

Table 1.2-3: Types of U categories (adopted from (IAEA, 2005)).

Uranium type	^{235}U
Depleted U (DU)	$< 0.71\%$
Natural U (NU)	0.71%
Low enriched U (LEU)	$> 0.71\%$ and $< 20\%$
High enriched U (HEU)	$\geq 20\%$
Weapons-grade U	$\geq 90\%$

The identification of the U enrichment can be helpful for identifying undeclared nuclear activities. E.g. ^{235}U enrichment greater than 90 % indicates the presence of weapons-grade U. Moreover, the minor U isotopes ^{234}U and ^{236}U are valuable for identifying the type of uranium feed used in an enrichment process as their content will vary according to the origin of the feed (i.e. uranium ore, DU, recycled U or commercial-grade NU). Both recycled and commercial-grade NU may contain ^{236}U (IAEA, 2005) and ^{234}U outside the range of natural U (Axelsson et al., 2009). Furthermore, the presence of ^{236}U in nuclear material is, together with Pu and fission products, an indicator that U has been irradiated (IAEA, 2005). However, the determined U and Pu isotopic compositions of irradiated fuel should be consistent with the predicted compositions. Modeling implies the knowledge of the initial fuel composition, burn-up and cooling time (Donohue, 1998). Both isotopic compositions are good indicator of the reactor history and the used source material.

Considering the $^{236}\text{U}/^{238}\text{U}$ isotope ratio, Boulyga and Heumann (Boulyga and Heumann, 2006) demonstrated the use of this isotope ratio for monitoring environmental contaminations by low amounts of uranium from spent fuel. They observed that $^{236}\text{U}/^{238}\text{U}$ is a more sensitive and accurate indicator than $^{235}\text{U}/^{238}\text{U}$ as $^{235}\text{U}/^{238}\text{U}$ originating from reactor uranium is mixed with natural U (Boulyga and Heumann, 2006).

Pu is solely generated in a nuclear reactor. Hence its isotopic composition varies with regard to the used source material and irradiation history (see also 1.2.2) (Ketterer and Szechenyi, 2008). In Fig. 1.2-5 $^{240}\text{Pu}/^{239}\text{Pu}$ isotope ratios of various potential nuclear contamination sources are shown.

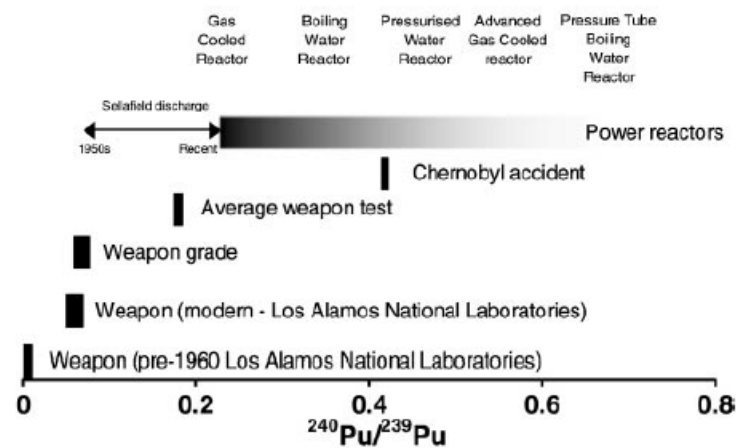


Fig. 1.2-5: $^{240}\text{Pu}/^{239}\text{Pu}$ in potential nuclear contamination sources (adopted from Taylor et al. (Taylor et al., 2001)).

Plutonium is often characterized by the quantity of fissile material available (i.e. ^{239}Pu). However, Plutonium grades (see Table 1.2-4) are expressed as a percentage of ^{240}Pu as this isotope decays by spontaneous fission and is considered as an impurity by weapons manufacturers (IAEA, 2005).

Table 1.2-4: Pu grades (adopted from (IAEA, 2005)).

Plutonium grade	^{240}Pu	^{239}Pu
Super-grade	< 3 %	
Weapons-grade	< 7 %	> 90 %
Fuel-grade	7 % to 18 %	
Reactor-grade	> 18 %	< 60 %

Plutonium isotopes are useful for age determination of nuclear material as well. For this purpose, the four parent/daughter relations are used: $^{238}\text{Pu}/^{234}\text{U}$, $^{239}\text{Pu}/^{235}\text{U}$, $^{240}\text{Pu}/^{236}\text{U}$ and $^{241}\text{Pu}/^{241}\text{Am}$. The age is the time span since the last chemical separation and provides important indication with respect to the origin of the nuclear material. Information about the age can help to exclude production or reprocessing plants that were not operating at a given time as origin sources (Wallenius et al., 2007).

Moreover, the Pu isotopic fingerprint is a useful tracer for assessing e.g. soil and sediment erosion (Everett et al., 2008; Schimmack et al., 2002) or ocean processes, including circulation, sedimentation and biological productivity (Lindahl et al., 2010).

1.3 Radioactive particles

According to the IAEA (Fesenko, 2011) 'radioactive particles are defined as localized aggregation of radioactive atoms that give rise to an inhomogeneous distribution of radionuclides significantly different from that of the matrix background'. As the particles exhibit high specific activities compared with that of the bulk material, they are often referred to as 'hot particles' (Vajda, 2001). Vajda (Vajda, 2001) emphasized that a clear definition of hot particles with respect to the particle size and the activity cannot be given, but that hot particles are often referred to as particles having sizes larger than 0.5 μm (Vajda, 2001). However, radionuclides that are released into the environment can be classified into five main groups (Fesenko, 2011):

- fuel particles or particles of fissile material with sizes from sub- μm to fragments (> 2 mm) (e.g. U/Pu particles)
- condensed aggregates or molecular particles, or particles formed due to condensation of volatile radionuclides
- discrete radioactive particles or clusters (e.g. Ru particles)
- colloids or pseudo-colloids with sizes ranging from 1-450 nm
- low molecular species (e.g. complexes, chelates) with sizes smaller than 1 nm and a nominal molecular mass less than 1 kDa

Considering the emission of radioactive particles, the following sources can be distinguished (Salbu and Lind, 2005):

- nuclear weapons tests (Marshall Islands; Nevada test site, U.S.; Maralinga, Australia; Semipalatinsk, Kazakhstan; Mururoa, French Polynesia; Novaya Zemlya, Russian Federation),
- use of depleted U munitions in the Gulf war and the Balkan Conflict
- accidents with nuclear devices, i.e. US B52 aircrafts and reactor driven Soviet satellite Cosmos 954 (Palomares, Spain; Thule, Greenland; Canada)
- nuclear accidents (e.g. Windscale, UK (former Sellafield); Chernobyl)
- nuclear facilities (e.g. nuclear power plants and reprocessing plants)
- dumped nuclear waste

Radioactive particles emitted and deposited in the environment represent point sources of short and long-term radioecological significance. Inhalation of respiratory (≤ 10 μm) particles and skin doses due to surface contaminations are attributed to short-term effects, whereas long-term

effects relate to an ecosystem transfer as a consequence of the mobilization of radionuclides from radioactive particles due to weathering (Salbu and Lind, 2005). The weathering rate is influenced by the particle matrix (e.g. fuel matrix), structural changes (e.g. transformation of UO_2 to U_3O_8) and chemical conditions (i.e. pH, redox, microbial activity) at the deposition site (Fesenko, 2011; Salbu et al., 1998). The ecosystem transfer finally results in an incorporation of radionuclides into the biosphere. The knowledge of their chemical, physical and transport properties is a necessity to assess potential human health risks. In addition, it helps to respond to emergency cases and to facilitate the environmental management of contaminated areas (Fesenko, 2011).

It should be noted that in this section just a brief general introduction about radioactive particles is given. Comprehensive compendiums can be found elsewhere (Admon, 2009; Fesenko, 2011; Vajda, 2001). Admon (Admon, 2009) paid particular attention to single particles handling, discussing for instance algorithms for particle re-location. Fesenko (Fesenko, 2011) and Vajda (Vajda, 2001) focused on radioactive particles in the environment, including their release from various sources and their identification, localization and characterization (i.e. morphology, elemental and isotopic composition, etc.) by nuclear analytical as well as micro-analytical techniques and mass spectrometry. In addition to the description of analytical principles, characteristics of particles released from individual sources (e.g. Chernobyl, nuclear weapon tests, etc) are given as well. Analytical techniques that are closely related to the subject of this thesis and that are currently applied in international safeguards for radioactive particle analysis are discussed in section 1.4. Hot particles released from the accidental Chernobyl nuclear power plant are discussed in section 2.3 of this thesis.

1.4 Analytical techniques currently applied in international safeguards for the determination of U and Pu isotopic signatures of single particles collected by swipe sampling

Analytical techniques that are applied in international safeguards for the analysis of swipe samples can be broadly divided into techniques used for 1) sample screening (e.g. gamma spectrometry, x-ray fluorescence spectrometry), 2) bulk analysis (e.g. TIMS, ICPMS) and 3) particle analysis (e.g. SEM, FT-TIMS, SIMS) (Zendel et al., 2011).

Bulk analysis mainly aims at the detection of uranium (U) and plutonium (Pu) at the lowest possible levels and the measurement of both concentration and isotopic composition. It involves the analysis of the entire swipe, which is typically destructed by high-temperature ashing followed by acid dissolution. U and or Pu concentration measurements are usually performed by isotope dilution (Zendel et al., 2011) using thermal ionization mass spectrometry (TIMS) or inductively coupled plasma mass spectrometry (ICPMS). Sample preparation and separation procedures that are applied are given elsewhere (Donohue, 2002; Zendel et al., 2011). Other bulk analytical techniques that are applied in international safeguards are low-background high resolution gamma spectrometry (HRGS), alpha spectrometry, liquid scintillation counting, delayed neutron activation analysis (DNAA) and accelerator mass spectrometry (AMS). HRGS is used for the determination of gamma-emitting fission and activation products (e.g. ^{241}Am , ^{131}I , ^{137}Cs , etc.), whereas alpha and beta emitters are detected by means of liquid scintillation counting. AMS is a useful method to measure very low abundant isotopes such as ^{129}I and ^{236}U in environmental samples as well as trace amounts of Pu (IAEA, 2005).

While bulk analysis yields an average value of U and/or Pu isotopic compositions, particle analysis involves the analysis of individual micro-meter sized particles. This allows detecting even small amounts of for example enriched U in the presence of large amounts of natural or depleted U (see 1.2.1). In bulk analysis, these small amounts would be most likely masked (Donohue, 1998). Thus, particle analysis is especially useful for identifying the presence of multiple nuclear signatures present on a swipe sample (IAEA, 2005). Moreover, particle analysis is powerful as:

- “ 1. Fine particulate material or aerosols are often released in the handling of nuclear material.
2. The particles are representative of the original material and their composition provides specific information about the source.
3. The released particles are highly mobile and can be found in many locations at a nuclear facility.
4. It is difficult to clean up and remove the released particles.
5. Samples taken at a facility that has been operated over a long period provide an insight into the entire history of the operation.” (Ranebo et al., 2009)

In the following chapters techniques that are currently applied in international safeguards for the U and Pu isotopic analysis of single particles collected by swipe sampling are described in more detail. Information about other techniques used for the characterization (i.e. elemental analysis, morphology, etc.) of radioactive particles can be found elsewhere (Fesenko, 2011; Vajda, 2001).

1.4.1 Particle identification and localization

This section is dedicated to a short overview about commonly applied techniques for the identification and localization of single particles containing U and/or Pu for subsequent isotopic analysis. These single particles are typically embedded in an environmental matrix (dust, soil, pollen, fibers, etc. (Zendel et al., 2011)) when collected by swipe sampling. This step ensures that only single particles containing U and/or Pu are selected and analyzed for their isotopic compositions.

1.4.1.1 Fission track

Fission track (FT) (Esaka et al., 2004; Lee et al., 2007a; Lee et al., 2005; Lee et al., 2007b; Park et al., 2006; Shen et al., 2008; Stetzer et al., 2004) is applied for the identification of single particles containing fissile isotopes (i.e. ^{233}U , ^{235}U , ^{239}Pu). Typically, the subsequent analysis is performed by means of TIMS (see 1.4.2.1) (IAEA, 2005). Fission track is a highly selective method as only fissile isotopes producing fission fragments due to the irradiation with thermal neutrons are leaving tracks in the detector. Natural U particles yield smaller number of tracks than HEU particles at the same neutron flux. Therefore, the number of tracks compared to the particle size indicates the presence of enriched U or Pu (Zendel et al., 2011).

Particles are typically removed from swipes by ashing or ultrasonic treatment in a suitable suspension medium such as ethanol or siloxane (Zendel et al., 2011). This is followed by spreading the particles onto a plastic track etch film in a layer of collodion (nitrocellulose). Lexan® is typically used as detector and collodion for fixing the particles (IAEA, 2005). However, other procedures for removing particles from swipes (Esaka et al., 2004) as well as other detectors such as mica (Shen et al., 2008) were investigated as well. Esaka et al. (Esaka et al., 2004), for example, suggested to collect the particles on a polycarbonate membrane filter using a filtration system which is similar to a vacuum impactor (see 5.1.1). Dissolution of the film and drying of the suspension yields a membrane, in which the particles are embedded. Moreover, Shen et al. (Shen et al., 2008) proposed to use a Lexan® sheet as substrate and mica as FT-detector.

The detectors are subsequently irradiated for several minutes with thermal neutrons ($\sim 1 \times 10^{15}$ n/cm²) in a nuclear reactor, whereupon fissile isotopes undergo fission and leave damage tracks in the detector (IAEA, 2005; Zendel et al., 2011). The tracks can be made visible under a light microscope after etching (IAEA, 2005), e.g. using NaOH (Park et al., 2006) or HF (Shen et al., 2008). The particles are selected upon their number of fission fragments, their size and appearance (IAEA, 2005). Finally, the selected particles are removed from the film and placed onto filaments for TIMS analysis (see also 1.4.2.1) (IAEA, 2005).

Concerning the localization of radioactive particles in environmental samples (e.g. soil, sediment, dust, etc.) a SEM-grid coated with e.g. boron (Lee et al., 2007b) or thorium (Lee et al., 2005) can be applied as reference grid in order to get reference points for the localization of particles after etching of the detector. However, localization of alpha emitting radioactive particles, which contain Pu and/or ²⁴¹Am isotopes, in environmental samples is also very often performed by alpha track analysis (Boulyga et al., 1997; Boulyga et al., 1999a; Boulyga et al., 1999b; Lee et al., 2007b; Zhuk et al., 1995), which is also a nuclear track radiography method. In alpha track analysis the sample is placed in firm contact with a solid state nuclear track detector (SSNTD) that records the tracks resulting from alpha emitting nuclides. On the contrary to fission track, no reactor irradiation is required (Lee et al., 2007b). The exposure to the detector usually lasts for several days to weeks. Alpha track analysis allows in addition to the identification of particles the determination of their alpha activities and their sizes (Boulyga et al., 1999a; Boulyga et al., 1999b; Zhuk et al., 1995). Moreover, it was shown by Lee et al. (Lee et al., 2011) that alpha track analysis is helpful for detecting particles containing Pu present in a matrix of U and Pu particles, when combined with fission track analysis.

1.4.1.2 Scanning electron microscopy combined with energy-dispersive x-ray spectrometry

Scanning electron microscopy (SEM) combined with energy dispersive x-ray (EDX) spectrometry is an excellent tool for searching and locating particles (sizes down to 0.1 μm), and determining their elemental composition (overall detection limit: 10^{-15} g) (IAEA, 2005) from which the stoichiometric compositions can be derived (Ciurapinski et al., 2002). It should be noted that as a consequence of the average path length of an electron in U and Pu (i.e. $\sim 2 \mu\text{m}$ when using an impinging energy of 30 keV) only surface elemental compositions can be determined (Ranebo et al., 2007).

A SEM-EDX instrument allows performing an automated search of the sample planchet, whereupon elements containing high Z (atomic number) are detected by means of a backscattered electron detector (Zendel et al., 2011). After identification and localization of particles containing U and/or Pu, the particles can be additionally analyzed by means of a wavelength-dispersive x-ray (WDX) detector, which has superior energy resolution but lower x-ray efficiency (≤ 10 times lower compared to EDX). Another disadvantage is that only one element can be measured at a time (Ciurapinski et al., 2002).

Single particle analysis using SEM-EDX in combination with SIMS (see 1.4.2.2) was proven to be very useful for the morphological and isotopic characterization of particles (Donohue et al., 2008; Erdmann et al., 2000; Kips et al., 2007; Ranebo et al., 2007; Ranebo et al., 2010). Ranebo et al. (Ranebo et al., 2007), for example, combined these two methods for the characterization of mixed Pu and U particles originating from the Thule accident in Greenland. Two different surface morphologies were identified by SEM. SIMS depth profiling enabled to determine a heterogeneous distribution of U and Pu present in the particles. Donohue et al. (Donohue et al., 2008) even further applied focused ion beam (FIB) etching in order to examine the interior of particles by SEM-EDX. The relocation of particles in the FIB instrument (1540XB, Zeiss cross-beam machine combining a high-resolution (3 nm) Schottky field emission SEM with a scanning micro-focused (< 6 nm) Ga ion beam gun) was feasible by using reference marks (i.e. three SEM grids) and a relocation algorithm. After SEM and FIB analyses the particles were manipulated for SIMS analysis for determining the Pu and U isotopic composition (Donohue et al., 2008).

Both SEM and SIMS analyses require that the particles are deposited on a polished flat and conducting surface (i.e. pyrolytic graphite planchets). The particles can either be removed from a (heptane) suspension or the particles can be deposited by applying a vacuum impactor

technique (see also 5.1.1) (Zendel et al., 2011). Another strategy was presented by Donohue et al. (Donohue et al., 2008) who used a conductive adhesive tape attached to an aluminum SEM stub for removing the particles from the swipes.

1.4.2 U and Pu isotopic analysis of single particles

In the following chapters (1.4.2.1 and 1.4.2.2) the main analytical methods that are currently applied in international safeguards for analyzing the U and Pu isotopic composition of single particles are explained. Laser ablation - multi collector - inductively coupled plasma mass spectrometry (LA-MC-ICPMS), the technique that was applied in this thesis, is explained in detail in chapter 1.5.

1.4.2.1 Thermal ionization mass spectrometry

TIMS allows determining both U and Pu isotopic compositions from the same particle, with detection limits in the picogram (10^{-12}) range (IAEA, 2005). As just one particle can be analyzed per filament, a pre-selection of particles, typically performed by fission track (see 1.4.1.1), is a pre-requisite for subsequent analysis. Usually, the particle of interest is removed from the fission track film and placed on a zone-refined rhenium (Re) filament (IAEA, 2005). Other filaments that can be used are tungsten (W) or tantalum (Ta). The filaments are heated in the vacuum system by passing a current of several amperes through the filaments. At temperatures of 1400°C – 1800 °C U and Pu are evaporating from the particle and positive ions are generated. However, a competition between evaporation of analyte atoms and ionization poses a challenge, which is more pronounced for single filament TIMS compared to the use of two separate filaments for evaporation and ionization. The latter, however, suffers from reduced ionization efficiency (i.e. 0.1-1 % under best conditions) (Zendel et al., 2011). Detailed explanations about the basic concepts of TIMS can be found elsewhere (Becker, 2007; Smith, 2000) .

1.4.2.2 Secondary ion mass spectrometry

Secondary ion mass spectrometry (SIMS) is a well implemented technique in international safeguards and nuclear forensics for single particle analysis (Betti et al., 1999; Donohue, 1998; Donohue, 2002; Esaka et al., 2007; IAEA, 2005; Tamborini, 2004; Tamborini and Betti, 2000; Tamborini et al., 2002; Zendel et al., 2011). Regarding international safeguards SIMS is mainly

applied for determining the U isotopic composition only (IAEA, 2005). However, particle characterization with respect to the Pu isotopic composition is also feasible (Betti et al., 1999; Tamborini, 2004; Tamborini and Betti, 2000; Tamborini et al., 2002).

SIMS analyses require the particles to be deposited on a flat, polished and conducting sample substrate, which is often referred to as planchet (see also 1.4.1.2). After insertion of the planchet into a vacuum chamber, an energetic beam of primary ions (i.e. typically O_2^+ with an energy of 10-15 keV) is applied to the sample (Zendel et al., 2011). As a consequence of the impact of the primary ion beam on the sample surface and the resulting collision cascade, primary particles are implanted into the surface, resulting in a reshuffling of 50-500 matrix atoms (Betti, 2005). A fraction of the sputtered material is released as secondary ions that are accelerated into the mass analyzer part, e.g. a double-focusing mass spectrometer (Zendel et al., 2011).

SIMS allows performing raster scanning of the sample surface for the generation of an ion image (Zendel et al., 2011) by using an imaging detection system (i.e. channel plate/ resistive anode encoder system, which registers the x and y locations of individual ions) (Donohue, 2002). In this so called ion microscope mode a defocused primary ion beam (5-300 μm) is used for the fast scanning of large surface areas (Betti, 2005; Donohue, 1998). The resulting ion images of the isotopes measured (i.e. ^{235}U and ^{238}U) enable locating the particles of interest having diameters in the range of 0.5 μm to 10 μm . Moreover, enrichments can be determined by comparing the ion images of ^{235}U and ^{238}U . Scanning of one cm^2 of a planchet area with ion field sizes of ca. 150 x 150 μm takes about 6-8 hours (Zendel et al., 2011). However, particles of special interest can be re-analyzed for determining the complete U isotopic composition, including the minor U isotopes ^{234}U and ^{236}U , of a particle (IAEA, 2005). This is accomplished by using the so called ion microprobe mode in which a focused ion beam is used (Betti, 2005; Donohue, 1998).

Pre-selection of single particles — as is the case for TIMS (1.4.2.1) — is due to the use of an ion microscope mode not a necessity for SIMS analyses. However, Esaka et al. (Esaka et al., 2007) demonstrated the usefulness of U particle pre-selection using SEM. The isolation of U particles from Pb particles present in a simulated swipe sample enabled to reduce biases of $^{234}\text{U}/^{238}\text{U}$ and $^{236}\text{U}/^{238}\text{U}$ isotope ratio measurements as contributions from isobaric interferences (i.e. $^{206}\text{Pb}^{12}\text{C}^{16}\text{O}^+$ and $^{208}\text{Pb}^{12}\text{C}^{16}\text{O}^+$) were reduced. Increased deviations from the certified values were observed with increasing $^{208}\text{Pb}/^{238}\text{U}$ intensity ratios (Esaka et al., 2007).

Generally, isobaric interferences occurring especially at the m/z of the minor U isotopes ^{234}U and ^{236}U are a main limitation with regard to SIMS analyses, especially when the uranium

particle itself contains interfering elements. Moreover, interferences may also result from organic clusters occurring at the masses of interest (Ranebo et al., 2009). In Table 1.4-1 common isobaric interferences for swipe samples are given.

Table 1.4-1: Common isobaric interferences for swipe samples at the masses of U, and required mass resolutions (MRP = mass resolving power). The table was adopted from Ranebo et al. (Ranebo et al., 2009).

Isotope	Interference	MRP ($M/\Delta M$)
^{234}U	$^{208}\text{Pb}^{26}\text{Mg}$	2864
	$^{207}\text{Pb}^{27}\text{Al}$	2802
	$^{206}\text{Pb}^{28}\text{Si}$	2613
	$^{92}\text{Mo}^{94}\text{Mo}^{16}\text{O}_3$	958
	$^{138}\text{Ba}^{32}\text{S}^{16}\text{O}_4$	1272
	$^{116}\text{Sn}^{118}\text{Sn}$	985
	$^{48}\text{Ti}_2^{138}\text{Ba}$	975
	$^{208}\text{Pb}^{27}\text{Al}$	2741
	$^{207}\text{Pb}^{28}\text{Si}$	2580
	$^{92}\text{Mo}^{95}\text{Mo}^{16}\text{O}_3$	953
^{235}U	$^{117}\text{Sn}^{118}\text{Sn}$	982
	$^{116}\text{Sn}^{119}\text{Sn}$	984
	$^{48}\text{Ti}^{49}\text{Ti}^{138}\text{Ba}$	968
	$^1\text{H}^{234}\text{U}$	48490
	$^{208}\text{Pb}^{28}\text{Si}$	2566
	$^{92}\text{Mo}^{96}\text{Mo}^{16}\text{O}_3$	947
	$^{118}\text{Sn}_2$	974
	$^{116}\text{Sn}^{120}\text{Sn}$	977
	$^{48}\text{Ti}^{50}\text{Ti}^{138}\text{Ba}$	953
	$^{182}\text{W}^{54}\text{Fe}$	1496
^{236}U	$^1\text{H}^{235}\text{U}$	38152
	$^{206}\text{Pb}^{16}\text{O}_2$	2752
	$^{208}\text{Pb}^{30}\text{Si}$	2372
	$^{94}\text{Mo}^{96}\text{Mo}^{16}\text{O}_3$	929
	$^{95}\text{Mo}_2^{16}\text{O}_3$	936
	$^{92}\text{Mo}^{98}\text{Mo}^{16}\text{O}_3$	938
	$^{118}\text{Sn}^{120}\text{Sn}$	964
	$^{182}\text{W}^{12}\text{C}_2^{16}\text{O}_2$	2112
	$^{182}\text{W}^{56}\text{Fe}$	1419
	$^{50}\text{Ti}_2^{138}\text{Ba}$	930
^{238}U	$^{207}\text{Pb}^{16}\text{O}_2$	2574
	$^{95}\text{Mo}^{96}\text{Mo}^{16}\text{O}_3$	908
	$^{94}\text{Mo}^{97}\text{Mo}^{16}\text{O}_3$	910
	$^{183}\text{W}^{56}\text{Fe}$	1378
	$^{238}\text{U}^1\text{H}$	

A strategy to overcome the isobaric interferences given in Table 1.4-1 is the use of large geometry (LG)-SIMS instruments providing high mass resolution and high transmission due to a larger radius of the magnetic sector (compared to small geometry (SG)-SIMS instruments). However, it should be noted that it is not possible to resolve hydrogen interferences: $^1\text{H}^{234}\text{U}$ and $^1\text{H}^{235}\text{U}$. While the contribution of $^1\text{H}^{234}\text{U}$ is usually neglected, corrections are typically applied for the $^1\text{H}^{235}\text{U}$ hydrogen interference occurring at the m/z of ^{236}U .

Moreover, LG-SIMS instruments are equipped with a multi collector, which is advantageous with respect to the useful yield (i.e. ratio of ions measured relative to the number of atoms in the sample) (Ranebo et al., 2009).

1.5 Laser ablation – (multi collector) – inductively coupled plasma mass spectrometry

Since its introduction in the 1980s (Gray, 1985), laser ablation (LA) in combination with inductively coupled plasma mass spectrometry (ICPMS) has evolved to a widely used technique for the direct analysis of solid samples determining major, minor and trace elements and isotope ratios in geology (Cottle et al., 2009; Leisen et al., 2012; Pettke et al., 2011a), archaeology (Golitzko and Terrell, 2012; Wagner et al., 2012), authenticity (Brunner et al., 2010; Swoboda et al., 2008) and provenancing studies (Fontaine et al., 2010), environmental monitoring (Cizdziel et al., 2012; Holá et al., 2011) and migration studies (Hobbs et al., 2012; Zitek et al., 2010), biomonitoring and –imaging (Becker et al., 2008; Sela et al., 2007; Stadlbauer et al., 2005; Waentig et al., 2012) as well as in forensics (Abrego et al., 2012; Grainger et al., 2012; Pointurier et al., 2012), to just cite examples.

LA is a quasi non-destructive sampling technique on the macroscopic scale that requires minimal or no sample preparation, which makes the technique especially attractive for chemically resistant samples (Koch and Günther, 2011). In comparison to sample preparation for liquid nebulization, contamination risks are reduced as well as the loss of volatile components. Furthermore, high spatial and in-depth resolutions enable to determine sample heterogeneities (Russo et al., 2002b).

Especially the combination of LA and multi-collector (MC)-ICPMS exhibits an excellent tool for directly determining and resolving isotopic compositions of solid samples (Duffin et al., 2012; Fontaine et al., 2010; Iizuka et al., 2011; Iizuka and Hirata, 2005; Souders and Sylvester, 2008, 2010) as MC-ICPMS instruments yield superior performance — compared to instruments equipped with a single collector — in terms of accuracy and precision of isotope ratio measurements (Albarède et al., 2004; Ingle et al., 2003; Lacan et al., 2010; Morgan et al., 2011; Rehkämper et al., 2001; Wieser and Schwieters, 2005).

The relevance of LA as solid sample introduction technique for ICPMS is highlighted by the number of review and trend articles dedicated to this topic (e.g. (Fernández et al., 2007; Garcia et al., 2009; Günther-Leopold et al., 2005; Koch and Günther, 2007, 2011; Russo et al., 1998; Russo et al., 2002b; Russo et al., 2004; Shaheen et al., 2012)) as well as by the yearly increasing number of publications (see Fig. 1.5-1). Alone in 2011 almost 400 entries for ‘laser ablation inductively coupled plasma mass spectrometry’ were registered in *SciFinder*.

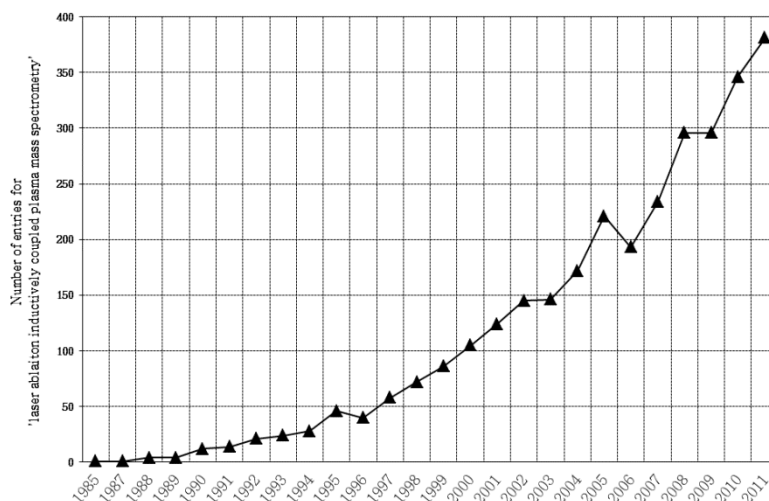


Fig. 1.5-1: Number of entries in *SciFinder* for 'laser ablation inductively coupled plasma mass spectrometry'.

In the last years, LA-(MC)-ICPMS has been recognized more and more as a useful method for the U and Pu isotopic characterization of nuclear fuel samples or samples that are of special relevance for nuclear forensics (Becker, 2005; Boulyga et al., 2003; Cizdziel et al., 2008; Guillong et al., 2007; Günther-Leopold et al., 2008; Marin et al., 2012; Stefánka et al., 2008). Moreover, LA-ICPMS has proven to be a promising technique for determining the U and Pu isotopic compositions of single particles (Aregbe et al., 2011; Becker et al., 2008; Boulyga and Prohaska, 2008; Lloyd et al., 2009; Pointurier et al., 2012; Pointurier et al., 2011; Varga, 2008).

The usefulness of LA-MC-ICPMS as a complementary technique to (FT-)TIMS and SIMS (see 1.4) results from its potential to overcome current limitations of these two methods. However, it has to be stressed that each method provides merits (e.g. precision, accuracy, time-effectiveness, high sensitivity, reduced molecular interferences, etc.) for specific safeguards related questions. Thus, taking advantage of the benefits of each technique helps to extend the amount of safeguards-relevant information.

In comparison to TIMS, LA-(MC)-ICPMS offers higher sensitivity, which is of advantage for the analysis of particles with sizes in the (sub)- μm range and U amounts in the low pg range. Such particle analyses pose a challenge for TIMS (Pointurier et al., 2011). In addition, high sensitivities are also important for the analysis of environmental matrices (Boulyga and Prohaska, 2008). Thus, LA-(MC)-ICPMS is a very promising technique for the analysis of particles embedded in complex matrices containing organic compounds and heavy metals. In addition, it is less prone to molecular interferences than SIMS, which use may be limited for such samples because of molecular interferences present at the mass-to-charge ratios of the

isotopes of interest (Ranebo et al., 2009). Moreover, in LA-(MC)-ICPMS non-conducting samples can be readily analyzed, whereas in SIMS samples have to be provided with a conductive layer (Boulyga and Prohaska, 2008).

Pre-selection, using either FT or SEM, of particles with sizes down to the sub- μm range is regarded as a pre-requisite for fast LA-(MC)-ICPMS analyses (Pointurier et al., 2012; Pointurier et al., 2011). FT offers the advantage that highly enriched particles are definitely detected, whereas they might be overlooked in SIMS and SEM-LA-ICPMS (Pointurier et al., 2011).

Pointurier et al. (Pointurier et al., 2011) estimated the time needed for the analysis of 60 U particles for SIMS, FT-TIMS, FT-LA-ICPMS and SEM-LA-ICPMS. The analysis steps that were taken into account included: deposition on disk, irradiation (including transport and cooling of the samples), particle deposition on filament, particle localization and isotope ratio measurements (including instrument optimization and calculation). SIMS and SEM-LA-ICPMS yielded comparable overall analysis times with 4 and 3.5 days, respectively, whereas 21 and 13 days were estimated for FT-TIMS and FT-LA-ICPMS, respectively. FT-LA-ICPMS provides a shorter analysis time than FT-TIMS as the isotopic analysis can be performed in less time. It was estimated that isotope ratio measurements of 60 particles by means of LA-ICPMS can be performed in 1.5 days, whereas 6 days would be required for TIMS analyses. In addition, no micro-handling and individual loading of particles is necessary. In case of SIMS, 3 days were estimated for the isotopic analysis of 60 particles (Pointurier et al., 2011)

Pointurier et al. (Pointurier et al., 2011) additionally compared FT-LA-ICPMS, FT-TIMS and SIMS with respect to accuracy and precision. SIMS yielded the best precision (i.e. 0.7 % (n=30) and the smallest deviation from the certified value (i.e. 0.5 % (n=30)), followed by TIMS (i.e. precision: 4.8 % (n=18), bias from certified value: 2.7 % (n=18)) and LA-ICP-QMS measurements (i.e. precision: 24.2 % (n=19), bias from certified value: 11.5 % (n=19)) (Pointurier et al., 2011). However, it has to be stressed that in that study a single collector ICP-QMS instrument was applied for the analysis of $^{235}\text{U}/^{238}\text{U}$ (Pointurier et al., 2011). Improvements in precision and smaller biases from the certified value could be achieved by applying a multi collector-ICPMS. In addition, the use of a MC-ICPMS instrument would also allow measuring the minor U isotopes ^{234}U and ^{236}U .

1.5.1 Basic concepts of laser ablation

1.5.1.1 Laser ablation fundamentals

Ablation for removing a portion of a sample requires energy absorption. In case of laser ablation this energy is provided by laser light energy, which results in mass leaving the surface of the sample in form of electrons, ions, atoms, molecules, clusters and particles. The ablation mechanism is significantly influenced by laser parameters such as pulse duration (i.e. ns and fs) and wavelength (i.e. IR, UV and vacuum UV); with both having a great impact on stoichiometric sampling of the solid of interest. However, the significance of the influence of a laser parameter on e.g. stoichiometric sampling is highly dependent on the sample material properties (e.g. transparent *versus* opaque or metal *versus* isolator, etc.) (Russo et al., 2007).

Ablation mechanism

The ablation mechanism can be divided into three main processes: 1) bond breaking and plasma ignition, 2) plasma expansion and cooling and 3) particle ejection and condensation. However, the mechanisms occurring due to the incident of laser light strongly depend on the irradiation (i.e. energy per unit area and time in $W\text{ cm}^{-2}$) and the pulse duration of the applied laser. While thermal vaporization is the dominant mechanism for nanosecond (ns) laser pulses with irradiances less than 10^8 W cm^{-2} , Coulomb explosion is the main bond breaking mechanism for femtosecond laser pulses with irradiances higher than 10^{13} W cm^{-2} (Russo et al., 2007). In fs-LA higher irradiances are always applied for the same fluences as in ns-LA as the laser energy hits the sample in much shorter time (Glaus et al., 2010). However, if the laser irradiance is high enough in ns-LA non-thermal mechanisms are existing in addition to thermal ones. Thermal mechanisms comprise phase transition from solid to liquid, liquid to vapor and vapor to plasma. Thus, the sample surface will melt and vaporize. On the contrary laser ablation using fs laser pulses comprise a direct solid-vapor (or solid-plasma) transition. Thermal conduction can be neglected as the lattice is heated by non-thermal melting, which is followed by the creation of a laser-induced plasma with rapid expansion rates (Russo et al., 2007).

Laser-induced plasma is generated due to the ionization of vaporized mass by absorption of incident laser light. The laser-induced plasma causes plasma shielding, which is more pronounced for ns-LA as the plasma does not decay as fast as plasma induced by a fs laser pulse.

In case of ns laser pulses, the plasma is reheated by the absorption of the later part of a pulse. On the contrary, in case of fs laser pulses plasma shielding can be neglected. After ending of the laser pulse, the laser-induced plasma is expanding into the ambient, which is referred to as plume. Plasma expansion in form of a shockwave from ns laser pulses takes place in a three dimensional way whereas fs pulse durations yield one dimensional (i.e. perpendicular to the sample surface) plasma expansions (Russo et al., 2007).

The last stage of the LA processes comprises particle formation from condensed vapor, liquid sample ejection and solid-sample exfoliation. Condensation of vapor results in the formation of nanoparticles, whereby their sizes are determined by the cooling time and the density of the vapor. Generally, condensation starts when the vapor reaches the boiling temperature (~ 3000 K) of the material and stops when the condensation temperature (~ 2000 K) is reached. Liquid sample ejection takes place as a consequence of high pressure gradient forces at the molten surface. Ejection of solid particles results from thermal stress forces that are breaking the sample into particles (Russo et al., 2007). However, melting of the surface and solid ejection are more prominent for ns-LA than for fs-LA (Fernández et al., 2007; Liu et al., 2004; Russo et al., 2007).

1.5.1.2 Elemental fractionation during laser ablation

Laser parameters such as pulse duration and laser wavelength have a major influence on elemental fractionation (Fryer et al., 1995; Longerich et al., 1996) and stoichiometric sampling (i.e. laser aerosol composition is representative for the bulk composition (Koch and Günther, 2011)) as they strongly influence the particle size and distribution and the chemical composition of the laser generated aerosol (Glaus et al., 2010; Koch et al., 2004; Kuhn and Günther, 2004; Liu et al., 2005). Elemental fractionation is regarded as one of the main limitations of LA-ICPMS for performing quantitative analyses of elemental concentrations in the absence of matrix matched calibration standards (e.g. (Glaus et al., 2010; Günther-Leopold et al., 2005; Koch and Günther, 2007, 2011)), which availability is limited for many applications (Koch and Günther, 2007). Generally, elemental fractionation does not only occur at the ablation site (Glaus et al., 2010; Liu et al., 2004) but also during transport to the ICP (Koch et al., 2002) and in the ICP itself (Guillong and Günther, 2002; Guillong et al., 2003; Krosiakova and Günther, 2007; Kuhn and Günther, 2003, 2004).

The use of laser ablation systems providing shorter wavelengths and pulse durations helped to minimize elemental fractionation (e.g. (Glaus et al., 2010; Liu et al., 2004; Poitrasson et al.,

2003)), and thus to improve quantification capabilities without the use of matrix matched calibration standards (Koch and Günther, 2007). However, other parameters such as laser fluence (i.e. laser energy density) (Claverie et al., 2009a; Garcia et al., 2008; Koch et al., 2005; Koch et al., 2004; Koch et al., 2006; Russo et al., 2002a) and repetition rate (Claverie et al., 2009a; Gonzalez et al., 2008) have to be additionally taken into account. A comprehensive review dealing with the influence of various laser parameters (i.e. pulse duration, wavelength, beam profile, pulse frequency, power density and fluence) and ablation cell peculiarities (i.e. ambient atmosphere, configuration and transport system) on the performance of ns- and fs-LA can be found in (Shaheen et al., 2012). This section only provides a brief discussion about the influence of pulse duration, laser wavelength and carrier gas on LA-ICPMS analyses.

Influence of pulse duration on LA-ICPMS analyses

LA results in the generation of particles having different sizes and size-dependent chemical compositions (Glaus et al., 2010; Koch et al., 2005; Koch et al., 2004; Kuhn and Günther, 2004; Liu et al., 2005). In fs-LA smaller particles with a more uniform particle size distribution are produced compared to ns-LA (Koch et al., 2004; Liu et al., 2004). The presence of smaller particles results in reduced elemental fractionation due to reduced incomplete vaporization and ionization in the ICP as is the case for larger particles (Aeschliman et al., 2003; Kuhn and Günther, 2003; Liu et al., 2004). Considering ns-LA, Kuhn and Günther (Kuhn and Günther, 2003) ablated brass using ns laser pulses and observed that particles larger than 100 nm were Zn depleted whereas particles smaller than 20 nm were enriched in Zn (measurements conducted by SEM-EDX).

Liu et al. (Liu et al., 2004) observed that fs pulses yielded particles with sizes of 100-200 nm that formed large agglomerates of irregular shape with sizes of 5-10 μm when ablating brass. On the contrary, ns laser ablation produced single spherical entities with sizes ranging from 10-1000 nm. Single large droplets that most likely ejected from the molten surface were observed in ns laser ablation but not in fs ablation. In addition, a raised rim around the crater perimeter, caused by re-solidification of molten brass, could be identified for ns laser ablation. Compared to ns laser ablation, enhanced signal intensities and improved precisions were observed for fs laser ablation, even though large agglomerates were produced. However, the authors assumed that these agglomerates were more effectively digested in the ICP than larger single particles that resulted in spike signals in ns laser ablation. In addition, the use of fs laser pulses allowed improving the precision of elemental ratios as elemental fractionation was less pronounced compared to ns laser ablation. Moreover, a larger (~ 10 -15 times) crater volume for fs laser

ablation demonstrated the enhanced ablation efficiency compared to ns laser ablation (Liu et al., 2004). Generally, fs laser pulses are enabling higher ablation rates than ns pulses as they are not affected by plasma shielding. In addition, less pulse energy is lost by thermal diffusion (heat affected zone) in the sample (Russo et al., 2007).

Different morphologies and elemental compositions of aerosol particles generated by ns and fs laser ablation were observed by Glaus et al. (Glaus et al., 2010) who investigated silicate, metal and semiconductor samples. Fs laser generated aerosols showed less matrix dependence and similar particle morphologies for all samples compared to ns laser ablation, where morphological differences were found for silicate and metal and semiconductor, respectively, samples. No wavelength dependency with respect to particle morphology could be identified for fs-UV-LA and fs-IR-LA. Even though no obvious fractionation could be observed by ICPMS measurements, electron microscopy measurements revealed different chemical compositions of fs laser generated aerosol. In case of zircon, large particles consisted of almost pure zirconium dioxide whereas nanoparticle agglomerates consisted of silicon dioxide (for both fs-UV-LA and fs-IR-LA). No separation could be found for aerosol generated by ns laser ablation of zircon. The analysis of brass revealed the enrichment of Cu in large particles for both ns and fs generated aerosol. However, the elemental separation was less distinct for fs-UV-LA, for which—as well as for fs-IR-LA— no significant Cu/Zn fractionation could be observed in contrast to ns laser pulses. No elemental separation according to particle size as well as fractionation during ICPMS measurements could be identified for pyrite, representing a semiconductor sample, and for stainless steel. It was assumed that gas-to-particle conversion in the vapor phase and hydrodynamic sputtering of the remaining liquid led to the formation of nanoparticle agglomerates and large spherical particles, respectively, in case of ns-LA. Temporal fractionation of e.g. Cu/Zn ratios may be observed due to the loss of droplets, which are enriched in Cu, with increasing crater depth and the formed debris around the crater. In case of fs-LA it was assumed that droplets and vapor may be released in the same expansion process at a much higher kinetic energy, which led to reduced elemental fractionation. However, the elemental separation into individual particle sizes was regarded as a major limitation with respect to quantitative analyses without using matrix-matched standards, even for fs-LA (Glaus et al., 2010).

Garcia et al. (Garcia et al., 2008) determined that elemental fractionation was independent of the matrix (i.e. binary metallic, semiconductor samples and multi-component glass) and that at high shot numbers stoichiometric sampling could be accomplished when applying fs-IR-LA. Elemental fractionation could be observed during the first shots whereas at higher shots the elemental ratios approached an asymptotic fluence-independent value. It was stressed that elemental fractionation depended on the fluence, whereupon larger effects could be observed at

the ablation threshold. The application of high fluences yielded constant elemental ratios after the second shot (Garcia et al., 2008).

Moreover, Poitrasson et al. (Poitrasson et al., 2003) observed that fs-UV-LA was superior to ns-UV-LA in terms of precision, accuracy and repeatability for elemental Pb/U and Pb/Th ratios as well as for Pb isotopic ratios analyzed in glass, monazite and zircon samples.

Influence of laser wavelength on LA-ICPMS analyses

Generally, shorter wavelengths — UV *versus* IR — provide higher photon energies (1064 nm: 1.16 eV, 266 nm: 4.7 eV, 213 nm: 5.8 eV, 193 nm: 6.4 eV) for bond breaking and ionization of the sample. If the photon energy is higher than the bond energy (typically a few eV) of the sample, non-thermal mechanisms become more pronounced. Moreover, more energy per unit volume is provided for ablation by UV wavelengths because of the shorter optical penetration depth (Russo et al., 2007). UV wavelengths are also more efficiently penetrating the laser-induced plasma and thus bond-breaking is directly initiated (Russo et al., 2002b). Advantages for the LA process (e.g. reduced elemental fractionation) by applying shorter wavelengths, particularly with regard to samples such as silicate glass, were demonstrated by several authors (Guillong and Günther, 2002; Guillong et al., 2003; Horn et al., 2001; Russo et al., 2000). The use of shorter wavelengths (i.e. 193 nm < 213 nm < 266 nm) for the ablation of e.g. silicates results in smaller ablation rates (amount of ablated mass per laser pulse per unit area) and reduced heat-affected zones as the laser energy is more effectively coupled into the sample (increased absorption for shorter wavelengths) (Günther-Leopold et al., 2005).

Horn et al. (Horn et al., 2001) observed more uniform ablation rates for NIST glass samples (i.e. NIST 610 (dark blue), NIST 612 (light blue) and NIST 614 (transparent)) when applying a wavelength of 193 nm compared to 266 nm. At 193 nm similar sample removal rates per pulse were observed for all three glasses, resulting from similar absorption behaviors at 193 nm. In case of 266 nm, ablation of NIST 614 glass, representing the sample with the highest transparency for 266 nm, resulted in higher ablation rates and the formation of larger particles because of longer optical penetration depths and absorption of the laser energy in larger volumes (Horn et al., 2001).

Guillong and Günther (Guillong and Günther, 2002) observed wavelength-dependent particle size distributions when analyzing NIST glass samples. The analysis of transparent samples using 266 nm as laser wavelength yielded particle size distributions that were dominated by particle sizes > 1 µm, whereas smaller particle sizes (< 0.2 µm) were observed for opaque samples. However, a direct comparison of particle size distributions with regard to the different

wavelengths could not be conducted due to the detection capabilities of the particle measurement system for particles produced by means 193 nm ($< 0.1 \mu\text{m}$). Differences in the particle size distributions were nonetheless evident. In addition, the ratio of small to large particles increased with increasing crater depth. Filtering of particles larger than $0.8 \mu\text{m}$ allowed reducing elemental fractionation during LA using a 266 nm laser, indicating a reduction of ICP induced elemental fractionation due to incomplete vaporization of large particles (Guillong and Günther, 2002). In another study, Guillong et al. (Guillong et al., 2003) investigated the influence of three different wavelengths (193 nm versus 213 nm and 266 nm) on the analysis of silicate samples. Except for the wavelength all laser parameters were kept constant. As shorter wavelengths have shorter penetration depths the aerosol consisted of more small particles, which resulted in better signal stabilities and reduced elemental fractionation for all analyzed NIST glass samples (i.e. from opaque to transparent (NIST 610, NIST 612 and NIST 614)). In case of 213 nm and 266 nm reduced signal stabilities and enhanced elemental fractionation were observed with increasing transparency of the glass samples, resulting from increased mean particle sizes and the incomplete vaporization of larger particles in the ICP (Guillong et al., 2003).

Considering the analysis of NIST 610 silicate glass by means of fs-UV-LA using wavelengths of $\sim 200 \text{ nm}$ and $\sim 265 \text{ nm}$ both aerosols mainly consisted of nano-sized particles and/or agglomerates with sizes ranging from 50-250 nm. Nonetheless, the particle fraction consisting of 100-250 nm particles increased when applying a wavelength of $\sim 265 \text{ nm}$ (Koch et al., 2006). The study conducted by Koch et al. (Koch et al., 2006) demonstrates that a wavelength-dependent particle size distribution for opaque silicate samples is less pronounced in fs LA than in ns LA.

In case of metallic samples the optical penetration depth seems not to be as relevant due to energy losses through reflection on the sample and thermal conductivity (Horn et al., 2001). Kuhn and Günther (Kuhn and Günther, 2003) observed that the use of a 266 nm laser yielded Cu/Zn ratios having less deviations from the certified value than the use of 193 nm, for which 14 % higher Cu/Zn ratios were reported.

In Table 1.5-1 typical applications of laser wavelengths and pulse durations are given. In order to review state-of-the-art applications and because of the large number of papers yearly published, special emphasis was put on applications published in 2012 with regard to ns-LA. Considering fs-LA, applications published from 2000 to 2012 were taken into account because of the small number of papers compared to ns-LA. However, it should be noted that the list cannot be regarded as exhaustive. As can be seen in Table 1.5-1, in 2012 only wavelengths in the

UV range were applied for the analysis of various matrices in ns-LA. In case of fs-LA the applied wavelengths ranged from the deep UV to the IR. The use of fs-LA is limited to only a few non-fundamental investigations, whereas ns-LA is widely applied for various matrices ranging from e.g. minerals to tumor tissue sections. Hence, it is evident that shorter pulse durations are not yet widely used in the community, most likely resulting from higher acquisition costs for fs-LA systems compared to ns-LA systems. However, this may change in the next years. Regarding the list of laser ablation systems currently available on the market (see Table 1.5-2) it is obvious that fs-LA systems have successfully entered the market. The nowadays availability of easy-to-use and stand-alone systems may contribute to a more widespread use of fs-LA systems.

Influence of carrier gas on LA-ICPMS analyses

The particle-size distribution is also strongly dependent on the laser ablation carrier gas, especially in case of shorter wavelengths (Horn and Günther, 2003). In comparison to Ar, the use of He results in enhanced transport efficiencies of the generated aerosol to the ICP (Eggins et al., 1998; Kuhn and Günther, 2003), which yields enhanced signal intensities and reduced deposition of ablated material on the sample surface (Eggins et al., 1998). The gain in sensitivity under He atmosphere can be explained by the generation of much more smaller particles due to a more rapid end of condensational particle growth from vapor. The laser-induced plasma under He atmosphere is smaller compared to that using Ar as ablation carrier gas. Moreover, He has a higher thermal conductivity which enables a faster removal of thermal energy away from the ablation site. However, enhanced transport efficiencies under He atmosphere are less pronounced when a wavelength of 266 nm is applied for LA as at this wavelength less vapor and more primary particles are generated (Horn and Günther, 2003). Guillong and Günther (Guillong and Günther, 2002) observed a 3 fold signal enhancement by applying He for the transport of 193 nm produced particles, whereas no influence in the transport efficiency, using either Ar or He as carrier gas, could be detected for particles generated by applying a wavelength of 266 nm.

Table 1.5-1: Typical applications of laser wavelengths and pulse durations for LA-ICPMS analyses
(ns-LA: emphasis on applications published in 2012 but also selected applications from the years before; fs-LA: applications published from 2000 to 2012)

Wave-length	Pulse duration	Laser	Field	Sample type	Note	References
193 nm	ns	ArF Excimer	Geology/ geochronology	Zircon		(Helbig et al., 2012)
193 nm	ns	ArF excimer	Geology	Quartz-hosted fluid inclusions		(Leisen et al., 2012)
193 nm	ns	ArF excimer	Environmental monitoring/ heavy metal exposure	Teeth		(Shepherd et al., 2012)
193 nm	ns	excimer	Geology/ geochronology	Zircon		(Tollstrup et al., 2012)
193 nm	ns	ArF excimer	Migration	Fish otoliths		(Chang et al., 2012)
193 nm	ns	Nd:YAG	Nuclear forensics	Glass particles doped with U		(Kappel et al., 2012)
193 nm	ns	ArF excimer	Geology/geochronology	Speleothems		(Drysdale et al., 2012)
193 nm	ns	ArF excimer	Geology/geochronology	Zircon		(Georgiev et al., 2012)
193 nm	ns	ArF excimer	Archaeology	Kiln sherds		(Zhu et al., 2012)
193 nm	ns	ArF excimer	Bioimaging	Tumor tissue sections (rat)		(Gholap et al., 2012)
193 nm	ns	ArF excimer	Other	Lead fire assay button		(Compernelle et al., 2012)
193 nm 213 nm	ns ns	Nd:YAG Nd:YAG	Geology	Stalagmite, ostracod shells (calcium carbonate)	Comparison of 193 nm and 213 nm for the samples of interest, need for matrix-matched calibration; application of 193 nm yielded more precise data, reduced elemental fractionation, less pronounced mass load and matrix effects	(Jochum et al., 2012)
213 nm	ns	Nd:YAG	Nuclear forensics	Uranium oxide particles		(Pointurier et al., 2012)
213 nm	ns	Nd:YAG	Archaeology/provenancing	Ceramics		(Golitzko and Terrell, 2012)
213 nm	ns	Nd:YAG	Geology / geochronology	Allanite		(Darling et al., 2012)
213 nm	ns	Nd:YAG	Environmental monitoring	Green leaves		(Cizdziel et al., 2012)
213 nm	ns	Nd:YAG	Environmental monitoring/chemical imaging	Fern rhizomes		(Koelmel and Amarasiriwardena, 2012)
213 nm	ns	Nd:YAG	Bioimaging	Kidney (rats)		(Moreno-Gordaliza et al., 2011)

213 nm	ns	Nd:YAG	Bioimaging	Liver (fish /gar)		(Barst et al., 2011)
213 nm	ns	Nd:YAG	Forensics	Automotive glass		(Grainger et al., 2012)
213 nm	ns	Nd:YAG	Archaeology	Glass vessels		(Panighello et al., 2012)
213 nm	ns	Nd:YAG	Migration	Fish otoliths		(Reis-Santos et al., 2012)
213 nm	ns	Nd:YAG	Food monitoring	Herbal supplements		(Bu et al., 2012)
213 nm	ns	Nd:YAG	Bioimaging	Mouse brain, chicken breast standard	Use of H ₂ as reaction gas	(Lear et al., 2012)
213 nm	ns	Nd:YAG	Biomonitoring	Tobacco, wheat		(Judy et al., 2012)
213 nm	ns	Nd:YAG	Bioimaging	Western blot immunoassay		(Waentig et al., 2012)
213 nm	ns	Nd:YAG	Nuclear industry	Ni-based alloy, pure Ni, Fe with Ni coating		(Vaculovic et al., 2012)
213 nm	ns	Nd:YAG	Environmental monitoring	Rock coatings		(Mantha et al., 2012)
213 nm	ns	Nd:YAG	Environmental monitoring/ heavy metal exposure	Teeth		(Abdullah et al., 2012)
213 nm	ns	Nd:YAG	Migration	Fish otoliths		(Hobbs et al., 2012)
213 nm	ns	Nd:YAG	Fundamental investigations	Cu CRMs, Cu powder pellets	Evaluation of powder pellets as calibration standards	(Traub et al., 2010)
213 nm	ns	Nd:YAG	Other	Thin film coated glasses	Depth-profile analysis	(Konz et al., 2011b)
213 nm	ns	Nd:YAG	Bioimaging	Human serum sample (gels from gel electrophoresis)		(Konz et al., 2011a)
213 nm	ns	Nd:YAG	Environmental monitoring	Fish scales		(Holá et al., 2011)
213 nm	ns	Nd:YAG	Fundamental investigations	Titanite	Phase and composition changes during LA	(Fliegel et al., 2010)
213 nm	ns	Nd:YAG	Nuclear forensics	Uranium oxide particles		(Pointurier et al., 2011)
213 nm	ns	Nd:YAG	Archaeology/provenancing	Glass		(Walton et al., 2012)
213 nm	ns	Nd:YAG	Bioimaging	Selenium-containing proteins (extract of sunflower leafs, polyacrylamide gels from gel electrophoresis)		(da Silva and Arruda, 2012)
266 nm	ns	Nd:YAG	Bioimaging	Urine (single droplets)		(Kumtabtim et al., 2011)
266 nm	ns	Nd:YAG	Nuclear forensics	Uranium oxide pellet, HEU rod	Minimization of mass fractionation using soft ablation and defocusing beam strategy	(Marin et al., 2012)
266 nm	ns	Nd:YAG	Bioimaging	Bark		(Siebold et al., 2012)
266 nm	ns	Nd:YAG		IDA-chip bioelectronic	imaging	(Zoriy et al., 2009)

				device		
266 nm	ns	Nd:YAG	Bioimaging	Brain (rat, pig)		(Pugh et al., 2012)
266 nm	ns	Nd:YAG	Bioimaging	Tissue sections (snails)		(Santos et al., 2009)
355 nm	ns	Nd:YAG	Bioimaging	Brain (rats)		(Wu and Becker, 2012)
532 nm	ns	Nd:YAG	Fundamental investigations	Interdigitated electrode array (IDA) chips	Near field LA for measurements at nanometer scale	(Zoriy et al., 2009)
532 nm	ns	Nd:YAG	Fundamental investigations	20 nm Au film deposited onto a Si substrate	Near field LA for measurements at nanometer scale	(Zoriy et al., 2008)
532 nm	ns	Nd:YAG	Fundamental investigations	Copper isotopic standard reference material NIST SRM 976 and tungsten-molybdenum alloy NIST SRM 480	Near field LA for measurements at nanometer scale	(Zoriy and Becker, 2009)
196 nm	fs	Ti: sapphire	Fundamental investigations	Silicate glass, baddeleyite, zircon, metal, oxide, hydroxide, carbonate and sulfide	Absence of elemental and isotopic fractionation using 196 nm fs-LA	(Horn and von Blanckenburg, 2007)
200 nm	fs	Ti: sapphire	Fundamental investigations	Silicate glass and minerals	Comparison of 193 nm ns-LA with 200 nm fs-LA	(Kimura and Chang, 2012)
265 nm	fs	Ti: sapphire	Fundamental investigations	Metals Brass, silicate glasses	Evaluation of liquid standard calibration	(Wälle et al., 2008)
265 nm	fs	Ti: sapphire	Fundamental investigations	Cr thin layer on a Ni substrate	Depth-profiling analysis	(Pisonero et al., 2007)
266 nm	fs	Ti: sapphire	Fundamental investigations	Silicate glass	Influence of repetition rate and scan speed on LA-ICPMS analysis	(Gonzalez et al., 2008)
343 nm	fs	Yb:KWG	Other	Silicate glass	U isotopic analysis of NIST glass	(Duffin et al., 2012)
785 nm	fs	Ti: sapphire	Fundamental investigations	Sediment reference material	Determination of the chemical composition of seven sediment reference materials	(Shaheen and Fryer, 2011)
785 nm	fs	Ti: sapphire	Fundamental investigations	Glass		(Shaheen et al., 2008)
785 nm	fs	Ti: sapphire	Fundamental investigations	Glass	Addition of hydrogen and nitrogen to the central gas flow	(Shaheen and Fryer, 2010)
795 nm	fs	Ti: sapphire	Fundamental investigations	Cu and Zn CRMs and powder pellets	Evaluation of powder pellets as calibration standards	(Traub et al., 2009)
795 nm	fs	Ti: sapphire		Lead fire assay buttons		(Vanhaecke et al., 2010)

795 nm	fs	Ti: sapphire	Fundamental investigations	Brass, aluminum, silicate Glass	Investigation of the applicability of non-matrix matched calibration	(Bian et al., 2006)
795 nm	fs	Ti: sapphire	Fundamental investigations	Brass, Ag-Cu, Ni-Fe, Cr-Fe, Pb-Sb, GaAs, NIST glass	Influence of laser fluence on elemental fractionation	(Garcia et al., 2008)
795 nm	fs	Ti: sapphire	Fundamental investigations	Silicate glass	Characterization of dielectric aerosol with respect to elemental fractionation; influence of laser fluence	(Koch et al., 2005)
800 nm	fs	Ti: sapphire	Fundamental investigations	Silicate glass	Influence of laser laser fluence on fractionation	(Russo et al., 2002a)
800 nm	fs	Ti: sapphire	Geology	Silicate (NIST 610) and sulfide (Po-726 and Cpy-RM) reference material, natural pyrite	Non-matrix dependence of fs-LA	(Velásquez et al., 2011)
800 nm	fs	Ti: sapphire	Fundamental investigations	Monazite	Influence of laser parameters on laser-induced aerosols	(D'Abzac et al., 2011)
800 nm	fs	Ti: sapphire	Fundamental investigations	Monazite	Influence of energy and pulse width on LA-ICPMS analysis	(D'Abzac et al., 2010)
800 nm	fs	Ti: sapphire	Geology	Quartz-hosted melt inclusions		(Borisova et al., 2008)
1030 nm	fs	Yb:KWG	Migration	Fish otoliths		(Martin et al., 2010)
1030 nm	fs	Yb:KGW	Other	Crude oils	Matrix effects (transparent versus crude oil)	(Ricard et al., 2011)
1030 nm	fs	Yb:KWG	Fundamental investigations	Soil and sediment	Matrix matched quantification by solid-spike isotope dilution	(Fernández et al., 2008b)
1030 nm	fs	Yb:KWG	Fundamental investigations	Soil and sediment	In-cell isotope dilution	(Fernández et al., 2008a)
1030 nm	fs	Yb:KWG	Fundamental investigations	Selenoproteins (polyacrylamide gels)	Laser-induced aerosol characterization	(Claverie et al., 2009b)
1030 nm	fs	Yb:KWG	Fundamental investigations	Glass	Influence of high repetition rate on elemental fractionation	(Claverie et al., 2009a)
1030 nm	fs	Yb:KWG	Environmental monitoring	Calcite shell (Great Scallop)		(Tabouret et al., 2012)
1030 nm	fs	Yb:KWG	Migration	Fish otoliths		(Feutry et al., 2012)
193 nm 266 nm 800 nm	ns ns fs	ArF excimer Nd:YAG Ti: sapphire	Archaeology	Corning archeological reference glasses		(Wagner et al., 2012)
193 nm 266 nm	ns ns	ArF excimer Nd:YAG	Fundamental investigations	Fe-based samples	Evaluation of quantification capabilities (matrix and non-	(Mozná et al., 2006)

265 nm	fs	Ti: sapphire			matrix matched calibration)	
193 nm 795 nm	ns fs	ArF excimer Ti: sapphire	Authenticity and provenancing	Andesine		(Fontaine et al., 2010)
193nm 780 nm	ns fs	ArF excimer Ti: sapphire	Fundamental investigations	Pyrite, zircon, glass	Comparison ns-LA versus fs-LA	(Hirata and Kon, 2008)
193 nm 265 nm 795 nm	ns fs fs	ArF excimer Ti: sapphire Ti: sapphire	Fundamental investigations	Brass, Stainless steel, Pyrite, Galenite, Zircon, Multicomponent glass	Comparison ns-LA versus fs-LA; characterization of laser generated aerosol	(Glaus et al., 2010)
200 nm 265 nm	fs fs	Ti: sapphire Ti: sapphire	Fundamental investigations	Silicate glass, brass	Comparison of different UV wavelengths using fs-LA; Less dependency of signal ratios on wavelength and repetition rate but on laser fluence	(Koch et al., 2006)
266 nm 266 nm	ns fs	Nd:YAG Ti: sapphire	Fundamental investigations	Brass	Comparison ns-LA versus fs-LA performance; aerosol characterization	(Liu et al., 2004)
266 nm 266 nm	ns fs	Nd:YAG Ti: sapphire	Fundamental investigations	Glass, monazite, zircon	Comparison UV-fs-LA and UV-ns-LA; less matrix dependency for UV-fs-LA	(Poitrasson et al., 2003)
266 nm 266 nm	ns fs	Nd:YAG Ti: sapphire	Fundamental investigations	NIST glass	Comparison ns-LA versus fs-LA; UV-fs-LA produced less spike signals	(Gonzalez et al., 2007a)
266 nm 266 nm	ns fs	Nd:YAG Ti: sapphire	Fundamental investigations	High purity zinc, zinc alloy, zinc-aluminum alloy and aluminum alloy	Comparison ns-LA versus fs-LA	(Gonzalez et al., 2007b)
266nm 1030 nm	ns fs	Nd:YAG Yb:KWG	Fundamental investigations	Heteroatom-containing proteins (polyacrylamide gels from gel electrophoresis)	Comparison ns-LA versus fs-LA	(Ballihaut et al., 2007)
266 nm 1045 nm	ns fs	Nd:YAG Yb:KWG	Fundamental investigations	Brass and urban dust	Comparison ns-LA versus fs-LA, evaluation of particle effects	(Perdian et al., 2008)
775 nm 775 nm	ns fs	Ti: sapphire Ti: sapphire	Fundamental investigations	Brass	Comparison ns-LA versus fs-LA; particle size distributions and compositions	(Koch et al., 2004)

Table 1.5-2: Laser ablation systems currently available on the market.

Manufacturer	Brand name	Laser	Wave-length	Pulse duration	Max Energy	Rep. Rate	Spot size	Fluence
Applied Spectra, Inc. (ASI)	J100 Femto	Yb:KWG (amplitude laser head)	1030 nm	< 480 fs	< 1mJ	1 - 100 kHz	5 - 100 μ m	n.a.
Applied Spectra, Inc. (ASI)	J100-UV Femto	Yb:KWG (amplitude laser head)	343 nm	< 480 fs	< 150 μ J	1 - 100 kHz	3 - 100 μ m	n.a.
Applied Spectra, Inc. (ASI)	Pegasus Tandem LA-LIBS	Nd:YAG	213 nm	< 5ns	n.a.	n.a.	n.a.	n.a.
CETAC Technologies and Photon Machines Inc.	LSX-266	Nd:YAG	266 nm	ns	n.a.	n.a.	n.a.	n.a.
CETAC Technologies and Photon Machines Inc.	LSX-213 G2	Nd:YAG	213 nm	5 ns	> 4.5 mJ	n.a.	5 - 200 μ m	n.a.
CETAC Technologies and Photon Machines Inc.	Analyte Excite	ArF excimer; ATL head	193 nm	< 4 ns	n.a.	1 - 300 Hz	2 - 150 μ m	n.a.
CETAC Technologies and Photon Machines Inc.	Analyte G2	ArF excimer; ATL head	193 nm	< 4ns	n.a.	n.a.	> 2 μ m	n.a.
CETAC Technologies and Photon Machines Inc.	Excite Pharos FS	Yb:KGW (Pharos laser head)	800 nm, 257 nm, sub 200 nm	< 200 fs	n.a.	n.a.	> 2 μ m	n.a.
Coherent Inc.	GeoLasPro	ArF excimer	193 nm	ns			4 - 160 μ m	45 J/cm ² ; >120 μ m: 35 j/cm ²
Electro Scientific Industries, Inc.	NWRFemto Laser Ablation System	Yb:KGW (Pharos laser head modified)	800 nm, 257 nm, 205 nm	< 200 fs	n.a.	1 - 1000 Hz	n.a.	UV: >3J/cm ² ; VUV >1j/cm ²
Electro Scientific Industries, Inc.	NWR193 Laser Ablation System	ArF excimer	193 nm	2 ns	n.a.	n.a.	n.a.	n.a.
Electro Scientific Industries, Inc.	NWR213 Laser Ablation System	Nd:YAG	213 nm	< 5 ns	n.a.	n.a.	n.a.	n.a.
Electro Scientific Industries, Inc.	NWR266 Large Beam Laser Ablation System	Nd:YAG	266 nm	< 5 ns	n.a.	n.a.	n.a.	n.a.
Resonetics	RESolution M-50 HR	Excimer - Compex Pro Coherent laser head (ArF)	193 nm	20 ns	200 mJ	100 Hz	5 - 380 μ m	30 J/cm ²
Resonetics	RESolution M-50 LR	Excimer - Compex Pro Coherent laser head (ArF)	193 nm	20 ns	200 mJ	20 Hz	5 - 380 μ m	30 J/cm ²
Resonetics	RESolution	Excimer - Compex Pro	193 nm	5 ns	8 mJ	300 Hz	4 - 100 μ m	15 J/cm ²

	M-50 E	Coherent laser head (ArF)						
Resonetics	RESolution S-50 LR	ArF excimer (ATL laser head)	193 nm	5 ns	8 mJ	300 Hz	4 - 100 μm	15 J/cm ²
NovaLase SA; Amplitude Systèmes; Nexeya	Alfamet IR	Yb:KWG (amplitude laser head)	1030 nm	fs	n.a.	1 - 100 kHz	25 - 200 μm	30, 80, 112 μm : 276, 31, 17 J/cm ²
NovaLase SA; Amplitude Systèmes; Nexeya	Alfamet UV	Yb:KWG (amplitude laser head)	257 nm	fs	n.a.	1 - 100 kHz	6 - 100 μm	18, 54, 72 μm : 325, 36, 20 J/cm ²
NovaLase SA; Amplitude Systèmes; Nexeya	Alfamet L3	Yb:KWG (amplitude laser head)	515 nm	fs	n.a.	1 - 100 kHz	variable	8, 16, 32 μm : 298, 74, 18 J/cm ²

1.5.2 Basic principles of (multi collector) – inductively coupled plasma mass spectrometry

This section is dedicated to a short overview about the basic principles of ICPMS in general and MC-ICPMS in particular. If the reader is interested in more detailed information about (MC)-ICPMS, it is recommended to consult one of many ICPMS handbooks (Jarvis et al., 1992; Sylvester, 2001; Nelms, 2005; Becker, 2007) or review articles (Jakubowski et al., 2011; Rehkämper et al., 2001; Wieser and Schwieters, 2005) for further reading. In this section special emphasis is put on the description of detectors typically applied in a multi collector array (see 1.5.2.3) and on multi collector block configurations for the simultaneous analysis of U and Pu (see 1.5.2.4).

1.5.2.1 ICPMS fundamentals

ICPMS is regarded as one of the most important analytical techniques in atomic spectroscopy (Jakubowski et al., 2011), not at least due to its capabilities to perform multi-element analyses at ultra-trace concentration levels (i.e. down to the sub-ppt level) and isotope ratio analyses. In the following the principle of ICPMS is shortly described.

Sample introduction

Sample introduction systems for introducing liquid samples and laser ablation systems that are applied for generating an aerosol from solid samples have to be considered as main systems. Laser ablation as sample introduction is described in 1.5.1.

A sample introduction system for introducing liquid samples into the ion source usually consists of two main parts, namely the nebulizer that generates an aerosol and the spray chamber for removing large droplets from the aerosol introduced into the ICP. The most commonly used nebulizer-spray chamber combinations consist of a pneumatic nebulizer that is coupled to a Scott type double pass spray chamber or a cyclonic spray chamber. The pneumatic concentric nebulizer has a narrow capillary in its center and is fixed to a cylindrical main body. Nebulization takes place with the help of an argon gas flow, which emerges at high velocity through the annulus between the inner capillary and the external body. A Scott type double-pass spray chamber consists of two concentric tubes. After passing the first tube the aerosol has to change its path by 180° (Todoli and Vanhaecke, 2005). The cyclonic spray chamber is shown in

Fig. 1.5-2. The nebulizer is tangentially introduced into the spray chamber. Benefits over Scott type spray chambers are faster wash-out characteristics, higher aerosol transport efficiency, less spiking and low internal volume (Elemental Scientific. Cyclonic Spray Chambers.).



Fig. 1.5-2: Quartz cyclonic spray chamber. The figure was adopted from (Elemental Scientific. Cyclonic Spray Chambers.)

However, in order to increase sensitivity and to reduce the water load into the ICP, spray chambers are often combined with heating or cooling modules or membrane desolvation units. The sample introduction system that was used within the course of this thesis was the DSN-100 (i.e. DeSolvation Nebulizer System, Nu Instruments Ltd., Wrexham, U.K.). The liquid sample is usually nebulized by means of a self-aspirating PFA nebulizer having a sample uptake rate of about $120 \mu\text{L min}^{-1}$. The generated aerosol is then introduced into a heated spray chamber where it is vaporized. Heating of the spray chamber walls is accomplished by a hot gas flow, which additionally prevents the condensation of the aerosol at the walls. Afterwards, the aerosol enters a heated (i.e. $110 \pm 10 \text{ }^\circ\text{C}$) semi-porous PTFE membrane. The solvent passes the membrane and is carried away by means of a counter-directed Ar membrane gas flow (Nu Instruments Ltd. DSN-100 - DeSolvation Nebulizer System). Finally, a dried aerosol is introduced into the ion source. The reduction of the water load into the ICP results in a reduction of interferences resulting from H_2O and in increased sensitivity.

Ion source - Inductively coupled plasma

The ion source most widely used in inorganic mass spectrometry is the inductively coupled plasma (ICP), which is operated at atmospheric pressure ($\sim 1000 \text{ mbar}$). Typically a quartz torch is placed in a load coil to which a radiofrequency (RF) power between 750 W and 1700 W is applied. An alternating current oscillates (i.e. 27.1 MHz or 40.6 MHz) within the field, setting up electrical and magnetic fields at the top of the torch. The application of a spark using a Tesla coil results in a release of electrons from argon (Ar) atoms present due to the gas flow flowing

through the torch. The released electrons are then accelerated in the magnetic field, which is referred to as inductive coupling. The fast moving electrons are colliding with neutral Ar atoms, which results again in the emission of electrons. Generally, the plasma consists of neutral Ar atoms, positively charged Ar ions and electrons. The collision processes are responsible for the high temperature of the plasma. Depending on the region of the plasma, the plasma is at a temperature between 6000 K and 10000 K. Because of these high temperatures desolvation, vaporization, atomization and finally ionization of the introduced sample aerosol take place. It should be mentioned that the extent of ionization is a function of an element's first ionization potential relative to that of Ar (i.e. 15.76 eV), whereby most elements of the periodic table produce predominantly singly charged ions. However, some elements such as cerium (Ce) or barium (Ba) have second ionization potentials low enough so that a significant amount of doubly charged ions is generated (Hill et al., 2005).

Ion extraction and focusing

While the ICP is at atmospheric pressure, the mass analyzer requires high vacuum (i.e. 10^{-7} mbar to 10^{-8} mbar). The interface is the region where the first pressure reduction takes place in addition to the extraction of ions generated in the ICP. The ICP flame is focused on the sampler cone (i.e. nickel, platinum, copper, aluminum) which exhibits an orifice with a diameter of ca. 1 mm. The sampling cone is usually mounted on a water cooled plate in order to circumvent it from melting due to the high temperature of the ICP. The expansion chamber is directly located behind the sampler cone and is pumped by a rotary pump, which yields a pressure of about 2-5 mbar. After the expansion chamber the skimmer cone having an orifice with a diameter of ca. 0.4 – 0.7 mm is located (Hill et al., 2005).

Recently, Thermo Fisher Scientific Inc. introduced a so called Jet Interface, with which increased sensitivities can be obtained. This interface uses a high capacity dry interface pump and a specially designed set of cones (i.e. x-skimmer and jet-sampler)(Thermo Fisher Scientific Inc. Thermo Scientific Jet Interface). Increased sensitivities can also be achieved in MC-ICPMS instruments manufactured by Nu Instruments by applying so called high-performance cones.

After the ions have been extracted from the ICP, they have to be focused and guided into the mass analyzer. This focusing is achieved by means of the ion optics, which consist of electrostatically controlled lens components. These components that are at high voltage can either be a series of metal plates, barrels or cylinders (Thomas, 2001).

In the case of a magnetic sector field instrument the extracted ions are accelerated up to 10 keV by a high extraction potential (Batey et al., 2005). The high voltage is either supplied to the interface with the analyzer at ground potential or to the analyzer part. In the later case the interface is kept at ground. Worth mentioning is, however, that both variants are available in commercial instruments. E.g. Nu Instruments Ltd. uses the first variant, whereas Thermo Fisher Scientific keeps the interface at ground potential.

Mass analyzer

The mass analyzer, which is under high vacuum (i.e. $\sim 10^{-8}$ mbar), is the part of an ICPMS instrument where the separation of ions according to their mass-to-charge (m/z) ratio takes place. Three types of analyzers are typically applied in inorganic mass spectrometry: 1) quadrupole mass analyzer, 2) double focusing sector-field analyzer and 3) time-of-flight analyzer (Batey et al., 2005). As the MC-ICPMS instrument (i.e. Nu Plasma HR, Nu Instruments Limited, Wrexham, U.K.) that was used in this study consisted of a double-focusing sector field analyzer with Nier-Johnson geometry, the principle of this mass analyzer will be briefly discussed.

A double-focusing sector field instrument consists of both an electrostatic analyzer and a magnetic sector analyzer. Ions generated in an ICP typically have an ion kinetic energy distribution between 5 eV and 10 eV. In order to reduce this energy distribution by energy focusing, the ions are passing an electrostatic analyzer before entering the magnetic sector analyzer. This geometry is referred to as Nier-Johnson geometry if a 90° electrostatic analyzer is combined with a 60° magnetic sector. However, the electrostatic analyzer can also be located after the magnet according to the reversed Nier-Johnson geometry (Batey et al., 2005).

Detection system

A comprehensive overview about detection systems applied in (MC)-ICPMS instruments is given in 1.5.2.3.

1.5.2.2 Multi collector – ICPMS

Traditionally, thermal ionization mass spectrometry (TIMS) has been the method of choice for achieving the highest accuracy and precision of isotope ratios (Yang, 2009). However, in TIMS elements having a high ionization potential are difficult to analyze (Rehkämper et al., 2001;

Wieser and Schwieters, 2005; Yang, 2009). As elements with high ionization potentials can be easily ionized in the ICP and because accurate and precise isotope ratios comparable to TIMS can be determined (Yang, 2009), MC-ICPMS became a complementary technique to TIMS. The enhanced use of MC-ICPMS since its introduction in the 1990s is also demonstrated by the increasing number of publications over the years (Fig. 1.5-3). Merits of MC-ICPMS are its simple and robust sample introduction, high sample throughput and high mass resolution (Yang, 2009) which enables to get rid of particular spectroscopic interferences.

In a MC-ICPMS instrument an ICP ion source is combined with a magnetic sector mass spectrometer and multiple detectors (e.g. Faraday cups, secondary electron multiplier) (Rehkämper et al., 2001). Typically, MC-ICPMS instruments are based on a Nier-Johnson double-focusing geometry. The Thermo Scientific Inc. 'Neptune', for example, uses the ICP interface of the 'Element 2', a single collector ICPMS instrument, and the multi-collector technology of the 'Triton', which is a Thermo Scientific Inc. TIMS instrument (Jakubowski et al., 2011). On the contrary to the 'Neptune', the ICP interface of the Nu Instruments Ltd. 'Nu Plasma HR' MC-ICPMS instrument that was used in this study is under high voltage, whereas the analyzer and the collector part are at ground potential. Detailed descriptions of MC-ICPMS instruments that have been commercially available since their introduction in the 1990s can be found in various reviews (Jakubowski et al., 2011; Rehkämper et al., 2001; Wieser and Schwieters, 2005; Yang, 2009).

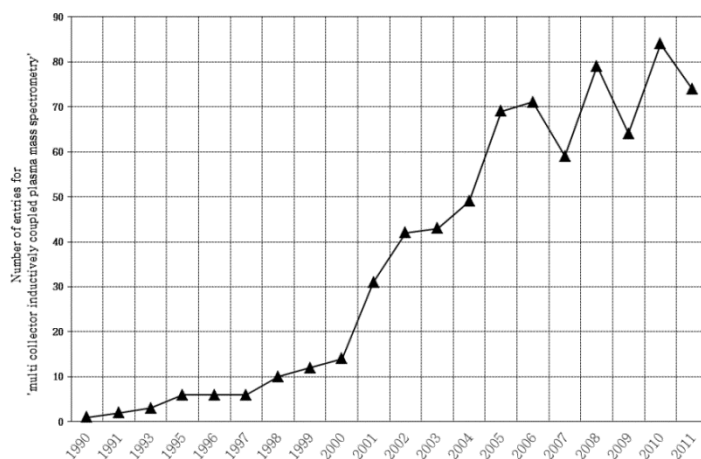


Fig. 1.5-3: Number of entries in SciFinder for 'multi collector inductively coupled plasma mass spectrometry'.

1.5.2.3 Detectors typically used in a multi collector array

Faraday cups

Faraday cups are regarded as the detectors of choice for high precise isotope ratio measurements, not at least due to their high stability and linearity (Longerich and Diegor, 2001). Moreover, their width, which is about 3.5 mm in the case of a 'Neptune *Plus*' Faraday cup (Tuttas et al.) and about 2 mm in the case of a 'NU Plasma HR' Faraday cup, respectively, allows to easily arrange them in parallel to each other in a multi collector array for the simultaneous detection of incoming ions.

Faraday cups are typically applied for the detection of relatively high ion currents (Becker, 2007; Rehkämper et al., 2001). Based on analogue detection the intensity of the ion beam (current = charge per unit time) is measured, in contrast to pulse counting where the number of ions are detected (Rehkämper et al., 2001).

Faraday cups are usually designed as a rectangular metal box with one open end into which the ions are entering. The box is connected to an amplifier with a high impedance input (Meyers, 2000). Typically $10^{11} \Omega$ high value resistors are used in MC-ICPMS (Nu Instruments Ltd. NP Manual V2) or TIMS instruments. However, it is also feasible to apply resistors $> 10^{11} \Omega$ (Tuttas et al.) for extending the dynamic range. When ions are entering the box electrons are released in order to neutralize the incoming positively charged ions (Meyers, 2000). The electron current are flowing through the resistor, across which they are creating a potential difference (Longerich and Diegor, 2001). The detection efficiency is close to 100 % as all incoming ions are detected. In addition, gain stability is given as the gain does only depend on the resistor value (Longerich and Diegor, 2001). However, the loss of secondary electrons that are emitted after ions are impinging on the inner surface of the Faraday cups may lead to increased ion current readings. Therefore, an electron suppressor and permanent magnets are used in order to hinder the escape of secondary electrons (Meyers, 2000).

In the following the Faraday cups that are used in the 'Nu Plasma HR' multi collector array are described in order to get a more detailed picture of these detectors (see also Fig. 1.5-4).

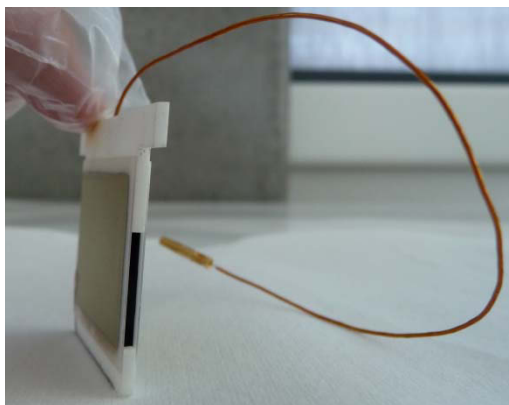


Fig. 1.5-4: 'Nu Plasma HR' Faraday cup.

The Faraday detectors applied in the 'Nu Plasma HR' multi collector array consist of a ceramic body with sapphire sides. While the outer walls are gold coated, the interior ones are coated with graphite. However, the rear of the detector interior consists of a graphite block. The gold coating is grounded when the Faraday cup is mounted in the detector block in order to eliminate charging when ions pass along the outer walls of the detector. An electron suppressor is located near the opening of the Faraday cup (Nu Instruments Ltd. NP Faraday detectors). This electron suppressor has a potential of -50 V to -100 V (Nu Instruments Ltd. NP Manual V2) and ensures that secondary electrons are not released from the detector. However, reduction of secondary electron generation is accomplished by the graphite coating of the inner walls. Moreover, small magnets that are located above and below the collector block send surface ejected electrons into a circular path, which additionally hinders the escape of electrons (Nu Instruments Ltd. NP Faraday detectors). In addition, the Faraday cups are designed in a way so that the electron escape angle is minimized, which is achieved by increasing the Faraday cup length (Nu Instruments Ltd. NP Manual V2).

The Faraday cups that are used in the 'NU Plasma HR' multi collector array are having a dynamic range of 10 V, whereas the ones used in the 'Nu Plasma II' (latest generation of Nu Instruments Ltd. MC-ICPMS) are having a dynamic range of 55 V (Nu Instruments Ltd. Nu Plasma II). In both cases $10^{11} \Omega$ resistors are used. On the other hand, the Thermo Scientific Inc. 'Neptune' MC-ICPMS is available with Faraday cups having a dynamic range of 55 V (Ball et al., 2008).

The lower end of the dynamic range is limited by the detector noise (i.e. Johnson noise) that is associated with the resistance value (Nu Instruments Ltd. NP Manual V2). The relationship between the random noise and the resistance (Nu Instruments Ltd. NP Manual V2) is given in eq (1.5-1)

$$i_n = \sqrt{\frac{4 k_B T \Delta f}{R}} \quad (1.5-1)$$

where i_n is the random noise in amps rms, k_B the Boltzmann constant in J/K, T the absolute temperature in K, Δf the measurement bandwidth in Hz and R the resistance in Ω . Thus, the noise current limit for a one second measurement period is 4×10^{-16} amps rms., assuming that all other noise sources have been eliminated. However, the limit can be improved by increasing the measurement period (Nu Instruments Ltd. NP Manual V2).

Typically, modern Faraday cups that are employed in a multi collector array do not have to be cross calibrated against each other because they have uniform registration efficiency. The gain calibration factors of the individual amplifiers are usually determined by sequentially connecting the amplifier inputs to a stable reference current. The response of the amplifier is measured, whereupon the ratios of the measured signals yield the gain or cross calibration factors (Wieser and Schwieters, 2005). According to Wieser and Schwieters, the uncertainty of the calibration factor for a Faraday cup, resulting from a cross calibration of two amplifiers, is 5 ppm (1 RSD). Taking this uncertainty into account for calculating the uncertainty of the external reproducibility, an uncertainty of 7 ppm (1 RSD) is obtained for the external reproducibility. As the uncertainty is determined by the uncertainty of the calibration factor, the reproducibility achievable for one isotope ratio is limited to 7 ppm. In order to enable more precise isotope ratio measurements, Thermo Fischer Scientific Inc. implemented a so called 'Virtual Amplifier' design for the Faraday cup cross calibration (see Fig. 1.5-5). The advantage of this design is that biases resulting from uncertainties in the gain calibration are eliminated. In comparison to a classical approach, in which each Faraday cup is connected to an individual amplifier, the 'Virtual Amplifier' design uses a relay matrix, whereby the amplifiers can be switched between different Faraday cups (Wieser and Schwieters, 2005). The principle of this design is described in detail in (Wieser and Schwieters, 2005).

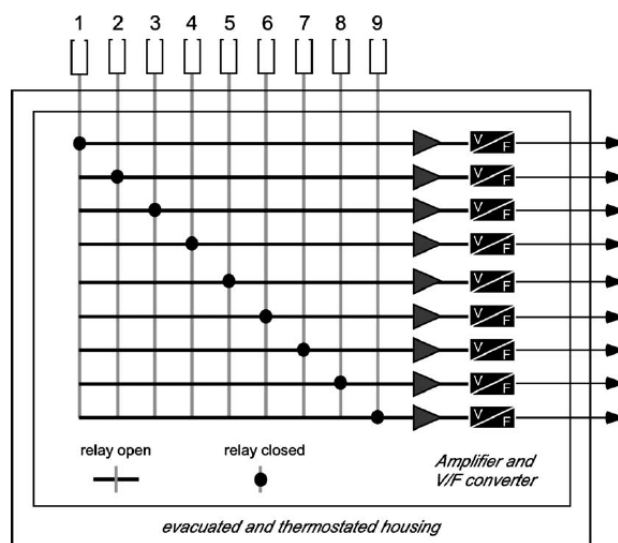


Fig. 1.5-5: Schematic diagram of the Thermo Scientific Inc. Virtual Amplifier. The figure was adopted from Wieser and Schwieters (Wieser and Schwieters, 2005).

Another peculiarity employed by Thermo Fisher Scientific Inc. is the use of a larger ion optical magnification (i.e. $M=2$), which results in an improved Faraday cup performance. Since the mass dispersion is directly proportional to the ion optical magnification, the Faraday cups can be enlarged (i.e. twice as wide with $M=2$) in comparison to an ion optical magnification of $M=1$. As the angular divergence of the ion beam at the detector is proportionally reduced with the ion optical magnification, the effective depth at which the ions strike the side walls of the Faraday cup is increased. Hence, there is a higher chance that secondary electrons are not escaping from the cup. A schematic description of the effects of the larger ion optical magnification is given in Fig. 1.5-6.

It was already mentioned above that Faraday cups are the detectors of choice for precise isotope ratio measurements. However, when it comes to the data acquisition of short, fast changing signals as it is the case with transient signals resulting from e.g. laser ablation, Faraday amplifier outputs are lagging behind input signals after a change in signal intensities. These differences in amplifier response times are leading to signal intensities that are enhanced or reduced relative to each other (Pettke et al., 2011b), whereby a drift in the measured isotope ratios is observed over a transient (Hirata et al., 2003). A detailed discussion about differences in amplifier response times is given in section 2.2 of this thesis.

Noteworthy is that nowadays Faraday cups are also employed together with a dual mode (i.e. pulse-counting for low ion intensities and analogue detection for high ion currents combined in one detector) secondary electron multiplier (SEM) in single collector ICPMS instruments for

increasing the linear dynamic range. Thermo Scientific Inc., for example, states that the linear dynamic range is increased up to $> 10^{12}$ orders of magnitude by incorporating a Faraday cup in the ELEMENT XR*. The dual mode SEM is linear over nine orders of magnitude. Hence, the additional use of a Faraday cup enhances the dynamic range by three orders of magnitude (Thermo Fisher Scientific Inc. Thermo Scientific ELEMENT 2 & ELEMENT XR).

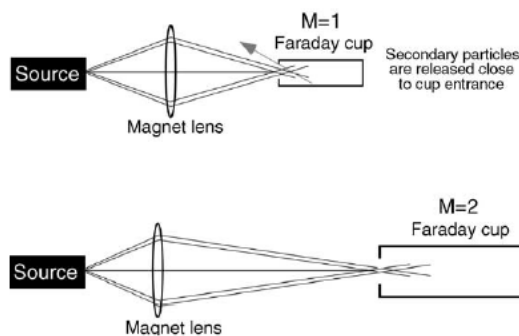


Fig. 1.5-6: Schematic description of the effects resulting from ion optical magnification (i.e. $M=2$).

At $M=2$ the Faraday cup is enlarged and the ion beam strikes the wall at a deeper position compared to $M=1$. The figure was adopted from Wieser and Schwieters (Wieser and Schwieters, 2005).

Electron multipliers

Generally, there are two different types of electron multipliers that are used in MC-ICPMS instruments: discrete-dynode secondary electron multipliers (SEMs) and continuous dynode or channel electron multipliers (CEMs) (Hunter and Stresau, 2005). Generally, both detectors are based on signal multiplying induced by emission of secondary electrons due to impinging ions. Discrete-dynode secondary electron multipliers are the most used detectors in single collector ICPMS instruments, in which they can be operated according to a dual mode. The principle of SEMs operating in analogue and dual, respectively, mode is given elsewhere (Hunter and Stresau, 2005; Richter et al., 2001).

Channel electron multiplier

Channel electron multipliers (CEMs) were used in early single collector ICPMS instruments as they were more stable in air than the discrete-dynode secondary electron multipliers (SEMs) that were available at these times. However, the development of air-stable dynode materials in SEMs favored the replacement of CEMs in single collector ICPMS instruments by discrete-dynode SEMs during the 1990s, mainly due to their higher dynamic range (Hunter and Stresau, 2005).

However, Thermo Fisher Scientific Inc. applied miniaturized channeltron type detectors in their 'Neptune' MC-ICPMS and 'Triton' MC-TIMS, respectively, instrument. These detectors were applied as discrete dynode SEMs, having a width of about 20 mm, were not compatible with the tight space requirements in a multi collector array. The channeltron type detectors with a width of 3.5 mm had the same dimensions as the applied Faraday cups. Disadvantageous was that they were limited with respect to their dynamic range (Tuttas et al.).

Recently, Thermo Fisher Scientific Inc. started to employ compact discrete dynode (CDD) multipliers (see also 1.5.2.4) in the multi collector array as an alternative to previously applied MIC detectors. In comparison to these detectors, CDD multipliers, having about twice the width of the applied standard Faraday cups (i.e. ~ 6-7 mm), are giving the same dynamic (i.e. 1 cps to 1 400 000 cps) range and performance as standard sized discrete dynode SEMs (Tuttas et al.).

A classical CEM consists of a curved glass tube with an internal diameter of about 1 mm (O'Connor and Evans, 2007). The interior is coated with a lead oxide semiconducting material (Jarvis et al., 1992) having an inner high resistance (O'Connor and Evans, 2007). A schematic diagram of a CEM is given in Fig. 1.5-7.

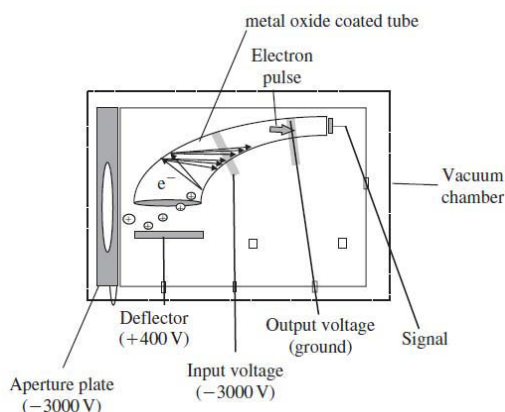


Fig. 1.5-7: Schematic diagram of a continuous dynode electron multiplier. adopted from O'Connor and Evans (O'Connor and Evans, 2007).

Typically, voltages of -2600 V and -3500 V are applied to the multiplier, whereby ions are attracted into the funnel opening (O'Connor and Evans, 2007). The back of the tube near the collector is held at ground potential (Jarvis et al., 1992). Ions that have entered the glass tube are impinging on the surface, which results in an ejection of secondary electrons from the surface. These electrons are accelerated down the tube as a result of the potential gradient across the tube (O'Connor and Evans, 2007), resulting from the continuous varying of the resistance of the interior coating across the tube (Jarvis et al., 1992). The accelerated electrons

are again colliding with the tube's inner surface. As a consequence further emissions of secondary electrons and multiplying (i.e. $10^7 - 10^8$) of the ion's incident signal are taking place. At the end the electron pulses (i.e. 50 mV to 100 mV), which last about 10 ns, are recorded (O'Connor and Evans, 2007).

Discrete-dynode secondary electron multipliers

In addition to their use as detection systems in single collector ICPMS instruments, discrete-dynode secondary electron multipliers (SEMs) are applied in MC-ICPMS instruments as well. In contrast to Faraday cups, which are used for the detection of high ion intensities, SEMs are employed for measuring low ion signal intensities. According to Richter et al. (Richter et al., 2001) they are currently among the most sensitive detectors for measuring extremely small ion currents (i.e. $< 10^{-15}$ A), which is a prerequisite for the detection of low abundant isotopes and or isotopes that are present in very small concentrations, respectively. Typically, the dynamic range goes up to $10^5 - 10^6$ cps (Richter et al., 2001).

In MC-ICPMS instruments SEMs manufactured by ETP (SGE Analytical Science Pty Ltd., Victoria, Australia) have been widely employed (Nu Instruments Ltd. NP Multiplier Operation; Ball et al., 2008; Hoffmann et al., 2005). Recently, Thermo Fisher Scientific Inc. and MasCom developed a new generation of SEMs, which show improved linearity (Richter et al., 2009) (see below). SEMs are usually positioned off-axis to the focal plane of the mass analyzer (Rehkämper et al., 2001) as they are too large in size for being incorporated in the collector block as is the case with e.g. Faraday cups or CDD detectors.

SEM design

A schematic diagram of a SEM is shown in Fig. 1.5-8.

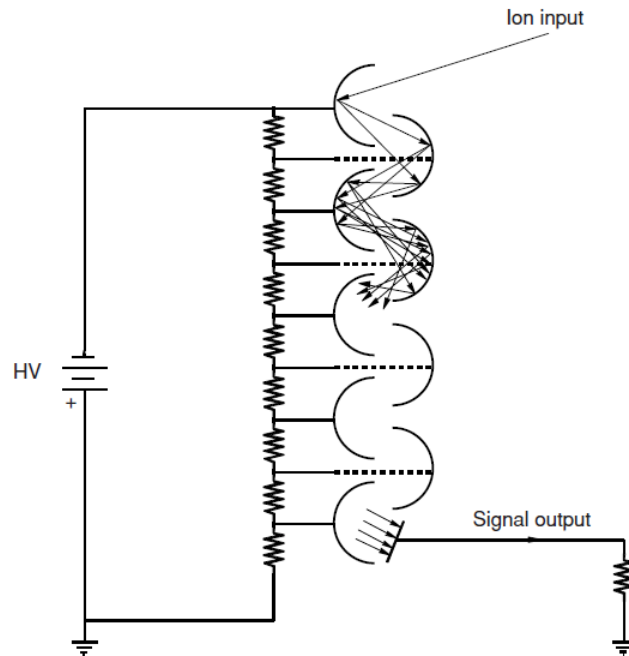


Fig. 1.5-8: Schematic diagram of a discrete-dynode secondary electron multiplier, adopted from Hunter and Stresau (Hunter and Stresau, 2005).

As can be seen a high voltage is applied to the dynode array. The dynodes used in SEMs consist of layered metals (i.e. Be on Cu, Mg on Ag) and are constructed in a curved way in order to focus the electrons onto the following dynode (Meyers, 2000). Ions that are entering the detector are accelerated to the first (or conversion) dynode, from which electrons are emitted as a consequence of an impinging ion. The secondary electrons are then accelerated by means of the electron-optics to the next dynode, where again several secondary electrons are generated per incident electron (Hunter and Stresau, 2005). Thereby an electron cascade (i.e. $10^7 - 10^8$ electrons) (Richter et al., 2001) over the SEM having several stages (i.e. typically 21-26 for pulse-counting) is created. The single electron pulse that is generated from a single incident ion is finally collected at the detector's output electrode.

The detector's output is referred to as gain, which is defined as the average number of electrons collected for each input ion initiating an electron cascade. The gain can be adjusted by means of the high voltage applied to the multiplier, whereby higher gains are achieved with higher voltages. Thus, the inter-dynode voltage is adjusted and as a consequence the electron impact energy as well (Hunter and Stresau, 2005).

The ion detection efficiency depends on the mass and the energy of an incident ion as these parameters determine the average number of secondary electrons emitted at the first dynode, whereby proportional relationships are given between the ion-to-electron conversion yield and 1) the ion impact energy and 2) the reciprocal of the square root of the mass of the ion. Generally, higher ion-to-electron yields are resulting in higher ion detection efficiencies, whereby the number of secondary electrons that are emitted is determined by Poisson statistics. E.g. an average ion-to-electron yield of 1.0 results in a detection efficiency of about 63 %, whereas a detection efficiency of about 95 % will be obtained by a yield of 3.0 (Hunter and Stresau, 2005).

High voltage setting

Noteworthy is that the high voltage yielding the maximum gain cannot be considered as the high voltage optimum for the operation of the multiplier (Nu Instruments Ltd. NP Multiplier Operation). In Fig. 1.5-9 a typical ion counting plateau curve (Hunter and Stresau, 2005) showing the relationship between the high voltage applied to the multiplier and the count rate is given.

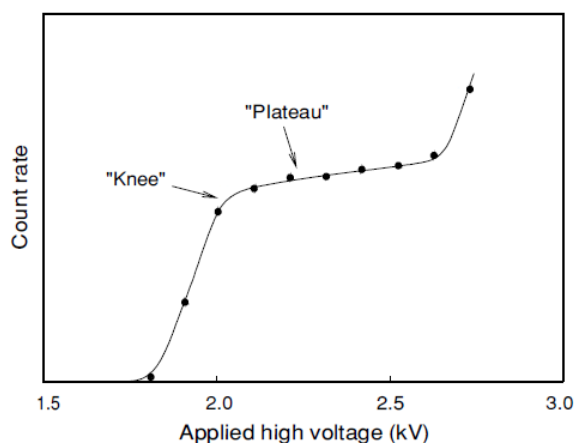


Fig. 1.5-9: Ion counting plateau curve adopted from Hunter and Stresau (Hunter and Stresau, 2005). Please note that the Figure was slightly modified.

Generally, the optimal voltage should be set just above the knee of the plateau as this is the region of best ion detection sensitivity, linearity, gain stability and operating life. At the plateau region slight changes of any applied voltage just have small effects on the measured count rates.

On the other hand, at e.g. the knee of the curve already small voltage fluctuations are leading to a pronounced increase or decrease of the count rate.

The curve shown in Fig. 1.5-9 is derived by step-wise increasing the voltage applied to the multiplier. At the beginning a very low operating voltage is applied so that no signal pulses are measured. In this case the voltage is set to below the discrimination threshold, which is the threshold voltage that has to be exceeded in order to assign pulses to signal outputs coming from the multiplier. Below this threshold pulses coming from the multiplier and pulses coming from the dark noise (i.e. measured output signal in the absence of any input signal) are not distinguishable. At a certain voltage a measurable count rate is observed, whereas further increasing of the voltage yields a steep increase of the count rate. However, at some point —at the plateau region —increasing voltages just have a small effect on the observed count rates. After the plateau increasing voltages yield again a sharp increase of the count rate, which can be attributed to 1) ion-feedback in the SEM and 2) electronic double-counting of pulses. Ion-feedback occurs as a consequence of the generation of positively charged residual gas molecule ions within the multiplier. These ions are striking a dynode, thus generating additional secondary electrons. Hence, a second pulse can be initiated. Electronic double-counting is a result of an impedance mismatch between the signal output electrode and the detection electronics (Hunter and Stresau, 2005). These so called after-pulsing (Ramebäck et al., 2001) effects result in a gain of measured count rates. That means that more counts are detected as one would expect from just ions entering the detector.

Dead time

Another phenomenon accompanied with pulse-counting SEMs is the dead time, which is the time during which a new incoming event is neglected (Ramebäck et al., 2001). On the contrary to after-pulsing dead time results in count rate losses. Thus lower count rates are observed than are actually occurring (Jarvis et al., 1992).

Ion counting systems are classified either into a paralyzable or a non-paralyzable system (Hunter and Stresau, 2005; Müller, 1973). However, in practice the SEM behaves in a way that is in between these two (Nelms et al., 2001). Williamson et al. (Williamson et al., 1988) attributed both the detector and the amplifier discriminator to the paralyzable system, whereas the electronic components (i.e. pulse shaper within the amplifier discriminator and counter) were attributed to the non-paralyzable system. Thus dead time is a feature of both the detector and the ion counting electronics (Nelms et al., 2001).

In a paralyzable system the dead time can be extended indefinitely as each pulse resulting from an ion entering the detector leads to an extension of the dead time, whether or not the pulse itself is counted. On the other hand, in non-paralyzable systems the precedent impact of an ion creates a dead time, during which a subsequent ion is not counted. Other than in a paralyzable system, no extension of the dead time takes place due to the impact of an ion (Hunter and Stresau, 2005; Williamson et al., 1988).

The dead time results in a non-linear behavior (see below) of the SEM, whereupon non-linearity and count rate losses are more pronounced at higher count rates (Jarvis et al., 1992). Hence taking non dead time corrected raw intensities into account for the computation of e.g. isotope ratios may result in non- accurate ratios. The equation usually applied for correcting the raw intensities for the dead time (Müller, 1973; Nelms et al., 2001) is given in eq (1.5-2) (see also 2.1, eq (2.1-1)):

$$I_t = \frac{I_0}{(1-I_0\tau)} \quad (1.5-2)$$

where I_t is the intensity (in cps) corrected for the dead time, I_0 is the measured intensity not dead time corrected and τ is the dead time of the SEM. The equation given above (i.e. 1.3-2) is only valid for non-paralyzable systems. However, at count rates $\ll 1/\tau$ the paralyzable and the non-paralyzable model are approximating each other (Hunter and Stresau, 2005; Nelms et al., 2001).

A common approach for determining the dead time of SEMs applied in ICPMS instruments is based on isotope ratio measurements as a function of the analyte concentration (Vanhaecke et al., 1998). Nelms et al. (Nelms et al., 2001), for example, compared four different methods of dead time calculations with regard to their ease of application and accuracy. Three of these methods were based on lead (Pb) isotope ratio measurements. However, another method for determining the dead time is based on pulse-to-pulse timing measurements, in which the time distribution of the pulses from the amplifier is recorded. In this approach the observed dead time is the time during which no pulse is recorded (Ramebäck et al., 2001). Ramebäck et al. (Ramebäck et al., 2001) observed discrepancies between ratio and electronically determined dead times. As the ratio determined dead time was shorter than the electronically determined one, the discrepancies were attributed to secondary effects (i.e. after-pulsing, see above). The authors additionally stressed that after-pulsing may result in negative dead times. After-pulsing was assigned to a combination of a wrong voltage setting (i.e. too high) applied to the multiplier together with the use of an impedance mismatching cable between the multiplier and the amplifier. E.g. after-pulsing was not observed when using a 50 Ω cable instead of a 75 Ω one.

Mass dependence of the dead time

Investigations of the possibility of a mass dependence of the detector dead time were accomplished by several authors (e.g. (Nelms et al., 2001; Vanhaecke et al., 1998)). While Nelms et al. (Nelms et al., 2001) and Richter et al. (Richter et al., 2001) did not identify such a dependency (Nelms et al., 2001), Vanhaecke et al. (Vanhaecke et al., 1998) observed a dependency of the dead time on the analyte mass when using a channeltron electron multiplier installed in a ICP-QMS. No such dependency was observed by the same authors when using a SEM that was installed in a single collector ICP-SFMS instrument (Vanhaecke et al., 1998).

SEM linearity

Considering the linearity of a SEM, ideally a linear relationship between the ions entering the SEM and the measured count rate should be given. The slope of this linear relationship represents the relative yield (i.e. ratio of the measured count rate and the actual number of ions entering the SEM) of the SEM, whereas the intercept represents the dark noise. If a linear relationship is given, the relative yield, which is also referred to as gain, is independent of the count rate. Typically, the relative yield/gain, which is usually given in comparison to the yield/gain of a Faraday cup, is between 90 % and 100 % when the high voltage is set to a value just above the knee of the plateau (see above). It should be mentioned that the Faraday cup ion detection efficiency is close to 100 % (Richter et al., 2009; Richter et al., 2001)

It was stressed above that dead time results in a non-linear behavior of the SEM, which results in the determination of non-accurate isotope ratios as less counts are measured than are actually generated from incidents ions (Jarvis et al., 1992). However, Richter et al. (Richter et al., 2001) discussed measurement data from Rosman et al. (Rosman et al., 1987), who performed SEM linearity studies in analogue mode. As the investigated SEM showed a non-linear behavior in analogue mode, it was concluded that non-linearity is not necessarily an effect resulting from the dead time (Richter et al., 2001). It was assumed that the observed non-linearity was rather caused in the SEM itself than in the amplifier electronics. Thus, non-linearity is depending on the linearity of both the SEM itself and the amplifier electronics (Richter et al., 2009). However, as both systems might exhibit different linearity characteristics (i.e. linear vs. logarithmic), both systems should be investigated separately. If e.g. the dead time of the pulse amplifier was electronically determined by means of e.g. an oscilloscope, residual non-linearities could be observed after applying corrections using the before electronically determined dead time (Richter et al., 2009). Richter et al. (Richter et al., 2009) stated that the electronically

determined dead time is not traceable to the SI-system, though. The use of electronically determined dead times to reduce measurement uncertainty has been discussed by Nygren et al. (Nygren et al., 2006).

Richter et al. (Richter et al., 2001) observed a non-linear behavior with respect to ETP and MasCom detectors when performing TIMS measurements. A so called RLR-algorithm (i.e. restricted logarithmic rate effect) was established and applied for correcting for deviations due to a non-linear behavior of the SEM. According to Richter et al. (Richter et al., 2009) a SEM is linear for count rates below a certain limiting count rate, whereas the SEM response increases logarithmically with the count rate. However, this is only true for count rates below the certain limiting count rate. In the case of the SEMs investigated by Richter et al. (Richter et al., 2001) a counting rate limit of ca. 2×10^4 was observed. On the contrary to the dead time, more pulses are detected at higher count rates due to SEM non-linearity. If the increase of the SEM efficiency was ignored in the presence of relatively small dead times (e.g. 20 ns), negative dead times could be observed as well (Richter et al., 2009). In addition, it should be mentioned that if the SEM of interest showed a non-linear behavior, dead time determinations by isotope ratio measurements using certified isotopic reference materials (see below) would yield incorrect results. The determined dead times are typically too low when compared to the electronically determined dead times of the pulse amplifier (Richter et al., 2001).

Hoffmann et al. (Hoffmann et al., 2005) performed SEM linearity studies using a 'Neptune' MC-ICPMS. In this study non-linearity of an ETP detector was additionally observed for count rates below 10^4 cps, whereby non-linearity already started at a count rate of 10 cps. After exceeding 10^4 to 10^5 cps an additional non-linear behavior was observed, which is in good accordance with Richter et al. (Richter et al., 2001).

A reason for observing an increase in the count rate response with increasing count rates may be a count rate-dependent memory effect. Some surface charge may be trapped at the last set of dynodes where the charge density of the electron pulse is greatest. This surface charge may fade away following an exponential function. In the case of high count rates the decay of the surface charge would take longer as compared to low count rates. Thus, the voltage distribution within the dynode/resistor array would take some time reaching stable conditions again (Richter et al., 2001). Considering non-linearity at low count rates, Hoffman et al. (Hoffmann et al., 2005) suggested that thermal effects, resulting from ion impact and secondary electron avalanches, could have an influence. Heating could e.g. increase the rate of released electrons or add additional kinetic energy to the secondary electrons. In both cases the final pulse height could be increased.

As it is assumed that the mechanisms resulting in the observed non-linearity are taking place at the last dynodes, no elemental dependency on the non-linearity should be observed (Richter et al., 2001). Hoffman et al. (Hoffmann et al., 2005) checked for elemental dependency by measuring U and Th solutions, but could not identify any relationship between non-linearity and the element analyzed.

Generally, certified isotopic reference materials are applied for performing linearity studies. The applied CRMs should have multiple isotopes differing in relative abundances by several orders of magnitude. In addition, in order to be able to correct for mass bias without being influenced by possible non-linearity effects, the material should have two isotopes which ratio is close to unity (Richter et al., 2009; Richter et al., 2001). This is especially important when all isotopes are measured with the same SEM according to a so called peak-jumping routine (see below). Richter et al. (Richter et al., 2009) proposed to use the IRMM-072, IRMM-073 or the IRMM-074 series for linearity studies as these certified isotopic reference materials are fulfilling all requirements.

Noteworthy is that the IRMM-073 series was diluted from the IRMM-072 series in order to facilitate shipment and use of this material in environmental U mass spectrometry. The IRMM-074 series on the other hand was prepared in order to replace the quite popular IRMM-072 series. Worth mentioning is that the IRMM-072 series consisted of 15 individual certified isotopic reference materials, whereupon the $^{235}\text{U}/^{238}\text{U}$ isotope ratio was held constant at a value close to unity. The $^{233}\text{U}/^{235}\text{U}$ isotope ratios varied in 15 steps across the series from 1.0 to 1.0×10^{-6} . The IRMM-074 series was designed in order to cover the same working range, although in 10 steps, using the same isotope pairs for linearity studies (Richter et al., 2009).

Recently Richter et al. (Richter et al., 2009) suggested two procedures for SEM linearity studies and dead time determination using the IRMM-073/-074 series. While it is recommended to use the static procedure for linearity studies of SEMs installed in MC-ICPMS instruments, the dynamic procedure was designed for measurements with MC-TIMS. A static procedure was also recommended by Hoffman et al. (Hoffmann et al., 2005) for SEM linearity studies using MC-ICPMS. The static procedure is independent on plasma instabilities. Hence the precision of MC-ICPMS isotope ratio measurements is improved compared to the use of the dynamic procedure (Hoffmann et al., 2005). In the dynamic procedure, the authors additionally observed a memory effect (i.e. elevated SEM yield) as a consequence of applying high ion beam intensities to the SEM before measuring a less abundant isotope (Hoffmann et al., 2005).

In the static procedure proposed by Richter et al. (Richter et al., 2009) ^{233}U is measured with the SEM of interest at various intensity levels using the IRMM-073/1-15 or IRMM-074/1-10 series.

Thus the entire range of count rates can be covered. The major U isotopes ^{235}U and ^{238}U are measured with Faraday cups at a uniform intensity level. The SEM-Faraday cup inter-calibration is performed by additionally measuring ^{235}U with the SEM. The dead time can be determined by detecting ^{233}U at different count rates. It is derived from the slope of a regression line with $(^{233}\text{U}/^{235}\text{U})_{\text{measured}}/(^{235}\text{U}/^{238}\text{U})_{\text{certified}} - 1$ on the y-axis and with the ^{233}U count rate on the x-axis. Linearity is observed when the measured data points are well fitted by the regression line. Considering linearity studies and dead time determinations with TIMS, the static procedure is not recommended as it is difficult to realize uniform intensity levels for different standard solutions loaded on different filaments. In the case of TIMS, one standard of the IRMM-073/-074 series, preferably having a $^{233}\text{U}/^{235}\text{U}$ isotope ratio of about 0.01, is measured at various intensity levels in a so called peak-jumping mode. The dead time can be again determined from the slope of a linear regression. On the contrary to the static procedure, the dead time is determined by measuring ^{235}U at the different count rates. But it has to be accounted for the dead time effect resulting from the measurement of ^{233}U with the same SEM as well. Therefore the slope has to be divided by the following term: $1 - (^{233}\text{U}/^{235}\text{U})_{\text{certified}}$. Worth mentioning is that if the dynamic procedure is applied for MC-ICPMS dead time determinations, typically larger uncertainties, mainly resulting from plasma instabilities, are observed compared to TIMS (Richter et al., 2009). Furthermore, Richter et al. (Richter et al., 2009) reported that the SEMs of interest in the latest study did not show any detector-inherent non-linearity. The detectors, which have been developed by Thermo Fisher Scientific Inc. in collaboration with MasCom in 2006, were linear within 0.1 % and required only dead time correction for the pulse amplifier (Richter et al., 2009).

1.5.2.4 Multi collector configurations for the simultaneous analysis of U and Pu in ICPMS

Both Nu Instruments Ltd. and Thermo Fisher Scientific Inc. provide multi collector configurations for the simultaneous measurement of U and Pu, respectively. In the following the 'Nu Plasma HR' collector block configurations that have been applied within the course of this PhD studies are described. The 'Neptune Plus' L5 ion counter package collector block configuration is additionally discussed in order to give an example of a latest generation multi collector configuration for U and Pu analysis.

'Nu Plasma HR' collector block configurations

The 'Nu Plasma HR' standard collector block configuration used throughout these studies consists of twelve Faraday cups (see also 1.5.2.3) and three SEMs (see also 1.5.2.3). As the collector array is fixed, peak alignment of the ion beams entering the collectors is accomplished by means of a patented zoom lens system. The standard collector block configuration enables the simultaneous determination of the minor U isotopes ^{234}U and ^{236}U with SEMs together with the simultaneous detection of the major U isotopes ^{235}U and ^{238}U with Faraday cups (see Fig. 1.5-10). H6 to H1 refers to Faraday cups located at the high mass side, whereas L1 to L5 refers to the ones located at the low mass side. Ax stands for the center Faraday cup. The application of the 'Nu Plasma HR' standard collector block arrangement for U isotope ratio measurements is also described in detail in 2.1.

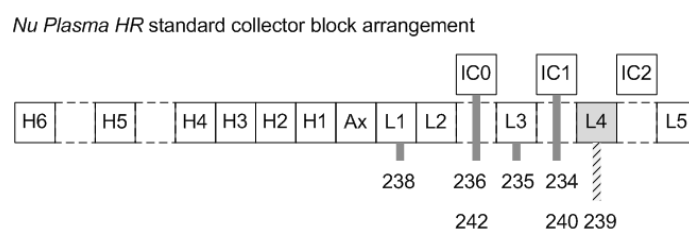


Fig. 1.5-10: 'Nu Plasma HR' (Nu Instruments Ltd.) standard collector block configuration. (H...Faraday cup high mass side, Ax...Faraday cup axial mass, L...Faraday cup low mass side, IC...ion counting multiplier (i.e. secondary electron multiplier)).

Peak tailing

^{236}U is typically measured with the SEM called IC0 as a deceleration filter is installed in front of this detector. Depending on the instrument manufacturer the deceleration filter may also be referred to as retardation filter, WARP (wide-angle energy retarding filter) or RPQ (retarding potential quadrupole) filter. The deceleration filter reduces this so called peak tailing as it reduces the amount of ions with low kinetic energy (Nu Instruments Ltd. NP Abundance Sensitivity). Peak tailing is often expressed as abundance sensitivity (Batey et al., 2005), which is defined as the ratio of the maximum ion current recorded at a mass m to the ion current arising from the same species recorded at an adjacent mass ($m \pm 1$) (IUPAC Compendium of Chemical Terminology (1997)). Low kinetic energy ions are a result of collisions with residual gas molecules and/or scattering processes at the edges of the beam defining apertures. Moreover these processes might also result in a slight change of the ion optical flight path (Wieser and Schwieters, 2005). The low kinetic energy ions are appearing at a different position

in the mass spectrum as the magnetic sector deflects ions with reduced kinetic energy with a smaller radius compared to ions having a higher energy. Thus, a tail is built up on the low mass side of the major peak (Wieser and Schwieters, 2005) which results in an increase of the background at neighboring masses (Thermo Fisher Scientific Inc. Another step ahead in MC-ICPMS). Wieser and Schwieters stated abundance sensitivities, without applying a filter, in the range of 1-5 ppm for state of the art multi collector instruments (Wieser and Schwieters, 2005).

In the case of U isotope ratio measurements, ^{238}U ions are tailing into the mass of ^{236}U , which is usually present in extremely low quantities compared to ^{235}U and ^{238}U , respectively. A schematic diagram of the ^{238}U peak tailing effect is shown in Fig. 1.5-11. It can be seen that the application of the deceleration filter reduces the amount of ^{238}U ions tailing into the mass of ^{236}U . Boulyga et al. (Boulyga et al., 2006) for example observed a $^{236}\text{U}/^{238}\text{U}$ abundance sensitivity improvement from 1.5×10^{-6} to 3×10^{-9} when applying the deceleration filter for the determination of ^{236}U . Richter et al. determined a detection limit of 1.2×10^{-10} by applying a RPQ deceleration lens system for $^{236}\text{U}/^{238}\text{U}$ isotope ratio measurements by means of thermal ionization mass spectrometry. $^{236}\text{U}/^{238}\text{U}$ detection limits ranging from 10^{-10} (Zhao et al., 1994) to 10^{-12} (Paul et al., 2000) were observed using acceleration mass spectrometry.

Noteworthy is that a simultaneous detection of $^{238}\text{U}^1\text{H}$ together with the other U isotopes of interest is not feasible using the 'Nu Plasma HR' collector block configuration. In this case ^{238}U can be measured with L3 whereas its respective hydride is then measured with IC0 at $m/z=239$.

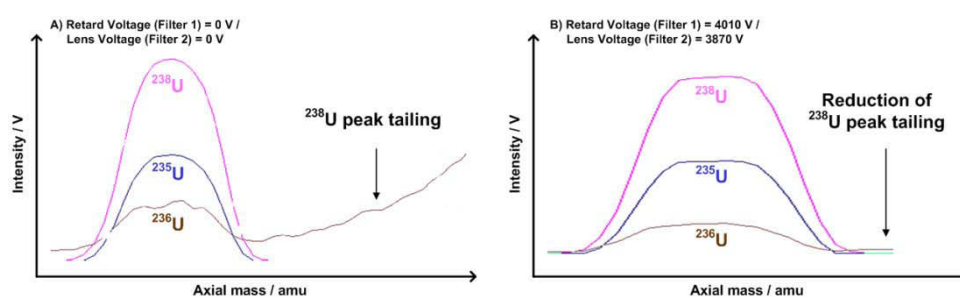


Fig. 1.5-11: Schematic description of the ^{238}U peak tailing effect. Mass scanning was performed using a 'Nu Plasma HR' MC-ICPMS (A) ^{238}U peak tailing when no deceleration filter (i.e. voltages = 0) is applied, (B) Reduction of ^{238}U peak tailing when applying a deceleration filter). Different peak shapes in A) and B) are resulting from different x-y-scalings.

Modified collector block configuration

Considering the analysis of Pu, Faraday cups are mostly not sensitive enough for the detection of Pu isotopes. Pu isotopes are present in very low concentrations, especially in environmental samples such as soil or sediment (e.g. 10^{-12} to 10^{-11} g g⁻¹ (Boulyga et al., 2004)). Regarding the 'Nu Plasma HR' standard collector block configuration in Fig. 1.5-10, it can be seen that only ²⁴⁰Pu and ²⁴²Pu can be simultaneously detected by means of SEMs as the ²³⁹Pu beam is directed into the L4 Faraday cup. In order to enable the simultaneous measurement of ²³⁹Pu, ²⁴⁰Pu and ²⁴²Pu by means of SEMs, a so called 'dog leg' deflector was inserted at the L4 Faraday cup position, thus guiding the ion beam of ²³⁹Pu from the L4 position into IC2. A schematic diagram of the modified collector block configuration is shown in Fig. 1.5-12. In addition, the modified collector block enables the simultaneous determination of ²³⁵U, ²³⁶U and ²³⁸U with SEMs. Thus, it is feasible to sequentially analyze U and Pu in the same sample as was performed with respect to the analysis of micro-samples originating from the vicinity of the Chernobyl NPP (see 2.3).

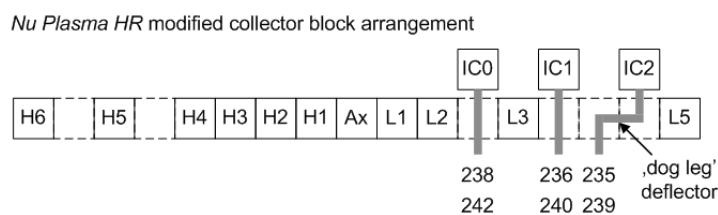


Fig. 1.5-12: 'Nu Plasma HR' (Nu Instruments Ltd.) modified collector block configuration. (H...Faraday cup high mass side, Ax...Faraday cup axial mass, L...Faraday cup low mass side, IC...ion counting multiplier (i.e. secondary electron multiplier))

'Neptune Plus' collector block configuration

The 'Neptune Plus' MC-ICPMS L5 ion counter package collector block arrangement that is shown in Fig. 1.5-13 is a special Multi Ion Counting (MIC) setup for U and Pu isotope ratio analyses. The collector block shown in Fig. 1.5-13 consists of nine Faraday cups, three SEMs (i.e. SEM 1-3) and two CDDs (i.e. CDD 4 and CDD 5). Older instrument were equipped with nine Faraday cups and eight miniaturized channeltron type (see also 1.5.2.3) detectors (Wieser and Schwieters, 2005).

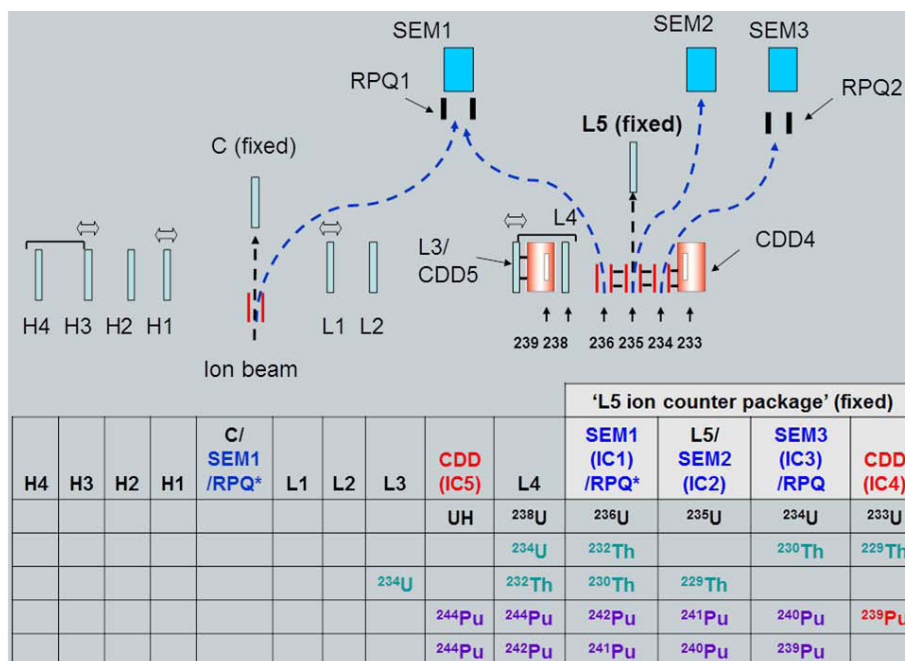


Fig. 1.5-13: 'Neptune Plus' (Thermo Fisher Scientific Inc.) L5 ion counter package collector block configuration for U and Pu analysis.

The SEM and the CDD detectors are both referred to as ion counter detectors. As can be seen in Fig. 1.5-13 the configuration consists of moveable and switchable IC/Faraday cup detectors. Peak alignment is achieved by mechanically moving the detectors. This is, as aforementioned, contrary to the 'Nu Plasma HR' collector array, in which the detectors are at fixed positions and where peak alignment is performed by means of a zoom lens system. In the 'Neptune Plus' the L5 detector is, for example, fixed, whereas the L4 detector is moveable. It can be driven by the L3 detector via a clip. The CDD 5 detector is attached to L3, thus, it is also moved by L3. Both L4 and CDD5 can be moved towards the 'L5 ion counter package' platform, which allows recording $m/z=237$ with L4 and ^{238}U with CDD5. In this case a mass dispersion of one mass unit is applied with respect to all detectors. However, a mass dispersion of one mass unit is not feasible for the L3 and the CDD5 detector as they are installed in a fixed way.

The 'L5 ion counter package collector block configuration is designed in a way so that ^{238}U , ^{236}U , ^{235}U , ^{234}U , ^{233}U can be simultaneously detected together with the $^{238}\text{U}^1\text{H}$. While the major U isotopes ^{235}U and ^{238}U are detected with Faraday cups (i.e. L5 and L4, respectively), ^{234}U and ^{236}U are measured with SEM 3 and SEM 1, respectively. As both SEM 1 and SEM3 are equipped with a RPQ Filter, $^{236}\text{U}/^{238}\text{U}$ and $^{234}\text{U}/^{235}\text{U}$ abundance sensitivities can be improved as a result of decreased ^{238}U and ^{235}U peak tailing.

1.5.3 Application of LA-ICPMS for the analysis of single particles – literature review

LA-ICPMS shows great potential for the analysis of particles with respect to both isotopic and elemental signatures, mostly in environmental and nuclear forensics (see 1.5.3.4) as well as for the characterization of crime scene evidence. As this thesis aimed at the evaluation of the capability of LA-(MC)-ICPMS for single particle analysis a comprehensive literature review dealing with this topic is given in the following.

1.5.3.1 Analysis of airborne particulate matter and fly ash

The first approaches of using LA-ICPMS for single particle analysis were applied to the characterization of airborne particulates. Tanaka et al. (Tanaka et al., 1998) used LA-ICP-QMS for the determination of Al, Ti, V, Cr, Mn, Fe, Co, Ni, Cu, Zn, As, Se, Cd, Sb and Pb in airborne particulate matter collected in Tokyo, Japan from January 1996 to May 1996. Calibration was accomplished by means of four cellulose nitrate membrane filters, which had been prepared by dropping different aliquots of standard solutions onto it. The same filters were applied for collecting the particulate matter. Standard solutions were prepared from multi-element standard solutions, whereupon two different concentration ranges were chosen for the elements of interest (i.e. major and minor elements). The elemental concentrations (i.e. Al (110-510 ng m⁻³), Ti (14-50 ng m⁻³), V (3-4.5 ng m⁻³), Cr (2.6-7.3 ng m⁻³), Mn (13-32 ng m⁻³), Fe (470-1000 ng m⁻³), Co (0.24-0.34 ng m⁻³), Ni (2.4-3.9 ng m⁻³), Cu (26-47 ng m⁻³), Zn (110-310 ng m⁻³), As (1.6-3.4 ng m⁻³), Se (0.9-1.7 ng m⁻³), Cd (1.1-2.2 ng m⁻³), Sb (5.7-16 ng m⁻³) and Pb (53-120 ng m⁻³)) determined by analyzing filter samples by LA-ICPMS were in good agreement with results determined by means of instrumental neutron activation analysis (INAA) and x-ray fluorescence spectrometry (XRF) (Tanaka et al., 1998).

Another procedure for preparing calibration standards using standard reference materials (i.e. NIST SRM 1648 and BCR 176) for the elemental analysis of airborne particulate matter by LA-ICP-QMS was proposed by Wang et al. (Wang et al., 1998). Standard filters were generated by means of a specially designed sample preparation chamber described in (Wang et al., 1998). Calibration curves were derived by analyzing different standard filters with varying amounts of loaded SRM particulates. The study showed that the PTFE-membrane filter's loading capacity should be limited to about 2 mg/filter in order to get a linear calibration curve (Wang et al., 1998). In subsequent studies Cr (Wang et al., 1999a) and Si (Wang et al., 1999b) were determined by LA-ICP-QMS in airborne particulate matter collected from monitoring stations in

Taiwan, using the procedure proposed above for preparing filter calibration standards. NIST SRM 1648 was applied as certified standard reference material (Wang et al., 1999a; Wang et al., 1999b).

Okuda et al. (Okuda et al., 2004) used LA-ICP-QMS for the determination of trace metal concentrations (i.e. Al, Ti, V, Cr, Mn, Fe, Co, Ni, Cu, Zn, As, Se, Cd, Sb and Pb) in aerosol particles collected on cellulose nitrate filters in Beijing, China from March 2001 to August 2003. A comparison of daily average metal concentrations of about 700 samples of total suspended particulate matter (TSP) collected in Beijing with average metal concentrations of TSP originating from the center of Tokyo showed 1.7 – 21.8 times higher concentrations for Beijing (Okuda et al., 2004). In another study Okuda et al. (Okuda et al., 2006) monitored concentrations of the same trace metals as in a previous study (Okuda et al., 2004) in TSP samples collected at Rishiri Island, Hokkaido, Japan from May 2001 to October 2003. Typically, lower concentration levels were observed compared to Beijing, China and Tokyo, Japan. However, elevated trace metal concentrations were determined several times per year, most likely resulting from long-range emission transports. The use of sector analysis in which the area surrounding Rishiri Island was classified into four air mass inflow sectors (i.e. marine, Japan, China and Siberia) together with the knowledge of the trace metal concentrations allowed drawing conclusions about the emission source. Especially Pb/Zn, As/V and Pb/V ratios were useful indices for deriving emission sources (Okuda et al., 2006).

Recently, Hsieh et al. (Hsieh et al., 2011) developed a strategy for the determination of absolute elemental contents (i.e. Na, Mg, Al, Si, K, Ca, Ti, V, Cr, Mn, Fe, Ni, Cu, Zn, As, Sr, Cd, Ba and Pb) in nanometer- and sub-micrometer-sized airborne particulate matter, which were collected on polytetrafluoroethylene (PTFE) membrane filters by means of an electrical low-pressure impactor (ELPI). The use of an ELPI enabled to collect particles segregated into different particle sizes (i.e. 0.030 – 0.108 μm , 0.108 – 1.000 μm and 1.000 – 9.970 μm). Calibration was accomplished by analyzing PTFE membranes, on which defined amounts of standard solutions had been dropped. Grid patterns (grid spacing: 300 μm , spot size: 110 μm) were applied for the ablation of individual impaction spots. Moreover, a standard addition method was applied for validation of the proposed method (Hsieh et al., 2011).

Gligorovski et al. (Gligorovski et al., 2008) applied LA-ICP-QMS in combination with an image analysis software for multi-elemental mapping of size-segregated aerosol particles. Both industrial-influenced and urban aerosols were collected using cascade impactors with different collection stages to collect different size ranges (i.e. industrial-influenced aerosol: 0.17 – 10 μm ; urban aerosol: 0.038 – 16 μm). An air particulate standard reference material (NIST 2783; PM_{2.5}) certified for V, Fe, Zn, As, Sb, Ba and Pb concentrations (ng cm^{-2}) was used for calibration

purposes. Elemental maps were generated by rastering the laser beam over whole aerosol impaction spots on the cascade impactor foils, whereas the use of an image analysis software allowed to study the elemental distributions in the analyzed spots. E.g. high Zn and low Pb concentrations were determined for the largest particles of industrial-influenced aerosol (Gligorovski et al., 2008). Moreover, LA-ICP-QMS was also applied for the qualitative analysis of Pb, As, Cr, Sb, Sn, Zn, Si, Al, Mn, Cu, Fe, Ca, Mg, Sr in aerosol particles deposited on tree barks in order to assess the presence of particle deposits (Suzuki, 2006).

Spears (Spears, 2004) applied LA-ICP-QMS for the analysis of fly ash. The analysis of individual particles was not feasible, mainly due to identification problems and lack of sensitivity for minor elements by applying a laser spot size of 10 μm . Therefore transects were analyzed by scanning the laser beam (spot size: $\sim 30 \mu\text{m}$) over a layer of particles resulting from scattering the particles onto a resin-coated microscope slide. Two different scans were performed in order to cover the analysis of both the minor (Al, S, K, V, Cr, Fe, Cd, As and Hg) and the major (K, Cu, Zn, Ga, Ge, Se, Mo, Tl, Pb and U) elements. Interpretation of the data was accomplished by correlation matrices. E.g. it was determined that As, U, Pb, Tl, Mo, Se and Ge and Ga to a lesser extent, are mainly present on the surfaces of the fly ash particles (Spears, 2004).

1.5.3.2 Analysis of particles containing platinum group elements

Rauch et al. (Rauch et al., 2002) applied LA-ICP-quadrupole (Q)MS for the analysis of particles containing platinum group elements (PGE) (i.e. platinum (Pt), palladium (Pd) and rhodium (Rh)). The particulate samples were distributed onto a sticky tape, which was ablated by applying line scans. The analysis of PGE in automobile emission particles and particles in road and river sediments was of special interest as PGE emitted into the environment from automobile catalysts pose risks for both humans and the environment. In all analyzed samples, PGE were associated with cerium (Ce), a major catalyst component (i.e. wash-coat). The co-existence of both Ce and PGE in particles was determined to be a useful fingerprint for tracing particles containing PGE back to automobile catalysts and to determine environmental transport mechanisms. In addition it was concluded that relative Pt/Pd/Rh signal intensities might give an indication about specific automobile catalysts (Rauch et al., 2002). Moreover, LA-ICP-QMS was applied for analyzing road sediment samples (particles $< 63 \mu\text{m}$) for identifying Pb and PGE associations to geochemical fractions (i.e. carbonates, hydrous Fe, Mn oxides and silicate phases) in such samples. Pb showed a high degree of association to Ca/Mg/Sr and Fe/Mn phases but a lesser degree to the Si/Al/K phase. However, no associations were identified for Pt, which was studied as a representative for PGE, to the studied geochemical

fractions. Laser ablation was again accomplished by applying line scans on the road sediments fixed on a tape (Rauch et al., 2000a). Rauch et al. (Rauch et al., 2000b) further applied LA-ICP-QMS for the assessment of PGE distributions in airborne particulate matter sampled by means of a filter, and for the identification of individual airborne particles having high PGE concentrations.

1.5.3.3 Analysis of crime scene evidence

Scadding et al. (Scadding et al., 2005) studied the application of LA-ICP-time of flight (TOF)-MS for the forensic analysis of micro debris (i.e. spherules left behind after cutting open a steel safe door with an oxy-acetylene gas cutter). Two different measurement approaches were successfully applied: 1) analysis of an entity of debris consisting of 10 spherules and 2) analysis of single spherules. In both cases three different steel safe doors were distinguishable with respect to their elemental distribution patterns. In addition, the analysis of three different spherule fractions ($> 63 \mu\text{m} < 150 \mu\text{m}$; $> 150 \mu\text{m} < 250 \mu\text{m}$ and $> 250 \mu\text{m} < 500 \mu\text{m}$) did not yield a significant difference in the determined patterns. Spherules collected from the clothing of the person who cut the safe doors, showed the same elemental distribution patterns as the respective doors. Thus, it was demonstrated that elemental distribution patterns allow linking a person of interest (POI) to a crime scene (Scadding et al., 2005). LA-ICP-QMS was further applied for the qualitative characterization of gunshot residue (GSR) particles, typically revealing sizes between $0.5 \mu\text{m}$ and $5 \mu\text{m}$, from firearm discharges. The qualitative characterization included the analysis of elements that are considered to be present in GRS (i.e. Al, Si, P, S, Cl, K, Ca, Fe, Ni, Cu, Zn, Sn, Sb, Ba, Pb), whereupon Pb, Sb and Ba are considered as the key elements. GSR particles collected by means of tape lifts from skin surfaces could be directly analyzed by applying a raster scanning ablation pattern (spot size: $160 \mu\text{m}$). Moreover, it could be demonstrated that skin cells covering the GSR particles do not have an impact on the analysis as is the case with respect to SEM-EDX, which is commonly applied for the characterization of GSR and in which particles covered by skin cells cannot be detected (Abrego et al., 2012).

1.5.3.4 Application of LA-ICPMS for single particle analysis in nuclear forensics

In a study conducted by Choi et al. (Choi et al., 2010) a variety of microparticles was analyzed with respect to their gadolinium (Gd) isotopic compositions by means of LA-ICP-TOF-MS. The authors analyzed the Gd isotopic composition in two single Gd_2O_3 particles ($\sim 10 \mu\text{m}$) using a slightly defocused laser beam ($\sim 2\text{mm}^2$) for a low sample consumption rate and stable ion

signals. The Gd_2O_3 particles were mixed with deionized water for dispersing them onto a tantalum (Ta) plate for analysis. A collodion solution was used for fixing the particles on the substrate. Matrix effects of used metal plates were additionally investigated by analyzing single Gd coated silica particles ($\sim 60 \mu m$; 50 ng Gd/particle) loaded onto a Cu, Zn and Ta, respectively, plate. Cu and Ta showed better S/N ratios than Zn. In addition, a swiped-mixed particle sample consisting of Gd_2O_3 ($\sim 10 \mu m$), Ni ($\sim 3 \mu m$) and Pd ($\sim 1 \mu m$) metal particles was analyzed, which demonstrated the applicability of LA-ICP-TOF-MS for the analysis of particle samples collected by means of swipes in international safeguards. All determined Gd isotopic compositions were in good agreement with the natural isotopic composition (Choi et al., 2010).

LA-MC-ICPMS equipped with three discrete-dynode secondary electron multipliers was used for the determination of $^{235}U/^{238}U$, $^{236}U/^{238}U$, $^{145}Nd/^{143}Nd$, $^{146}Nd/^{143}Nd$, $^{101}Ru/(^{99}Ru+^{99}Tc)$ and $^{102}Ru/(^{99}Ru+^{99}Tc)$ isotope ratios in micro-samples originating from the Chernobyl fallout (Boulyga and Prohaska, 2008). Pre-identification of the micro-samples, with sizes ranging from about 100 μm to 1 mm and surface alpha activities of 3-38 mBq, in the collected soil samples was accomplished by means of nuclear track radiography. Switching between the isotopic systems allowed the sequential measurement of all isotopes with SEMs. If the particles were large enough (i.e. $> 200 \mu m$) all isotopic systems could be sequentially analyzed. Smaller particles were only analyzed with respect to their U isotopic composition. However, the complete analysis of one micro-sample could be accomplished in 15-20 min, excluding the time needed for optimization and calibration. The latter was performed by liquid standards that were introduced by a membrane desolvator system additionally coupled to the LA-MC-ICPMS set-up. In general the usefulness of LA-ICPMS for obtaining spatially resolved isotopic information on the microscopic level, which is of particular use for the assessment of environmental contaminations with nuclear waste was demonstrated. E.g. heterogeneities in the U isotopic composition within one micro-sample (consisting of five subsamples) as well as isotopic variations between individual micro-samples ($n=10$) could be identified (Boulyga and Prohaska, 2008).

MC-ICPMS coupled to a laser ablation system was further employed by Lloyd et al. (Lloyd et al., 2009) for the analysis of single DU uranium-oxide grains ($n=115$) retrieved from contaminated soil and dust samples. Prior to the LA-MC-ICPMS analysis the uranium-oxide particles were 1) concentrated from the bulk samples by inter alia using dense-liquid for the separation of low-density silicates and uranium-oxide grains larger than 20 μm and 2) embedded in epoxy resin. Natural uraninite grains were analyzed for quality control purposes. The analysis time for one uranium-oxide grain was about 2 minutes, whereas a complete analysis including particle location and the measurement of reference materials could be accomplished in 16 minutes.

Relative expanded uncertainties (2σ) of 0.2-1.8 % and 2.3-4.0 % were reported for $^{235}\text{U}/^{238}\text{U}$ and $^{236}\text{U}/^{238}\text{U}$, respectively, isotope ratios. Using LA-MC-ICPMS for the analysis of single uranium-oxide grain samples, the variability of the isotopic compositions of DU could be studied (Lloyd et al., 2009).

Varga (Varga, 2008) applied LA-ICP-(sector field)SF-MS for the determination of the U isotopic composition of uranium oxide powder samples having depleted, natural and low enriched U isotopic compositions. A highly enriched uranium-oxide powder stemming from a Round robin exercise was additionally analyzed for validation purposes. The uranium oxide powder samples, with sizes ranging from 10 μm to 30 μm , were distributed on a double-sided tape and covered by another tape to circumvent dislocation of particles during laser ablation. Single particle analysis was accomplished by partially ablating an individual particle and calculating the average composition from three to five parallel measurements. This multiple-spot approach enabled improving the precision of a particle measurement and was useful for the estimation of the uncertainty. In addition, soft ablation using low laser energy yielded more data points per transient signal which also resulted in an improvement of precision. Medium mass resolution ($R=4000$) was applied in order to eliminate molecular interferences, which were contributing especially to the signal intensities of the minor isotopes (i.e. ^{234}U and ^{236}U) in low mass resolution. Applying medium resolution, the determined $^{234}\text{U}/^{238}\text{U}$, $^{235}\text{U}/^{238}\text{U}$ and $^{236}\text{U}/^{238}\text{U}$ isotope ratios of the particles were in good agreement with solution nebulization based data. The major isotope ratio $^{235}\text{U}/^{238}\text{U}$ of single particles having dimensions of about 19 μm x 25 μm could be determined with precisions ranging from 0.9-5.1 % relative standard deviations (Varga, 2008).

Sub-micrometer sized particles containing U were analyzed by Pointurier et al. (Pointurier et al., 2011) applying LA-ICP-QMS. $^{235}\text{U}/^{238}\text{U}$ isotope ratios of individual particles of two different samples (i.e. NUSIMEP-6 interlaboratory comparison sample and IAEA swipe-field sample) were analyzed after pre-selection by means of fission track. The minor isotope ratio $^{234}\text{U}/^{238}\text{U}$ could be determined for one particle, which showed the highest number of fission tracks. In case of all other particles the count rates for the minor isotopes ^{234}U and ^{236}U were too low for detection. The determined isotope ratios of the NUSIMEP-6 particles ($n=19$) were in good agreement with the certified value. Relative uncertainties (coverage factor =1) ranged from 2.0 % to 37 %. However, in comparison to TIMS and SIMS measurements of the NUSIMEP-6 samples LA-ICPMS measurements were less precise (i.e. LA-ICPMS: 24.2 % RSD ($n=19$), FT-TIMS: 4.8 % RSD ($n=18$), SIMS: 0.7 % RSD ($n=30$)). In addition, the average $^{235}\text{U}/^{238}\text{U}$ isotope ratio also showed a larger deviation from the certified value (i.e. LA-ICPMS: 11.5 % ($n=19$), FT-TIMS: 2.7 % ($n=18$), SIMS: 0.5 % ($n=30$)). Single particle analyses of the IAEA swipe-field sample yielded a relative

standard deviation of 22.9 % (n=24). TIMS measurements were again more precise with a relative standard deviation of 5.3 % (n=19). Particles having natural and low enriched U isotopic compositions could be identified in the swipe samples. The authors assumed that the larger dispersion of the isotope ratios determined by LA-ICP-QMS resulted from a 'mixing effect' as a consequence of the simultaneous analysis of several particles present on the substrate. Moreover, an overall ionization efficiency (i.e. ratio of the number of detected U ions to the number of U atoms in a particle) ranging from 1.2×10^{-4} to 3.9×10^{-4} was determined for LA-ICP-QMS (Pointurier et al., 2011).

Recently Pointurier et al. (Pointurier et al., 2012) used LA-ICP-QMS for the determination of $^{235}\text{U}/^{238}\text{U}$ isotope ratios of single particles deposited on the NUSIMEP-7 single deposition test sample. This test sample was distributed by the Institute for Reference Materials and Measurements (IRMM) in the course of an interlaboratory comparison. Pre-selection of particles was also accomplished by fission track. The isotope ratios of seven particles were in good agreement with the certified value provided by the IRMM and with the isotope ratios determined by means of FT-TIMS and SIMS. However, the average $^{235}\text{U}/^{238}\text{U}$ isotope ratio determined by LA-ICP-QMS showed a bias of 3 % from the certified value, whereas FT-TIMS and SIMS measurements yielded average isotope ratios with biases of -2.7 % and -2.6 %, respectively. In comparison to SIMS and FT-TIMS larger relative standard uncertainties as well less precise isotope ratios were determined by LA-ICP-QMS. Standard uncertainties (k=1) of 7.1 %, 4.5 % and 3.0 % were determined for LA-ICP-QMS, FT-TIMS and SIMS, respectively. Considering the precision, both SIMS and FT-TIMS yielded relative standard deviations of 3.0 %, whereas LA-ICP-QMS yielded 9.6 %. The estimated detection capability of LA-ICP-QMS was equivalent to TIMS but below (i.e. by a factor of 15) that of SIMS. However, the authors assumed that the use of a double-focusing ICPMS having higher sensitivity would yield a detection capability comparable to SIMS. In addition, the use of an ICPMS equipped with a multi-collector would reduce the measurement uncertainty and facilitate the determination of the minor isotopes. The measurement yield of LA-ICP-QMS was comparable to that obtained by conventional solution nebulization ICP-QMS (i.e. $\sim 10^{-4}$). Nonetheless, it was smaller than that of FT-TIMS and SIMS (i.e. by a factor of 10 and 20, respectively) (Pointurier et al., 2012).

Becker et al. (Becker et al., 2008) applied LA-ICP-sector field (SF)-MS for the determination of the average $^{235}\text{U}/^{238}\text{U}$ isotopic composition (i.e. 0.032 ± 0.004 ; n=10) of single UO_2 particles ($\leq 1 \mu\text{m}$).

Please note that three other studies (i.e. outcome of this thesis) dealing with single particle analysis by LA-MC-ICPMS are given in chapter 2.

2 Applications

The aim of this thesis was to study the performance and applicability of LA-MC-ICPMS for the determination of U and Pu isotopic signatures of single particles.

Even though most reliable and state-of-the-art techniques are applied for particle analysis within international safeguards, it is important to look into complementary analytical techniques as well. The objective is to provide reference values as well as to promote improvements in analysis and to extend the amount of safeguards-relevant information that can be gained from the analysis of swipe and/or environmental samples. The applicability of LA-MC-ICPMS for particle analysis was evaluated as this technique offers some advantages over well, in international safeguards, implemented mass spectrometric techniques. SIMS reveals limitations with respect to the analysis of samples having complex matrices (i.e. environmental matrices containing organic compounds, heavy elements, etc.), whereas the analysis of particles with U amounts in the low pg range poses a challenge for TIMS due to its lower sensitivity compared to LA-MC-ICPMS. In comparison to SIMS, LA-MC-ICPMS is less prone to molecular interferences, which is advantageous for the analysis of particles embedded in environmental matrices. In addition, there is no need of a conducting substrate. Thus, environmental samples can be readily analyzed.

The scientific work required for fulfilling the aim of this thesis can be divided into three categories:

- I) “Method development and validation, including full total combined uncertainty computations, and demonstration of the capabilities of LA-MC-ICPMS for the direct determination of the U isotopic signature in distinct single, μm -sized particles.”

The outcome of this work (see 2.1) is presented in form of a publication (Kappel et al., 2012) that was published in the Journal of Environmental Radioactivity. The layout of this paper was adapted for the sake of layout conformity within this thesis. The presented text, figures and tables correspond to the printed version.

- II) “Assessment of the applicability of different data treatment strategies for the computation of U isotope ratios from transient signals in order to determine accurate and precise isotope ratios of single particles having different isotopic compositions” (see 2.2).

The outcome of this work, which is provisionally accepted with major revisions in Analytical and Bioanalytical Chemistry, is presented in 2.2. Recommended revisions have been considered in the manuscript presented in this thesis. However, the final published version might slightly divert from the presented text.

- III) “Investigation of the applicability of LA-MC-ICPMS for 1) analyzing Pu isotope ratios in particles embedded in environmental matrices and 2) the identification of nuclear contamination sources” (see 2.3). The results of this study are presented in form of a paper prepared for submission.

All references are integrated in chapter 4.

2.1 Application I

Direct Uranium Isotope Ratio Analysis of Single Micrometer-Sized Glass Particles¹

Stefanie Kappel^a, Sergei F. Boulyga^b, and Thomas Prohaska^{a,*}

^aUniversity of Natural Resources and Life Sciences, Vienna, Department of Chemistry, Division of Analytical Chemistry–VIRIS-Laboratory, Konrad Lorenzstrasse 24, 3430 Tulln, Austria

^b Safeguards Analytical Services, Department of Safeguards, International Atomic Energy Agency, Wagramer Strasse 5, 1400 Vienna, Austria

* Corresponding author: Thomas Prohaska, University of Natural Resources and Life Sciences, Vienna, Department of Chemistry, Division of Analytical Chemistry–VIRIS-Laboratory (UFT Campus Tulln), Konrad Lorenzstrasse 24, 3430 Tulln, Austria, E-mail: thomas.prohaska@boku.ac.at. Phone: (+43 1) 47654-6092. Fax: (+43 1) 47654-6059.

¹ Published in Journal of Environmental Radioactivity 113 (2012) 8-15

ABSTRACT

We present the application of nanosecond laser ablation (LA) coupled to a 'Nu Plasma HR' multi collector inductively coupled plasma mass spectrometer (MC-ICP-MS) for the direct analysis of U isotope ratios in single, 10–20 micrometer-sized, U-doped glass particles. Method development included studies with respect to (1) external correction of the measured U isotope ratios in glass particles, (2) the applied laser ablation carrier gas (i.e. Ar versus He) and (3) the accurate determination of lower abundant $^{236}\text{U}/^{238}\text{U}$ isotope ratios (i.e. 10^{-5}). In addition, a data processing procedure was developed for evaluation of transient signals, which is of potential use for routine application of the developed method. We demonstrate that the developed method is reliable and well suited for determining U isotope ratios of individual particles. Analyses of twenty-eight S1 glass particles, measured under optimized conditions, yielded average biases of less than 0.6 % from the certified values for $^{234}\text{U}/^{238}\text{U}$ and $^{235}\text{U}/^{238}\text{U}$ ratios. Experimental results obtained for $^{236}\text{U}/^{238}\text{U}$ isotope ratios deviated by less than –2.5 % from the certified values. Expanded relative total combined standard uncertainties U_c ($k=2$) of 2.6 %, 1.4 % and 5.8 % were calculated for $^{234}\text{U}/^{238}\text{U}$, $^{235}\text{U}/^{238}\text{U}$ and $^{236}\text{U}/^{238}\text{U}$, respectively.

Keywords: Laser ablation; multi collector ICP-MS; uranium isotope ratio analysis; particle analysis; nuclear forensics; nuclear safeguards

1. Introduction

The isotopic fingerprints of uranium (U) and plutonium (Pu) are of particular interest for international safeguards (Axelsson et al., 2009) and nuclear forensics (Mayer et al., 2007) as the knowledge of these signatures enables to link nuclear material to its respective nuclear processes and activities (Donohue, 2002). U and/or Pu isotopic signatures are stored in micrometer-sized particles (Donohue, 1998) that can be emitted during nuclear processes. The absolute amount of nuclear material in such particles usually ranges from picograms to nanograms (Axelsson et al., 2009). Sampling of such material is performed in nuclear facilities (e.g. enrichment facilities, hot cells, etc.) and the nearby environment by means of swipes (Donohue, 1998; Donohue, 2002). Analyzing individual particles has the advantage that possible signatures of unknown isotopic compositions can be detected, even if they are masked by dust particles or other matrices that have declared or natural isotopic signatures. In comparison, bulk analysis, which comprises the analysis of the entire swipe, would only yield an average value of different isotopic signatures present on the swipe (Donohue, 1998).

Fission track-thermal ionization mass spectrometry (FT-TIMS) (Esaka et al., 2004; Lee et al., 2007a) and secondary ionization mass spectrometry (SIMS) (Betti et al., 1999; Ranebo et al., 2009; Tamborini, 2004) are usually applied for the isotopic characterization of single, micrometer-sized particles from safeguards samples (Donohue, 1998). The performance of TIMS in terms of accuracy and precision of isotope ratio measurements is unquestioned (Heumann et al., 1998); however, the need for a nuclear reactor for irradiation (Lee et al., 2007a) of the FT detector with thermal neutrons is the main drawback of FT-TIMS. SIMS offers the advantage of combining the localization of particles collected by means of swipes and the determination of the isotopic information in one instrument (Betti et al., 1999). Moreover, scanning electron microscopy combined with energy-dispersive X-ray spectrometry (SEM-EDX) is applied for the localization of particles and the determination of the elemental composition (Ciurapinski et al., 2002; Donohue et al., 2008), as well as morphological characterization of the particles (Kips et al., 2007; Ranebo et al., 2007).

Even though both TIMS and SIMS are state-of-the-art techniques, the International Atomic Energy Agency (IAEA) is pursuing improvements and new method developments in order to obtain a complete picture of a particle's history and to help verifying the absence of undeclared activities. Recently, laser ablation-inductively coupled plasma mass spectrometry (LA-ICP-MS) was applied for direct actinide isotope analysis of single particles (Boulyga and Prohaska, 2008; Lloyd et al., 2009; Varga, 2008). Varga analyzed U isotope ratios of U_3O_8 powder particles (i.e. depleted, natural, low enriched and high enriched U)—having lateral dimensions of 10–30 micrometer—by employing a high resolution double-focusing ICP sector-field mass spectrometer equipped with a single collector. The U amount in a 10 μm particle was estimated to approximately 0.46 ng, assuming a spherical particle (Varga, 2008). Depleted uranium oxide particles (i.e. larger than 20 μm), embedded in dust and surface soil, were directly analyzed by Lloyd et al. (Lloyd et al., 2009) by employing LA-multi collector (MC)-ICP-MS for the determination of $^{235}\text{U}/^{238}\text{U}$ and $^{236}\text{U}/^{238}\text{U}$. The sampling volume corresponded to approximately 4 ng U (Lloyd et al., 2009). The applicability of LA-MC-ICP-MS for isotope ratio analyses of U and fission products of micro-samples (i.e. dimensions ranging from 100 μm to 1 mm) collected in the vicinity of Chernobyl was demonstrated by Boulyga and Prohaska (Boulyga and Prohaska, 2008).

The present work describes the application of ns laser ablation coupled to MC-ICP-MS for the direct determination of $^{234}\text{U}/^{238}\text{U}$, $^{235}\text{U}/^{238}\text{U}$ and $^{236}\text{U}/^{238}\text{U}$ isotope ratios in single, U-doped, 10–20 micrometer-sized glass particle reference material (Raptis et al., 2002). The purpose of the glass particles applied in this study is the simulation of environmental samples (e.g. soil,

sediment or dust) that contain hot particles (Raptis et al., 2002), which is of interest considering a future application of the presented method for such samples. Hence, method development and the merits of this analytical technique are demonstrated by means of this reference material, in which absolute U amounts are in the picogram range. To the authors' knowledge it is the first time that certified reference material is used for the validation of LA-MC-ICP-MS for U isotope ratio analyses in single particles. The full evaluation and validation of the presented method is described. In addition, a novel approach for operator-independent data processing, including non-laborious external correction of the isotope ratios of interest is presented in this work.

2. Materials and Methods

2.1. Reagents, standards and certified reference materials

Analytical reagent grade nitric acid (65 % (m/m), Merck KGaA, Darmstadt, Germany) underwent double sub-boiling distillation (Milestone-MLS GmbH, Leutkirch, Germany) prior to use. 1% (m/m) HNO₃ was prepared by diluting purified 65 % (m/m) HNO₃ with reagent grade type I water (18.2 MΩ · cm at 25 °C, Ultra Clear Basic Reinstwassersystem, SG Wasseraufbereitung und Regenerierstation GmbH, Barsbüttel, Germany) that was also purified by sub-boiling distillation (Milestone-MLS GmbH, Leutkirch, Germany) prior to use. Certified isotope reference materials — CRM U500 (New Brunswick Laboratory, U.S. Department of Energy, Washington, DC, U.S.) and IRMM-187 (European Commission-JRC, Institute for Reference Materials and Measurements, Geel, Belgium) — were applied for external correction and the determination of the secondary electron multiplier yields. An in-house prepared mixture, having a ²³⁶U/²³⁸U isotope ratio of 8.96 x 10⁻⁷, of IRMM-184 (European Commission-JRC, Institute for Reference Materials and Measurements, Geel, Belgium) and U500, was used for optimizing the deceleration filter. This mixture was obtained by diluting and gravimetric mixing of both IRMM-184 and U500 in order to obtain a solution with a ²³⁶U/²³⁸U isotope ratio that is approximately twice as high as the ²³⁶U/²³⁸U abundance sensitivity that was determined without applying the deceleration filter. Determination of the abundance sensitivity for uranium isotopes at the mass m-2 u was employed with a ²³³U isotopic spike solution ((99.4911 atom percent of ²³³U; CRM 111-A (New Brunswick Laboratory, U.S. Department of Energy, Washington, DC, U.S.)). A natural U solution (IRMM-184) was used for the determination of the UH⁺/U⁺ hydride ratio when introducing liquid standards. Dilution of the standards was accomplished with 1 % (m/m) HNO₃ in order to get solutions exhibiting concentrations in the

low ng g⁻¹ range (i.e. smaller than 10 ng g⁻¹). The isotope amount ratios of the certified reference materials used in this study are given in Table 2.1-1.

Table 2.1-1: Isotope amount ratios of certified reference materials used in this study.

	²³⁴ U/ ²³⁸ U	²³⁵ U/ ²³⁸ U	²³⁶ U/ ²³⁸ U
S1 (U in glass)	0.000 055 7(11)	0.007 304 5(36)	0.000 010 08(11)
S3(U in glass)	0.000 279 6(17)	0.043 343(22)	0.000 424 8(10)
IRMM-184	0.000 053 138(32)	0.007 262 3(22)	0.000 000 124 46(17)
IRMM-187	0.000 387 00(16)	0.047 325(14)	0.000 071 965(39)
CRM U500 ^a	0.010 422(19)	0.999 6(14)	0.001 518 7(62)

^a the given isotope amount ratios and uncertainties (k=2) were calculated from the certified atom percents of ²³⁴U, ²³⁵U, ²³⁶U and ²³⁸U, and respective uncertainties stated in the certificate

S1 and S3 glass particles that are doped with U of certified isotopic composition (European Commission-JRC, Institute for Reference Materials and Measurements, Geel, Belgium) were used for method development, optimization, validation and proof of principle. The particles were produced by the IRMM for the IRMM support programme to the International Atomic Energy Agency (IAEA) and for the IRMM external NUSIMEP quality control programme (Nuclear Signatures Interlaboratory Measurement Evaluation Programme). Matrix glass, consisting of 70 % SiO₂, 15 % B₂O₃, 10 % Na₂O, 4 % CaO and 1 % Al₂O₃ (i.e. borosilicate glass), was mixed with U₃O₈, in order to produce U-containing glass particles. Afterwards the U doped glass was blended with matrix glass in order to simulate environmental samples (e.g. soil, sediment or dust) that contain hot particles. A detailed description of the preparation of the used glass particles is given in Raptis et al., 2002. The analysis of the matrix glass enabled to exclude interferences occurring from matrix elements (e.g. Al, Pb, Si, etc.). The size of the glass particles was between 10 and 20 µm (Raptis et al., 2002). Certified isotope amount ratios of the utilized particles are given in Table 2.1-1. The estimated U amount per 10 micrometer-sized glass particle was less than 100 pg when assuming (1) a spherical shape, (2) a borosilicate glass density of 2.5 g cm⁻³ and (3) an U₃O₈ amount of 5 % (m/m) (Raptis et al., 2002). About 1.1 mg of each glass particle standard were distributed on a cellulose acetate membrane filter (OE 67, Whatman GmbH, Dassel, Germany) and treated in a closed glass Petri dish with acetone vapor for about 30 minutes. The transparent membranes were then affixed, using customary glue, to a glass object plate. Both the membrane and the glass object plate were screened for their U blank.

2.2. Instrumentation

All isotope ratio measurements were accomplished with a double-focusing high resolution sector field MC-ICP-MS (Nu Plasma HR, Nu Instruments Limited, Wrexham, U.K.) A solid state nanosecond laser ablation system (UP 193, ESI-NWR Division, Electro Scientific Industries, Inc., Portland, CA, U.S.) was coupled to the MC-ICP-MS in order to perform direct analyses of the glass particles of interest. Both Ar and He were employed as carrier gas. A membrane desolvation system (DSN-100, Nu Instruments Limited, Wrexham, U.K.) was connected in parallel to the LA-MC-ICP-MS setup. This setup enables liquid sample introduction without the necessity of decoupling the laser system for the measurement of the liquid U reference material. No liquid solution was aspirated during laser ablation of the glass particles. A schematic diagram of this setup is given elsewhere (Boulyga and Prohaska, 2008). The desolvation of the liquid samples by means of the membrane system allows introducing a dry aerosol into the ICP. Hence hydride generation is reduced compared to the introduction of a wet aerosol. Instrumental parameters are summarized in Table 2.1-2.

2.2.1. Collector block configuration

The 'Nu Plasma HR' MC-ICP-MS is equipped with twelve Faraday cups and three discrete-dynode secondary electron multipliers. This configuration enables the simultaneous determination of the isotopes of interest. The major U isotopes, ^{235}U and ^{238}U , were measured with Faraday cups (i.e. L1 and L3), whereas the minor isotopes, ^{234}U and ^{236}U , were analyzed with secondary electron multipliers (i.e. IC0 and IC1). IC0, the secondary electron multiplier with which ^{236}U was measured, has a deceleration filter installed to eliminate ions with low kinetic energies in order to improve abundance sensitivity. Yield variations of the secondary electron multipliers (i.e. IC0 and IC1) were determined by means of U500 according to standard-sample bracketing before and after the analyses of the glass particles. The UH^+/U^+ hydride ratio for both liquid measurements and laser ablation was assessed by analyzing ^{238}U with L3 whereas its respective hydride was measured with IC0 at $m/z=239$. The determination of the $^{236}\text{U}/^{238}\text{U}$ abundance sensitivity was accomplished with a ^{233}U isotopic spike solution. Ion currents of ions having a mass-to-charge ratio of 231 and 233, respectively, were measured with the same secondary electron multiplier (i.e. IC0) and Faraday cup (i.e. L1), respectively, that were employed for the determination of ^{236}U and ^{238}U .

Table 2.1-2: Instrumental parameters.

Laser (New Wave 'UP 193')	
Ablation mode	Static point ablation
Wavelength / nm	193
Pulse length / ns	3
Energy density / J cm ⁻²	0.78–8.75
Power density / GW cm ⁻²	0.28–3.16
Repetition rate / Hz	10
Spot size / μm	10–15
Ar mix gas / L min ⁻¹	0.9
He mix gas / L min ⁻¹	0.9
Liquid sample introduction system (DSN-100)	
Nebulizer	PFA 100
Sample uptake rate / μL min ⁻¹	130
Nebulizer gas pressure / Pa	1.4 x 10 ⁵ –1.7 x 10 ⁵
Hot gas / L min ⁻¹	0.07–0.35
Membrane gas / L min ⁻¹	1.65–3.09
Spraychamber temperature / °C	112–117
Membrane temperature / °C	119–123
MC-ICP-MS (Nu Plasma HR)	
RF power / W	1300
Auxiliary gas / L min ⁻¹	1.2
Cool gas / L min ⁻¹	13
Cones	Ni
Isotopes monitored with Faraday cup at axial mass position	234, 239, 242
Mass separation	1
Acceleration voltage / V	4000
Resolution m/Δm	300 (low resolution)
Detection system	Faraday cups IC0 ^a , IC1 ^a
Voltages applied to deceleration filter	
Retard (Filter 1) / V	4010
Lens (Filter 2) / V	3870
Data acquisition mode	TRA ^b (acquisition time per data point: 1 s)

^aSecondary electron multiplier^bTime resolved analysis

2.3. Data Processing

Ar or He was measured as blank for about ten minutes prior to the analyses of the S1 and S3 glass particles. Blank determination for the liquid certified reference materials (i.e. U500 and IRMM-187) was performed by measuring 1 % (m/m) HNO₃ for ten minutes. The blank signal of each isotope of interest was calculated as an average of six blocks. Prior to this each block had been assessed as an average of 100 single data points. The blanks of the isotopes of interest were then subtracted from the single recorded signal intensities of the glass particles and the liquid certified reference materials, respectively.

Afterwards, the signal intensities, recorded in V, were converted into counts per second (cps) by using a factor of 6.24150965×10^7 . Since ²³⁴U and ²³⁶U were measured with discrete-dynode secondary electron multipliers, dead time correction of these intensities was performed according to eq (2.1-1) (Nelms et al., 2001)

$$I_t = \frac{I_0}{(1 - I_0 \tau)} \quad (2.1-1)$$

where I_t is the intensity (in cps) corrected for the dead time, I_0 is the raw intensity and τ is the dead time of the secondary electron multiplier. Dead times of 34 ns ($U_c = 9$ ns) and 4 ns ($U_c = 1.5$ ns) were applied for IC0 and IC1, respectively. The dead time and the linearity of the secondary electron multipliers were determined according to the dynamic procedure published by Richter et al. (Richter et al., 2009). Different concentrations of IRMM-073/7 (European Commission-JRC, Institute for Reference Materials and Measurements, Geel, Belgium) were used for determining the deviation of ²³³U/²³⁵U isotope ratios from the certified ratio at increasing ²³⁵U count rates. Mass bias correction was performed by measuring ²³⁵U/²³⁸U in these solutions.

The ²³⁴U/²³⁸U, ²³⁵U/²³⁸U and ²³⁶U/²³⁸U isotope ratios of the liquid certified reference materials were calculated by dividing the average signal intensities, which were obtained with respect to the procedure already described for assessing the average blank signals, of the isotopes of interest. The calculation of the external correction factors is given in eq (2.1-2)

$$CF_{xU/^{238}U} = \frac{(^{xU/^{238}U})_{\text{certified}}}{(^{xU/^{238}U})_{\text{Bl and } \tau \text{ corrected, lq}}} \quad x = 234, 235 \text{ or } 236 \quad (2.1-2)$$

where $CF_{xU/^{238}U}$ is the external correction factor, $(^{xU/^{238}U})_{\text{certified}}$ is the isotope ratio of the certified reference material and $(^{xU/^{238}U})_{\text{Bl and } \tau \text{ corrected, lq}}$ is the blank and dead time

corrected isotope ratio of interest of the liquid (lq) sample. The external correction factor was determined twice a day according to standard-sample bracketing. The average of the daily determined external correction factors was applied for the correction of the glass particle isotope ratios. Signal intensities of the time resolved ablation profiles were corrected for blank and dead time. An ablated single particle and a typical ablation profile are given in Fig. 2.1-1.

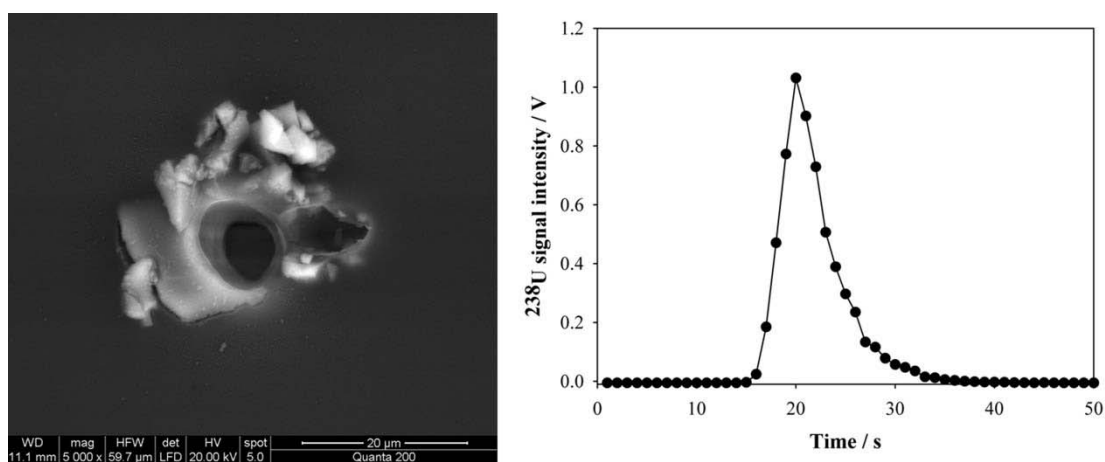


Fig. 2.1-1: Scanning electron micrograph of an ablated S1 glass particle (left) and typical time resolved ablation profile (right). The ablation profile is shown by means of the ^{238}U signal intensity. A laser ablation spot size of $10\ \mu\text{m}$ was applied.

In order to enhance the precision of the background, the gas blank, used for blank correction, was determined by measuring it for ten minutes as already described above. Additional gas blanks were recorded for about 15 seconds prior to the particle ablation and after it in order to monitor the complete wash-out of the previously analyzed samples. The blank and dead time corrected signal intensities were subject to a so-called logical test, which aimed at setting an operator-independent threshold for the selection of intensities used for further evaluation. The threshold was set to twenty times the standard deviation of the determined blank signal. The signal intensities of the isotope that yielded the smallest number of single data points above this threshold, defined the peak area used for further evaluation. Then the intensities of each isotope were integrated over the defined peak area, and the $^{234}\text{U}/^{238}\text{U}$, $^{235}\text{U}/^{238}\text{U}$ and $^{236}\text{U}/^{238}\text{U}$ isotope ratios were calculated by dividing the integrated signal intensities of the isotopes. Integration was performed by summing up the single recorded signal intensities (i.e. recorded in time resolved analysis mode with an acquisition time of one second per data point) in Microsoft Excel 2007. Integrating over the defined peak area was performed because of counting statistics, thereby reducing the influence of small count rates on the isotope ratio. Finally, the blank and dead time corrected isotope ratios $(^X\text{U}/^{238}\text{U})_{\text{Bl}}$ and $\tau_{\text{corrected,GP}}$ of the glass particle (GP) were

multiplied with the respective external correction factors $CF_{xU/^{238}U}$ in order to obtain the final glass particle isotope ratio $(^{x}U/^{238}U)_{\text{corrected,GP}}$ (see eq 2.1-3).

$$(^{x}U/^{238}U)_{\text{corrected,GP}} = (^{x}U/^{238}U)_{\text{Bl and } \tau \text{ corrected,GP}} \times CF_{xU/^{238}U} \quad (2.1-3)$$

$x = 234, 235 \text{ or } 236$

2.3.1. Uncertainty Evaluation

Expanded total combined standard uncertainties (U_c) were calculated according to ISO/GUM (ISO/IEC Guide 98-3:2008) and Eurachem (EURACHEM / CITAC Guide CG 4) using the GUM Workbench Pro software (version 2.4, Metrodata GmbH, Weil am Rhein, Germany). The single parameters that were propagated for computing the expanded total combined standard uncertainties of the $^{234}\text{U}/^{238}\text{U}$, $^{235}\text{U}/^{238}\text{U}$ and $^{236}\text{U}/^{238}\text{U}$ isotope ratio measurements of the glass particles are given in Table 2.1-3. No significant contributions to the expanded total combined standard uncertainties could be identified with respect to Faraday cup gain calibration and different signal response/decay times of Faraday cups and secondary electron multipliers. Thus, these effects were not included in the uncertainty budget.

Table 2.1-3: Propagated parameters for computing the expanded total combined standard uncertainties of glass particle isotope ratio measurements.

Parameter	$^{234}\text{U}/^{238}\text{U}$	$^{235}\text{U}/^{238}\text{U}$	$^{236}\text{U}/^{238}\text{U}$
$(^{x}\text{U}/^{238}\text{U})_{\text{certified}}^{\text{a}}$	X	X	X
$(^{x}\text{U}/^{238}\text{U})_{\text{measured}}^{\text{a}}$	X	X	X
Blank ^{a,b}	X	X	X
Dead time ^{234}U or ^{236}U ^{a,b}	X		X
$^{238}\text{U}^+$ peak tailing ^{a,b}			X
Yield variation IC0 or IC1 ^{a,b}	X (IC1)		X (IC0)
UH ⁺ /U ⁺ ^{a,b}			X

^a liquid certified reference material measurement

^b glass particle measurement

3. Results and discussion

3.1. Selection of isotope standard for calibration

U500 and IRMM-187 were investigated for the determination of the external correction factor. The utilization of U500 was determined as this certified reference material exhibits an almost 1:1 $^{235}\text{U}/^{238}\text{U}$ isotope ratio, which is regarded as preferable for the determination of mass bias

effects. The applicability of IRMM-187, which is a low-enriched U isotopic reference material, was additionally studied as its U isotope amount ratios have lower expanded uncertainties compared to U500.

The external correction factor corrects in one step for all effects present during the analysis, except for the liquid-solid matrix dissimilarity. The effects that are considered in the external correction factor are: mass bias (for $^{234}\text{U}/^{238}\text{U}$, $^{235}\text{U}/^{238}\text{U}$ and $^{236}\text{U}/^{238}\text{U}$), secondary electron multiplier yield and its variation (for $^{234}\text{U}/^{238}\text{U}$ and $^{236}\text{U}/^{238}\text{U}$), peak tailing from $^{238}\text{U}^+$ ions (for $^{236}\text{U}/^{238}\text{U}$) and $^{235}\text{U}^1\text{H}^+ / ^{235}\text{U}^+$ hydride rate (for $^{236}\text{U}/^{238}\text{U}$). The $^{235}\text{U}^1\text{H}^+ / ^{235}\text{U}^+$ hydride rate for both laser ablation and liquid measurements (i.e. introduction of dry aerosol) was about 1×10^{-6} . The standard solution concentrations in the low ng g^{-1} range were applied in order to not overload the secondary electron multipliers. The maximum count rate determined for ^{234}U was set to approximately 9.5×10^5 cps. Applying an external correction factor determined by means of IRMM-187 did not result in a significant difference, compared to U500 (see Fig. 2.1-2).

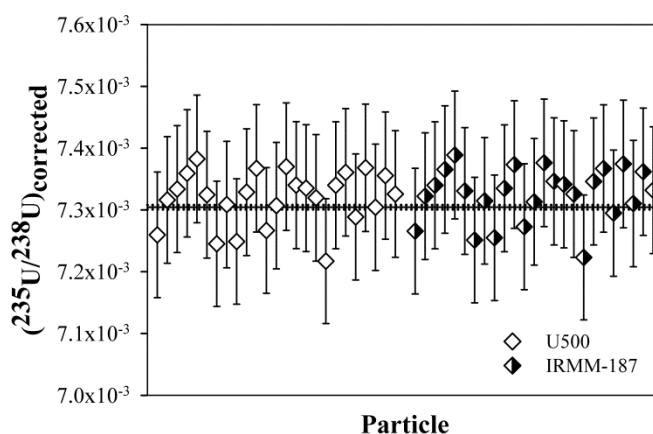


Fig. 2.1-2: Comparison of S1 $^{235}\text{U}/^{238}\text{U}$ isotope ratios corrected with U500 (white diamonds) and IRMM-187 (semi-filled diamonds), respectively, external correction factors. The solid line represents the certified isotope ratio ($^{235}\text{U}/^{238}\text{U} = 0.0073045(36)$), whereas the dotted lines indicate the certified range. Spot sizes of $10 \mu\text{m}$ were applied. Error bars are indicating the expanded uncertainty of $^{235}\text{U}/^{238}\text{U}$ isotope ratios ($k=2$).

Correction with IRMM-187 yielded a bias of 0.28 % of the average ($n=25$) $^{235}\text{U}/^{238}\text{U}$ glass particle isotope ratio, whereas the average of $^{235}\text{U}/^{238}\text{U}$ isotope ratios that were corrected with U500 showed a bias of 0.20 % from the certified value. Both corrections resulted in accurate $^{235}\text{U}/^{238}\text{U}$ glass particle isotope ratios (see Fig. 2.1-2). The lower uncertainties of the isotope amount ratios of IRMM-187, compared to U500, were not reflected in the expanded total combined uncertainty as the main contribution to the uncertainty results from the repeatability

of the glass particle measurements (see below). It was decided to apply U500 for external correction, as determined mass bias effects are independent of detector non-linearities. We also investigated the applicability of using lower concentrations of U500 for calibration in order to account for low laser ablation signals. The final solution concentration was selected around 4 ng g⁻¹ in order not to overload IC detectors and as lower concentrations led to higher uncertainties (i.e. 2.8 % and 1.5 % for ²³⁴U/²³⁸U and ²³⁵U/²³⁸U when applying a 0.4 ng g⁻¹ standard compared to 2.6 % and 1.4 % at 4 ng g⁻¹). In Fig. 2.1-3 both ²³⁴U/²³⁸U and ²³⁵U/²³⁸U glass particle isotope ratios that were corrected with U500 (4 ng g⁻¹) are shown.

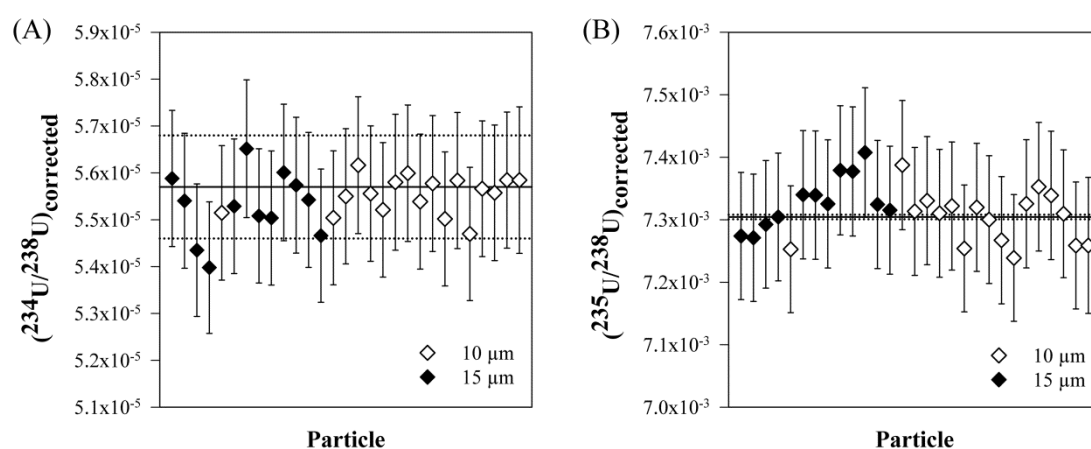


Fig. 2.1-3: S1 ²³⁴U/²³⁸U (A) and ²³⁵U/²³⁸U (B) isotope ratios corrected with U500 external correction factors. The solid lines represent the certified isotope ratios (²³⁴U/²³⁸U = 0.000 055 7(11); ²³⁵U/²³⁸U = 0.007 304 5(36)), whereas the dotted lines indicate the certified range. Spot sizes of 10 μm (white diamonds) and 15 μm (black diamonds) were applied. Error bars are indicating the expanded uncertainty of ²³⁴U/²³⁸U and ²³⁵U/²³⁸U isotope ratios (k=2).

These ratios were determined by applying spot sizes of 10 μm and 15 μm. The average ²³⁴U/²³⁸U and ²³⁵U/²³⁸U isotope ratios (see Fig. 2.1-3) measured in 28 S1 particles yielded biases of -0.51 % and 0.15 %, respectively. The maximum observed ²³⁸U signal intensities ranged from about 0.14 V to 2.1 V for the analyzed glass particles. Considering the combined standard uncertainties, 2.6 % and 1.4 % expanded uncertainties (k=2) were computed for ²³⁴U/²³⁸U and ²³⁵U/²³⁸U isotope ratio measurements. Comparing the biases and the uncertainties of the isotope ratios, it can be concluded that the isotope ratios are in good agreement with the certified range. Moreover, an underestimation of the individual uncertainty contributions can be excluded. The main contribution to the uncertainty budget is produced by the repeatability of the measurements (i.e. 85.5 % and 96.5 % for ²³⁴U/²³⁸U and ²³⁵U/²³⁸U). In addition, it is evident that

the different spot sizes do not influence the final results and can be chosen upon the size of the analyzed particles. The same applies for the other ratios (data not shown).

3.2. Laser ablation carrier gas

It is well known (Eggins et al., 1998; Guillong and Günther, 2002; Günther and Heinrich, 1999; Horn and Günther, 2003) that the application of He as laser ablation carrier gas has certain advantages for particular sample matrices (e.g. smaller particle size distribution, enhanced signal intensities, increased transport efficiency, minimized elemental fractionation) over Ar, especially if a laser wavelength of 193 nm is applied. In this work, both carrier gases were investigated with respect to their influence on the accuracy and precision of the isotope ratio analysis of glass particles. The analyses of the glass particles were, apart from the used carrier gas, performed under the same measurement conditions, applying spot sizes of 10 μm and an external correction factor determined by means of U500. Laser ablation under He atmosphere resulted in an average $^{235}\text{U}/^{238}\text{U}$ isotope ratio (n=31) of 0.00733(10), which deviated 0.41% from the certified ratio. In comparison, the average $^{235}\text{U}/^{238}\text{U}$ ratio (n=25) of 0.00732(10) that was obtained by using Ar as carrier gas showed a bias of 0.20% from the certified value. The given uncertainties of the average isotope ratios are total combined uncertainties. The applied carrier gas was not reflected in the expanded uncertainty, which was 1.4% for both applications. Therefore, no significant difference in the $^{235}\text{U}/^{238}\text{U}$ isotope ratios was observed (see also Fig. 2.1-4).

This was additionally confirmed by the fact that no significant signal enhancement on the average laser signals of the particles was observed when He was used. Applying a spot size of 10 μm , the maximum observed ^{238}U glass particle signal intensities ranged from 0.2 V to 0.7 V, both for Ar and He. Isotope ratios that were determined by means of ablation under He atmosphere exhibit a slightly better repeatability (i.e. 0.49%) compared to particles ablated under Ar atmosphere (i.e. 0.60%). However, the use of He was not regarded to be advantageous for the presented purpose. Therefore, Ar was used as carrier gas for further investigations.

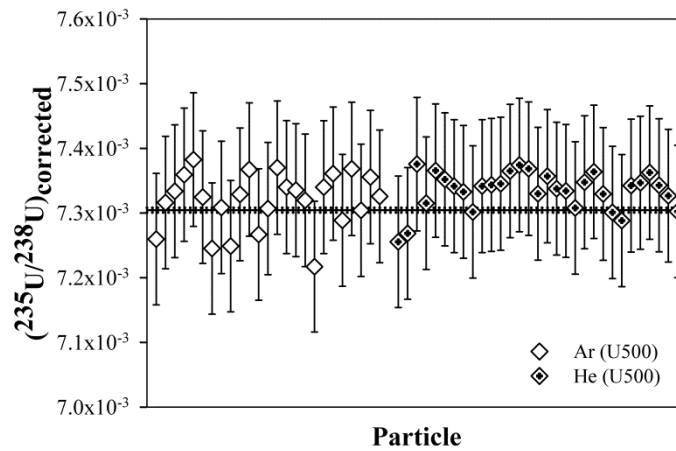


Fig. 2.1-4: S1 $^{235}\text{U}/^{238}\text{U}$ isotope ratios that were determined by using Ar (white diamonds) and He (x-hair diamonds), respectively, as laser ablation carrier gases. The solid line represents the certified isotope ratio ($^{235}\text{U}/^{238}\text{U} = 0.007\,304\,5(36)$), whereas the dotted lines indicate the certified range. Spot sizes of $10\ \mu\text{m}$ were applied. Error bars are indicating the expanded uncertainty of $^{235}\text{U}/^{238}\text{U}$ isotope ratios ($k=2$).

3.3. Determination of $^{236}\text{U}/^{238}\text{U}$ Isotope Ratios

The determination of low $^{236}\text{U}/^{238}\text{U}$ isotope ratios is usually difficult because of significant peak tailing from $^{238}\text{U}^+$ ions on the mass of ^{236}U , and interference by $^{235}\text{U}^1\text{H}^+$ ions. The peak tailing in a magnetic sector-field mass spectrometer mainly results from low-energy ions, which originate from ion collisions with residual gas molecules and ion energy variations after the ESA and magnetic sector (Boulyga et al., 2006). In order to reduce the amount of these low energy ions and decrease the $^{236}\text{U}/^{238}\text{U}$ abundance sensitivity, a deceleration filter was applied for the determination of ^{236}U . The optimization of the deceleration filter is described in detail elsewhere (Boulyga et al., 2006). The ablation of the S1 glass particles was accomplished using Ar as the carrier gas. External correction was performed by means of U500 $CF_{^{236}\text{U}/^{238}\text{U}}$ correction factors. Applying the deceleration filter improved the $^{236}\text{U}/^{238}\text{U}$ abundance sensitivity by almost one order of magnitude (i.e. 1.26×10^{-7} compared to 1.06×10^{-6} with the filter turned off) and led to a reduced bias from the certified range and significantly reduced uncertainties. Results that were obtained with and without deceleration filter are given in Fig. 2.1-5.

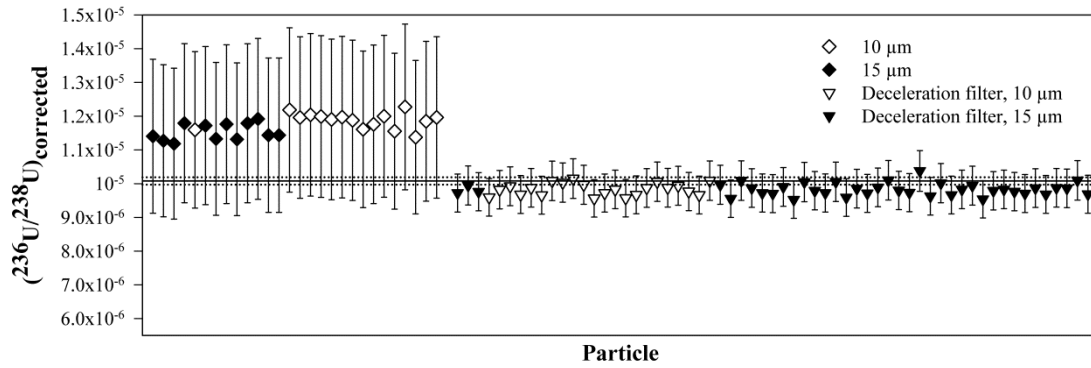


Fig. 2.1-5: Comparison of S1 $^{236}\text{U}/^{238}\text{U}$ isotope ratios that were determined by measuring ^{236}U applying (triangle) and not applying (diamond) a deceleration filter. The solid line represents the certified isotope ratio ($^{236}\text{U}/^{238}\text{U} = 0.00001008(11)$), whereas the dotted lines indicate the certified range. Spot sizes of 10 μm (white symbols) and 15 μm (black symbols) were applied. Error bars are indicating the expanded uncertainty of $^{236}\text{U}/^{238}\text{U}$ isotope ratios ($k=2$).

The average of 61 particles of $^{236}\text{U}/^{238}\text{U}$ isotope ratios yielded a bias of -2.48% from the certified value. In contrast, the average of 28 particles, which were analyzed with the deceleration filter turned off, yielded a bias of 16.3%, which was mainly caused by the poor abundance sensitivity. The calculation of combined standard uncertainties for $^{236}\text{U}/^{238}\text{U}$ glass particle isotope ratio measurements yielded an expanded uncertainty of 20% ($k=2$) for measurements with the deceleration filter turned off (see Table 2.1-4). The main contribution to the expanded total combined uncertainty budget was assigned to the peak tailing from $^{238}\text{U}^+$ ions, which accounts for 78.9% of the expanded total combined standard uncertainty (see Table 2.1-4).

However, the application of the deceleration filter reduced the expanded uncertainty to 5.8% ($k=2$) and the contribution of the $^{238}\text{U}^+$ peak tailing to the uncertainty budget to 19.4% (see Table 2.1-4). In the later case, the repeatability of the measurements was the main contributor to the expanded total combined uncertainty budget as it accounted for 26.4%.

Table 2.1-4: Relative contributions of single parameters to the expanded total combined standard uncertainty of $^{236}\text{U}/^{238}\text{U}$ glass particle measurements.

Parameters	Relative contributions / %	
	Deceleration filter	
	No	Yes
$(^{236}\text{U}/^{238}\text{U})_{\text{certified, lq}}$	0.0	0.5
$(^{236}\text{U}/^{238}\text{U})_{\text{measured, lq}}$	0.2	13.6
^{236}U blank (1 % HNO_3), lq	0.0	0.0
^{238}U blank (1 % HNO_3), lq	0.0	0.0
Dead time IC0 (for ^{236}U), lq	0.0	1.5
$^{238}\text{U}^+$ peak tailing (for ^{236}U), lq	0.0	0.0
Yield variation IC0 (for ^{236}U), lq	0.3	6.2
UH^+/U^+ (for ^{236}U), lq	4.9	1.6
$(^{236}\text{U}/^{238}\text{U})_{\text{measured, GP}}$	13.5	26.4
^{236}U gas blank, GP	0.0	11.0
^{238}U gas blank, GP	0.0	0.4
Dead time IC0 (for ^{236}U), GP	0.0	0.0
$^{238}\text{U}^+$ peak tailing, GP	78.9	19.4
Yield variation IC0 (for ^{236}U), GP	0.2	12.4
UH^+/U^+ (for ^{236}U), GP	2.0	6.8
$RSU (k=2) / \%$	20.0	5.8

Lq...liquid certified reference material measurement
GP...glass particle measurement

3.4. Reproducibility

$^{235}\text{U}/^{238}\text{U}$ isotope ratio measurements of S1 glass particles, applying Ar as the carrier gas and spot sizes of 10 μm , were performed within two independent measurement series for investigating the reproducibility of the method. The second measurement series was repeated after nine months. The reproducibility, calculated as RSD of forty-two $^{235}\text{U}/^{238}\text{U}$ isotope ratio measurements, is 0.62 %. An external repeatability (calculated as RSD) of 0.65 % (n=17) and 0.60 % (n=25), respectively, was observed for the 1st and the 2nd measurement series for $^{235}\text{U}/^{238}\text{U}$, $^{234}\text{U}/^{238}\text{U}$ and $^{236}\text{U}/^{238}\text{U}$ isotope ratio measurements yielded an external repeatability of 0.71 % (n=17) and 1.84 % (n=22), respectively, for analyses using 10 μm spot ablation and Ar as the carrier gas. A summary of the U isotope ratio measurements of S1 glass particles is given in Table 2.1-5.

Table 2.1-5: $^{234}\text{U}/^{238}\text{U}$, $^{235}\text{U}/^{238}\text{U}$ and $^{236}\text{U}/^{238}\text{U}$ determined isotope ratios of S1 glass particles.

	$^{234}\text{U}/^{238}\text{U}$	$^{235}\text{U}/^{238}\text{U}$ (a)	$^{235}\text{U}/^{238}\text{U}$ (b)	$^{236}\text{U}/^{238}\text{U}$
	(n=17)	(n=17)	(n=25)	(n=22)
Average	5.55×10^{-5}	7.31×10^{-3}	7.32×10^{-3}	9.84×10^{-6}
SD	3.96×10^{-7}	4.78×10^{-5}	4.38×10^{-5}	1.81×10^{-7}
RSD / %	0.71	0.65	0.60	1.84
RSU / %	2.6	1.4	1.4	5.8
Repeatability / %	0.71	0.65	0.60	1.84
Bias / %	0.26	-0.16	0.20	-2.41
Certified isotope amount ratios	$5.57(11) \times 10^{-5}$	$7.3045(36) \times 10^{-3}$	$7.3045(36) \times 10^{-3}$	$1.008(11) \times 10^{-5}$

a...first measurement series

b...second measurement series

In comparison, Varga reported precisions of 0.9–5.1 % for the $^{235}\text{U}/^{238}\text{U}$ isotope ratio analysis of individual U_3O_8 particles, with lateral dimensions ranging from 10–30 μm . The reported precision for the single collector measurements was achieved by performing partial ablation of the particles, together with applying low laser energy (Varga, 2008). A relative precision of 0.22 % (2σ) for $^{235}\text{U}/^{238}\text{U}$ LA-MC-ICP-MS isotope ratio measurements, applying spots of approximately $25 \times 14 \mu\text{m}$, of 138 natural uraninite grains was reported by Lloyd et al. (Lloyd et al., 2009)

3.5. Demonstration of applicability of developed method by means of S3 glass particle measurements

S3 glass particles were analyzed under optimized conditions (i.e. carrier gas: Ar; external correction: U500; application of deceleration filter) to demonstrate the applicability of the developed method for the investigation of low-enriched uranium particles. Laser ablation of the particles was accomplished by using Ar as the carrier gas. Spot sizes of 10 μm and 15 μm were applied for ablation of S3 glass particles. The maximum ^{238}U signal intensities ranged from about 0.05 V to 1.5 V.

The determined $^{234}\text{U}/^{238}\text{U}$, $^{235}\text{U}/^{238}\text{U}$ and $^{236}\text{U}/^{238}\text{U}$ isotope ratios of the S3 glass particles, which are shown in Table 2.1-6, were in good accordance with the certified value.

Relative expanded uncertainties ($k=2$) of 3.8 % ($^{234}\text{U}/^{238}\text{U}$), 0.8 % ($^{235}\text{U}/^{238}\text{U}$) and 6.7 % ($^{236}\text{U}/^{238}\text{U}$) were calculated for the isotope ratio measurements (see Table 2.1-6). In case of $^{234}\text{U}/^{238}\text{U}$ and $^{235}\text{U}/^{238}\text{U}$, the main contribution to the expanded total combined uncertainty

budget (i.e. 89.9% and 75.9% for $^{234}\text{U}/^{238}\text{U}$ and $^{235}\text{U}/^{238}\text{U}$, respectively) resulted again, as already observed for S1 particles, from the repeatability of the glass particle measurements. Considering the relative distribution of parameters propagated for the expanded total combined standard uncertainty of $^{236}\text{U}/^{238}\text{U}$ isotope ratio measurements, the main contributors are the variation of the IC0 yield (i.e. 46.3%) and the repeatability (i.e. 15.7%). In contrast to S1 glass particles, no contribution was assigned to the peak tailing from $^{238}\text{U}^+$ ions. ^{238}U peak tailing does less affect the determination of ^{236}U of S3 glass particles as they exhibit an about 42 times higher $^{236}\text{U}/^{238}\text{U}$ isotope ratio than S1 particles (see Table 2.1-1).

4. Conclusions

We demonstrated the applicability, reliability and robustness of LA-MC-ICP-MS for the direct analysis of distinct individual particles with respect to their U isotopic composition (i.e. $^{234}\text{U}/^{238}\text{U}$, $^{235}\text{U}/^{238}\text{U}$ and $^{236}\text{U}/^{238}\text{U}$). Glass particles, which were produced by the IRMM in order to simulate environmental samples containing hot particles, were used for the full evaluation of the presented method. The used particles are certified with respect to their U isotopic composition, including ^{236}U , and they are exhibiting a particle size down to 10 μm with U amounts in the low picogram range. As U-containing particles were blended with inactive matrix glass, matrix interferences resulting from, for example, Al, Pb or Si could be excluded by analyzing the inactive matrix glass. Thus, the glass particles were ideal for performing a full validation of LA-MC-ICP-MS for the presented aim by means of certified reference materials.

The application of a deceleration filter was proven to be a prerequisite in particular for the accurate determination of very low $^{236}\text{U}/^{238}\text{U}$ isotope ratios (i.e. 10^{-5}). Expanded total combined standard uncertainty calculations revealed the main contributors to the uncertainty budgets and helped to optimize the analytical procedure. It is evident that combined uncertainties have to be evaluated according to the abundance ratio as contributors may change significantly when ratios vary within orders of magnitude. The presented semi-automatic evaluation approach may result in a future use of this technique in safeguards and/or (nuclear) forensics with respect to the analysis of environmental samples. However, pre-selection of U-containing particles by means of, for example, SEM/EDX prior to LA-MC-ICP-MS analysis is regarded to be advantageous for the application of the presented method for routine analysis.

Table 2.1-6: $^{234}\text{U}/^{238}\text{U}$, $^{235}\text{U}/^{238}\text{U}$ and $^{236}\text{U}/^{238}\text{U}$ determined isotope ratios of S3 glass particles.

	$^{234}\text{U}/^{238}\text{U}$ (n=9)	<i>SU</i> (k=2)	$^{235}\text{U}/^{238}\text{U}$ (n=9)	<i>SU</i> (k=2)	$^{236}\text{U}/^{238}\text{U}$ (n=13)	<i>SU</i> (k=2)
	2.74 x 10 ⁻⁴	1.04 x 10 ⁻⁵	4.30 x 10 ⁻²	3.22 x 10 ⁻⁴	4.19 x 10 ⁻⁴	2.80 x 10 ⁻⁵
	2.78 x 10 ⁻⁴	1.06 x 10 ⁻⁵	4.31 x 10 ⁻²	3.23 x 10 ⁻⁴	4.19 x 10 ⁻⁴	2.81 x 10 ⁻⁵
	2.74 x 10 ⁻⁴	1.04 x 10 ⁻⁵	4.30 x 10 ⁻²	3.22 x 10 ⁻⁴	4.18 x 10 ⁻⁴	2.80 x 10 ⁻⁵
	2.74 x 10 ⁻⁴	1.04 x 10 ⁻⁵	4.32 x 10 ⁻²	3.24 x 10 ⁻⁴	4.28 x 10 ⁻⁴	2.86 x 10 ⁻⁵
	2.79 x 10 ⁻⁴	1.06 x 10 ⁻⁵	4.33 x 10 ⁻²	3.25 x 10 ⁻⁴	4.19 x 10 ⁻⁴	2.81 x 10 ⁻⁵
	2.70 x 10 ⁻⁴	1.02 x 10 ⁻⁵	4.33 x 10 ⁻²	3.25 x 10 ⁻⁴	4.18 x 10 ⁻⁴	2.80 x 10 ⁻⁵
	2.78 x 10 ⁻⁴	1.06 x 10 ⁻⁵	4.33 x 10 ⁻²	3.24 x 10 ⁻⁴	4.22 x 10 ⁻⁴	2.83 x 10 ⁻⁵
	2.78 x 10 ⁻⁴	1.06 x 10 ⁻⁵	4.33 x 10 ⁻²	3.25 x 10 ⁻⁴	4.22 x 10 ⁻⁴	2.83 x 10 ⁻⁵
	2.77 x 10 ⁻⁴	1.05 x 10 ⁻⁵	4.34 x 10 ⁻²	3.25 x 10 ⁻⁴	4.19 x 10 ⁻⁴	2.81 x 10 ⁻⁵
					4.17 x 10 ⁻⁴	2.79 x 10 ⁻⁵
					4.20 x 10 ⁻⁴	2.81 x 10 ⁻⁵
					4.21 x 10 ⁻⁴	2.82 x 10 ⁻⁵
					4.19 x 10 ⁻⁴	2.81 x 10 ⁻⁵
Average	2.76 x 10 ⁻⁴		4.32 x 10 ⁻²		4.20 x 10 ⁻⁴	
SD	3.07 x 10 ⁻⁶		1.39 x 10 ⁻⁴		2.73 x 10 ⁻⁶	
RSD / %	1.11		0.32		0.65	
RSU / %	3.8		0.8		6.7	
Repeatability / %	1.11		0.32		0.65	
Bias / %	-1.35		-0.31		-1.15	
Certified isotope amount ratios	2.796(17) x 10 ⁻⁴		4.3343(22) x 10 ⁻²		4.248(10) x 10 ⁻⁴	

Acknowledgement

We thank Urs Klötzli from the Department of Lithospheric Research at the University of Vienna for providing the in-house U solution and the laser ablation system. Stefan Bürger from the Department of Safeguards (International Atomic Energy Agency) is acknowledged for his help with uncertainty calculations. Jane Poths and Dave Donohue from the Department of Safeguards (International Atomic Energy Agency) are acknowledged for the fruitful discussion of all aspects related to uranium isotope ratio measurements in particles. The authors thank Thomas Konegger from the Institute of Chemical Technologies and Analytics at the Vienna University of Technology for performing the scanning electron microscope analyses of the glass particles. The Austrian Science Fund FWF (START project 267-N11) and the International Atomic Energy Agency are highly acknowledged for financial support.

2.2 Application II

Evaluation strategies for isotope ratio measurements of single particles by LA-MC-ICPMS²

Stefanie Kappel^a, Sergei F. Boulyga^b, Ladina Dorta^c, Detlef Günther^c, Bodo Hattendorf^c, Daniel Koffler^d, Gregor Laaha^d, Friedrich Leisch^d and Thomas Prohaska^{a,*}

^a University of Natural Resources and Life Sciences, Vienna, Department of Chemistry, Division of Analytical Chemistry–VIRIS-Laboratory, Konrad Lorenzstrasse 24, 3430 Tulln, Austria

^b Safeguards Analytical Services, Department of Safeguards, International Atomic Energy Agency, Wagramer Strasse 5, 1400 Vienna, Austria

^c Swiss Federal Institute of Technology Zurich (ETH Zurich), Department of Chemistry and Applied Biosciences, Laboratory of Inorganic Chemistry, Wolfgang-Pauli-Strasse 10, 8093 Zurich

^d University of Natural Resources and Life Sciences, Vienna Department of Landscape, Spatial and Infrastructure Sciences, Institute of Applied Statistics and Computing, Gregor Mendel Straße 33, 1180 Vienna, Austria

* Corresponding author: Thomas Prohaska, University of Natural Resources and Life Sciences, Vienna, Department of Chemistry, Division of Analytical Chemistry–VIRIS-Laboratory (UFT Campus Tulln), Konrad Lorenzstrasse 24, 3430 Tulln, Austria, E-mail: thomas.prohaska@boku.ac.at. Phone: (+43 1) 47654-6092. Fax: (+43 1) 47654-6059.

² Major revisions requested (submitted to Analytical and Bioanalytical Chemistry)

ABSTRACT

Data evaluation is a crucial step when it comes to the determination of accurate and precise isotope ratios computed from transient signals measured by multi collector – inductively coupled plasma mass spectrometry (MC-ICPMS) coupled to for example laser ablation (LA). In the present study, the applicability of different data evaluation strategies (i.e. ‘point by point’, ‘integration’ and ‘linear regression slope’ method) for the computation of $^{235}\text{U}/^{238}\text{U}$ isotope ratios measured in single particles by LA-MC-ICPMS was investigated. The analyzed uranium oxide particles (i.e. 9073-01-B, CRM U010 and NUSIMEP-7 test samples) having sizes down to the sub- μm range are certified with respect to their $^{235}\text{U}/^{238}\text{U}$ isotopic signature, which enabled to evaluate the applied strategies with respect to precision and accuracy. The different strategies were also compared with respect to their expanded uncertainties. Even though the point to point method proved to be superior the other methods are advantageous as they are taking weighted signal intensities into account. For the first time the use of a ‘finite mixture model’ is presented for the determination of an unknown number of different U isotopic compositions of single particles present on the same planchet. The model uses an algorithm that determines the number of isotopic signatures by attributing individual data points to computed clusters. The $^{235}\text{U}/^{238}\text{U}$ isotope ratios are then determined by means of the slopes of linear regressions estimated for each cluster. The model was successfully applied for the accurate determination of different $^{235}\text{U}/^{238}\text{U}$ isotope ratios of particles deposited on the NUSIMEP-7 test samples.

Keywords: U isotope ratios, laser ablation MC-ICPMS, single particles, short transient signals, data evaluation strategies, finite mixture model

1. Introduction

Particles containing radionuclides are emitted during processes related to the nuclear fuel cycle (e.g. in enrichment facilities, in nuclear reactors, etc.). The knowledge of the uranium (U) and/or plutonium (Pu) isotopic signatures of such particles is highly valuable for international safeguards (Axelsson et al., 2009) and nuclear forensics (Mayer et al., 2007) as it helps to verify the absence of undeclared nuclear activities. International Atomic Energy Agency (IAEA) inspectors are collecting these particles, which are typically exhibiting sizes in the low micrometer range, by means of cotton swipes during routine inspections of nuclear facilities and the near-by environment (Donohue, 1998; Donohue, 2002).

Considering the analysis of the sampled particles, individual analysis of single particles is preferred over bulk analysis of the entire swipe. The swipe may contain a small number of particles with hidden isotopic signatures together with a large number of particles having known or natural isotopic composition. In such a case, bulk analysis of the entire swipe would yield a 'mixed' U or Pu isotopic composition and isotopic signatures of suspicious particles would eventually not be detected (Axelsson et al., 2009; Donohue, 1998). However, it has to be stressed that bulk analysis, including the measurement of U and Pu concentrations and isotopic compositions, is equally important for verifying the completeness and correctness of States Declarations (Zendel et al., 2011).

A promising technique for U isotope ratio analyses of single particles is laser ablation – (multi collector) – inductively coupled plasma mass spectrometry (LA-(MC)-ICPMS) (Aregbe et al., 2011; Boulyga and Prohaska, 2008; Kappel et al., 2012; Lloyd et al., 2009; Pointurier et al., 2011; Varga, 2008). Laser ablation of single particles with sizes in the low micrometer range typically yields transient signals that often only last a few milliseconds.

However, transient signals are also generated by other sample introduction techniques such as high performance liquid chromatography (HPLC) (Günther-Leopold et al., 2004), gas chromatography (GC) (Epov et al., 2010; Krupp and Donard, 2005; Krupp et al., 2001), flow-injection (Galler et al., 2007) or gold trap (Evans et al., 2001; Xie et al., 2005). Compared to continuous steady-state signals measured after solution nebulization, transient signals usually lead to less precise isotope ratios (Günther-Leopold et al., 2004; Hirata and Yamaguchi, 1999), which is mainly attributed to shorter measurement times, lower signal intensities due to lower analyte concentrations introduced and isotope ratio drifts over the transient signal (Rodríguez-González et al., 2011). Moreover, precision of individual data points, which is often referred to as 'internal' precision in literature (Evans et al., 2001; Krupp and Donard, 2005), varies over the transient signal as a result of varying signal intensities. According to counting statistics (Skoog and Leary, 1992) in which the relative standard deviation is expressed as the square root of the reciprocal of the registered counts, higher counts are yielding a smaller relative standard deviation and more precise isotope ratio data. Günther-Leopold et al. (Günther-Leopold et al., 2004), for example, observed the smallest isotope ratio (point-to-point) fluctuations at the top of the peak when performing neodymium (Nd) measurements by HPLC-MC-ICPMS. In LA-MC-ICPMS analyses, improved signal-to-noise ratios can be achieved by applying a laser cell with fast washout of the generated aerosol (Cottle et al., 2009). In addition, high spatial resolution analysis is enabled as a mixing of aerosol from different spots is avoided (Fricker et al., 2011).

Isotope ratio drifts over the transient signal have been reported by several authors using GC (Dzurko et al., 2009; Krupp et al., 2004; Krupp and Donard, 2005; Wehmeier et al., 2003), HPLC

(Günther-Leopold et al., 2005; Günther-Leopold et al., 2004) and LA (Hirata et al., 2003; Pettke et al., 2011b) as sample introduction techniques for MC-ICPMS. Krupp and Donard (Krupp and Donard, 2005) considered four effects as potential causes for the observed drifts in lead (Pb) and mercury (Hg), respectively, isotope ratio measurements by GC-MC-ICPMS. They studied instrumental mass bias, chromatographic fractionation in the GC column, a rise in the background signal during peak elution and the influence of analyte concentration and peak shape. As only an influence with respect to the peak width was identified, the authors pointed out the possibility that the relative change in analyte intensity per time might be the most pronounced effect driving the extent of the isotope ratio drift (Krupp and Donard, 2005). Hence and due to the fact that isotope ratio drifts were observed applying different MC-ICPMS instruments (i.e. 'Axiom' (Thermo, Winsford) (Krupp and Donard, 2005), 'Isoprobe' (GV Instruments, Manchester) (Krupp and Donard, 2005), 'Neptune' (Thermo Fisher Scientific, Germany) (Günther-Leopold et al., 2004)), it was assumed that the data acquisition system design behind the Faraday cups might lead to problems with respect to the acquisition of short, fast changing signals (Krupp and Donard, 2005). The same postulation was given by Dzurko et al. (Dzurko et al., 2009) and Günther-Leopold et al. (Günther-Leopold et al., 2005). During the simultaneous acquisition of transient signals, Faraday amplifier outputs are lagging behind input signals after a change in signal intensities. Thus, any difference in the amplifier response times leads to signal intensities that are enhanced or reduced relative to each other (Pettke et al., 2011b). Hirata et al. (Hirata et al., 2003) investigated the effect of fast increasing or decreasing copper (Cu) isotope ratios over a transient signal, whereat changing Cu isotope ratios were also attributed to the slow response of Faraday preamplifiers. The introduction of a correction factor enabled to minimize the systematic increase of Cu isotope ratios with prolonged laser ablation from 3-5 ‰ to < 1 ‰ (Hirata et al., 2003).

A drift of Pb isotope ratios during the course of LA-MC-ICPMS measurements of fluid inclusions using a 'Nu Plasma 1700' MC-ICPMS (Nu Instruments Limited, Wrexham, U.K.) was observed by Pettke et al. (Pettke et al., 2011b), who again attributed this observation to Faraday amplifier response differences. The authors investigated two different signal decay functions (i.e. Tau-correction) as well as two different integration methods for the determination of accurate Pb isotope ratios of fluid inclusions, whereupon integration of single intensities over the entire transient signal was regarded as method of choice. In addition, applying Tau-correction allowed accounting for differences in Faraday amplifier responses (Pettke et al., 2011b). Cottle et al. (Cottle et al., 2009) observed differing detector response times with respect to Faraday detectors and ion counting multipliers (i.e. discrete-dynode secondary electron multipliers) when performing Pb/U isotope ratio measurements by means of a 'Nu Plasma' MC-ICPMS (Nu

Instruments Limited, Wrexham, U.K.). Both signals rose at a similar rate but the Faraday signal was delayed by about 0.2 s relative to the ion counting multiplier. The influence of this time-offset as well as of the Faraday amplifier response effects on the determined isotope ratios was circumvented by integrating the single measured signal intensities over the whole transient signal prior to the calculation of the isotope ratios (Cottle et al., 2009).

Recently, Fietzke et al. (Fietzke et al., 2008) proposed a new data evaluation strategy for transient LA-MC-ICPMS signals. In their approach strontium (Sr) isotope ratios were derived from the slope of a linear regression, with the isotope representing the numerator on the y-axis and the denominator on the x-axis. The authors highlighted several advantages such as (1) the avoidance of a subjective influence that might occur by setting integration limits, (2) the use of all data (i.e. including background data), (3) the contribution of each data point, dependent on its signal intensity, to the linear regression and (4) the detection of interferences or fractionation due to deviations from the ideal linear fit (Fietzke et al., 2008). In comparison to conventional data reduction (i.e. separate background correction and calculation of $^{87}\text{Sr}/^{86}\text{Sr}$ isotope ratios for each individual point), 4-5 times better precision and accuracy could be achieved for LA-MC-ICPMS $^{87}\text{Sr}/^{86}\text{Sr}$ isotope ratio measurements of a carbonate sample. Moreover, the authors stated that the $^{87}\text{Sr}/^{86}\text{Sr}$ isotope ratios determined within their study were almost as precise as those measured by means of conventional liquid-nebulization MC-ICPMS (Fietzke et al., 2008). Epov et al. (Epov et al., 2010) compared three data reduction methods (i.e. 'peak area integration', 'point by point' and 'linear regression slope' method) for the determination of Hg isotopic compositions by means of GC-MC-ICPMS. It was demonstrated that the method using the slope of a linear regression typically yielded more precise and accurate δ Hg values than the other strategies. In addition, Rodríguez-Castrillón (Rodríguez-Castrillón et al., 2012) applied this new data evaluation strategy for the determination of Sr and Nd isotope ratios by means MC-ICPMS coupled to on-line liquid chromatography.

The above discussed publications dealing with isotope ratio determinations from transient signals illustrate well that data treatment is a crucial step. However, the analytical community strives towards new data evaluation strategies in order to reduce bias and uncertainty of isotope ratios from transient signals as was recently shown by various authors (Epov et al., 2010; Fietzke et al., 2008; Rodríguez-Castrillón et al., 2012). This work aimed at investigating the applicability of different data treatment strategies for the computation of individual major U isotope ratios (i.e. $^{235}\text{U}/^{238}\text{U}$) from single particle measurements.

2. Experimental

2.1. Reagents and certified reference materials

Certified reference materials (CRM) that are certified with respect to their U isotope ratios—IRMM-184 (European Commission-JRC, Institute for Reference Materials and Measurements, Geel, Belgium, (IRMM, 2005)), CRM U030-A (New Brunswick Laboratory, U.S. Department of Energy, Washington, DC, U.S., (New Brunswick Laboratory, CRM U030-A)) and CRM U500 (New Brunswick Laboratory, U.S. Department of Energy, Washington, DC, U.S., (New Brunswick Laboratory, CRM U500)) — were used for the determination of external correction factors for correcting mass bias. The certified reference materials were introduced by solution nebulization after dilution to concentrations less than 10 ng g^{-1} by 1 % (m/m) HNO_3 . 1 % (m/m) HNO_3 was prepared by diluting 65 % (m/m) HNO_3 (Merck KGaA, Darmstadt, Germany) with ultrapure water (18 $\text{M}\Omega \text{ cm}$ at 25 °C; PURELAB® Classic, Veolia Water Systems Austria GmbH, Wien, Austria at BOKU Vienna; Milli-Q® Element, Millipore, Millipore Corporation, Billerica, MA, U.S. at ETH Zurich). Ultrapure water and 65 % (m/m) HNO_3 were purified by sub-boiling distillation (Savillex Corporation, Eden Prairie, MN, USA at BOKU Vienna; DuoPUR, Milestone S.r.l., Italy at ETH Zurich) prior to use.

The following single uranium oxide particles, which are certified for their U isotopic compositions, were measured: 9073-01-B ($\text{UO}_2 \cdot 2 \text{H}_2\text{O}$ particles, European Commission-JRC, Institute for Reference Materials and Measurements, Geel, Belgium, (IRMM, 1997)), CRM U010 (U_3O_8 particles, New Brunswick Laboratory, U.S. Department of Energy, Washington, DC, U.S., (New Brunswick Laboratory, CRM U010)) and NUSIMEP-7 test samples (U_3O_8 particles, Nuclear Signatures Interlaboratory Measurement Evaluation Programme, European Commission-JRC, Institute for Reference Materials and Measurements, Geel, Belgium, (Truyens et al., 2011)). NUSIMEP-7 was an interlaboratory comparison (ILC) organized by the Institute for Reference Materials and Measurements. Participating laboratories received two test samples with U particles with undisclosed U isotope ratios. The ‘single deposition’ sample had one U isotopic composition whereas the ‘double deposition’ sample had two different isotopic compositions. The average diameter of the NUSIMEP-7 samples was reported to be $(0.327 \pm 0.139) \mu\text{m}$ (Truyens et al., 2011), whereas the particle sizes of 9073-01-B and CRM U010, which were determined by means of scanning electron microscopy at the TU Vienna (Quanta 200, FEI, Oregon, U.S.), ranged from about 1 to 5 μm . The used particle reference materials are considered to be representative for particles collected by IAEA inspectors using swipe sampling, even though they are exhibiting a broad particle size distribution. However, swipe samples may

contain particles of different origins, and thus of different chemical compositions and sizes. The certified isotope ratios of the used CRMs are listed in Table 2.2-1.

Table 2.2-1: Certified isotope ratios of CRMs measured in the course of this study.

	$^{235}\text{U}/^{238}\text{U}$	Reference
IRMM-184 ^a	0.007 262 3(22)	(IRMM, 2005)
CRM U030-A (U_3O_8) ^b	0.031 366 6(83)	(New Brunswick Laboratory, CRM U030-A)
CRM U500 (U_3O_8) ^b	0.999 6(14)	(New Brunswick Laboratory, CRM U500)
CRM U010 (U_3O_8) ^b	0.010 140(10)	(New Brunswick Laboratory, CRM U010)
9073-01-B ($\text{UO}_2 \cdot 2 \text{H}_2\text{O}$)	0.007 255 7(36)	(IRMM, 1997)
NUSIMEP-7 single deposition (U_3O_8)	0.009 072 6(45)	(Truyens et al., 2011)
NUSIMEP-7 double deposition (U_3O_8)	0.009 072 6(45)	(Truyens et al., 2011)
	0.034 148(17)	

^a chemical form is not stated in the certificate

^b the stated isotope amount ratios and according uncertainties ($k=2$) were calculated from the certified atom percents of ^{235}U and ^{238}U and their uncertainties as stated in the certificates.

2.2. Particle preparation for LA-MC-ICPMS analyses

Particle preparation for LA-MC-ICPMS analyses of 9073-01-B ($\text{UO}_2 \cdot 2 \text{H}_2\text{O}$) and CRM U010 (U_3O_8) particles was performed in a class 100 clean room at the IAEA Safeguards Analytical Laboratory in Seibersdorf, Austria. The 9073-01-B and CRM U010 particles were distributed on cotton swipes, from which they were sampled onto silicon planchets by means of a vacuum impactor. Silicon planchets are routinely used for particle preparation for subsequent LA-MC-ICPMS analysis in our laboratory as particles are more easily identifiable from the planchets background via the laser camera compared to carbon planchets. In addition, the use of carbon planchets may lead to the generation of clusters interfering at the masses of interest. However, the particles of the NUSIMEP-7 samples were already distributed on graphite planchets. Carbon planchets are routinely used for particle preparation for secondary ion mass spectrometry (SIMS). The generation of carbon clusters interfering at the masses of interest was monitored by measuring blank planchtes. No interferences were detected.

All planchets were covered with a colorless, commercially available nail polish, which was mixed 1:1 (v/v) with acetone (acetone p.a., Merck KGaA, Darmstadt, Germany). This step ensured that the particles were not moved during the laser ablation process.

2.3. LA-MC-ICPMS

U isotope ratio measurements of 9073-01-B and CRM U010 single U particles were accomplished at the ETH Zurich with a double-focusing high resolution sector field MC-ICPMS ('Nu Plasma HR', Nu Instruments Limited, Wrexham, U.K.). The instrument was coupled with a femtosecond (fs) laser ablation system operating at a wavelength of 795 nm. The fs laser ablation system uses a chirped pulse amplification Ti-sapphire-based laser system (Legend, Coherent Inc., Santa Clara, CA, U.S.). A large ablation cell with fast washout (i.e. decrease to signal intensities as low as 0.1 – 1 % within 1.3 – 2.6 s) was used (Fricker et al., 2011).

U isotope ratio measurements of the NUSIMEP-7 test samples were performed at the BOKU Vienna by coupling a nanosecond excimer-based laser ablation system (NWR 193, ESI-NWR Division, Electro Scientific Industries, Inc., Portland, CA, USA) with a 'Nu Plasma HR' MC-ICPMS (Nu Instruments Limited, Wrexham, U.K.). The used laser cell also enabled a fast washout (i.e. decrease to signal intensities as low as 1 % within less than 1.5 s) of the generated laser aerosol. The dark background of the planchets and the particle sizes (ca. 0.3 - 5 μm) hampered the identification of individual particles with the observation systems attached to the laser ablation systems. Therefore, line or raster scans were applied.

In both cases, a desolvating nebulizer system (DSN-100, Nu Instruments Limited, Wrexham, U.K.) was connected in parallel to the laser ablation system by means of a laminar flow adapter. The DSN-100 was used for solution nebulization to produce a dry aerosol for determining external correction factors. Blank correction of the solution nebulized CRMs was accomplished by 1 % (m/m) HNO_3 . No solution was aspirated during laser ablation to minimize possible blank influences during the ablation process.

Faraday cups (i.e. L1 and L3) were used for the detection of the major U isotopes ^{235}U and ^{238}U on both instruments. Operating parameters are given in Table 2.2-2.

2.4. Data treatment

IRMM-184, U030-A and U500, respectively, were measured before and after the particle analyses for the determination of the external correction factor $CF_{R_{235\text{U}/238\text{U}}}$, which corrects primarily for mass bias in the case of $^{235}\text{U}/^{238}\text{U}$ measurements (Kappel et al., 2012).

Signal intensities of the U isotopes during LA-ICPMS measurements were recorded in time resolved analysis mode. The blank signals were calculated from the U background signals of blank planchets (i.e. planchets with no particles but covered with nail polish).

Table 2.2-2: Operating parameters for LA-MC-ICPMS analyses.

Laser parameter	fs-LA-MC-ICPMS (ETH Zurich)	ns-LA-MC-ICPMS (BOKU Vienna)
Ablation mode	Line scan	Raster scan
Wavelength / nm	795	193
Pulse duration	~ 150 fs	3 ns
Fluence / J cm ⁻²	1	20
Repetition rate / Hz	4	15
Spot size / μm	~ 70	5
Scan speed / μm sec ⁻¹	10	2
He carrier gas / L min ⁻¹	0.9	0.8
DSN-100		
Nebulizer	Micromist	PFA 100
Nebulizer gas pressure / Pa	~ 2.1 x 10 ⁵	~ 2.0 x 10 ⁵ - 2.4 x 10 ⁵
Hot gas / L min ⁻¹	~0.3	~ 0.25 – 0.3
Membrane gas / L min ⁻¹	~3.15	~ 3.2 – 3.5
Spraychamber temperature / °C	112 – 116	112 – 116
Membrane temperature / °C	119 – 123	119 – 123
Nu Plasma HR MC-ICPMS		
RF power / W	1300	1300
Auxiliary gas / L min ⁻¹	0.75	0.8
Cool gas / L min ⁻¹	13	13
Cones	Ni	Ni
Mass separation	1	1
Isotopes monitored	²³⁵ U, ²³⁸ U	²³⁵ U, ²³⁸ U
Acceleration voltage / V	6000	4000
Resolution m/Δm	300 (low resolution)	300 (low resolution)
Detection system	Faraday cups L1 and L3	Faraday cups L1 and L3
Voltages applied to deceleration filter		
Retard (Filter 1) / V	5993	4012
Lens (Filter 2) / V	5840	3850
Data acquisition mode	TRA ^a (acquisition time per data point: 0.2 s)	TRA ^a (acquisition time per data point: 0.1 s)

^aTime resolved analysis

Typically the average of up to 500 readings was used for assessing the blank signals. After blank correction a threshold was set. Only signals higher than 3 x the standard deviation of the blank of ^{235}U (lower abundant isotope) were considered for further data processing. Excluding subjective influence for the selection of peak area limits is of particular importance considering a routine application of this method.

Different data evaluation approaches were investigated for the calculation of $^{235}\text{U}/^{238}\text{U}$ isotope ratios.

'Point by point' method (PBP): Calculation of U isotope ratios was accomplished by averaging the U isotope ratios derived from dividing individual, simultaneously acquired data points. All data points are contributing equally, independent on the signal intensity.

'Integration' method: $^{235}\text{U}/^{238}\text{U}$ isotope ratios were calculated by dividing the signal intensities which were integrated over the selected peak area. Small count rates contribute to a lesser extent to the isotope ratio than higher count rates. This approach is commonly applied in chromatography (Günther-Leopold et al., 2004; Krupp et al., 2004; Krupp et al., 2001; Rodríguez-González et al., 2011).

'Linear regression slope' method (LRS): The U isotope ratios were calculated by means of the slope of a linear regression using the 'least squares' method of the regression analysis. All selected data points (i.e. > 3 x standard deviation of the blank) are contributing to the linear fit (i.e. $y=ax$), whereupon higher signal intensities are having a larger impact. Moreover, the LRS method was applied to not blank corrected data. As both the blank and the particle signal intensities (not blank corrected) were taken into account the linear regression was not forced through the origin (i.e. $y = ax + b$).

'Finite mixture model': The 'finite mixture model' was applied for the determination of an unknown number of different $^{235}\text{U}/^{238}\text{U}$ isotopic signatures. The isotope ratios are again derived from the slopes of linear regression lines. In the 'finite mixture model' an algorithm applying fixed residual variances is used for clustering of the data points of interest and subsequent estimation of the slopes of the linear regression lines. The number of clusters, which represent the isotopic compositions, is estimated by the algorithm. A detailed description of the 'finite mixture model' is given in Leisch (Leisch, 2004). Computation was done in R (R Development Core Team, 2012), Version 2.15.0, using Grün and Leisch's flexmix package (Grün and Leisch, 2008). The raw data of ^{235}U and ^{238}U measurements were imported to the script. Blank correction and data selection by means of 3 x SD was directly accomplished in R.

Finally the U isotope ratios were multiplied with the external correction factor $CF_{R_{235\text{U}/238\text{U}}}$ to correct the isotope ratio for mass bias.

Data from 9073-01-B particle measurements (single isotopic composition) were used for the comparison of the ‘point by point’, the ‘integration’ and the ‘linear regression slope’ method. Data sets from 9073-01-B and CRM U010 were combined to one data set for the development of the ‘finite mixture model’. The NUSIMEP-7 test samples (multiple isotopic compositions) were evaluated by means of the ‘finite mixture model’ and compared to the commonly applied ‘point by point’ method.

2.5. Calculations of combined standard measurement uncertainties

Computation of expanded (k=2) uncertainties (U) was performed according to ISO/GUM (ISO/IEC Guide 98-3:2008) and EURACHEM (EURACHEM / CITAC Guide CG 4) guidelines with the GUM Workbench Pro software (version 2.4, Metrodata GmbH, Weil am Rhein, Germany). The applied model equations are described in the following (i.e. eq (2.2-1 – 2.2-3)):

$$R_{235U/238U, Particle, final} = R_{235U/238U, Particle, measured} * CF_{R_{235U/238U}} + \delta_{blank-LA, 235U} + \delta_{blank-LA, 238U} \quad (2.2-1)$$

$$CF_{R_{235U/238U}} = \frac{R_{235U/238U, CRM_{lq}, certified}}{R_{235U/238U, CRM_{lq}, measured, final}} \quad (2.2-2)$$

$$R_{235U/238U, CRM_{lq}, measured, final} = R_{235U/238U, CRM_{lq}, measured} + \delta_{blank-lq, 235U} + \delta_{blank-lq, 238U} \quad (2.2-3)$$

where $R_{235U/238U, Particle, final}$ is the final $^{235}U/^{238}U$ isotope ratio of the measured particle; $R_{235U/238U, Particle, measured}$ is the measured — blank corrected — $^{235}U/^{238}U$ isotope ratio; $CF_{R_{235U/238U}}$ is the external correction factor, which was derived from the ratio of the certified (i.e. $R_{235U/238U, CRM_{lq}, certified}$) and the final, measured $^{235}U/^{238}U$ isotope ratio of the liquid CRM (i.e. $R_{235U/238U, CRM_{lq}, measured, final}$). $R_{235U/238U, CRM_{lq}, measured, final}$ was expressed in a separate equation (i.e. eq (3.3-3)) in order to not only account for the standard uncertainty (u) of the measurement of the liquid CRM, but also for standard uncertainties resulting from blank

contributions. $R_{235\text{U}/238\text{U}, \text{CRM}_{\text{LQ}}, \text{measured}}$ is the measured — blank corrected — $^{235}\text{U}/^{238}\text{U}$ isotope ratio. Standard measurement uncertainties resulting from ^{235}U and ^{238}U , respectively, blank contributions from both LA and liquid measurements were accounted for by using so called δ -factors (European co-operation for Accreditation; Bürger et al., 2010) (i.e. $\delta_{\text{blank-LA}, ^{235}\text{U}}; \delta_{\text{blank-LA}, ^{238}\text{U}}; \delta_{\text{blank-lq}, ^{235}\text{U}}; \delta_{\text{blank-lq}, ^{238}\text{U}}$).

The combined standard measurement uncertainties u_c were multiplied with a coverage factor of 2 (i.e. $k=2$) in order to obtain expanded uncertainties (U).

3. Results and Discussion

3.1. Comparison of data evaluation methods for particles with single isotopic composition (CRM 9073-01-B)

A typical transient signal record of single particle measurements by LA-MC-ICPMS is shown in Fig. 2.2-1.

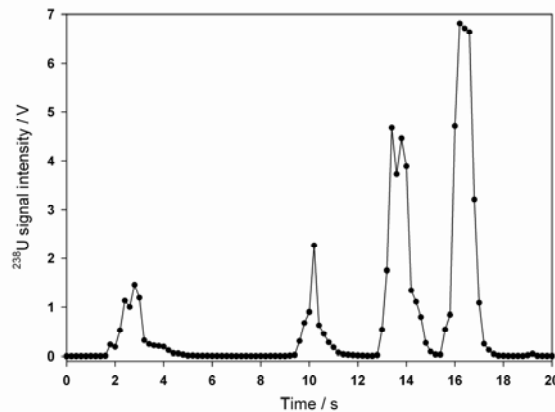


Fig. 2.2-1: LA-MC-ICPMS transient signal recorded during line scanning of 9073-01-B particles (1-5 μm).

The maximum ^{238}U signal intensities of all analyzed 9073-01-B particles ranged from about 0.5 V to 9.7 V. (Higher signal intensities led to a saturation of the detector and were not taken into account.) In Fig. 2.2-1 it can be seen that some peaks are exhibiting two or more peak maxima, which most likely result from adjacent particles entering the ICP almost simultaneously. To simplify matters for further evaluation, data points that belonged to one peak were regarded as signal intensities of one single particle. This simplification was considered as justified because the investigated test material has one certified U isotopic composition. Considering the ‘LRS’

method, two different evaluation approaches (i.e. $y = ax$ and $y = ax + b$) were compared. In case of blank corrected data, the regression line was forced through the origin (i.e. $y = ax$), whereas the intercept ($y = ax + b$) was taken into account for not blank corrected data. External correction was accomplished by means of IRMM-184. A summary of the different evaluation strategies is given in Table 2.2-3.

Table 2.2-3: Comparison of the 'PBP', 'integration' and 'LRS' method for n=118 particles.

	PBP	integration	LRS (data blank corrected, $y=ax$)	LRS (data not blank corrected, $y=ax + b$)
Average $^{235}\text{U}/^{238}\text{U}$ isotope ratio (n=118)	0.00729	0.00733	0.00736	0.00740
SD	0.00008	0.00011	0.00017	0.00022
RSD / %	1.1	1.5	2.3	3.0 %
Bias / %	0.5	1.0	1.5	2.0 %
RU* (k=2) / %	1.8	2.1	3.1	3.9 %
Certified $^{235}\text{U}/^{238}\text{U}$ isotope ratio	0.0072557(36)	0.0072557(36)	0.0072557(36)	0.0072557(36)

*relative expanded uncertainty

All evaluation strategies yield average $^{235}\text{U}/^{238}\text{U}$ isotope ratios that are in accordance with the certified value and that are overlapping within their uncertainties. Although the 'PBP' method yielded the best precision and the smallest bias from the certified value in this study, the other strategies can be advantageous from a statistical point of view as they are taking weighted signal intensities into account. A comparison of the 'LRS method' with regard to its application to blank and not blank corrected data yielded better precision and a smaller bias from the certified value for the blank corrected data, from which isotope ratios were computed by forcing the regression line through the origin. Moreover, forcing the regression line through the origin is regarded as advantageous as in this case it is ensured that high intensities are dominating the regression.

The uncertainties of single particle measurements with different maximum ^{238}U signal intensities were calculated. Typically, apart from the 'LRS' ($y = ax + b$) method, the largest relative expanded uncertainties (RU) were observed for particles with the lowest signal intensities, whereas similar uncertainties were observed for particles with peak intensities higher than about 1.5 V. In Table 2.2-4 relative expanded uncertainties (RU) and relative contributions of input parameters are given for three single particles with different maximum ^{238}U signal intensities.

Table 2.2-4: Relative expanded uncertainties (RU) and relative contributions of input parameters of $^{235}\text{U}/^{238}\text{U}$ isotope ratio measurements of single particles.

Data evaluation strategy	PBP			integration			LRS (data blank corrected, $y = ax$)			LRS (data not blank corrected, $y = ax + b$)		
Maximal ^{238}U signal intensities of individual particles/V	0.5	3.1	9.7	0.5	3.1	9.7	0.5	3.1	9.7	0.5	3.1	9.7
RU (k=2) / %	3.5	2.3	2.3	4.0	3.3	3.1	5.8	4.7	4.8	6.0	6.1	6.2
Relative contributions / %												
$R_{^{235}\text{U}/^{238}\text{U}, \text{CRM}_{\text{Iq}}, \text{certified}}$	< 0.05	< 0.05	< 0.05	< 0.05	< 0.05	< 0.05	< 0.05	< 0.05	< 0.05	< 0.05	< 0.05	< 0.05
$R_{^{235}\text{U}/^{238}\text{U}, \text{CRM}_{\text{Iq}}, \text{measured}}$	< 0.05	0.2	0.1	< 0.05	< 0.05	< 0.05	< 0.05	< 0.05	< 0.05	< 0.05	< 0.05	< 0.05
$\delta_{\text{blank-Iq}, ^{235}\text{U}}$	< 0.05	0.2	0.2	< 0.05	0.1	0.1	< 0.05	< 0.05	< 0.05	< 0.05	< 0.05	< 0.05
$\delta_{\text{blank-Iq}, ^{238}\text{U}}$	< 0.05	< 0.05	< 0.05	< 0.05	< 0.05	< 0.05	< 0.05	< 0.05	< 0.05	< 0.05	< 0.05	< 0.05
$R_{^{235}\text{U}/^{238}\text{U}, \text{Particle}, \text{measured}}$	37.8	90.0	87.8	55.4	86.0	98.9	78.4	99.1	99.1	100	100	100
$\delta_{\text{blank-LA}, ^{235}\text{U}}$	62.2	9.6	11.9	44.6	13.9	1.0	21.6	0.9	0.9	n.c.	n.c.	n.c.
$\delta_{\text{blank-LA}, ^{238}\text{U}}$	< 0.05	< 0.05	< 0.05	< 0.05	< 0.05	< 0.05	< 0.05	< 0.05	< 0.05	n.c.	n.c.	n.c.

n.c. ...not considered

The reproducibility (i.e. $R_{235\text{U}/238\text{U}, \text{Particle, measured}}$) was identified as the main contributor to the uncertainty. This is also in good accordance to previous work (Kappel et al., 2012). However, an exception from this was observed for the RU of the $^{235}\text{U}/^{238}\text{U}$ isotope ratio with the lowest maximal ^{238}U signal intensity of the ‘PBP’ method. In this case, the main contribution resulted from the ^{235}U laser ablation blank (i.e. 62.2 %), followed by the reproducibility (i.e. 37.8 %). ^{235}U blank contributions were also pronounced for the ‘integration’ and the ‘LRS’ ($y = ax$) method with respect to particles with the lowest peak intensities. The influence of the ^{235}U laser ablation blank is significantly reduced at higher signal intensities for the ‘integration’ and the ‘LRS’ ($y = ax$) method as compared to the ‘PBP’ method. This can be explained by the fact that in the ‘PBP’ method high and low intensities are contributing equally to the isotope ratio.

3.2. ‘Finite mixture model’

Evaluation methods taking weighted signal intensities into account are considered as data evaluation strategies of choice when dealing with short transient signals resulting from LA-MC-ICPMS analyses. Considering real safeguards samples the typical situation is that one has to deal with an unknown number of particles that can differ in their isotopic signatures.

In Fig. 2.2-2 a typical transient signal recorded during raster scanning of a NUSIMEP-7 test sample is shown. Laser ablation of NUSIMEP-7 particles having an average diameter of $(0.327 \pm 0.139) \mu\text{m}$ yields very sharp signals with maximal ^{238}U signal intensities below 1 V. In most cases only one data point per particle was observed in the transient signal.

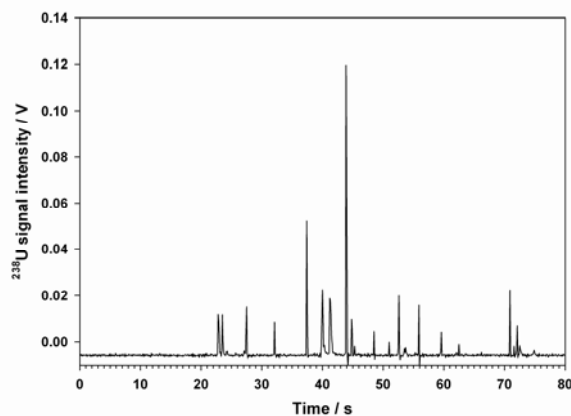


Fig. 2.2-2: LA-MC-ICPMS transients signal recorded during raster scanning of a NUSIMEP-7 interlaboratory comparison test sample.

Thus, applying the integration method to individual peaks is not possible. The commonly applied approach for determining multiple isotopic signatures from transient signals is the 'PBP method' and plotting the isotope ratios in ascending order. In Fig. 2.2-3 the results of the 'PBP method' for the 'double deposition' NUSIMEP-7 test sample, which was expected to have two different isotopic compositions, is shown. As can be seen, two different major areas (i.e. two steps in the graph) of isotope ratios could be identified, indeed. In order to determine the isotopic compositions, the averages of the isotope ratios of these two areas were calculated. The data set was divided in two groups at the deflection point. Isotope ratios that were not within two times the standard deviation were not considered for calculating the average values. Isotope ratios that are between the two areas are typically considered as mixed ratios, whereas those at the lower and the upper end are typically regarded, dependent on their number, as other isotopic compositions or outliers resulting from the measurement.

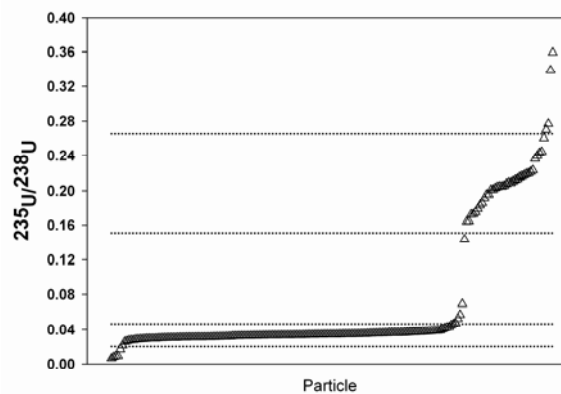


Fig. 2.2-3: Use of the 'PBP' method for the evaluation of the NUSIMEP-7 'double' deposition measurement data. $^{235}\text{U}/^{238}\text{U}$ isotope ratios are plotted in ascending order. The dotted lines are indicating the lower and the upper ends of the standard deviations (2σ).

Based on the 'PBP' method, two main isotopic compositions (i.e. 0.0340(76) and 0.210(46)) were identified. However, a comparison with the certified isotopic compositions (Table 2.2-1) yields that the sample had been contaminated with an ^{235}U enrichment of about 21 % from an unknown source and that one certified isotopic composition (i.e. 0.0090726(45)) was not identified. The isotope ratios at the lower and upper end of the step-profile were regarded as outliers as their number was rather small compared to the main isotopic compositions (one certified isotopic composition and the contamination). The drawbacks of this evaluation strategy for multiple isotopic signatures are evident: 1) low and high signal intensities are contributing equally to the isotope ratio, 2) the determination of the main compositions

depends on the judgment of the analyst and 3) other isotopic compositions present may be hidden by the major constituents.

In order to improve the data evaluation we made use of the principle of the linear regression slope method. All signal intensities of interest are plotted in an x-y-chart. Data from 9073-01-B and CRM U010 particle measurements were combined for a test data set in order to simulate a sample with particles of different known isotopic compositions. In Fig. 2.2-4A the scatter plot of this test data set is shown.

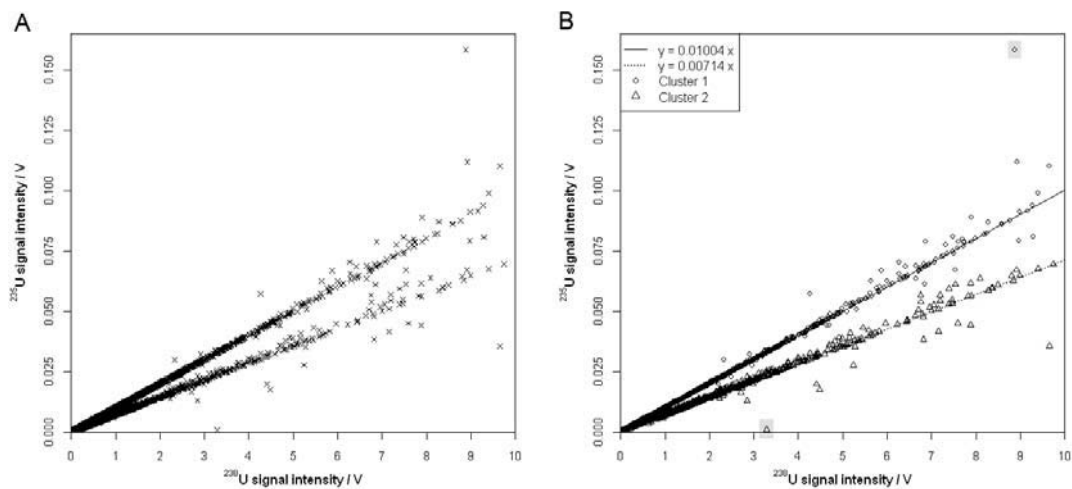


Fig. 2.2-4: Determination of two different $^{235}\text{U}/^{238}\text{U}$ isotope ratios by means of the slopes of linear regression lines applying the 'finite mixture model'. A) Scatter plot of a data set of 9073-01-B and CRM U010 particle measurements that were combined to one test data set. B) Application of the 'finite mixture model' to the test data set: the circles and the triangles are representing the two clusters (i.e. two isotopic signatures) that are distinguishable. The isotopic signatures are determined by means of the slope of the linear regression lines. The in the legend stated slopes are not externally corrected. Outliers are marked by grey colored rectangles.

At this step no differentiation between the data points of different isotopic compositions can be accomplished. A 'finite mixture model' was applied for the deconvolution of this data set to determine the different $^{235}\text{U}/^{238}\text{U}$ isotopic signatures. The data points are clustered, which is demonstrated by the two different symbols (i.e. circle and triangle) (Fig. 2.2-4B). Finally, the slopes of the linear relationships and the respective uncertainties of the clustered data points are estimated by the model (Grün and Leisch, 2008; Leisch, 2004). All selected data points are contributing to each linear fit and the regression lines are forced through the origin. Higher signal intensities have a larger leverage effect on the slope than lower ones, which is given by the model. In an additional step, the isotope ratios that are derived from the slope of the regression lines have to be corrected by means of the external correction factor $CF_{R_{^{235}\text{U}/^{238}\text{U}}}$

(equal to the other data evaluation strategies). In the case of the test data set, external correction was accomplished by means of IRMM-184.

Fixed residual variances, which are empirically determined by the model, were applied in order to circumvent the generation of a 'ghost' cluster that would collect all data points that are far off from the linear relationships with random distribution. Such a 'ghost' cluster would reflect a U isotopic composition not present in the particles.

The script of the 'finite mixture model' enables to easily trace back single data points that are far off from the computed linear regression lines to the raw data set. The test data set consists of two known certified $^{235}\text{U}/^{238}\text{U}$ isotopic signatures. Data points that are outside the uncertainty of the computed isotopic compositions (i.e. slopes) can be excluded and the model is recalculated. The principle of outlier detection is discussed for two data points marked in Fig. 2.2-4B. The outliers resulted from different decay times of the applied Faraday detectors. The transient signals revealed that the Faraday detector L1 (^{238}U) had been saturated just before the signal of the outlier was recorded. Therefore these data points were regarded as measurement artifacts and excluded from the regression. Outlier elimination resulted in a reduction of the bias of the determined isotopic signatures from the certified values (from 0.2 % to -0.03 % for 9073-01-B and from 0.6 % to 0.5 % for U010) and reduced the uncertainties of the slope (from 14 % to 10 % for 9073-01-B and from 10 % to 7 % for U010). Expanded uncertainties (eqs. 2-4) of 19 % ($k=2$) and 14 % ($k=2$), were computed for the $^{235}\text{U}/^{238}\text{U}$ isotopic signature of 9073-01-B (i.e. 0.00725) and U010 (i.e. 0.01019), respectively. The major contributor to the uncertainty is the uncertainty of the slope which is determined by the fixed residual variances of the model.

3.3. Application of the 'finite mixture model' to NUSIMEP-7 interlaboratory comparison test samples

The 'finite mixture model' was applied to the ^{235}U and ^{238}U measurement data of the NUSIMEP-7 interlaboratory comparison test samples in order to investigate its applicability for the determination of different unknown U isotopic compositions. The clusters and linear regression lines that were computed for both the 'single' and the 'double' deposition samples by the 'finite mixture model' are shown in Fig. 2.2-5.

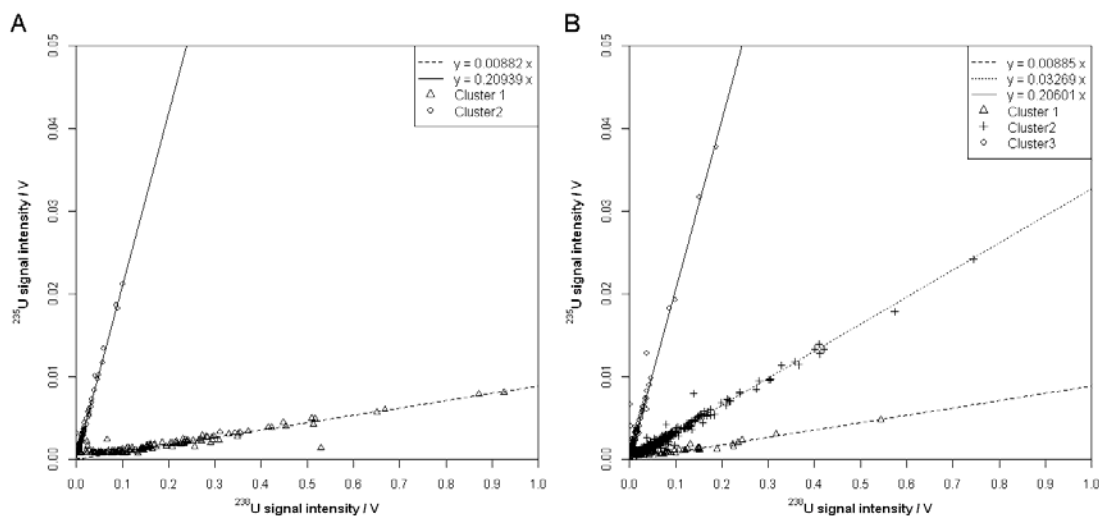


Fig. 2.2-5: Application of the finite mixture model to the blank corrected ^{235}U and ^{238}U measurement data of the NUSIMEP-7 inter-laboratory comparison test samples (A: NUSIMEP 7 single deposition; B: NUSIMEP 7 double deposition). A contamination during sample handling with a ^{235}U enrichment of about 21 % was detected on both planchets.

The ‘finite mixture model’ yielded $^{235}\text{U}/^{238}\text{U}$ isotopic compositions that were, within their uncertainties, in good agreement with the certified values (see Table 2.2-5). Both test samples had been contaminated with a ^{235}U enrichment of about 21 %. Thus, one additional isotopic composition was determined for both the ‘single’ and ‘double deposition’ test samples. The additional isotopic composition of the contaminant is in agreement between the two test samples indicating the same (unknown) source of contamination.

Table 2.2-5: Summary of NUSIMEP-7 results

NUSIMEP-7 test sample	$^{235}\text{U}/^{238}\text{U}$	CRM for external correction	RU (k=2) / %	Bias from certified value	z score [‡]	zeta score [‡]	Cluster size / data points
‘single’ deposition	0.00898(90)	IRMM-184	10.0	-1.0 %	-2.04	-0.21	144
	0.2130(10)	CRM U500	0.5	*	*	*	119
‘double’ deposition	0.0090(11)	IRMM-184	12.2	-0.7 %	-1.60	-0.13	29
	0.0332(10)	CRM U030-A	3.0	-2.6 %	-5.55	-1.89	633
	0.2096(11)	CRM U500	0.5	*	*	*	122

* contamination

[‡]interpretation of scores: $|\text{score}| \leq 2$: satisfactory result; $2 < |\text{score}| < 3$: questionable result; $|\text{score}| > 3$: unsatisfactory result

Moreover, z and zeta scores were calculated in order to assess the performance of LA-MC-ICPMS measurements, using the ‘finite mixture model’ for data evaluation, with respect to the stringent performance criteria of the NUSIMEP-7 ILC for the major U ($^{235}\text{U}/^{238}\text{U}$) isotope ratio (Truyens et al., 2011). As can be seen in Table 2.2-5, some measurements could not be performed in accordance with measurements considered as good practice for IAEA Network Analytical Laboratories (NWAL). However it has to be stressed that less than 50 % of the NUSIMEP-7 participants reported satisfactory results (i.e. 47 % for the ‘single’ deposition, 41 % for the 1st enrichment and 35 % for the 2nd enrichment of the ‘double deposition’). In case of the 2nd enrichment, satisfactory results were only achieved by large geometry-secondary ion mass spectrometry (LG-SIMS), nanoSIMS and secondary electron microscope-thermal ionization mass spectrometry (SEM-TIMS) measurements. In addition, laboratories, including also NWAL laboratories, using small geometry SIMS instruments could not achieve satisfactory z scores as well, even though SIMS is a mainstay technique for the analysis of the particle samples of interest (Truyens et al., 2011). Worth mentioning is that the organizers stated in their NUSIMEP-7 report (Truyens et al., 2011) that questionable results would still have been satisfactory when applying the less stringent performance criteria from NUSIMEP-6, the previous ILC (Truyens et al., 2011). However, disregarding the z scores, reported isotopic compositions that were determined by LA-ICPMS were in good agreement within their uncertainties — which were larger than uncertainties reported for e.g. SIMS measurements — with the certified values (Truyens et al., 2011). A good agreement with the certified isotopic compositions was also achieved, as aforementioned, in this study by applying the ‘finite mixture model’ to LA-MC-ICPMS ^{235}U and ^{238}U measurement data.

Regarding the zeta scores, satisfactory results (i.e. $|\text{score}| \leq 2$) were achieved for all isotopic compositions, which indicates that the estimate of the uncertainties are consistent with the deviations from the reference value (Truyens et al., 2011).

In the ‘finite mixture model’ the whole computation — blank correction, data selection by means of $3 \times \text{SD}$, determination of the number of clusters, computation of the slope and of its uncertainty — of the data set having about 50000 data points (including the blank measured in between the particle signals) is accomplished automatically by the applied algorithm. Thus, information about the isotopic composition is readily available. Moreover, data evaluation is not influenced by the analyst. In addition, the application of the ‘finite mixture model’ to the NUSIMEP-7 ‘double deposition’ sample (Table 2.2.-5) demonstrated the model’s strength for the determination of an accurate isotopic signature of a rather small population (i.e. 29 data points) present besides two larger ones (i.e. 122 and 633 data points).

4. Conclusions

In this study four different data treatment strategies for the computation of $^{235}\text{U}/^{238}\text{U}$ isotope ratios of single particles from transient signals were evaluated. Generally, strategies in which higher signal intensities are having a higher impact on the isotope ratio ('integration' and 'linear regression slope' method) are regarded as advantageous from a statistical point of view. However, these methods can only be applied if individual particles can be analyzed and if the resulting peak consists of multiple data points. Considering real safeguards samples, an individual selection of the particles to be analyzed is often not feasible using LA-MC-ICPMS without pre-selection by means of for example fission track or scanning electron microscopy. Hence, the resulting peak may consist of data points from several particles having different isotopic compositions. Moreover, depending on the size of the particles only one data point may be available for subsequent data treatment. The in this case commonly applied 'point by point' method bears the danger to overlook isotopic compositions of particles being underrepresented on the planchet. A 'finite mixture model' based on linear regression enables to identify an unknown number of entities of different isotopic composition, thus providing a significant contribution to fields dealing with multiple isotope ratios in mixed samples.

Using the 'finite mixture' model for the evaluation of LA-MC-ICPMS measurement data resulting from the analysis of NUSIMEP-7 ILC particles allowed accurately determining the $^{235}\text{U}/^{238}\text{U}$ certified isotopic compositions of both the 'single' and the 'double' deposition sample. Zeta scores revealed that the estimates of the uncertainties were consistent with the deviations from the reference values. The reproducibility, which is presented by the slope of the linear regression, was identified as main contributor. Even though in this study only results for the major U isotope ratio ($^{235}\text{U}/^{238}\text{U}$) were shown, the model is equally applicable for the determination of $^{234}\text{U}/^{238}\text{U}$ and $^{236}\text{U}/^{238}\text{U}$. The minor U isotope ratios are equally important in nuclear safeguards and forensics for verifying the absence of undeclared nuclear activities. The applicability of LA-MC-ICPMS for the determination of the minor U isotopes was demonstrated in a recent study (Kappel et al., 2012) as well as by others that used LA-ICPMS within the course of the NUSIMEP-7 ILC (Truyens et al., 2011). LA-MC-ICPMS is a promising technique for single particle analysis as its use may extend safeguards-relevant information that can be gained from the analysis of swipe and/or environmental samples. It offers higher sensitivity than TIMS, which is of advantage for the analysis of particles with low U amounts as well as for the analysis of environmental matrices. Another advantage of LA-MC-ICPMS for analyzing particles embedded in complex matrices is that it is less prone to molecular interferences than SIMS, which use for the analysis of such samples may be limited due to the occurrence of molecular

interferences at the mass-to-charge ratios of the U isotopes of interest. Nonetheless, LA-MC-ICPMS is limited with regard to the individual selection of particles for analysis, which bears the danger of determining mixed isotope ratios. Thus, pre-selection of particles is regarded as a necessity for subsequent LA-MC-ICPMS analysis.

Acknowledgements

The Austrian Science Fund FWF (START project 267-N11) and the International Atomic Energy Agency are highly acknowledged for financial support. The authors also thank Thomas Konegger from the Institute of Chemical Technologies and Analytics at the Vienna University of Technology for performing the scanning electron microscope analyses of the particles. We also thank Stefan Bürger for the fruitful discussions about uncertainty propagations of U isotope ratio measurements. We thank Andreas Zitek for supporting this work with regard to the deconvolution of multiple isotope ratios in mixed samples.

2.3 Application III

Spatially Resolved Analysis of Plutonium Isotopes in Environmental Samples by using Laser Ablation MC-ICPMS³

Stefanie Kappel^a, Sergei F. Boulyga^{b*} and Thomas Prohaska^a

^aUniversity of Natural Resources and Life Sciences, Vienna, Department of Chemistry, Division of Analytical Chemistry–VIRIS-Laboratory, Konrad Lorenzstrasse 24, 3430 Tulln, Austria

^b Safeguards Analytical Services, Department of Safeguards, International Atomic Energy Agency, Wagramer Strasse 5, 1400 Vienna, Austria

* Corresponding author: Sergei F. Boulyga, Safeguards Analytical Services, Department of Safeguards, International Atomic Energy Agency, Wagramer Strasse 5, 1400 Vienna, Austria, E-mail: s.bulyha@iaea.org

³ Prepared for submission

ABSTRACT

This study discusses the application of laser ablation (LA) – multi collector (MC) – ICPMS for spatially resolved plutonium fingerprinting in micro-samples (particles with sizes of 50 μm to 1000 μm) that originate from the vicinity of the Chernobyl nuclear power plant in order to investigate the variation of the Pu isotopic composition in the Chernobyl fallout, which is reported here for the first time. Such analytical results are helpful for the identification of contamination sources, providing valuable information for emergency and response actions in the case of a nuclear incident. The determined $^{242}\text{Pu}/^{239}\text{Pu}$ and $^{240}\text{Pu}/^{239}\text{Pu}$ isotope ratios in the micro-samples reveal a correlation from low to high ratios, ranging from 0.007(2) to 0.047(8) for $^{242}\text{Pu}/^{239}\text{Pu}$ and from 0.183(13) to 0.577(40) for $^{240}\text{Pu}/^{239}\text{Pu}$. That variation reflects differences in the composition of spent fuel over the reactor core. The measured Pu isotopic signatures accord well with the Pu isotopic composition distribution that is typical for a RBMK-1000 reactor. Moreover, the average Pu isotope ratios calculated for all investigated micro-samples ($n=35$) correspond to previously published results of bulk Pu analysis in contaminated samples from the vicinity of Chernobyl.

Keywords: Plutonium Isotope Ratios, Environmental Contamination, Chernobyl Nuclear Power Plant, (MC)-ICP-MS, Laser Ablation

1. Introduction

Monitoring of environmental contaminations with actinides is of special interest for the assessment of hazards for humans (Perelygin and Chuburkov, 1997; Taylor, 1995), of the impact on flora and fauna as well as for the evaluation of radiation protection (Salbu, 2009). Moreover, the determination of origin and intended use of, for example, seized nuclear material as well as undeclared activities in a nuclear facility is of particular importance for nuclear safeguards (Donohue, 2002) and nuclear forensics (Mayer et al., 2007).

Radionuclides are mainly released into the environment during nuclear accidents or nuclear fuel cycle operations, which include releases from reprocessing plants or waste deposits (Hu et al., 2010; Salbu and Lind, 2005). Large amounts of Pu were released into the environment as a consequence of stratospheric nuclear weapons tests that took place between 1945 and 1975 (Carter and Moghissi, 1977). That Pu input into the ecosystem is known as ‘global fallout’, which reached its maximum around 1963 (Ketterer and Szechenyi, 2008). The Pu isotopic signature of this global fallout is well known. Kelley et al. (Kelley et al., 1999), for example, monitored 54

locations around the world in order to establish regional Pu isotopic baselines for recognizing additional Pu inputs into the ecosystem. The mean ^{239}Pu concentration for the surface soil level is approximately $10^{-13} \text{ g g}^{-1}$. Pu concentrations of $\geq 10^{-12} \text{ g g}^{-1}$ are regarded as hazardous level when accumulated in the human body (Perelygin and Chuburkov, 1997).

About 1-2 % of the total Pu content in the environment (Perelygin and Chuburkov, 1997) was emitted during the accident at the 4th unit of the Chernobyl nuclear power plant (ChNPP-4) on the 26th of April 1986, whereupon the 30 – 100 km zone was mainly contaminated with fuel particles emitted from the reactor core (Kashparov et al., 2011; Kashparov et al., 2003). In general, these so-called hot particles are localized aggregations of radionuclides typically having high specific activities compared to the surrounding bulk material (Fesenko, 2011). Pu was associated with the U fuel matrix of the Chernobyl reactor. The deposited fuel particles varied, according to the scenarios during the accident, in their chemical composition, morphology and oxidation states (Kashparov et al., 2000). The fate of fuel particles in the environment depends, apart from their chemical properties, on environmental conditions (Kashparov et al., 2011). Non-oxidized particles are regarded as relatively chemically stable, whereas the oxidized fraction is more susceptible to weathering (Salbu et al., 2001) and dissolution in soil (Kashparov et al., 2011). The oxidation of the grain matrix leads to superficial cracking of the particle. This results in enhanced effective surfaces for dissolution. Higher dissolution rates are observed in both acid and alkaline conditions, whereas minimum rates are found at neutral conditions. An infiltration of the fuel particles with water leads to weathering, leaching and mobilization of radionuclides into the ecosystem (Kashparov et al., 2011). The fate of Pu isotopes in soil depends inter alia on the presence of humic or fulvic acids and humus promoting the formation of low-mobile complexes (Sokolik et al., 2001). Furthermore, it was observed that Pu from underground nuclear tests at the Nevada Test Site is mobilized by groundwater in form of colloidal material (Kersting et al., 1999). Another study by Xu et al. (Xu et al., 2008) showed that Pu is leached due to its complexation by chelating groups deriving from siderophores bound to cutin-derived soil degradation products.

Furthermore, fuel particles with associated radionuclides can be transformed into radioactive clusters (i.e. micro-samples) that reveal sizes of several hundreds of micrometer (Boulyga and Prohaska, 2008). Boulyga and Prohaska (Boulyga and Prohaska, 2008) observed different U isotopic compositions in an individual cluster from the Chernobyl relocation zone, assuming a kind of encapsulation of particles with differing U isotopic compositions in one micro-sample. The range of measured U isotopic compositions in several micro-samples was in good accordance with the expected range resulting from different burn-ups (Kashparov et al., 2011) of the fuel assemblies used in the ChNPP-4 (Boulyga and Prohaska, 2008). Hence, the variation

of the burn-up over the reactor core was also reflected in the U isotopic compositions of the fuel particles (Kashparov et al., 2011) that were emitted into the environment during the accident.

Alpha-spectrometry (Chamizo et al., 2010; Hrnccek et al., 2005; Vajda and Kim, 2010) as well as mass spectrometric techniques (inductively coupled plasma mass spectrometry (ICP-MS), thermal ionization mass spectrometry (TIMS) (Jakopic et al., 2010), resonance ionization mass spectrometry (RIMS) (Erdmann et al., 1997; Nunnemann et al., 1998) and accelerator mass spectrometry (AMS) (Chamizo et al., 2010; Hrnccek et al., 2005) are applied for the analysis of Pu isotopes in environmental samples. Alpha-spectrometry is a well-established method for the determination of alpha-emitting actinides having half-lives less than 1000 years. The analysis of long-lived radionuclides, especially when only small sample amounts are available, often requires more sensitive mass spectrometric techniques, in particular if radionuclides have low specific activities that are typical for environmental samples. For such analyses long measurement times (i.e. days to weeks) would be required. Another drawback of alpha-spectrometry for Pu isotope analysis is that just a sum activity of ^{239}Pu and ^{240}Pu can be obtained due to the similar alpha energies of these two isotopes (5.16 MeV for ^{239}Pu and 5.17 MeV for ^{240}Pu). The sample matrix has to be completely separated from the actinides of interest for the improvement of resolution (Hrnccek et al., 2005; Kim et al., 2007; Taylor et al., 2001).

The relevance of mass spectrometric methods in general and ICP-MS in particular for radionuclide analysis is highlighted by the number of reviews (Becker, 2003; Becker, 2005; Boulyga, 2011; Hou and Roos, 2008; Lariviere et al., 2006) dedicated to this topic. Ketterer and Szechenyi (Ketterer and Szechenyi, 2008) and Kim et al. (Kim et al., 2007) put an emphasis on Pu analysis by ICP-MS, whereat easy sample preparation, relatively low analysis costs, high sample throughput due to short analysis times and high sensitivity are regarded as merits of ICP-MS. In addition, the use of multi-collector (MC)-ICP-MS allows improving the precision of actinide isotope ratio measurements at ultra-trace concentration levels (i.e. fg g^{-1}) in bulk environmental samples (Becker, 2005; Taylor et al., 2001). A further advantage of (MC)-ICP-MS is the feasibility of coupling a laser ablation (LA) system for the direct analysis of environmental samples in order to spatially resolve the isotopic information stored in such samples (Boulyga and Prohaska, 2008). LA-ICP-MS also allows analyzing targets prepared for alpha-spectrometry. Thus, both methods can be easily applied in a complementary approach for environmental Pu monitoring (Boulyga et al., 2003; Cizdziel et al., 2008).

This study describes the application of LA-MC-ICP-MS for spatially resolved Pu fingerprinting on the example of micro-samples originating from the vicinity of the Chernobyl NPP. The usefulness of LA-MC-ICP-MS with regard to its application for the assessment of environmental

contamination sources in response to accidental events that involve potential emissions of nuclear materials is demonstrated.

2. Experimental

2.1. Samples and sample preparation

Micro-samples (i.e. hot particles embedded in a soil matrix) from the Chernobyl accident were sampled in the vicinity of the Chernobyl NPP (8 km to the north-west of Chernobyl NPP) in 1992. The soil samples were taken in an area that has remained anthropogenically untouched since the accident. Sampling, sample preparation as well as nuclear track radiography analyses for particle identification and localization were performed at the Institute of Power Engineering, Minsk, Belarus in 1992. Experimental details are given elsewhere (Boulyga and Prohaska, 2008). The identified micro-samples, which were measured by nuclear track radiography, yielded sizes and surface alpha activities from about 50 μm to 1000 μm and from 3 mBq to 38 mBq, respectively. The micro-samples were embedded in transparent membranes that were affixed to glass plates by means of commercially available glue. The glass plates, which are typically used for optical microscopy, were directly put into the laser ablation cell.

2.2. Reagents and certified reference material

The analyses of the Chernobyl micro-samples included measurements of 1 % (m/m) HNO_3 as blank solution and CRM U500 (New Brunswick Laboratory, U.S. Department of Energy, U.S.), a liquid U certified isotope reference material, for optimization and determination of external correction factors for correcting mass bias and secondary electron multiplier gain. 65 % (m/m) HNO_3 (analytical reagent grade, Merck KGaA, Darmstadt, Germany) was diluted with reagent grade type I water (18.2 $\text{M}\Omega\text{ cm}$ at 25 $^\circ\text{C}$, Ultra Clear Basic Reinstwassersystem, SG Wasseraufbereitung und Regenerierstation GmbH, Barsbüttel, Germany). Both were purified by sub-boiling distillation (Milestone-MLS GmbH, Leutkirch, Germany) prior to use.

2.3. Instrumentation: LA-MC-ICPMS

LA-MC-ICP-MS was selected as analytical technique for spatially-resolved isotope analysis in order to assess the variations of the Pu isotopic composition in micro samples collected in the vicinity of the Chernobyl NPP. The use of laser ablation for sample introduction enabled the

direct generation of an aerosol for MC-ICPMS analyses of individual micro-samples of interest. The high sensitivity of MC-ICP-MS enabled Pu isotope analysis at very low concentration levels. An additional advantage was that the dry aerosol produced by laser ablation reduced interferences by molecular ions, such as oxides and hydrides (Boulyga and Prohaska, 2008; Boulyga et al., 2004), which could affect the accuracy of Pu isotope ratio measurements.

Pu isotope ratio measurements were accomplished with a double-focusing high resolution sector field MC-ICPMS (Nu Plasma HR, Nu Instruments Limited, Wrexham, U.K.) coupled to a solid state nanosecond laser ablation system (UP 193, ESI-NWR Division, Electro Scientific Industries, Inc., Portland, CA, U.S.). In order to measure a liquid U certified reference material (i.e. CRM U500) for the determination of external correction factors in between the analyses of the solid micro-samples, a membrane desolvation system (DSN-100, Nu Instruments Limited, Wrexham, U.K.) was connected in parallel to the laser ablation system. The desolvation unit allows introducing a dry aerosol into the ICP. No solution was aspirated during laser ablation. A schematic diagram of this setup is given elsewhere (Boulyga and Prohaska, 2008). Instrumental parameters are summarized in Table 2.3-1.

Table 2.3-1: Instrumental parameters

Laser (New Wave 'UP 193')	
Ablation mode	Static point ablation
Wavelength / nm	193
Pulse length / ns	3
Energy density / J cm ⁻²	1.70 – 5.83
Power density / GW cm ⁻²	0.66 – 2.06
Repetition rate / Hz	10
Spot size / μm	100 - 120
Ar mix gas / L min ⁻¹	0.7
Liquid Sample Introduction	
System type	DSN
Nebulizer	PFA 100
Sample uptake rate / μL min ⁻¹	130
Nebulizer gas pressure / Pa	~ 2 x 10 ⁵
Nebulizer gas flow rate / L min ⁻¹	-
Hot gas / L min ⁻¹	~0.25
Membrane gas / L min ⁻¹	~1.4
Spraychamber temperature / °C	112 – 116
Membrane temperature / °C	119 – 123

MC-ICPMS (Nu Plasma HR)	
RF power / W	1300
Auxiliary gas / L min ⁻¹	0.95
Cool gas / L min ⁻¹	13
Mass separation	1
Isotopes monitored	²³⁵ U, ²³⁶ U, ²³⁸ U, ²³⁹ Pu, ²⁴⁰ Pu, ²⁴² Pu
Resolution m/Δm	300 (low resolution)
Detection system	IC0 ^a , IC1 ^a , IC2 ^a
<i>High voltages, source and transfer lenses parameters</i>	Optimized for optimal sensitivity
<i>Voltages applied to collector and multiplier</i>	Optimized for optimal peak shape and alignment
Data acquisition mode	TRA ^b (acquisition time per data point: 1 s)

^aSecondary electron multiplier

^bTime resolved analysis

The 'Nu Plasma HR' MC-ICP-MS collector block is equipped with twelve Faraday cups and three discrete-dynode secondary electron multipliers (i.e. IC1, IC0 and IC2), which allows to perform precise isotope ratio measurements. However, Pu isotopes are present in very low concentrations in environmental samples. Boulyga et al. (Boulyga et al., 2004) determined Pu concentrations in soil and sediment samples collected in the 10 km to 30 km relocation zone of the ChNPP in the 10⁻¹² to 10⁻¹¹ g g⁻¹ range. As Faraday cups are not sensitive enough for the detection of these very low Pu ion signals the Pu isotope ratio measurements could only be performed by using secondary electron multipliers for the detection of Pu isotopes. In order to simultaneously detect ²³⁹Pu⁺, ²⁴⁰Pu⁺ and ²⁴²Pu⁺ ions with three secondary electron multipliers, the standard collector block arrangement was modified by using a 'dog leg' deflector, which was inserted at the L4 Faraday cup position in order to guide the ion beam of ²³⁹Pu from the L4 position into IC2. A schematic diagram of this modified collector block is shown in Fig. 2.3-1.

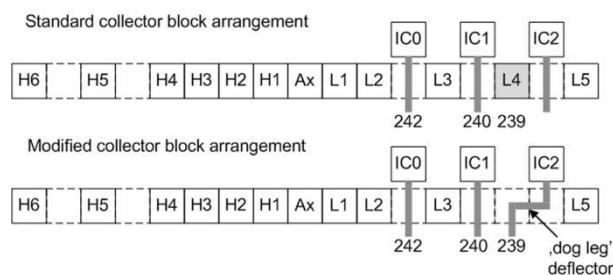


Fig. 2.3-1: Collector block arrangements of the 'Nu Plasma HR' MC-ICPMS (H...Faraday cup high mass side, Ax...Faraday cup axial mass, L...Faraday cup low mass side, IC...ion counting multiplier (i.e. secondary electron multiplier).

3. Data Processing

The measured ^{239}Pu , ^{240}Pu and ^{242}Pu signal intensities were recorded in time-resolved analysis mode with an acquisition time of one second per data point. A typical laser ablation analysis performing static point ablation lasted for about 20 – 40 seconds, excluding the time for the measurement of Ar as gas blank. Ar gas blanks were recorded for about ten seconds prior to the start of the ablation of the micro-samples in order to guarantee a complete wash-out of the previously performed analysis. The maximum recorded signal intensities per ablation ranged from about 160 – 600 000 cps for ^{239}Pu , 60 – 284 000 cps for ^{240}Pu and 7 – 19 000 cps for ^{242}Pu . Dead time correction of the measured intensities was automatically performed in the 'Nu Plasma' software, applying the previously determined dead times (i.e. IC0: 8.5 ns, IC1: 10 ns and IC2: 11 ns).

Calculation of the $^{242}\text{Pu}/^{239}\text{Pu}$ and $^{240}\text{Pu}/^{239}\text{Pu}$ isotope ratios was performed with the help of the slope of the regression lines of ^{242}Pu to ^{239}Pu and ^{240}Pu to ^{239}Pu scatter plots (Fietzke et al., 2008). The main advantage of this data processing strategy is that each data point, including the blank, is used for the evaluation and that the contribution of each data point to the linear fit depends on its signal intensity. Thus, higher signal intensities, usually yielding more precise data than lower signal intensities, are dominating the fit (Fietzke et al., 2008), which is of advantage when processing time resolved ablation profiles. Finally, the $^{242}\text{Pu}/^{239}\text{Pu}$ and $^{240}\text{Pu}/^{239}\text{Pu}$ isotope ratios were corrected for mass bias and secondary electron multiplier gain with external correction factors determined by measuring $^{238}\text{U}/^{235}\text{U}$ and $^{236}\text{U}/^{235}\text{U}$ isotope ratios in CRM U500 for at least ten minutes under the assumption of similar mass bias effects of Pu and U. ^{238}U was measured with IC0, whereas ^{236}U and ^{235}U were determined by means of IC1 and IC2. 1% (m/m) HNO_3 was analyzed for blank correction. Both the blank and the CRM U500 signal

intensities of the isotopes of interest were assessed by calculating an average of six blocks, where each block represented an average of 100 data points.

$^{242}\text{Pu}/^{239}\text{Pu}$ and $^{240}\text{Pu}/^{239}\text{Pu}$ isotope ratios of single static point ablations (i.e. number of LA analyses larger than two) on an individual micro-sample were pooled together if the isotope ratios yielded a homogenous distribution within the sample of interest. The $^{242}\text{Pu}/^{239}\text{Pu}$ and $^{240}\text{Pu}/^{239}\text{Pu}$ isotope ratios of one micro-sample were calculated as weighted means of replicate LA measurements, where the weighting factors were based on the theoretical precision of the measured signal intensities.

3.1. Uncertainty assessment

Computation of expanded ($k=2$) combined standard measurement uncertainties (U) was accomplished with the GUM Workbench Pro software (version 2.4, Metrodata GmbH, Weil am Rhein, Germany) according to ISO/GUM (ISO/IEC Guide 98-3:2008) and EURACHEM (EURACHEM / CITAC Guide CG 4) guidelines. Single parameters that were propagated for the expanded combined standard measurement uncertainties of both liquid and LA analyses included (1) blank (U500 measurements) and dark noise (analyses of micro-samples), (2) dead time, (3) secondary electron multiplier (SEM) gain and (4) repeatability of measurements. The within-measurement repeatability of the laser ablation analyses of micro-samples was calculated from the uncertainty of the slope of the linear regression, whereas the within-measurement repeatability of the liquid measurements was calculated from the standard deviation of six measurement blocks.

Uncertainties of the certified $^{238}\text{U}/^{235}\text{U}$ and $^{236}\text{U}/^{235}\text{U}$ isotope ratios and $^{238}\text{U}^+$ peak tailing at the mass $m-2 u$ (i.e. 1×10^{-6}) as well as $^{235}\text{U}^1\text{H}$ hydride formation were additionally propagated for U500 measurements. However, peak tailing did not significantly contribute to the expanded combined standard measurement uncertainties. This can be explained by the fact that peak tailing is less pronounced for small ratios as is the case for $^{236}\text{U}/^{235}\text{U}$ (i.e. 0.0015192(31)). Since the $^{242}\text{Pu}/^{239}\text{Pu}$ and $^{240}\text{Pu}/^{239}\text{Pu}$ isotope ratios of the Chernobyl samples were in the same order of magnitude or smaller, peak tailing of ^{239}Pu into the masses of ^{240}Pu and ^{242}Pu was neglected in the uncertainty propagation of the micro-samples.

Peak tailing effects of $^{238}\text{U}^+$ ions, originating from U present in the analyzed micro-sample cluster, into the masses of the Pu isotopes of interest were additionally propagated. Determination of this peak tailing effects was accomplished by measuring U500 at an axial mass of $m=245 u$. This procedure allowed assessing the peak tailing of $^{238}\text{U}^+$ ions at the masses $m+1 u$,

$m+2 u$ and $m+4 u$. The relative intensities at the masses $m=242 u$, $m=240 u$ and $m=239 u$ that have been normalized to the intensity of $^{238}\text{U}^+$ ions were about 4×10^{-7} , 3×10^{-6} and 3×10^{-5} . The relative intensities at the masses of $m=242 u$ and $m=240 u$ are reflecting the peak tailing from $^{238}\text{U}^+$ ions, whereas the relative intensities at the mass $m+1 u$ are representing both peak tailing and a contribution from the formation of $^{238}\text{U}^1\text{H}^+$ ions.

4. Results and Discussion

Fig. 2.3-2 presents measured Pu isotopic compositions in individual micro-samples that had smaller and larger sizes (Fig. 2.3-2A and Fig. 2.3-2B, respectively). An estimate of the sizes of the micro-samples can be derived from the respective ablation areas, which ranged from approximately 0.023 mm^2 – 0.034 mm^2 for smaller clusters and from 0.045 mm^2 – 0.147 mm^2 for larger ones. The isotopic compositions were calculated as weighted means of $^{242}\text{Pu}/^{239}\text{Pu}$ and $^{240}\text{Pu}/^{239}\text{Pu}$, respectively, isotope ratios determined per micro-sample if the isotope ratios did not yield a significant difference within the expanded ($k=2$) combined standard measurement uncertainties. The expanded uncertainties ($k=2$) for individual spot ablations ranged from 4.3 % to 46 % for $^{242}\text{Pu}/^{239}\text{Pu}$ and from 4.6 % to 12 % for $^{240}\text{Pu}/^{239}\text{Pu}$ isotope ratios. In case of $^{242}\text{Pu}/^{239}\text{Pu}$ isotope ratio measurements, repeatability of the LA measurements and ^{242}Pu blank were identified as main contributors, whereas blank contribution became less pronounced with higher ^{242}Pu count rates (i.e. larger than 100 cps). Repeatability of LA measurements and SEM gain variations for both liquid and LA measurements were identified as main contributors for $^{240}\text{Pu}/^{239}\text{Pu}$ isotope ratio measurements. The within-LA measurement repeatabilities for individual spot ablations ranged from 0.6 % to 34.0% and from 0.2 % to 5.1 % for $^{242}\text{Pu}/^{239}\text{Pu}$ and $^{240}\text{Pu}/^{239}\text{Pu}$, respectively. In comparison, external precisions (calculated as relative standard deviation of individual spot ablations per homogenous micro-sample) ranged from 0.3 % to 37.1 % and 0.2 % to 8.9 % for $^{242}\text{Pu}/^{239}\text{Pu}$ and $^{240}\text{Pu}/^{239}\text{Pu}$, respectively. All individual clusters presented in Fig. 2.3-2 were homogenous with regard to their Pu isotopic composition. However, significant differences were observed in the Pu isotope compositions measured in different micro-samples, whereas $^{242}\text{Pu}/^{239}\text{Pu}$ and $^{240}\text{Pu}/^{239}\text{Pu}$ isotope ratios of all micro-samples revealed a correlation from low to high ratios, ranging from 0.007(2) to 0.047(8) for $^{242}\text{Pu}/^{239}\text{Pu}$ and from 0.183(13) to 0.577(40) for $^{240}\text{Pu}/^{239}\text{Pu}$. As the majority of the investigated micro-samples (see Fig. 2.3-2) revealed a homogeneous isotopic composition, it can be concluded that those radioactive micro-samples were probably produced by particles that originated from the same reactor fuel assemblies.

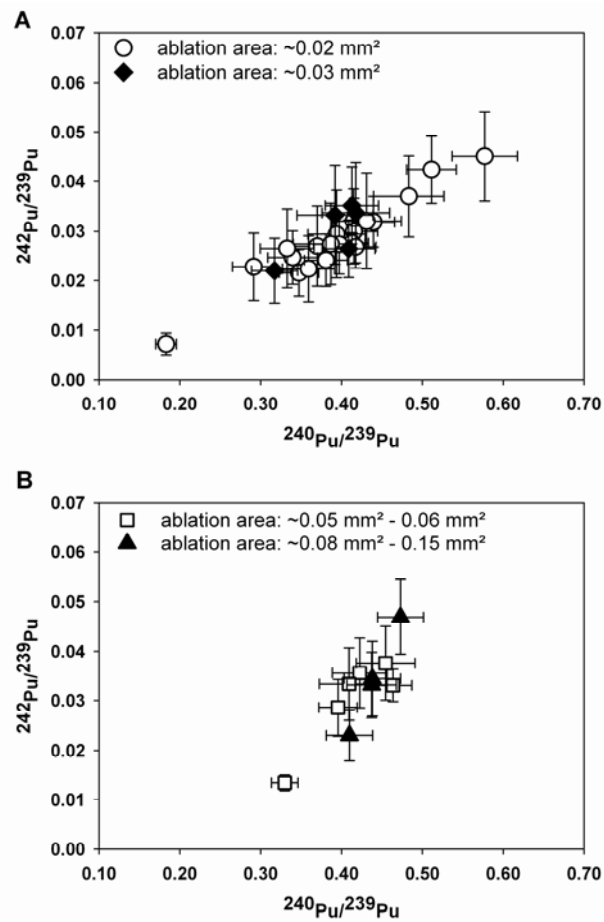


Fig. 2.3-2: Pu isotopic composition of micro-samples ($n=35$) collected in the vicinity of the ChNPP-4. The Pu isotope ratios were calculated as weighted means of $^{242}\text{Pu}/^{239}\text{Pu}$ and $^{240}\text{Pu}/^{239}\text{Pu}$, respectively, isotope ratios measured per micro-sample. The distribution of the Pu isotopic compositions is shown for smaller (A) and larger (B) clusters; the micro-sample size is expressed as size of the ablation area that was applied for Pu analysis. The error bars are indicating the expanded ($k=2$) combined standard measurement uncertainties.

If micro-samples were large enough it was possible to spatially resolve the Pu isotopic composition within individual micro-samples by applying several laser ablation spots to the micro-sample. Thus, two large micro-samples could be identified that yielded significant heterogeneities in the Pu isotopic composition (Fig. 2.3-3).

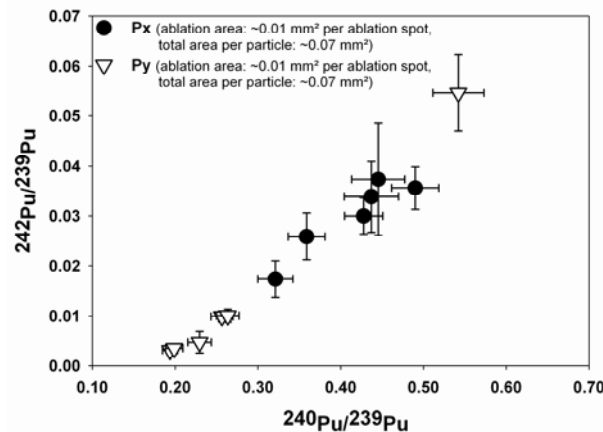


Fig. 2.3-3: Heterogeneous distribution of $^{242}\text{Pu}/^{239}\text{Pu}$ and $^{240}\text{Pu}/^{239}\text{Pu}$ isotope ratios measured in two micro-samples, Px and Py, collected in the vicinity of Chernobyl. The error bars are indicating the expanded ($k=2$) combined standard measurement uncertainties U_c ($k=2$).

These two micro-samples were obviously created by two or more particles, which originated from fuel assemblies with different burn-up grades, so that the isotopic composition of these micro-samples represent a mixture of several fuel particles with different burn-up grades. It should be noted that the mixed isotope ratios could also be produced due to insufficient spatial resolution of the applied analytical techniques, as both nuclear track radiography and laser ablation were not able to distinguish individual particles if distances between particles were smaller than $50\ \mu\text{m}$.

Boulyga and Prohaska (Boulyga and Prohaska, 2008) also observed heterogeneities in the U isotopic signature of micro-samples. They assumed a kind of encapsulation of particles with different U isotopic signatures in one micro-sample. It is still unclear if those particles got mixed during the explosion or during weathering and dissolution in soil. However, the presence of varying Pu or U isotopic signatures in one sample demonstrates the necessity of analytical methods that are capable of spatially resolving the inherent isotopic information.

An overview about previously published Pu isotope ratios determined in both soil and single hot particles is given in Table 2.3-2 for comparison. The average $^{242}\text{Pu}/^{239}\text{Pu}$ and $^{240}\text{Pu}/^{239}\text{Pu}$ isotope ratios calculated from the results of all micro-samples measured in this study are in a good agreement with the previously published results of bulk analysis of soil samples. However, it should be mentioned that very limited data have been published previously about the Pu isotope composition of individual particles (Boulyga et al., 1997; Wendt et al., 1999). The present study reports for the first time variations of Pu isotope ratios in the Chernobyl fallout, which could not be assessed previously. The observed variations can be explained by the fact that spent fuel was gradually replaced with freshly enriched uranium in the Chernobyl RBMK-

1000 reactor during its operation. That resulted in different irradiation histories, and thus, in varying burn-up grades of the fuel assemblies over the reactor core at the time of the accident (Begichev et al., 1990). The differences in the burn-up over the reactor core were reflected in different $^{242}\text{Pu}/^{239}\text{Pu}$ and $^{240}\text{Pu}/^{239}\text{Pu}$ isotope ratios in the fuel assemblies. While ^{239}Pu is generated via neutron capture in ^{238}U and subsequent β^- decay, ^{240}Pu , ^{241}Pu and ^{242}Pu are generated via neutron capture (n,γ) in ^{239}Pu . Hence, higher fuel burn-up led to an increase of the heavier Pu isotope fraction and as a consequence to higher $^{242}\text{Pu}/^{239}\text{Pu}$ and $^{240}\text{Pu}/^{239}\text{Pu}$ isotope ratios.

Table 2.3-2: Published Pu isotope ratios of Chernobyl fallout and reactor core.

Literature reference	$^{240}\text{Pu}/^{239}\text{Pu}$	$^{242}\text{Pu}/^{239}\text{Pu}$	Sample	Method
Muramatsu et al. (Muramatsu et al., 2000)	0.403(9)*	n.a.	Soil (n=8)	ICPMS
Boulyga and Becker (Boulyga and Becker, 2002)	0.396(14)*	n.a.	Soil (n=8)	ICPMS
Nunnemann et al. (Nunnemann et al., 1998)	0.394(2)‡	0.027(1)‡	Soil (n=1)	RIMS
Erdmann et al. (Erdmann et al., 1997)	0.378(2)*‡	0.024(1)*‡	Soil	RIMS
Boulyga et al. (Boulyga et al., 1997)	0.329(16)‡	0.021(3)‡	Hot particle (n=1)	RIMS
Wendt et al. (Wendt et al., 1999)	0.378(2)‡	0.088(1)‡	Hot particle (n=1)	RIMS
Kirchner and Noack (Kirchner and Noack, 1988)	0.56*†	0.044*†	Reactor core	Calculation
Begichev et al. (Begichev et al., 1990)	0.39*†	0.045*†	Reactor core	Calculation

*average values

‡ Isotope ratios were calculated from published isotopic compositions

† Isotope ratios were calculated from published activity data

Fig. 2.3-4 compares the measured Pu isotopic signatures in micro-samples with the Pu isotopic composition distribution that is typical for a RBMK-1000 reactor with the initial ^{235}U enrichment of about 2 %. The latter data was published by the Oak Ridge National Laboratory (ORIGEN-ARP, 2006). That study can be taken for comparison in the first approximation as the Chernobyl reactor exhibited similar characteristics. The Pu isotopic distribution, which is plotted according to increasing burn-ups of the spent-fuel of the RBMK-1000 reactor, follows a polynomial curve. As can be seen from Fig. 2.3-4 such a curve does also fit the distribution of the Pu isotopic signatures of all micro-samples analyzed in this study except in the case of just a few samples, which slightly deviate from the predicted distribution. Those deviations might occur due to the specific peculiarities of the nuclear core parameters of the Chernobyl reactor, which were not accounted for in the previous study (ORIGEN-ARP, 2006).

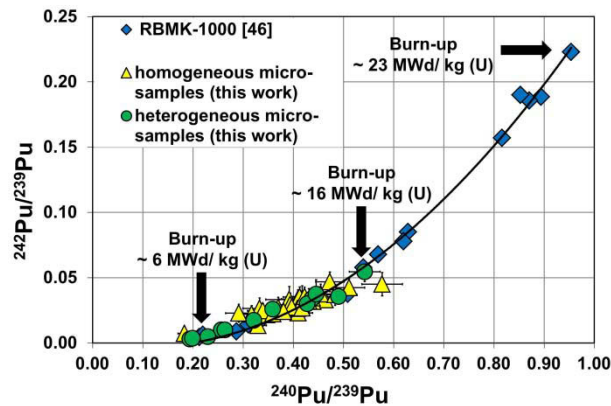


Fig. 2.3-4: Comparison of the Pu isotopic distribution with increasing burn-up in a RBMK-1000 reactor (ORIGEN-ARP, 2006)⁴ with the Pu isotopic distribution measured in micro-samples from the Chernobyl fallout.

5. Conclusions

Modern MC-ICP-MS instruments represent a highly efficient analytical tool for the analysis of Pu isotopic compositions of environmental samples, which allows identification of contamination sources and, thus provides valuable information for emergency and response actions in the case of a nuclear incident. In addition, implementation of laser ablation coupled to MC-ICP-MS allows a precise spatially resolved isotope analysis and provides more insight into specific signatures of contamination as has been demonstrated in this study on the example of $^{242}\text{Pu}/^{239}\text{Pu}$ and $^{240}\text{Pu}/^{239}\text{Pu}$ isotope ratio analysis in environmental micro-samples collected in the vicinity of Chernobyl NPP.

Acknowledgements

The Austrian Science Fund FWF (START project 267-N11) and the International Atomic Energy Agency are highly acknowledged for financial support. The authors also thank Urs Klötzli from the Department of Lithospheric Research at the University of Vienna for supporting us with the laser ablation system.

⁴ Please note that reference [46] in Fig. 2.3-4 refers to (ORIGEN-ARP, 2006). The different citation format results from the use of a different citation format in this thesis compared to that of the journal to which the manuscript will be submitted.

3 Summary and conclusions

In this thesis it was shown that LA-MC-ICPMS is a reliable and robust technique for providing high-quality U and Pu isotope ratio data measured in distinct individual particles (i.e. glass particles, uranium oxide particles, micro-samples from the Chernobyl fallout). Analytical method development and validation was accomplished using certified reference materials. Computation of expanded total combined standard uncertainty budgets enabled to assess the main contributors to the uncertainty, and thus to optimize the analysis.

Moreover, the evaluation of the applicability of different evaluation strategies was addressed as this step is crucial for determining accurate and precise isotope ratios. It was demonstrated that the newly developed data evaluation strategy using a so called 'finite mixture model' is a promising approach for the accurate determination of an unknown number of different isotopic compositions of an entity of particles. Apart from the potential use of this data processing strategy for swipe samples, the model may be useful in all fields dealing with the analysis of different isotopic signatures present in mixed samples.

The use of LA-MC-ICPMS additionally enabled to spatially resolve the Pu isotopic information stored in micro-samples from the Chernobyl fallout. Since no information about the variation of the Pu isotopic composition within the Chernobyl reactor core is available in literature, new insights are provided by the outcome of the accomplished work. Furthermore, the potential of LA-MC-ICPMS for analyzing and spatially resolving actinide isotopic compositions in environmental matrices could be demonstrated. The analysis of environmental matrices poses a challenge for both SIMS and TIMS. The application of SIMS is limited due to the presence of molecular interferences, whereas in TIMS the analysis of very low actinide amounts typically present in environmental samples is challenging due to its low sensitivity. In comparison, LA-MC-ICPMS provides higher sensitivity and is less prone to molecular interferences, which underlines the potential use of this technique for the analysis of environmental samples.

Summing up, it can be said that LA-MC-ICPMS is a state-of-the-art analytical technique for obtaining reliable isotopic information with regard to potentially safeguards-relevant particle samples. As LA-MC-ICPMS offers advantages especially for the analysis of environmental samples, it may most likely be routinely used in the future for resolving actinide isotopic information of particles embedded in environmental matrices. Nonetheless, as LA-MC-ICPMS is

also applicable for accurately determining the U isotopic compositions of individual particles, it may also be applied as a reference method in international safeguards for single particle analysis. However, an individual selection of particles with sizes in the low micrometer range is limited with this method, thus bearing the danger of determining mixed isotope ratios. Hence, future investigations have to focus on particle pre-selection, which is regarded as a pre-requisite for subsequent LA-MC-ICPMS analysis of individual particles.

The use of a fs-LA system is regarded as promising for improving U and Pu isotope ratio measurements in terms of accuracy and precision. The improvement of the precision is regarded as crucial as the reproducibility was identified as main contributor in combined uncertainty budgets. Thus, it represents the major parameter that has to be considered in future method development. Apart from the use of a fs-LA system, improved precision may also be achieved by increasing the sensitivity, using for example high-performance cones in combination with a high capacity interface pump. Increased sensitivity would result in higher signal intensities, and thus in more precise isotope ratio measurements.

In addition, future work should focus on the isotopic analysis of real safeguards samples in order to fully evaluate the applicability of LA-MC-ICPMS for a routine application. Moreover, representative safeguards particle samples should be analyzed with (FT-)TIMS, SIMS and LA-MC-ICPMS for a direct comparison in order to fully assess the merits and limitations of the different methods for different kinds of samples (i.e. uranium oxide particles, particles embedded in environmental matrices, etc.).

4 References

- Abdullah M, Ly A, Goldberg W, Clarke-Stewart K, Dudgeon J, Mull C, Chan T, Kent E, Mason A, Ericson J (2012) Heavy Metal in Children's Tooth Enamel: Related to Autism and Disruptive Behaviors? *Journal of Autism and Developmental Disorders* 42:929-936.
- Abrego Z, Ugarte A, Unceta N, Fernández-Isla A, Goicolea M A, Barrio R J (2012) Unambiguous Characterization of Gunshot Residue Particles Using Scanning Laser Ablation and Inductively Coupled Plasma-Mass Spectrometry. *Analytical Chemistry* 84:2402-2409.
- Admon U (2009). Single particles handling and analyses, In: Oughton D H, Kashparov V (Eds.), *Radioactive Particles in the Environment*. Springer Science + Business Media B.V.
- Aeschliman D B, Bajic S J, Baldwin D P, Houk R S (2003) High-speed digital photographic study of an inductively coupled plasma during laser ablation: comparison of dried solution aerosols from a microconcentric nebulizer and solid particles from laser ablation. *Journal of Analytical Atomic Spectrometry* 18:1008-1014.
- Albarède F, Telouk P, Blichert-Toft J, Boyet M, Agranier A, Nelson B (2004) Precise and accurate isotopic measurements using multiple-collector ICPMS. *Geochimica et Cosmochimica Acta* 68:2725-2744.
- Aregbe Y, Prohaska T, Stefanka Z, Széles É, Hubert A, Boulyga S (2011) Report on the Workshop on Direct Analysis of Solid Samples Using Laser Ablation-Inductively Coupled Plasma-Mass Spectrometry (LA-ICP-MS) -Organised by the ESARDA Working Group on Standards and Techniques for Destructive Analysis (WG DA). *Esarda Bulletin* 46:136-145.
- Argonne National Laboratory E (2005) Natural Decay Series: Uranium, Radium, and Thorium. Human Health Fact Sheet. <http://www.ead.anl.gov/pub/doc/natural-decay-series.pdf>. Accessed 7 November 2012
- Axelsson A, Fischer D M, Pécnin M V (2009) Use of data from environmental sampling for IAEA safeguards. Case study: Uranium with near-natural ^{235}U abundance. *Journal of Radioanalytical and Nuclear Chemistry* 282:725-729.
- Ball L, Sims K W W, Schwieters J (2008) Measurement of $^{234}\text{U}/^{238}\text{U}$ and $^{230}\text{Th}/^{232}\text{Th}$ in volcanic rocks using the Neptune MC-ICP-MS. *Journal of Analytical Atomic Spectrometry* 23:173-180.
- Ballihaut G, Clavierie F, Pécheyran C, Mounicou S, Grimaud R, Lobinski R (2007) Sensitive detection of selenoproteins in gel electrophoresis by high repetition rate femtosecond laser ablation-inductively coupled plasma mass spectrometry. *Analytical Chemistry* 79:6874-6880.
- Barst B D, Gevertz A K, Chumchal M M, Smith J D, Rainwater T R, Drevnick P E, Hudelson K E, Hart A, Verbeck G F, Roberts A P (2011) Laser Ablation ICP-MS Co-Localization of Mercury and Immune Response in Fish. *Environmental Science & Technology* 45:8982-8988.
- Batey J H, Prohaska T, Horstwood M, Nowell G M, Goenaga-Infante H, Eiden G C (2005). Mass Spectrometers, In: Nelms S M (ed), *Inductively Coupled Plasma Mass Spectrometry Handbook*. Blackwell Publishing Ltd, Blackwell Publishing Ltd.
- Becker J S (2003) Mass spectrometry of long-lived radionuclides. *Spectrochim Acta B* 58:1757-1784.
- Becker J S (2005) Inductively coupled plasma mass spectrometry (ICP-MS) and laser ablation ICP-MS for isotope analysis of long-lived radionuclides. *International Journal of Mass Spectrometry* 242:183-195.
- Becker J S, Sela H, Dobrowolska J, Zoriy M, Becker J S (2008) Recent applications on isotope ratio measurements by ICP-MS and LA-ICP-MS on biological samples and single particles. *International Journal of Mass Spectrometry* 270:1-7.
- Begichev S N, Borovoj A A, Burlakov E B, Gagarinsky A J, Demin V F, Khrulev A A, Khodakovskiy I L (1990). Fission product transport processes in reactor accidents, In: Rogers J T (ed). *Hemisphere New York*, pp. 717-734.
- Berglund M, Wieser M (2011) Isotopic compositions of the elements 2009 (IUPAC Technical Report). *Pure and Applied Chemistry* 83 (2):397-410.
- Betti M (2003) Civil use of depleted uranium. *Journal of Environmental Radioactivity* 64:113-119.

4 References

- Betti M (2005) Isotope ratio measurements by secondary ion mass spectrometry (SIMS) and glow discharge mass spectrometry (GDMS). *International Journal of Mass Spectrometry* 242:169-182.
- Betti M, Tamborini G, Koch L (1999) Use of Secondary Ion Mass Spectrometry in Nuclear Forensic Analysis for the Characterization of Plutonium and Highly Enriched Uranium Particles. *Analytical Chemistry* 71:2616-2622.
- Bian Q, Garcia C C, Koch J, Niemax K (2006) Non-matrix matched calibration of major and minor concentrations of Zn and Cu in brass, aluminium and silicate glass using NIR femtosecond laser ablation inductively coupled plasma mass spectrometry. *Journal of Analytical Atomic Spectrometry* 21:187-191.
- Bleise A, Danesi P R, Burkart W (2003) Properties, use and health effects of depleted uranium (DU): a general overview. *Journal of Environmental Radioactivity* 64:93-112.
- Borisova A Y, Freyrier R, Polvé M, Salvi S, Candaudap F, Aigouy T (2008) In situ multi-element analysis of the Mount Pinatubo quartz-hosted melt inclusions by NIR femtosecond laser ablation-inductively coupled plasma-mass spectrometry. *Geostandards and Geoanalytical Research* 32:209-229.
- Boulyga S F (2011) Mass spectrometric analysis of long-lived radionuclides in bio-assays. *International Journal of Mass Spectrometry* 307:200-210.
- Boulyga S F, Becker J S (2002) Isotopic analysis of uranium and plutonium using ICP-MS and estimation of burn-up of spent uranium in contaminated environmental samples. *Journal of Analytical Atomic Spectrometry* 17:1143-1147.
- Boulyga S F, Desideri D, Meli M A, Testa C, Becker J S (2003) Plutonium and americium determination in mosses by laser ablation ICP-MS combined with isotope dilution technique. *International Journal of Mass Spectrometry* 226:329-339.
- Boulyga S F, Erdmann N, Funk H, Kievets M K, Lomonosova E M, Mansel A, Trautmann N, Yaroshevich O I, Zhuk I V (1997) Determination of isotopic composition of plutonium in hot particles of the Chernobyl area. *Radiation Measurements* 28:349-352.
- Boulyga S F, Heumann K G (2006) Determination of extremely low $^{236}\text{U}/^{238}\text{U}$ isotope ratios in environmental samples by sector-field inductively coupled plasma mass spectrometry using high-efficiency sample introduction. *Journal of Environmental Radioactivity* 88:1-10.
- Boulyga S F, Kievitskaja A I, Kievets M K, Lomonosova E M, Zhuk I V, Yaroshevich O I, Perelygin V P, Petrova R, Brandt R, Vater P (1999a) Nuclear track radiography of "hot" aerosol particles. *Radiation Measurements* 31:191-196.
- Boulyga S F, Klötzli U, Prohaska T (2006) Improved abundance sensitivity in MC-ICP-MS for determination of $^{236}\text{U}/^{238}\text{U}$ isotope ratios in the 10^{-7} to 10^{-8} range. *Journal of Analytical Atomic Spectrometry* 21:1427-1430.
- Boulyga S F, Lomonosova E M, Zhuk I V, Yaroshevich O I, Kudrjashov V P, Mironov V P (1999b) Experimental study of radioactive aerosols in the vicinity of the Chernobyl Nuclear Power Plant. *Radiation Measurements* 30:703-707.
- Boulyga S F, Prohaska T (2008) Determining the isotopic compositions of uranium and fission products in radioactive environmental microsamples using laser ablation ICP-MS with multiple ion counters. *Analytical and Bioanalytical Chemistry* 390:531-539.
- Boulyga S F, Tibi M, Heumann K G (2004) Application of isotope-dilution laser ablation ICP-MS for direct determination of Pu concentrations in soils at pg g^{-1} levels. *Analytical and Bioanalytical Chemistry* 378:342-347.
- Brunner M, Katona R, Stefánka Z, Prohaska T (2010) Determination of the geographical origin of processed spice using multielement and isotopic pattern on the example of Szegedi paprika. *European Food Research and Technology* 231:623-634.
- Bu K, Cizdziel J V, Reidy L (2012) Analysis of herbal supplements for selected dietary minerals and trace elements by laser ablation- and solution-based ICPMS. *Microchemical Journal* 106:244-249.
- Bürger S, Essex R M, Mathew K J, Richter S, Thomas R B (2010) Implementation of Guide to the expression of Uncertainty in Measurement (GUM) to multi-collector TIMS uranium isotope ratio metrology. *Int J Mass Spectrom* 294:65-76.
- Carter M W, Moghissi A A (1977) Three Decades of Nuclear Testing. *Health Physics* 33:55-71.
- Chamizo E, Jiménez-Ramos M C, Enamorado S M, García-León M, García-Tenorio R, Mas J L, Masqué P, Merino J, Sanchez-Cabeza J A (2010) Characterisation of the plutonium isotopic composition of a sediment core from Palomares, Spain, by low-energy AMS and alpha-spectrometry. *Nucl Instrum Meth B* 268:1273-1276.
- Chang M-Y, Geffen A, Kosler J, Dundas S, Consortium F, Maes G (2012) The effect of ablation pattern on LA-ICPMS analysis of otolith element composition in hake, *Merluccius merluccius*. *Environmental Biology of Fishes* 95:509-520.

4 References

- Choi I, Song K, Park Y J, Kim J-Y, Yoo H-S (2010) Isotopic analysis of metallic and coated microparticles by laser ablation time-of-flight mass spectrometry (LA-TOF-MS). *Microchemical Journal* 95:38-42.
- Ciurapinski A, Parus J, Donohue D (2002) Particle analysis for a strengthened safeguards system: Use of a scanning electron microscope equipped with EDXRF and WDXRF spectrometers. *Journal of Radioanalytical and Nuclear Chemistry* 251:345-352.
- Cizdziel J, Bu K, Nowinski P (2012) Determination of elements in situ in green leaves by laser ablation ICP-MS using pressed reference materials for calibration. *Analytical Methods* 4:564-569.
- Cizdziel J V, Ketterer M E, Farmer D, Faller S H, Hodge V F (2008) 239 , 240 , 241 Pu fingerprinting of plutonium in western US soils using ICPMS: Solution and laser ablation measurements. *Analytical and Bioanalytical Chemistry* 390:521-530.
- Clark D L, Hecker S S, Jarvinen G D, Neu M P (2006). Plutonium, In: Morris L R, Edelstein N M, Fuger J, Katz J J (Eds.), *The Chemistry of the Actinide and Transactinide Elements*. 3rd edition. Volume 2. , 3rd ed. Springer.
- Claverie F, Fernandez B, Pecheyran C, Alexis J, Donard O F X (2009a) Elemental fractionation effects in high repetition rate IR femtosecond laser ablation ICP-MS analysis of glasses. *Journal of Analytical Atomic Spectrometry* 24:891-902.
- Claverie F, Pécheyran C, Mounicou S, Ballihaut G, Fernández B, Alexis J, Lobinski R, Donard O F X (2009b) Characterization of the aerosol produced by infrared femtosecond laser ablation of polyacrylamide gels for the sensitive inductively coupled plasma mass spectrometry detection of selenoproteins. *Spectrochimica Acta - Part B Atomic Spectroscopy* 64:649-658.
- Compernelle S, Wambeke D, De Raedt I, Vanhaecke F (2012) Evaluation of a combination of isotope dilution and single standard addition as an alternative calibration method for the determination of precious metals in lead fire assay buttons by laser ablation-inductively coupled plasma-mass spectrometry. *Spectrochimica Acta Part B: Atomic Spectroscopy* 67:50-56.
- Cottle J M, Horstwood M S A, Parrish R R (2009) A new approach to single shot laser ablation analysis and its application to in situ Pb/U geochronology. *J Anal At Spectrom* 24:1355-1363.
- D'Abzac F X, Poitrasson F, Freydier R, Seydoux-Guillaume A M (2010) Near Infra Red femtosecond Laser Ablation: The influence of energy and pulse width on the LA-ICP-MS analysis of monazite. *Journal of Analytical Atomic Spectrometry* 25:681-689.
- D'Abzac F X, Seydoux-Guillaume A M, Chmeleff J, Datas L, Poitrasson F (2011) Study of near infra red femtosecond laser induced particles using transmission electron microscopy and low pressure impactation: Implications for laser ablation-inductively coupled plasma-mass spectrometry analysis of natural monazite. *Spectrochimica Acta - Part B Atomic Spectroscopy* 66:671-680.
- da Silva M, Arruda M, 2012. Identification of selenium in the leaf protein of sunflowers by a combination of 2D-PAGE and laser ablation ICP-MS, *Microchimica Acta*. Springer Wien, pp. 131-136.
- Darling J R, Storey C D, Engi M (2012) Allanite U-Th-Pb geochronology by laser ablation ICPMS. *Chemical Geology* 292-293:103-115.
- Domingo J L (2001) Reproductive and developmental toxicity of natural and depleted uranium: a review. *Reproductive Toxicology* 15:603-609.
- Donohue D, Ciurapinski A, Cliff III J, Rüdener F, Kuno T, Poths J (2008) Microscopic studies of spherical particles for nuclear safeguards. *Applied Surface Science* 255:2561-2568.
- Donohue D L (1998) Strengthening IAEA safeguards through environmental sampling and analysis. *Journal of Alloys and Compounds* 271-273:11-18.
- Donohue D L (2002) Peer Reviewed: Strengthened Nuclear Safeguards. *Analytical Chemistry* 74:28 A-35 A.
- Drysdale R N, Paul B T, Hellstrom J C, Couchoud I, Greig A, Bajo P, Zanchetta G, Isola I, Spötl C, Banerchi I, Regattieri E, Woodhead J D (2012) Precise microsampling of poorly laminated speleothems for U-series dating. *Quaternary Geochronology* in press.
- Duffin A, Hart G, Hanlen R, Eiden G (2012) Isotopic analysis of uranium in NIST SRM glass by femtosecond laser ablation MC-ICPMS. *Journal of Radioanalytical and Nuclear Chemistry* 1-6.
- Dzurko M, Foucher D, Hintelmann H (2009) Determination of compound-specific Hg isotope ratios from transient signals using gas chromatography coupled to multicollector inductively coupled plasma mass spectrometry (MC-ICP/MS). *Analytical and Bioanalytical Chemistry* 393:345-355.

4 References

- Eggins S M, Kinsley L P J, Shelley J M G (1998) Deposition and element fractionation processes during atmospheric pressure laser sampling for analysis by ICP-MS. *Applied Surface Science* 127-129:278-286.
- Elemental Scientific. Cyclonic Spray Chambers. <http://www.icpms.com/products/cyclonic.php>. Accessed 13 November 2012.
- Meyers R A (ed) (2000). *Encyclopedia of Analytical Chemistry - Applications, Theory and Instrumentation*. John Wiley & Sons Ltd.
- Epov V N, Beraïl S, Jimenez-Moreno M, Perrot V, Pecheyran C, Amouroux D, Donard O F X (2010) Approach to Measure Isotopic Ratios in Species Using Multicollector-ICPMS Coupled with Chromatography. *Analytical Chemistry* 82:5652-5662.
- Erdmann N, Betti M, Stetzer O, Tamborini G, Kratz J V, Trautmann N, Van Geel J (2000) Production of monodisperse uranium oxide particles and their characterization by scanning electron microscopy and secondary ion mass spectrometry. *Spectrochimica acta, Part B: Atomic spectroscopy* 55:1565-1575.
- Erdmann N, Herrmann G, Huber G, Köhler S, Kratz J V, Mansel A, Nunnemann M, Passler G, Trautmann N, Turchin A, Waldek A (1997) Resonance ionization mass spectroscopy for trace determination of plutonium in environmental samples. *Fresenius' Journal of Analytical Chemistry* 359:378-381.
- Esaka F, Esaka K T, Lee C G, Magara M, Sakurai S, Usuda S, Watanabe K (2007) Particle isolation for analysis of uranium minor isotopes in individual particles by secondary ion mass spectrometry. *Talanta* 71:1011-1015.
- Esaka K T, Esaka F, Inagawa J, Iguchi K, Lee C G, Sakurai S, Watanabe K, Usuda S (2004) Application of fission track technique for the analysis of individual particles containing uranium in safeguard swipe samples. *Japanese Journal of Applied Physics* 43:915-916.
- EURACHEM / CITAC Guide CG 4 - Quantifying Uncertainty in Analytical Measurement (2000), 2nd edn.
- European co-operation for Accreditation. Expression of the Uncertainty of Measurement in Calibration. EA-4/02 M:1999.
- Evans R D, Hintelmann H, Dillon P J (2001) Measurement of high precision isotope ratios for mercury from coals using transient signals. *Journal of Analytical Atomic Spectrometry* 16:1064-1069.
- Everett S E, Tims S G, Hancock G J, Bartley R, Fifield L K (2008) Comparison of Pu and ¹³⁷Cs as tracers of soil and sediment transport in a terrestrial environment. *Journal of Environmental Radioactivity* 99:383-393.
- Fernández B, Claverie F, Pécheyran C, Alexis J, Donard O F X (2008a) Direct determination of trace elements in powdered samples by in-cell isotope dilution femtosecond laser ablation ICPMS. *Analytical Chemistry* 80:6981-6994.
- Fernández B, Claverie F, Pécheyran C, Donard O F X (2007) Direct analysis of solid samples by fs-LA-ICP-MS. *TrAC Trends in Analytical Chemistry* 26:951-966.
- Fernández B, Claverie F, Pécheyran C, Donard O F X (2008b) Solid-spiking isotope dilution laser ablation ICP-MS for the direct and simultaneous determination of trace elements in soils and sediments. *Journal of Analytical Atomic Spectrometry* 23:367-377.
- Fesenko S, 2011. *Radioactive particles in the Environment: Sources, Particle Characterization and Analytical Techniques*. International Atomic Energy Agency, Vienna.
- Feutry P, Tabouret H, Maeda K, Pécheyran C, Keith P (2012) Diadromous life cycle and behavioural plasticity in freshwater and estuarine Kuhlidae species (Teleostei) revealed by otolith microchemistry. *Aquatic Biology* 15:195-204.
- Fietzke J, Liebetrau V, Günther D, Gurs K, Hametner K, Zumholz K, Hansteen T H, Eisenhauer A (2008) An alternative data acquisition and evaluation strategy for improved isotope ratio precision using LA-MC-ICP-MS applied to stable and radiogenic strontium isotopes in carbonates. *Journal of Analytical Atomic Spectrometry* 23:955-961.
- Fisher D (1997) History of the International Atomic Energy Agency: the first forty years. http://www-pub.iaea.org/MTCD/publications/PDF/Pub1032_web.pdf. Accessed 21 August 2012.
- Fliegel D, Klementova M, Kosler J (2010) Phase and composition changes of titanite during laser ablation inductively coupled plasma mass spectrometry analysis. *Analytical Chemistry* 82:4272-4277.
- Fontaine G H, Hametner K, Peretti A, Günther D (2010) Authenticity and provenance studies of copper-bearing andesines using Cu isotope ratios and element analysis by fs-LA-MC-ICPMS and ns-LA-ICPMS. *Analytical and Bioanalytical Chemistry* 398:2915-2928.

- Fricker M B, Kutscher D, Aeschlimann B, Frommer J, Dietiker R, Bettmer J, Günther D (2011) High spatial resolution trace element analysis by LA-ICP-MS using a novel ablation cell for multiple or large samples. *International Journal of Mass Spectrometry* 307:39-45.
- Fryer B J, Jackson S E, Longerich H P (1995) The design, operation and role of the laser-ablation microprobe coupled with an inductively coupled plasma-mass spectrometer (LAM- ICP-MS) in the Earth sciences. *Canadian Mineralogist* 33:303-312.
- Galler P, Limbeck A, Boulyga S F, Stingeder G, Hirata T, Prohaska T (2007) Development of an On-Line Flow Injection Sr/Matrix Separation Method for Accurate, High-Throughput Determination of Sr Isotope Ratios by Multiple Collector-Inductively Coupled Plasma-Mass Spectrometry. *Analytical Chemistry* 79:5023-5029.
- Garcia C C, Lindner H, Niemax K (2009) Laser ablation inductively coupled plasma mass spectrometry-current shortcomings, practical suggestions for improving performance, and experiments to guide future development. *Journal of Analytical Atomic Spectrometry* 24:14-26.
- Garcia C C, Lindner H, von Bohlen A, Vadla C, Niemax K (2008) Elemental fractionation and stoichiometric sampling in femtosecond laser ablation. *Journal of Analytical Atomic Spectrometry* 23:470-478.
- Georgiev S, von Quadt A, Heinrich C A, Peytcheva I, Marchev P (2012) Time evolution of a rifted continental arc: Integrated ID-TIMS and LA-ICPMS study of magmatic zircons from the Eastern Srednogorie, Bulgaria. *Lithos* in press.
- Gholap D, Verhulst J, Ceelen W, Vanhaecke F (2012) Use of pneumatic nebulization and laser ablation-inductively coupled plasma-mass spectrometry to study the distribution and bioavailability of an intraperitoneally administered Pt-containing chemotherapeutic drug. *Analytical and Bioanalytical Chemistry* 402:2121-2129.
- Glaus R, Kaegi R, Krumeich F, Günther D (2010) Phenomenological studies on structure and elemental composition of nanosecond and femtosecond laser-generated aerosols with implications on laser ablation inductively coupled plasma mass spectrometry. *Spectrochimica Acta Part B: Atomic Spectroscopy* 65:812-822.
- Gligorovski S, Van Elteren J T, Grgic I (2008) A multi-element mapping approach for size-segregated atmospheric particles using laser ablation ICP-MS combined with image analysis. *Science of the Total Environment* 407:594-602.
- Goldschmidt B (1989) Uranium's Scientific History 1789-1939. <http://ist-socrates.berkeley.edu/~rochlin/ushist.html>. Accessed 17 August 2012.
- Goldschmidt P (1999) The IAEA Safeguards System moves into the 21st century. *Supplement to the IAEA Bulletin* 41(4):1-22.
- Golitzko M, Terrell J E (2012) Mapping prehistoric social fields on the Sepik coast of Papua New Guinea: ceramic compositional analysis using laser ablation-inductively coupled plasma-mass spectrometry. *Journal of Archaeological Science* 39:3568-3580.
- Gonzalez J J, Fernandez A, Oropeza D, Mao X, Russo R E (2008) Femtosecond laser ablation: Experimental study of the repetition rate influence on inductively coupled plasma mass spectrometry performance. *Spectrochimica Acta Part B: Atomic Spectroscopy* 63:277-286.
- Gonzalez J J, Liu C, Wen S B, Mao X, Russo R E (2007a) Glass particles produced by laser ablation for ICP-MS measurements. *Talanta* 73:577-582.
- Gonzalez J J, Liu C, Wen S B, Mao X, Russo R E (2007b) Metal particles produced by laser ablation for ICP-MS measurements. *Talanta* 73:567-576.
- Grainger M N C, Manley-Harris M, Coulson S (2012) Classification and discrimination of automotive glass using LA-ICP-MS. *Journal of Analytical Atomic Spectrometry* 27:1413-1422.
- Gray A L (1985) Solid sample introduction by laser ablation for inductively coupled plasma source mass spectrometry. *The Analyst* 110:551-556.
- Grün B, Leisch F (2008) FlexMix Version 2: Finite Mixtures with Concomitant Variables and Varying and Constant Parameters. *Journal of Statistical Software* 28:1-35.
- Guillong M, Günther D (2002) Effect of particle size distribution on ICP-induced elemental fractionation in laser ablation-inductively coupled plasma-mass spectrometry. *Journal of Analytical Atomic Spectrometry* 17:831-837.
- Guillong M, Horn I, Günther D (2003) A comparison of 266 nm, 213 nm and 193 nm produced from a single solid state Nd:YAG laser for laser ablation ICP-MS. *Journal of Analytical Atomic Spectrometry* 18:1224-1230.
- Günther-Leopold I, Waldis J K, Wernli B, Kopajtic Z (2005) Measurement of plutonium isotope ratios in nuclear fuel samples by HPLC-MC-ICP-MS. *International Journal of Mass Spectrometry* 242:197-202.

- Günther-Leopold I, Wernli B, Kopajtic Z, Günther D (2004) Measurement of isotope ratios on transient signals by MC-ICP-MS. *Analytical and Bioanalytical Chemistry* 378:241-249.
- Günther D, Heinrich C A (1999) Enhanced sensitivity in laser ablation-ICP mass spectrometry using helium-argon mixtures as aerosol carrier. *Journal of Analytical Atomic Spectrometry* 14:1363-1368.
- Jarvis K E, Gray A L, Houk R S (Eds.) (1992). *Handbook of Inductively Coupled Plasma Mass Spectrometry*. Blackie & Son Ltd.
- Helbig M, Keppie J D, Murphy J B, Solari L A (2012) U-Pb geochronological constraints on the Triassic-Jurassic Ayú Complex, southern Mexico: Derivation from the western margin of Pangea-A. *Gondwana Research* 22:910-927.
- Heumann K G, Gallus S M, Rädlinger G, Vogl J (1998) Precision and accuracy in isotope ratio measurements by plasma source mass spectrometry. *Journal of Analytical Atomic Spectrometry* 13:1001-1008.
- Hill S J, Fisher A, Liezers M (2005). *Plasma Generation, Ion Sampling and Focusing*, In: Nelms S M (ed), *Inductively Coupled Plasma Mass Spectrometry Handbook*. Blackwell Publishing Ltd.
- Hirata T, Hayano Y, Ohno T (2003) Improvements in precision of isotopic ratio measurements using laser ablation-multiple collector-ICP-mass spectrometry: reduction of changes in measured isotopic ratios. *Journal of Analytical Atomic Spectrometry* 18:1283-1288.
- Hirata T, Kon Y (2008) Evaluation of the analytical capability of NIR femtosecond laser ablation-inductively coupled plasma mass spectrometry. *Analytical Sciences* 24:345-353.
- Hirata T, Yamaguchi T (1999) Isotopic analysis of zirconium using enhanced sensitivity-laser ablation-multiple collector-inductively coupled plasma mass spectrometry. *Journal of Analytical Atomic Spectrometry* 14:1455-1459.
- Hobbs J, Castillo G, Tigan G, Lindberg J, Ikemiyagi N, Ramos G (2012) Tagging the next generation: validation of trans-generational chemical tagging for an endangered fish. *Environmental Biology of Fishes* in press.
- Hoffmann D L, Richards D A, Elliott T R, Smart P L, Coath C D, Hawkesworth C J (2005) Characterisation of secondary electron multiplier nonlinearity using MC-ICPMS. *International Journal of Mass Spectrometry* 244:97-108.
- Holá M, Kalvoda J, Nováková H, Skoda R, Kanický V (2011) Possibilities of LA-ICP-MS technique for the spatial elemental analysis of the recent fish scales: Line scan vs. depth profiling. *Applied Surface Science* 257:1932-1940.
- Horn I, Guillion M, Günther D (2001) Wavelength dependant ablation rates for metals and silicate glasses using homogenized laser beam profiles - implications for LA-ICP-MS. *Applied Surface Science* 182:91-102.
- Horn I, Günther D (2003) The influence of ablation carrier gasses Ar, He and Ne on the particle size distribution and transport efficiencies of laser ablation-induced aerosols: Implications for LA-ICP-MS. *Applied Surface Science* 207:144-157.
- Horn I, von Blanckenburg F (2007) Investigation on elemental and isotopic fractionation during 196 nm femtosecond laser ablation multiple collector inductively coupled plasma mass spectrometry. *Spectrochimica Acta Part B: Atomic Spectroscopy* 62:410-422.
- Hotchkis M A C, Child D, Fink D, Jacobsen G E, Lee P J, Mino N, Smith A M, Tuniz C (2000) Measurement of ²³⁶U in environmental media. *Nuclear Instruments and Methods in Physics Research Section B: Beam Interactions with Materials and Atoms* 172:659-665.
- Hou X, Roos P (2008) Critical comparison of radiometric and mass spectrometric methods for the determination of radionuclides in environmental, biological and nuclear waste samples. *Analytica Chimica Acta* 608:105-139.
- Hrnecek E, Steier P, Wallner A (2005) Determination of plutonium in environmental samples by AMS and alpha spectrometry. *Applied Radiation and Isotopes* 63:633-638.
- Hsieh Y-K, Chen L-K, Hsieh H-F, Huang C-H, Wang C-F (2011) Elemental analysis of airborne particulate matter using an electrical low-pressure impactor and laser ablation/inductively coupled plasma mass spectrometry. *Journal of Analytical Atomic Spectrometry* 26:1502-1508.
- Hu Q-H, Weng J-Q, Wang J-S (2010) Sources of anthropogenic radionuclides in the environment: a review. *Journal of Environmental Radioactivity* 101:426-437.
- Hunter K, Stresau D (2005). *Ion Detection*, In: Nelms S M (ed), *Inductively Coupled Plasma Mass Spectrometry Handbook*. Blackwell Publishing Ltd.
- IAEA (2001) IAEA Safeguards: Stemming the Spread of Nuclear Weapons. http://www.iaea.org/Publications/Factsheets/English/S1_Safeguards.pdf. Accessed 21 August 2012.

- Ketterer M E, Szechenyi S C (2008) Determination of plutonium and other transuranic elements by inductively coupled plasma mass spectrometry: A historical perspective and new frontiers in the environmental sciences. *Spectrochim Acta B* 63:719-737.
- Kim C-S, Kim C-K, Martin P, Sansone U (2007) Determination of Pu isotope concentrations and isotope ratio by inductively coupled plasma mass spectrometry: a review of analytical methodology. *Journal of Analytical Atomic Spectrometry* 22:827-841.
- Kimura J-I, Chang Q (2012) Origin of the suppressed matrix effect for improved analytical performance in determination of major and trace elements in anhydrous silicate samples using 200 nm femtosecond laser ablation sector-field inductively coupled plasma mass spectrometry. *Journal of Analytical Atomic Spectrometry* 27:1549-1559.
- Kips R, Leenaers A, Tamborini G, Betti M, Van Den Berghe S, Wellum R, Taylor P (2007) Characterization of uranium particles produced by hydrolysis of UF₆ using SEM and SIMS. *Microscopy and Microanalysis* 13:156-164.
- Kirchner G, Noack C C (1988) Core history and nuclide inventory of the Chernobyl core at the time of the accident. *Nuclear Safety* 29:1-3.
- Koch J, Feldmann I, Jakubowski N, Niemax K (2002) Elemental composition of laser ablation aerosol particles deposited in the transport tube to an ICP. *Spectrochimica Acta Part B: Atomic Spectroscopy* 57:975-985.
- Koch J, Günther D (2007) Femtosecond laser ablation inductively coupled plasma mass spectrometry: achievements and remaining problems. *Analytical and Bioanalytical Chemistry* 387:149-153.
- Koch J, Günther D (2011) Review of the state-of- The-art of laser ablation inductively coupled plasma mass spectrometry. *Applied Spectroscopy* 65:155A-162A.
- Koch J, Lindner H, von Bohlen A, Hergenroder R, Niemax K (2005) Elemental fractionation of dielectric aerosols produced by near-infrared femtosecond laser ablation of silicate glasses. *Journal of Analytical Atomic Spectrometry* 20:901-906.
- Koch J, von Bohlen A, Hergenroder R, Niemax K (2004) Particle size distributions and compositions of aerosols produced by near-IR femto- and nanosecond laser ablation of brass. *Journal of Analytical Atomic Spectrometry* 19:267-272.
- Koch J, Walle M, Pisonero J, Günther D (2006) Performance characteristics of ultra-violet femtosecond laser ablation inductively coupled plasma mass spectrometry at [similar]265 and [similar]200 nm. *Journal of Analytical Atomic Spectrometry* 21:932-940.
- Koelmel J, Amarasiriwardena D (2012) Imaging of metal bioaccumulation in Hay-scented fern (*Dennstaedtia punctilobula*) rhizomes growing on contaminated soils by laser ablation ICP-MS. *Environmental Pollution* 168:62-70.
- Konz I, Fernández B, Fernández M L, Pereiro R, Sanz-Medel A (2011a) Absolute quantification of human serum transferrin by species-specific isotope dilution laser ablation ICP-MS. *Analytical Chemistry* 83:5353-5360.
- Konz I, Fernandez B, Pereiro R, Fernandez M L, Sanz-Medel A (2011b) P, S and Cl trace detection by laser ablation double-focusing sector field ICP-MS to identify local defects in coated glasses. *Journal of Analytical Atomic Spectrometry* 26:1526-1530.
- Kroslakova I, Günther D (2007) Elemental fractionation in laser ablation-inductively coupled plasma-mass spectrometry: evidence for mass load induced matrix effects in the ICP during ablation of a silicate glass. *Journal of Analytical Atomic Spectrometry* 22:51-62.
- Krupp E, Péchéryran C, Meffan-Main S, Donard O X (2004) Precise isotope-ratio determination by CGC hyphenated to ICP- MCMS for speciation of trace amounts of gaseous sulfur, with SF₆ as example compound. *Analytical and Bioanalytical Chemistry* 378:250-255.
- Krupp E M, Donard O F X (2005) Isotope ratios on transient signals with GC-MC-ICP-MS. *International Journal of Mass Spectrometry* 242:233-242.
- Krupp E M, Péchéryran C, Pinaly H, Motelica-Heino M, Koller D, Young S M M, Brenner I B, Donard O F X (2001) Isotopic precision for a lead species (PbEt₄) using capillary gas chromatography coupled to inductively coupled plasma-multicollector mass spectrometry. *Spectrochimica Acta Part B: Atomic Spectroscopy* 56:1233-1240.
- Kuhn H-R, Günther D (2003) Elemental Fractionation Studies in Laser Ablation Inductively Coupled Plasma Mass Spectrometry on Laser-Induced Brass Aerosols. *Analytical Chemistry* 75:747-753.
- Kuhn H-R, Günther D (2004) Laser ablation-ICP-MS: particle size dependent elemental composition studies on filter-collected and online measured aerosols from glass. *Journal of Analytical Atomic Spectrometry* 19:1158-1164.

- Kumtabtim U, Siripinyanond A, Auray-Blais C, Ntwari A, Becker J S (2011) Analysis of trace metals in single droplet of urine by laser ablation inductively coupled plasma mass spectrometry. *International Journal of Mass Spectrometry* 307:174-181.
- Lacan F, Radic A, Labatut M, Jeandel C, Poitrasson F, Sarthou G, Pradoux C, Chmeleff J, Freydier R (2010) High-precision determination of the isotopic composition of dissolved iron in iron depleted seawater by double spike multicollector-ICPMS. *Analytical Chemistry* 82:7103-7111.
- Lariviere D, Taylor V F, Evans R D, Cornett R J (2006) Radionuclide determination in environmental samples by inductively coupled plasma mass spectrometry. *Spectrochim Acta B* 61:877-904.
- Lear J, Hare D J, Fryer F, Adlard P A, Finkelstein D I, Doble P A (2012) High-Resolution Elemental Bioimaging of Ca, Mn, Fe, Co, Cu, and Zn Employing LA-ICP-MS and Hydrogen Reaction Gas. *Analytical Chemistry* 84:6707-6714.
- Lee C-G, Suzuki D, Esaka F, Magara M, Kimura T (2011) Combined application of alpha-track and fission-track techniques for detection of plutonium particles in environmental samples prior to isotopic measurement using thermo-ionization mass spectrometry. *Talanta* 85:644-649.
- Lee C G, Iguchi K, Inagawa J, Suzuki D, Esaka F, Magara M, Sakurai S, Watanabe K, Usuda S (2007a) Development in fission track-thermal ionization mass spectrometry for particle analysis of safeguards environmental samples. *Journal of Radioanalytical and Nuclear Chemistry* 272:299-302.
- Lee M H, Douglas M, Clark S B (2005) Development of in situ fission track analysis for detecting fissile nuclides in contaminated solid particles. *Radiation Measurements* 40:37-42.
- Lee M H, Park Y J, Jee K Y, Kim W H, Clark S B (2007b) Study of an alpha track analysis and a fission track analysis for determining the hot particles contaminated with Pu and U isotopes. *Applied Radiation and Isotopes* 65:85-91.
- Leisch F (2004) FlexMix: A General Framework for Finite Mixture Models and Latent Class Regression in R. *Journal of Statistical Software* 11:1-18.
- Leisen M, Dubessy J, Boiron M-C, Lach P (2012) Improvement of the determination of element concentrations in quartz-hosted fluid inclusions by LA-ICP-MS and Pitzer thermodynamic modeling of ice melting temperature. *Geochimica et Cosmochimica Acta* 90:110-125.
- Lindahl P, Lee S-H, Worsfold P, Keith-Roach M (2010) Plutonium isotopes as tracers for ocean processes: A review. *Marine Environmental Research* 69:73-84.
- Liu C, Mao X, Mao S S, Greif R, Russo R E (2005) Particle Size Dependent Chemistry from Laser Ablation of Brass. *Analytical Chemistry* 77:6687-6691.
- Liu C, Mao X L, Mao S S, Zeng X, Greif R, Russo R E (2004) Nanosecond and Femtosecond Laser Ablation of Brass: Particulate and ICPMS Measurements. *Analytical Chemistry* 76:379-383.
- Lloyd N S, Parrish R R, Horstwood M S A, Chenery S R N (2009) Precise and accurate isotopic analysis of microscopic uranium-oxide grains using LA-MC-ICP-MS. *Journal of Analytical Atomic Spectrometry* 24:752-758.
- Longerich H, Günther D, Jackson S (1996) Elemental fractionation in laser ablation inductively coupled plasma mass spectrometry. *Fresenius' Journal of Analytical Chemistry* 355:538-542.
- Longerich H P, Diegor W (2001). Introduction to mass spectrometry, In: Sylvester P (ed), *Principles and Applications of Laser-Ablation ICP-Mass Spectrometry in the Earth Sciences*. Mineralogical Association of Canada, Short Course Series Vol. 29.
- Mantha N M, Schindler M, Kyser T K (2012) Silica- and sulfate-bearing rock coatings in smelter areas: Part II. Forensic tools for atmospheric metal(loid)- and sulfur-isotope compositions. *Geochimica et Cosmochimica Acta* 90:221-241.
- Marin R, Sarkis J, Nascimento M (2012) The use of LA-SF-ICP-MS for nuclear forensics purposes: uranium isotope ratio analysis. *Journal of Radioanalytical and Nuclear Chemistry* 1-6.
- Martin J, Daverat F, Pécheyran C, Als T D, Feunteun E, Réveillac E (2010) An otolith microchemistry study of possible relationships between the origins of leptocephali of European eels in the Sargasso Sea and the continental destinations and relative migration success of glass eels. *Ecology of Freshwater Fish* 19:627-637.
- Mayer K, Wallenius M, Fanghänel T (2007) Nuclear forensic science-From cradle to maturity. *Journal of Alloys and Compounds* 444-445:50-56.
- Mayer K, Wallenius M, Ray I (2005) Nuclear forensics - A methodology providing clues on the origin of illicitly trafficked nuclear materials. *Analyst* 130:433-441.
- Melo D, Burkart W (2004). Uranium, In: Merian E, Anke M, Ihnat M, Stoeppler M (Eds.), *Elements and their Compounds in the Environment*. 2nd edition. Wiley-VCH Verlag GmbH & Co. KGaA, Weinheim. .

4 References

- Moreno-Gordaliza E, Giesen C, Lázaro A, Esteban-Fernández D, Humanes B, Canas B, Panne U, Tejedor A, Jakubowski N, Gómez-Gómez M M (2011) Elemental Bioimaging in Kidney by LA-ICP-MS As a Tool to Study Nephrotoxicity and Renal Protective Strategies in Cisplatin Therapies. *Analytical Chemistry* 83:7933-7940.
- Morgan J L L, Gordon G W, Arrua R C, Skulan J L, Anbar A D, Bullen T D (2011) High-precision measurement of variations in calcium isotope ratios in urine by multiple collector inductively coupled plasma mass spectrometry. *Analytical Chemistry* 83:6956-6962.
- Možná V, Pisonero J, Holá M, Kanický V, Günther D (2006) Quantitative analysis of Fe-based samples using ultraviolet nanosecond and femtosecond laser ablation-ICP-MS. *Journal of Analytical Atomic Spectrometry* 21:1194-1201.
- Müller J W (1973) Dead-time problems. *Nuclear Instruments and Methods* 112:47-57.
- Muramatsu Y, Rühm W, Yoshida S, Tagami K, Uchida S, Wirth E (2000) Concentrations of ²³⁹Pu and ²⁴⁰Pu and their isotopic ratios determined by ICP-MS in soils collected from the Chernobyl 30-km zone. *Environmental Science and Technology* 34:2913-2917.
- Natural Decay Series: Uranium, Radium, and Thorium. Argonne National Laboratory, EVS. Human Health Fact Sheet, August 2005. <http://www.ead.anl.gov/pub/doc/natural-decay-series.pdf>. Accessed 16 August 2012.
- Nelms S M, Quérel C R, Prohaska T, Vogl J, Taylor P D P (2001) Evaluation of detector dead time calculation models for ICP-MS. *Journal of Analytical Atomic Spectrometry* 16:333-338.
- New Brunswick Laboratory - U.S. Department of Energy (2008) Certificate of Analysis CRM U010 - Uranium Isotopic Standard. http://www.nbl.doe.gov/docs/pdf/CRM_U010_5_milligram_Sample_Size_March_2008.pdf. Accessed 8 November 2012.
- New Brunswick Laboratory - U.S. Department of Energy (2008) Certificate of Analysis CRM U030-A - Uranium Isotopic Standard. http://www.nbl.doe.gov/docs/pdf/CRM_U030-A_10_milligram_Sample_Size_March_2008.pdf. Accessed 8 November 2012.
- New Brunswick Laboratory - U.S. Department of Energy (2008) Certificate of Analysis CRM U500 - Uranium Isotopic Standard. http://www.nbl.doe.gov/docs/pdf/CRM_U500_10_milligram_Sample_Size_March_2008.pdf. Accessed 8 November 2012.
- Nu Instruments Ltd. DSN-100 - DeSolvation Nebulizer System. Operator's Manual
- Nu Instruments Ltd. NP Abundance Sensitivity.
- Nu Instruments Ltd. NP Faraday detectors.
- Nu Instruments Ltd. NP Manual V2.
- Nu Instruments Ltd. NP Multiplier Operation.
- Nu Instruments Ltd. Nu Plasma II. Multi-collector ICP-MS. <http://www.nu-ins.com/pdf/Plasma-II-brochure.pdf>. Accessed 31 July 2012.
- Lieser K H (ed) (2008). *Nuclear and Radiochemistry: Fundamentals and Applications*. 2nd edition. Wiley-VCH.
- Nuclear Fuel Cycle Information System. IAEA-TECDOC-1613. http://www-pub.iaea.org/mtcd/publications/pdf/te_1613_web.pdf. Accessed 20 August 2012. (2009)
- Nunnemann M, Erdmann N, Hasse H U, Huber G, Kratz J V, Kunz P, Mansel A, Passler G, Stetzer O, Trautmann N, Waldek A (1998) Trace analysis of plutonium in environmental samples by resonance ionization mass spectroscopy (RIMS). *Journal of Alloys and Compounds* 271-273:45-48.
- Nygren U, Ramebäck H, Berglund M, Baxter D C (2006) The importance of a correct dead time setting in isotope ratio mass spectrometry: Implementation of an electronically determined dead time to reduce measurement uncertainty. *International Journal of Mass Spectrometry* 257:12-15.
- O'Connor G, Evans E H (2007). *Fundamental Aspects of Inductively Coupled Plasma - Mass Spectrometry (ICP-MS)*, In: Hill S J (ed), *Inductively Coupled Plasma Spectrometry and its Applications*, 2nd ed. Blackwell Publishing Ltd.
- Okuda T, Kato J, Mori J, Tenmoku M, Suda Y, Tanaka S, He K, Ma Y, Yang F, Yu X, Duan F, Lei Y (2004) Daily concentrations of trace metals in aerosols in Beijing, China, determined by using inductively coupled plasma mass spectrometry equipped with laser ablation analysis, and source identification of aerosols. *Science of the Total Environment* 330:145-158.
- Okuda T, Tenmoku M, Kato J, Mori J, Sato T, Yokochi R, Tanaka S (2006) Long-term observation of trace metal concentration in aerosols at a remote island, Rishiri, Japan by using inductively coupled plasma mass spectrometry equipped with laser ablation. *Water, Air and Soil Pollution* 174:3-17.

4 References

- ORIGEN-ARP Cross-Section Libraries for the RBMK-1000 System. http://www.ornl.gov/sci/scale/Publications/Murphy/ORNL_TM_2006_139.pdf. Accessed 7 March 2012. (2006)
- Panighello S, Orsega E F, van Elteren J T, Selih V S (2012) Analysis of polychrome Iron Age glass vessels from Mediterranean I, II and III groups by LA-ICP-MS. *Journal of Archaeological Science* 39:2945-2955.
- Park Y J, Song K, Pyo H Y, Lee M H, Jee K Y, Kim W H (2006) Investigation on the fission track analysis of uranium-doped particles for the screening of safeguards environmental samples. *Nuclear Instruments and Methods in Physics Research Section A: Accelerators, Spectrometers, Detectors and Associated Equipment* 557:657-663.
- Paul M, Berkovits D, Ahmad I, Borasi F, Caggiano J, Davids C N, Greene J P, Harss B, Heinz A, Henderson D J, Henning W, Jiang C L, Pardo R C, Rehm K E, Rejoub R, Seweryniak D, Sonzogni A, Uusitalo J, Vondrasek R (2000) AMS of heavy elements with an ECR ion source and the ATLAS linear accelerator. *Nuclear Instruments and Methods in Physics Research Section B: Beam Interactions with Materials and Atoms* 172:688-692.
- Perdian D C, Bajic S J, Baldwin D P, Houk R S (2008) Time-resolved studies of particle effects in laser ablation inductively coupled plasma-mass spectrometry: Part 1. Investigation of nanosecond and femtosecond pulse width lasers and devices for particle size selection. *Journal of Analytical Atomic Spectrometry* 23:325-335.
- Perelygin V P, Chuburkov Y T (1997) Man-made plutonium in environment - possible serious hazard for living species. *Radiation Measurements* 28:385-392.
- Pettke T, Oberli F, Audétat A, Guillong M, Simon A C, Hanley J J, Klemm L M (2011a) Recent developments in element concentration and isotope ratio analysis of individual fluid inclusions by laser ablation single and multiple collector ICP-MS. *Ore Geology Reviews* 44:10-38.
- Pettke T, Oberli F, Audétat A, Wiechert U, Harris C R, Heinrich C A (2011b) Quantification of transient signals in multiple collector inductively coupled plasma mass spectrometry: accurate lead isotope ratio determination by laser ablation of individual fluid inclusions. *Journal of Analytical Atomic Spectrometry* 26:475-492.
- Pisonero J, Koch J, Wälle M, Hartung W, Spencer N D, Günther D (2007) Capabilities of femtosecond laser ablation inductively coupled plasma mass spectrometry for depth profiling of thin metal coatings. *Analytical Chemistry* 79:2325-2333.
- Pointurier F, Hubert A, Pottin A C (2012) Performance of laser ablation: quadrupole-based ICP-MS coupling for the analysis of single micrometric uranium particles. *Journal of Radioanalytical and Nuclear Chemistry*
- Pointurier F, Pottin A C, Hubert A (2011) Application of nanosecond-UV laser ablation-inductively coupled plasma mass spectrometry for the isotopic analysis of single submicrometer-size uranium particles. *Analytical Chemistry* 83:7841-7848.
- Poitrasson F, Mao X, Mao S S, Freydier R m, Russo R E (2003) Comparison of Ultraviolet Femtosecond and Nanosecond Laser Ablation Inductively Coupled Plasma Mass Spectrometry Analysis in Glass, Monazite, and Zircon. *Analytical Chemistry* 75:6184-6190.
- Sylvester P (ed) (2001). *Principles and Applications of Laser-Ablation ICP-Mass Spectrometry in the Earth Sciences*. Mineralogical Association of Canada, Short Course Series Vol. 29.
- Pugh J, Cox A, McLeod C, Bunch J, Writer M, Hart S, Bienemann A, White E, Bell J (2012) Elemental imaging of MRI contrast agents: benchmarking of LA-ICP-MS to MRI. *Analytical and Bioanalytical Chemistry* 403:1641-1649.
- R Development Core Team (2012) *R: A language and environment for statistical computing*. R Foundation for Statistical Computing, Vienna, Austria. ISBN 3-900051-07-0, URL <http://www.R-project.org/>.
- Ramebäck H, Berglund M, Vendelbo D, Wellum R, Taylor P D P (2001) On the determination of the true dead-time of a pulse-counting system in isotope ratio mass spectrometry. *Journal of Analytical Atomic Spectrometry* 16:1271-1274.
- Ranebo Y, Eriksson M, Tamborini G, Niagolova N, Bildstein O, Betti M (2007) The use of SIMS and SEM for the characterization of individual particles with a matrix originating from a nuclear weapon. *Microscopy and Microanalysis* 13:179-190.
- Ranebo Y, Hedberg P M L, Whitehouse M J, Ingeneri K, Littmann S (2009) Improved isotopic SIMS measurements of uranium particles for nuclear safeguard purposes. *Journal of Analytical Atomic Spectrometry* 24:277-287.
- Ranebo Y, Niagolova N, Erdmann N, Eriksson M, Tamborini G, Betti M (2010) Production and Characterization of Monodisperse Plutonium, Uranium, and Mixed Uranium - Plutonium Particles for Nuclear Safeguard Applications. *Analytical Chemistry* 82:4055-4062.
- Raptis K, Ingelbrecht C, Wellum R, Alonso A, De Bolle W, Perrin R (2002) The preparation of uranium-doped glass reference materials for environmental measurements. *Nuclear Instruments and Methods in Physics Research, Section A: Accelerators, Spectrometers, Detectors and Associated Equipment* 480:40-43.

4 References

- Rauch S, Morrison G M, Moldovan M (2002) Scanning laser ablation-ICP-MS tracking of platinum group elements in urban particles. *Science of the Total Environment* 286:243-251.
- Rauch S, Morrison G M, Motelica-Heino M, Donard O F X, Muris M (2000a) Elemental association and fingerprinting of traffic-related metals in road sediments. *Environmental Science and Technology* 34:3119-3123.
- Rauch S b, Lu M, Morrison G M (2000b) Heterogeneity of Platinum Group Metals in Airborne Particles. *Environmental Science & Technology* 35:595-599.
- Rehkämper M, Schönbachler M, Stirling C H (2001) Multiple Collector ICP-MS: Introduction to Instrumentation, Measurement Techniques and Analytical Capabilities. *Geostandards Newsletter* 25:23-40.
- Reis-Santos P, Gillanders B M, Tanner S E, Vasconcelos R P, Elsdon T S, Cabral H N (2012) Temporal variability in estuarine fish otolith elemental fingerprints: Implications for connectivity assessments. *Estuarine, Coastal and Shelf Science* 112:216-224.
- Ricard E, Pécheyran C, Sanabria Ortega G, Prinzhofer A, Donard O F X (2011) Direct analysis of trace elements in crude oils by high-repetition-rate femtosecond laser ablation coupled to ICPMS detection. *Analytical and Bioanalytical Chemistry* 399:2153-2165.
- Richter S, Alonso A, Aregbe Y, Eykens R, Kehoe F, Kühn H, Kivel N, Verbruggen A, Wellum R, Taylor P D P (2009) A new series of uranium isotope reference materials for investigating the linearity of secondary electron multipliers in isotope mass spectrometry. *International Journal of Mass Spectrometry* 281:115-125.
- Richter S, Alonso A, De Bolle W, Wellum R, Taylor P D P (1999) Isotopic 'fingerprints' for natural uranium ore samples. *International Journal of Mass Spectrometry* 193:9-14.
- Richter S, Goldberg S A, Mason P B, Traina A J, Schwieters J B (2001) Linearity tests for secondary electron multipliers used in isotope ratio mass spectrometry. *International Journal of Mass Spectrometry* 206:105-127.
- Rodríguez-Castrillón J A, García-Ruiz S, Moldovan M, García Alonso J I (2012) Multiple linear regression and on-line ion exchange chromatography for alternative Rb-Sr and Nd-Sm MC-ICP-MS isotopic measurements. *Journal of Analytical Atomic Spectrometry* 27:611-618.
- Rodríguez-González P, Epov V N, Pecheyran C, Amouroux D, Donard O F X (2011) Species-specific stable isotope analysis by the hyphenation of chromatographic techniques with MC-ICPMS. *Mass Spectrometry Reviews* 31:504-521.
- Rosman K J R, Lycke W, Damen R, Werz R, Hendrickx F, Traas L, De Bièvre P (1987) The preparation and use of synthetic isotope mixtures for testing mass spectrometers. *International Journal of Mass Spectrometry and Ion Processes* 79:61-71.
- Russo R E, Mao X, Borisov O V (1998) Laser ablation sampling. *TrAC Trends in Analytical Chemistry* 17:461-469.
- Russo R E, Mao X, Gonzalez J J, Mao S S (2002a) Femtosecond laser ablation ICP-MS. *Journal of Analytical Atomic Spectrometry* 17:1072-1075.
- Russo R E, Mao X, Liu H, Gonzalez J, Mao S S (2002b) Laser ablation in analytical chemistry - a review. *Talanta* 57:425-451.
- Russo R E, Mao X L, Borisov O V, Liu H (2000) Influence of wavelength on fractionation in laser ablation ICP-MS. *Journal of Analytical Atomic Spectrometry* 15:1115-1120.
- Russo R E, Mao X L, Liu C, Gonzalez J (2004) Laser assisted plasma spectrochemistry: laser ablation. *Journal of Analytical Atomic Spectrometry* 19:1084-1089.
- Russo R E, Mao X L, Yoo J H, Gonzalez J J, Jagdish P S, Surya N T (2007). Chapter 3 - Laser Ablation, Laser-Induced Breakdown Spectroscopy. Elsevier, Amsterdam, pp. 49-82.
- Sahoo S (2009) Measurement of uranium and its isotopes at trace levels in environmental samples using mass spectrometry. *Indian Journal of Physics* 83:787-797.
- Salbu B (2009) Challenges in radioecology. *Journal of Environmental Radioactivity* 100:1086-1091.
- Salbu B, Krekling T, Lind O C, Oughton D H, Drakopoulos M, Simionovici A, Snigireva I, Snigirev A, Weitkamp T, Adams F, Janssens K, Kashparov V A (2001) High energy X-ray microscopy for characterisation of fuel particles. *Nuclear Instruments and Methods in Physics Research Section A: Accelerators, Spectrometers, Detectors and Associated Equipment* 467-468, Part 2:1249-1252.
- Salbu B, Krekling T, Oughton D H (1998) Characterisation of radioactive particles in the environment. *Analyst* 123:843-849.
- Salbu B, Lind O C (2005) Radioactive particles released from various nuclear sources. *Radioprotection* 40:27-32.

- Santos M C, Wagner M, Wu B, Scheider J, Oehlmann J, Cadore S, Becker J S (2009) Biomonitoring of metal contamination in a marine prosobranch snail (*Nassarius reticulatus*) by imaging laser ablation inductively coupled plasma mass spectrometry (LA-ICP-MS). *Talanta* 80:428-433.
- Scadding C J, Watling R J, Thomas A G (2005) The potential of using laser ablation inductively coupled plasma time of flight mass spectrometry (LA-ICP-TOF-MS) in the forensic analysis of micro debris. *Talanta* 67:414-424.
- Schimmack W, Auerswald K, Bunzl K (2002) Estimation of soil erosion and deposition rates at an agricultural site in Bavaria, Germany, as derived from fallout radiocesium and plutonium as tracers. *Naturwissenschaften* 89:43-46.
- Sela H, Karpas Z, Zoriy M, Pickhardt C, Becker J S (2007) Biomonitoring of hair samples by laser ablation inductively coupled plasma mass spectrometry (LA-ICP-MS). *International Journal of Mass Spectrometry* 261:199-207.
- Shaheen M, Fryer B J (2010) Improving the analytical capabilities of femtosecond laser ablation multicollector ICP-MS for high precision Pb isotopic analysis: The role of hydrogen and nitrogen. *Journal of Analytical Atomic Spectrometry* 25:1006-1013.
- Shaheen M, Gagnon J E, Yang Z, Fryer B J (2008) Evaluation of the analytical performance of femtosecond laser ablation inductively coupled plasma mass spectrometry at 785 nm with glass reference materials. *Journal of Analytical Atomic Spectrometry* 23:1610-1621.
- Shaheen M E, Fryer B J (2011) A simple solution to expanding available reference materials for Laser Ablation Inductively Coupled Plasma Mass Spectrometry analysis: Applications to sedimentary materials. *Spectrochimica Acta - Part B Atomic Spectroscopy* 66:627-636.
- Shaheen M E, Gagnon J E, Fryer B J (2012) Femtosecond (fs) lasers coupled with modern ICP-MS instruments provide new and improved potential for in situ elemental and isotopic analyses in the geosciences. *Chemical Geology*
- Shen Y, Zhao Y, Guo S L, Cui J, Liu Y, Li J, Xu J, Zhang H (2008) Study on analysis of isotopic ratio of uranium-bearing particle in swipe samples by FT-TIMS. *Radiation Measurements* 43:299-302.
- Shepherd T J, Dirks W, Manmee C, Hodgson S, Banks D A, Averley P, Pless-Mulloli T (2012) Reconstructing the life-time lead exposure in children using dentine in deciduous teeth. *Science of the Total Environment* 425:214-222.
- Siebold M, Leidich P, Bertini M, Deflorio G, Feldmann J, Krupp E, Halmschlager E, Woodward S (2012) Application of elemental bioimaging using laser ablation ICP-MS in forest pathology: distribution of elements in the bark of *Picea sitchensis* following wounding. *Analytical and Bioanalytical Chemistry* 402:3323-3331.
- Skoog D A, Leary J J (1992) *Principles of Instrumental Analysis*, 4th edn. Saunders College Publishing.
- Smith D H (2000). *Thermal Ionization Mass Spectrometry*, In: Barsick C M, Duckworth D C, Smith D H (Eds.), *Inorganic Mass Spectrometry - Fundamentals and Applications*. Practical Spectroscopy Series Volume 23. Marcel Dekker, Inc., New York.
- Sokolik G A, Ivanova T G, Leinova S L, Ovsianikova S V, Kimlenko I M (2001) Migration ability of radionuclides in soil-vegetation cover of Belarus after Chernobyl accident. *Environment International* 26:183-187.
- Spears D A (2004) The use of laser ablation inductively coupled plasma-mass spectrometry (LA ICP-MS) for the analysis of fly ash. *Fuel* 83:1765-1770.
- Stadlbauer C, Prohaska T, Reiter C, Knaus A, Stingeder G (2005) Time-resolved monitoring of heavy-metal intoxication in single hair by laser ablation ICP-DRCMS. *Analytical and Bioanalytical Chemistry* 383:500-508.
- Stetzer O, Betti M, Van Geel J, Erdmann N, Kratz J V, Schenkel R, Trautmann N (2004) Determination of the ²³⁵U content in uranium oxide particles by fission track analysis. *Nuclear Instruments and Methods in Physics Research, Section A: Accelerators, Spectrometers, Detectors and Associated Equipment* 525:582-592.
- Suzuki K (2006) Characterisation of airborne particulates and associated trace metals deposited on tree bark by ICP-OES, ICP-MS, SEM-EDX and laser ablation ICP-MS. *Atmospheric Environment* 40:2626-2634.
- Swoboda S, Brunner M, Boulyga S, Galler P, Horacek M, Prohaska T (2008) Identification of Marchfeld asparagus using Sr isotope ratio measurements by MC-ICP-MS. *Analytical and Bioanalytical Chemistry* 390:487-494.
- Tabouret H, Pomerleau S, Jolivet A, Pécheyran C, Riso R, Thébault J, Chauvaud L, Amouroux D (2012) Specific pathways for the incorporation of dissolved barium and molybdenum into the bivalve shell: An isotopic tracer approach in the juvenile Great Scallop (*Pecten maximus*). *Marine Environmental Research* 78:15-25.
- Tamborini G (2004) SIMS analysis of uranium and actinides in microparticles of different origin. *Microchimica Acta* 145:237-242.
- Tamborini G, Betti M (2000) Characterisation of radioactive particles by SIMS. *Mikrochimica Acta* 132:411-417.

4 References

- Tamborini G, Wallenius M, Bildstein O, Pajo L, Betti M (2002) Development of a SIMS Method for Isotopic Measurements in Nuclear Forensics Applications. *Microchimica Acta* 139:185-188.
- Tanaka S, Yasushi N, Sato N, Fukasawa T, Juari Santosa S, Yamanaka K, Ootoshi T (1998) Rapid and simultaneous multi-element analysis of atmospheric particulate matter using inductively coupled plasma mass spectrometry with laser ablation sample introduction. *Journal of Analytical Atomic Spectrometry* 13:135-140.
- Taylor D M (1995) Environmental plutonium in humans. *Applied Radiation and Isotopes* 46:1245-1252.
- Taylor D M (2011) *Plutonium: Environmental Pollution and Health Effects*. Elsevier B.V.
- Taylor R N, Warneke T, Milton J A, Croudace I W, Warwick P E, Nesbitt R W (2001) Plutonium isotope ratio analysis at femtogram to nanogram levels by multicollector ICP-MS. *Journal of Analytical Atomic Spectrometry* 16:279-284.
- Thermo Fisher Scientific Inc. Another step ahead in MC-ICPMS - Earth and Planetary Sciences, Nuclear Sciences. <http://www.thermoscientific.com/ecommservlet/techresource?storeId=11152&langId=1&taxonomy=4&resourceId=98925&contentType=Brochures&productId=11961870#>. Accessed 27 June 2012.
- Thermo Fisher Scientific Inc. Thermo Scientific ELEMENT 2 & ELEMENT XR. <http://www.thermoscientific.com/ecommservlet/productsdetail?productId=11961724&storeId=11152>. Accessed 1 August 2012.
- Thermo Fisher Scientific Inc. Thermo Scientific Jet Interface. http://www.thermo.com/eThermo/CMA/PDFs/Product/productPDF_56336.PDF. Accessed 13 August 2012.
- Thomas R (2001) A Beginner's Guide to ICP-MS Spectroscopy. http://www.geo.utep.edu/pub/jasper/isotope/pdf_notes/ICPMS.pdfhttp://www.geo.utep.edu/pub/jasper/isotope/pdf_notes/ICPMS.pdf. Accessed 13 August 2012
- Todoli J L, Vanhaecke F (2005). Liquid Sample Introduction and Electrothermal Vaporisation for ICP-MS: Fundamentals and Applications., In: Nelms S M (ed), *Inductively Coupled Plasma Mass Spectrometry Handbook*. Blackwell Publishing Ltd.
- Tollstrup D L, Xie L-W, Wimpenny J B, Chin E, Lee C-T, Yin Q-Z (2012) A trio of laser ablation in concert with two ICP-MSs: Simultaneous, pulse-by-pulse determination of U-Pb discordant ages and a single spot Hf isotope ratio analysis in complex zircons from petrographic thin sections. *Geochemistry, Geophysics, Geosystems* 13:Q03017.
- Traub H, Czerwensky M, Matschat R, Kipphardt H, Panne U (2010) Different calibration strategies for the analysis of pure copper metal by nanosecond laser ablation inductively coupled plasma mass spectrometry. *Journal of Analytical Atomic Spectrometry* 25:690-696.
- Traub H, Wälle M, Koch J, Panne U, Matschat R, Kipphardt H, Günther D (2009) Evaluation of different calibration strategies for the analysis of pure copper and zinc samples using femtosecond laser ablation ICP-MS. *Analytical and Bioanalytical Chemistry* 395:1471-1480.
- Truyens J, Stefaniak E, Mialle S, Aregbe Y (2011) NUSIMEP-7: Uranium isotope amount ratios in uranium particles. Interlaboratory Comparison Report. http://irmm.jrc.ec.europa.eu/interlaboratory_comparisons/nusimep/Nusimep-7/Documents/eur_25179_en%20nusimep_7_report_to_participants.pdf. Accessed 28 June 2012.
- Tuttas D, Schwieters J B, Bouman C, Deerberg M New Compact Discrete Dynode Multipliers Integrated into the Thermo Scientific TRITON Variable Multicollector Array. https://www.thermo.com/eThermo/CMA/PDFs/Product/productPDF_56696.PDF. Accessed 31 July 2012.
- Vaculovic T, Warchilova T, Simo T, Matal O, Otruba V, Mikuska P, Kanicky V (2012) Elemental mapping of structural materials for a nuclear reactor by means of LA-ICP-MS. *Journal of Analytical Atomic Spectrometry* 27:1321-1326.
- Vajda N (2001) *Radioactive Particles in the Environment. Occurrence, Characterization, Appropriate Analytical Techniques.*
- Vajda N, Kim C-K (2010) Determination of Pu isotopes by alpha spectrometry: a review of analytical methodology. *Journal of Radioanalytical and Nuclear Chemistry* 283:203-223.
- Vanhaecke F, de Wannemacker G, Moens L, Dams R, Latkoczy C, Prohaska T, Stingeder G (1998) Dependence of detector dead time on analyte mass number in inductively coupled plasma mass spectrometry. *Journal of Analytical Atomic Spectrometry* 13:567-571.
- Vanhaecke F, Resano M, Koch J, McIntosh K, Günther D (2010) Femtosecond laser ablation-ICP-mass spectrometry analysis of a heavy metallic matrix: Determination of platinum group metals and gold in lead fire-assay buttons as a case study. *Journal of Analytical Atomic Spectrometry* 25:1259-1267.

4 References

- Varga Z (2008) Application of laser ablation inductively coupled plasma mass spectrometry for the isotopic analysis of single uranium particles. *Analytica Chimica Acta* 625:1-7.
- Velásquez G, Borisova A Y, Salvi S, Béziat D (2011) In Situ Determination of Au and Cu in Natural Pyrite by Near-Infrared Femtosecond Laser Ablation-Inductively Coupled Plasma-Quadrupole Mass Spectrometry: No Evidence for Matrix Effects. *Geostandards and Geoanalytical Research* 36:315-324.
- Waentig L, Jakubowski N, Hardt S, Scheler C, Roos P H, Linscheid M W (2012) Comparison of different chelates for lanthanide labeling of antibodies and application in a Western blot immunoassay combined with detection by laser ablation (LA-)ICP-MS. *Journal of Analytical Atomic Spectrometry* 27:1311-1320.
- Wagner B, Nowak A, Bulska E, Hametner K, Günther D (2012) Critical assessment of the elemental composition of Corning archeological reference glasses by LA-ICP-MS. *Analytical and Bioanalytical Chemistry* 402:1667-1677.
- Wallenius M (2001) Origin determination of reactor produced plutonium by mass spectrometric techniques: application to nuclear forensic science and safeguards (Academic Dissertation). University of Helsinki, Finland. <http://ethesis.helsinki.fi/julkaisut/mat/kemia/vk/wallenius/originde.pdf>. Accessed 16 August 2012.
- Wallenius M, Lützenkirchen K, Mayer K, Ray I, de las Heras L A, Betti M, Cromboom O, Hild M, Lynch B, Nicholl A, Ottmar H, Rasmussen G, Schubert A, Tamborini G, Thiele H, Wagner W, Walker C, Zuleger E (2007) Nuclear forensic investigations with a focus on plutonium. *Journal of Alloys and Compounds* 444-445:57-62.
- Wallenius M, Mayer K, Ray I (2006) Nuclear forensic investigations: Two case studies. *Forensic Science International* 156:55-62.
- Walton M, Eremin K, Shortland A, Degryse P, Kirk S (2012) ANALYSIS OF LATE BRONZE AGE GLASS AXES FROM NIPPUR—A NEW COBALT COLOURANT. *Archaeometry* 54:835-852.
- Wang C-F, Chin C-J, Luo S-K, Men L-C (1999a) Determination of chromium in airborne particulate matter by high resolution and laser ablation inductively coupled plasma mass spectrometry. *Analytica Chimica Acta* 389:257-266.
- Wang C-F, Jeng S-L, Lin C C, Chiang P-C (1998) Preparation of airborne particulate standards on PTFE-membrane filter for laser ablation inductively coupled plasma mass spectrometry. *Analytica Chimica Acta* 368:11-19.
- Wang C-F, Tu F-H, Jeng S-L, Chin C-J (1999b) The determination of silicon in airborne particulate matter by XRF and LA-ICP-MS. *Journal of Radioanalytical and Nuclear Chemistry* 242:97-103.
- Wehmeier S, Ellam R, Feldmann J (2003) Isotope ratio determination of antimony from the transient signal of trimethylstibine by GC-MC-ICP-MS and GC-ICP-TOF-MS. *Journal of Analytical Atomic Spectrometry* 18:1001-1007.
- Wendt K, Blaum K, Bushaw B A, Grüning C, Horn R, Huber G, Kratz J V, Kunz P, Müller P, Nörtershäuser W, Nunnemann M, Passler G, Schmitt A, Trautmann N, Waldek A (1999) Recent developments in and applications of resonance ionization mass spectrometry. *Fresenius' Journal of Analytical Chemistry* 364:471-477.
- Wieser M E, Schwieters J B (2005) The development of multiple collector mass spectrometry for isotope ratio measurements. *International Journal of Mass Spectrometry* 242:97-115.
- Williamson J A, Kendall-Tobias M W, Buhl M, Seibert M (1988) Statistical evaluation of dead time effects and pulse pileup in fast photon counting. Introduction of the sequential model. *Analytical Chemistry* 60:2198-2203.
- World Nuclear Association. Mixed Oxide (MOX) Fuel. <http://www.world-nuclear.org/info/inf29.html>. Accessed 16 August 2012.
- World Nuclear Association. Plutonium. <http://www.world-nuclear.org/info/inf15.html>. Accessed 16 August 2012.
- Wu B, Becker J S (2012) Bioimaging of metals in rat brain hippocampus by laser microdissection inductively coupled plasma mass spectrometry (LMD-ICP-MS) using high-efficiency laser ablation chambers. *International Journal of Mass Spectrometry* 323-324:34-40.
- Xie Q, Lu S, Evans D, Dillon P, Hintelmann H (2005) High precision Hg isotope analysis of environmental samples using gold trap-MC-ICP-MS. *Journal of Analytical Atomic Spectrometry* 20:515-522.
- Xu C, Santschi P H, Zhong J Y, Hatcher P G, Francis A J, Dodge C J, Roberts K A, Hung C C, Honeyman B D (2008) Colloidal Cutin-Like Substances Cross-Linked to Siderophore Decomposition Products Mobilizing Plutonium from Contaminated Soils. *Environmental Science & Technology* 42:8211-8217.
- Yang L (2009) Accurate and precise determination of isotopic ratios by MC-ICP-MS: A review. *Mass Spectrometry Reviews* 28:990-1011.
- Zendel M, Donohue D L, Kuhn E, Deron S, Bíró T (2011). Nuclear Safeguards Verification Measurement Techniques, In: Vértés A, Nagy S, Klencsár Z, Lovas R G, Rösch F (Eds.), *Handbook of Nuclear Chemistry*. Springer Science + Business Media B.V.

4 References

- Zhao X L, Nadeau M J, Kilius L R, Litherland A E (1994) The first detection of naturally-occurring ^{236}U with accelerator mass spectrometry. *Nuclear Instruments and Methods in Physics Research Section B: Beam Interactions with Materials and Atoms* 92:249-253.
- Zhu T, Sun W, Zhang H, Wang H, Kuang G, Lv L (2012) Study on the provenance of xicun qingbai wares from the northern song dynasty of china *Archaeometry* 54:475-488.
- Zhuk I V, Lomonosova E M, Yaroshevich O I, Kievetz M K, Boulyga S F, Tzekhanovich I A, Mironov V P, Kudryashov V P, Drugachonok M A (1995) Application of solid state nuclear track detector method for determination of sizes and alpha-activity of "hot" particles of chernobyl fuel release. *Radiation Measurements* 25:419-420.
- Zitek A, Sturm M, Waidbacher H, Prohaska T (2010) Discrimination of wild and hatchery trout by natural chronological patterns of elements and isotopes in otoliths using LA-ICP-MS. *Fisheries Management and Ecology* 17:435-445.
- Zoriy M V, Becker J S (2009) Near-field laser ablation inductively coupled plasma mass spectrometry: A novel elemental analytical technique at the nanometer scale. *Rapid Communications in Mass Spectrometry* 23:23-30.
- Zoriy M V, Kayser M, Becker J S (2008) Possibility of nano-local element analysis by near-field laser ablation inductively coupled plasma mass spectrometry (LA-ICP-MS): New experimental arrangement and first application. *International Journal of Mass Spectrometry* 273:151-155.
- Zoriy M V, Mayer D, Becker J S (2009) Metal Imaging on Surface of Micro- and Nanoelectronic Devices by Laser Ablation Inductively Coupled Plasma Mass Spectrometry and Possibility to Measure at Nanometer Range. *Journal of the American Society for Mass Spectrometry* 20:883-890.

5 Appendices

5.1 Supplementary information

5.1.1 Particle sampling for subsequent LA-MC-ICPMS analysis

Sampling and treatment of single particles is a crucial step for subsequent LA-ICPMS analysis. Generally, the particles have to be sampled on a target, which can be easily put into the laser ablation cell. Furthermore, it has to be ensured that the particles are not loose on the target's surface in order to guarantee that individual particles are not relocated by the laser ablation carrier gas flowing through the laser cell. In addition, non-fixed particles may be disturbed by the shock wave generated at the ablation site, which would result in a relocation of adjacent particles or the particle of interest itself. E.g. if the particle of interest was laterally hit, only this fraction would be available for analysis as another fraction would most likely be relocated as a result of the shock wave.

Typically, particles analyzed for environmental safeguards are collected on cotton swipes (see also 1.1.1.1). As SIMS measurements demand a conductive surface, the collected particles have to be transferred onto such a surface. The particles are usually picked from the cotton swipe by means of so-called vacuum impactor sampling, which enables to transfer the particles from the cotton swipe onto a conductive graphite planchet. As this sampling strategy was regarded as very useful for the sampling of particle certified reference materials for LA-MC-ICPMS analysis, the sampling approach by means of vacuum impacting was adopted for such samples. In case of particle sampling for LA-MC-ICPMS Si planchets were used instead of graphite ones. Another modification was that particle fixation was not accomplished by means of an organic solvent and subsequent baking. The strategies that were applied within the course of this work are described below.

Sampling of particle certified reference materials by means of the vacuum impactor taking was accomplished in a clean room (class 100) in the Safeguards Analytical Laboratories in Seibersdorf, Lower Austria. The particle samples were handled in a glove bag, which was placed

in a laminar flow box in order to circumvent contaminations of the swipe and the surrounding working area, respectively. The vacuum impactor sampling included the following steps:

- Checking of particle counts of the sample preparation room.
- Examination of the polished surface of an unused planchet by means of an optical microscope.
- Cleaning of the surface by using an alcohol swipe and checking of the surface.
- Putting an o-ring into the vacuum impactor head.
- Placing the planchet on the o-ring.
- Placing of a glove bag into the laminar flow box.
- Putting of tweezers, the planchet case, a pair of gloves, the vacuum impactor (containing the planchet), a lab dish, the swipe (with particles on it) and a tygon tubing into the glove bag.
- Connecting one end of the tygon tubing with a filter.
- Unfolding the glove bag by means of filtered air.
- Removing of the air tubing and connecting the tygon tube with the tube going to the membrane pump. Prior to this, the opening of the glove bag where the tube is connected with the membrane pump and the air, respectively, has to be sealed with a Scotch tape.
- Closing of the other end of the glove bag (i.e. neck) by means of plastic rails.
- Connecting the vacuum impactor head with the end of the tygon tube placed in the glove bag.
- Putting both hands into the glove bag and putting on the gloves that were placed into the glove bag before.
- Connecting the vacuum impactor head with the end of the tygon tube placed in the glove bag.
- Putting of the swipe into the lab dish.
- Putting of the nozzle of the vacuum impactor head onto the swipe.
- Turning on of the membrane pump and swiping (3-5 s) of the particles.
- Repetition of the sampling for several times.
- After sampling, removing of the planchet from the vacuum impactor head using the tweezers and placing the planchet into a planchet case.
- Removing of the planchet from the glove bag.
- Checking of the surface with an optical microscope.

After particle sampling by means of a vacuum impactor, two different strategies for particle preparation for subsequent LA-MC-ICPMS analysis have been investigated: 1) transfer of the

particles from the planchet onto a cellulose acetate membrane and 2) fixation of the particles on the planchet using commercially available nail polish.

The first strategy is shown in Fig. 5.1-1. The Si planchet is put into a specially designed PTFE device, which consist of two parts. The lower part, which holds the planchet, is put into a glass petri dish slightly filled with acetone. Care must be taken that the planchet is not in direct contact with the acetone. The planchet holder was designed in a way so that this can be circumvented. A cellulose acetate membrane filter (OE 67, Whatman GmbH, Dassel, Germany) is put onto the planchet. Then the upper part of the PTFE device is put onto the device. This part is having a cut-out so that the acetone vapor present in the glass petri dish can easily interact with the membrane filter. This membrane-acetone interaction results in a dissolution of the membrane. Thus, the particles present on the planchet are transferred into the membrane. As soon as the membrane gets transparent it can be put out of the acetone vapor. The particles are then enclosed in the dry membrane, which can be fixed, using commercially available glue, on a glass slide typically used for microscopy. The glass slide can then be inserted into the laser ablation cell.



Fig. 5.1-1: Particle transfer onto a cellulose acetate membrane.

In the second strategy, the particles were directly fixed on the planchet's surface by means of commercially available transparent nail polish. The nail polish was diluted with acetone according to a 1:1 ratio in order to enable to pipette the mixture on the planchet's surface. The planchet can be directly put into the laser ablation cell.

It is recommended to use the second strategy for particle fixation as it is less time-consuming and easily applicable.

5.1.2 Dead time determination and linearity studies of secondary electron multipliers installed in the 'Nu Plasma HR' MC-ICPMS at BOKU, Vienna

Theoretical considerations regarding dead time determination and linearity studies are given in section 1.5.2.3.

Experimental

The applied measurement procedure was based on the dynamic procedure proposed by Richter et al. (Richter et al., 2009) for linearity studies performed by TIMS. In the proposed procedure a certified isotopic reference material, which fulfills the requirements for SEM linearity studies, is measured at different count rate intensities in a so called peak-jumping mode, in which the SEM detector only is applied (Richter et al., 2009).

In this study IRMM-073/7 (European Commission-JRC, Institute for Reference Materials and Measurements, Geel, Belgium) was applied for the performed measurements. This certified isotopic reference material consists of ^{233}U , ^{235}U and ^{238}U . While $^{233}\text{U}/^{235}\text{U}$ (i.e. 0.019993) was used to investigate the deviation of the measured from the certified isotope ratio, $^{235}\text{U}/^{238}\text{U}$ (i.e. 0.99317) was applied for determining the mass bias correction factors. The measured concentrations ranged from 0.006 ng g⁻¹ to ca. 20 ng g⁻¹. The ^{235}U count rate intensities ranged from about 5×10^{-4} to 1.8×10^{-6} cps.

Concerning TIMS measurements, the ion signal is very stable and does not show time dependent signal fluctuations that are occurring if an ICP is applied as ion source. Thus, the dynamic measurement procedure was modified for linearity studies of three discrete-dynode secondary electron multipliers (i.e. ion counting multiplier) that are installed in the 'Nu Plasma HR' MC-ICP-MS instrument at the BOKU Vienna. The applied cup configurations are shown in Table 5.1-1. The cup configurations and measurement cycles, respectively, were applied to internally determine the mass bias correction factors, the $^{233}\text{U}/^{235}\text{U}$ isotope ratio and the ion counter yield (i.e. IC yield) for each concentration.

The dead time has been set to zero prior to the measurements. The determination of the background was performed by measuring 1 % (w/w) HNO₃ for 10 minutes prior to the measurement of the different concentrations of IRMM-073/7. The different standard

concentrations have been measured from low to high concentrations. Instrumental parameters are given in Table 5.1-2.

Table 5.1-1: Cup configurations

Ion counter	Cycle	Cup configurations									
		H2	H1	Ax	L1	L2	IC0	L3	IC1	L4	IC2
IC0	1	238			235		233				
	2			238			235		233		
IC1	1	238			235		233				
	2			238			235		233		
	3					238		235		233	
	4	238			235		233				
IC2	1				238			235			
	2					238		235		233	
	3							238		235	
	4				238			235			

Table 5.1-2: Instrumental parameters

DSN parameter	
Nebuliser	PFA 100
Nebuliser pressure / Psi	25.1 - 31
Hot gas flow (Ar) / L·min ⁻¹	0.22-0.29
Membrane gas flow, /L·min ⁻¹	2.55-2.6
Spraychamber temperature / °C	113-116
Membrane temperature / °C	115-116
ICPMS (Nu Plasma HR) parameter	
RF power / W	1300
Auxiliary gas flow / L·min ⁻¹	1.2
Cool gas flow rate /L·min ⁻¹	13
Cones	Ni
Axial mass MC-ICPMS / m/z	236, 238 , 239, 240, 242
Masses monitored / m/z	
Zoom lens parameter	
Quad 1, V	44.0 to -49.7
Quad 2, V	-92.5 to -124.1
<i>High voltages, source and transfer lenses parameter</i>	Optimised for optimal sensitivity
<i>Voltages applied to the ion counters</i>	
Low mass IC / V	-321
High mass IC / V	-329
Dog leg IC / V	349
Dog leg skew /V	0
Cent def /V	-350
<i>Voltages applied to the multiplier</i>	
IC0	-2480
IC1	-2350
IC2	-2170
Data acquisition mode	10 cycles/block, 6 blocks
Integration time/measurement	10 s

Results

The measured intensities have been background corrected prior to further evaluation.

The applied mass bias correction factors were determined by measuring ^{235}U and ^{238}U with two Faraday cups (see Table 5.1-1). The mass bias correction factor of $^{235}\text{U}/^{238}\text{U}$ (eq. 5.1-1a) was used to calculate the mass bias per mass unit (eq. 5.1-1b) for the major U isotope ratio. The latter was applied for the calculation of the mass bias correction factor of $^{233}\text{U}/^{235}\text{U}$ (eq. 5.1-1c).

$$f_{MD,235/238} = \frac{R_{235/238cert}}{R_{235/238meas}} \quad (5.1-1a)$$

$$MD_{235/238} [\%] = \frac{(f_{MD,235/238}-1)*100}{(238-235)} \quad (5.1-1b)$$

$$f_{MD,233/238} = \frac{MD_{235/238}*(238-233)}{100} + 1 \quad (5.1-1c)$$

The $^{233}\text{U}/^{235}\text{U}$ isotope ratios of the measured concentrations of IRMM 073/7 were calculated according to eq. 5.1-2a, eq. 5.1-2b and eq. 5.1-2c:

$$R_{233/235_{IC0}} = \frac{233_{IC,cycle 1}/238_{FC,cycle 1}}{238_{FC,cycle 2}/235_{IC,cycle 2}} * f_{MD,233/235} \quad (5.1-2a)$$

$$R_{233/235_{IC1}} = \frac{233_{IC,cycle 2}/238_{FC,cycle 2}}{238_{FC,cycle 3}/235_{IC,cycle 3}} * f_{MD,233/235} \quad (5.1-2b)$$

$$R_{233/235_{IC2}} = \frac{233_{IC,cycle 2}/238_{FC,cycle 2}}{238_{FC,cycle 3}/235_{IC,cycle 3}} * f_{MD,233/235} \quad (5.1-2c)$$

In addition the $^{233}\text{U}/^{235}\text{U}$ isotope ratios were multiplied by a factor of 0.9996 to correct for the decay of ^{233}U since production date.

The relative difference between the determined, corrected by means of the mass bias and the decay of ^{233}U since certification date, from the certified isotope ratio was calculated according to eq. 5.1-3:

$$rel. diff. = (233/235_{corr})/(233/235_{cert}) - 1 \quad (5.1-3)$$

The ion counter yields were calculated according to the following equations:

$$Y_{IC0} = \frac{^{235}\text{IC,cycle 2}/^{238}\text{FC,cycle 2}}{^{235}\text{FC,cycle 1}/^{238}\text{FC,cycle 1}} \quad (5.1-4a)$$

$$Y_{IC1} = \frac{^{235}\text{IC,cycle 3}/^{238}\text{FC,cycle 3}}{^{235}\text{FC,cycle 1}/^{238}\text{FC,cycle 1}} \quad (5.1-4b)$$

$$Y_{IC2} = \frac{^{235}\text{IC,cycle 3}/^{238}\text{FC,cycle 3}}{^{235}\text{FC,cycle 1}/^{238}\text{FC,cycle 1}} \quad (5.1-4c)$$

Linearity of ion counting multipliers

It is well known that secondary electron multipliers tend to have a non-linear behavior, in particular at higher count rates ($> 10^{-5}$ cps) (Richter et al., 2001). This effect has to be corrected in order to perform accurate isotope ratio measurements. The non-linearity of the investigated ion counting multipliers is shown in Fig. 5.1-2. The slopes of the linear regression lines in Fig. 5.1-2 were used to calculate the dead times of the ion counter multipliers using eq. 5.1-5.

$$\tau [\text{ns}] = \text{slope}/(1 - 233/235_{\text{cert}}) * 10^{-9} \quad (5.1-5)$$

Dead times of 34 ns, 4 ns and 3 ns were determined for IC0, IC1 and IC2, respectively.

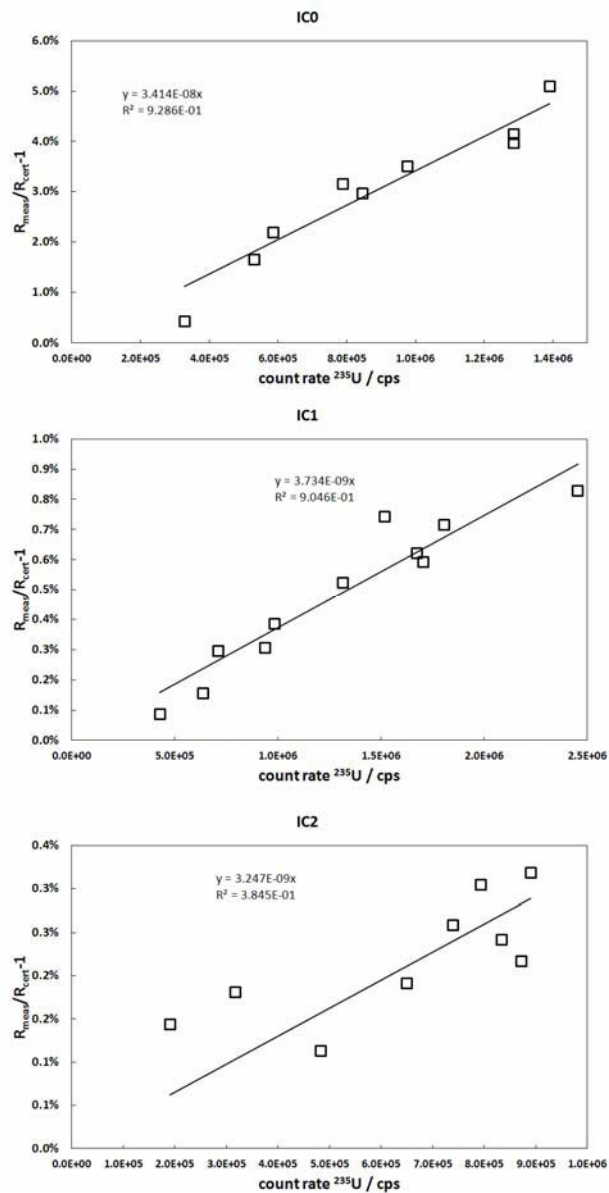
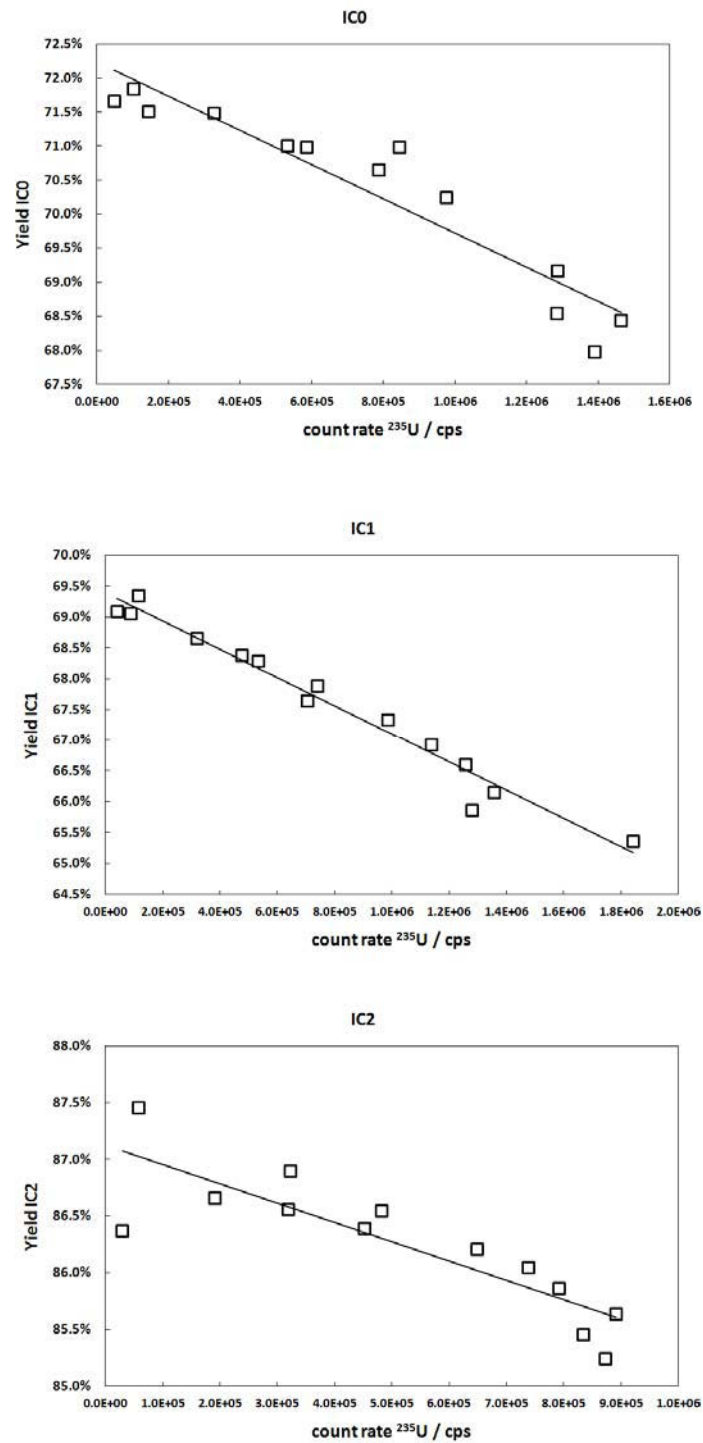


Fig. 5.1-2: Non-linear behavior of ion counting multipliers (i.e. IC0, IC1, IC2)

Dependence of ion counter yield on total counts

A linear relationship between the ion counter yield and the ^{235}U count rate was observed (see Fig. 5.1-3). The ion counter yields of all three ion counting multipliers decreased with increasing ^{235}U count rates. This demonstrates well that correction for the change in the ion counter yield is crucial for determining accurate isotope ratios.

Fig. 5.1-3: Correlation of ion counter yield with increasing ^{235}U count rate

5.2 List of Tables

Table 1.2-1: Properties of natural U isotopes.....	14
Table 1.2-2: IAEA Significant Quantities (SQ).....	23
Table 1.2-3: Types of U categories (adopted from (IAEA, 2005)).....	23
Table 1.4-1: Common isobaric interferences for swipe samples at the masses of U, and required mass resolutions (MRP = mass resolving power). The table was adopted from Ranebo et al.(Ranebo et al., 2009).....	34
Table 1.5-2: Laser ablation systems currently available on the market.	50
Table 2.1-2: Instrumental parameters.....	91
Table 2.1-4: Relative contributions of single parameters to the expanded total combined standard uncertainty of $^{236}\text{U}/^{238}\text{U}$ glass particle measurements.....	100
Table 2.1-5: $^{234}\text{U}/^{238}\text{U}$, $^{235}\text{U}/^{238}\text{U}$ and $^{236}\text{U}/^{238}\text{U}$ determined isotope ratios of S1 glass particles.	101
Table 2.1-6: $^{234}\text{U}/^{238}\text{U}$, $^{235}\text{U}/^{238}\text{U}$ and $^{236}\text{U}/^{238}\text{U}$ determined isotope ratios of S3 glass particles.	103
Table 2.2-1: Certified isotope ratios of CRMs measured in the course of this study.....	111
Table 2.2-2: Operating parameters for LA-MC-ICPMS analyses.	113
Table 2.2-4: Relative expanded uncertainties (RU) and relative contributions of input parameters of $^{235}\text{U}/^{238}\text{U}$ isotope ratio measurements.....	118
Table 2.2-5: Summary of NUSIMEP-7 results	123
Table 2.3-1: Instrumental parameters.....	132
Table 5.1-1: Cup configuration.....	163
Table 5.1-2: Instrumental parameters.....	163

5.3 List of Figures

Fig. 1.1-1: Cotton swipe sampling kit (adopted from (Zendel et al., 2011)).	12
Fig. 1.2-1: Natural decay series of ^{238}U (Natural Decay Series: Uranium, Radium, and Thorium). The symbols α and β are indicating alpha and beta decay, whereas the times are presenting the half-lives. The * symbol indicates isotopes that are also a gamma (γ) emitter (Argonne National Laboratory, 2005).	15
Fig. 1.2-2: Natural decay series of ^{235}U (Natural Decay Series: Uranium, Radium, and Thorium). The symbols α and β are indicating alpha and beta decay, whereas the times are presenting the half-lives. The * symbol indicates isotopes that are also a gamma (γ) emitter (Argonne National Laboratory, 2005).	16
Fig. 1.2-3: Schematic illustration of the nuclear fuel cycle (adopted from (IAEA NFCIS. Nuclear Fuel Cycle)).	18
Fig. 1.2-4: Major pathways for the formation of Pu isotopes in uranium fuels (Clark et al., 2006).	20
Fig. 1.2-5: $^{240}\text{Pu}/^{239}\text{Pu}$ in potential nuclear contamination sources (adopted from Taylor et al. (Taylor et al., 2001)).	24
Fig. 1.5-1: Number of entries in <i>SciFinder</i> for 'laser ablation inductively coupled plasma mass spectrometry'.	36
Fig. 1.5-2: Quartz cyclonic spray chamber. The figure was adopted from (Elemental Scientific. Cyclonic Spray Chambers.)	53
Fig. 1.5-3: Number of entries in <i>SciFinder</i> for 'multi collector inductively coupled plasma mass spectrometry'.	56
Fig. 1.5-4: 'Nu Plasma HR' Faraday cup.	58
Fig. 1.5-5: Schematic diagram of the Thermo Scientific Inc. Virtual Amplifier.	60
Fig. 1.5-6: Schematic description of the effects resulting from ion optical magnification (i.e. $M=2$). At $M=2$ the Faraday cup is enlarged and the ion beam strikes the wall at a deeper position.	61
Fig. 1.5-7: Schematic diagram of a continuous dynode electron multiplier. adopted from O'Connor and Evans (O'Connor and Evans, 2007).	62
Fig. 1.5-8: Schematic diagram of a discrete-dynode secondary electron multiplier, adopted from Hunter and Stresau (Hunter and Stresau, 2005).	64
Fig. 1.5-9: Ion counting plateau curve adopted from Hunter and Stresau (Hunter and Stresau, 2005). Please note that the Figure was slightly modified.	65
Fig. 1.5-10: 'Nu Plasma HR' (Nu Instruments Ltd.) standard collector block configuration. (H...Faraday cup high mass side, Ax...Faraday cup axial mass, L...Faraday cup low mass side, IC...ion counting multiplier (i.e. secondary electron multiplier).	72
Fig. 1.5-11: Schematic description of the ^{238}U peak tailing effect. Mass scanning was performed using a 'Nu Plasma HR' MC-ICPMS (A) ^{238}U peak tailing when no deceleration filter (i.e. voltages = 0) is applied, B) Reduction of ^{238}U peak tailing when applying a deceleration filter). Different peak shapes in A) and B) are resulting from different x-y-scalings.	73
Fig. 1.5-12: 'Nu Plasma HR' (Nu Instruments Ltd.) modified collector block configuration. (H...Faraday cup high mass side, Ax...Faraday cup axial mass, L...Faraday cup low mass side, IC...ion counting multiplier (i.e. secondary electron multiplier).	74
Fig. 1.5-13: 'Neptune Plus' (Thermo Fisher Scientific Inc.) L5 ion counter package collector block configuration for U and Pu analysis.	75
Fig. 2.1-1. Scanning electron micrograph of an ablated S1 glass particle (left) and typical time resolved ablation profile (right). The ablation profile is shown by means of the ^{238}U signal intensity. A laser ablation spot size of 10 μm was applied.	93

- Fig. 2.1-3: S1 $^{234}\text{U}/^{238}\text{U}$ (A) and $^{235}\text{U}/^{238}\text{U}$ (B) isotope ratios corrected with U500 external correction factors. The solid lines represent the certified isotope ratios ($^{234}\text{U}/^{238}\text{U} = 0.000\ 055\ 7(11)$; $^{235}\text{U}/^{238}\text{U} = 0.007\ 304\ 5(36)$), whereas the dotted lines indicate the certified range. Spot sizes of $10\ \mu\text{m}$ (white diamonds) and $15\ \mu\text{m}$ (black diamonds) were applied. Error bars are indicating the expanded uncertainty of $^{234}\text{U}/^{238}\text{U}$ and $^{235}\text{U}/^{238}\text{U}$ isotope ratios ($k=2$).....96
- Fig. 2.1-4: S1 $^{235}\text{U}/^{238}\text{U}$ isotope ratios that were determined by using Ar (white diamonds) and He (x-hair diamonds), respectively, as laser ablation carrier gases. The solid line represents the certified isotope ratio ($^{235}\text{U}/^{238}\text{U} = 0.007\ 304\ 5(36)$), whereas the dotted lines indicate the certified range. Spot sizes of $10\ \mu\text{m}$ were applied. Error bars are indicating the expanded uncertainty of $^{235}\text{U}/^{238}\text{U}$ isotope ratios ($k=2$).....98
- Fig. 2.1-5: Comparison of S1 $^{236}\text{U}/^{238}\text{U}$ isotope ratios that were determined by measuring ^{236}U applying (triangle) and not applying (diamond) a deceleration filter. The solid line represents the certified isotope ratio ($^{236}\text{U}/^{238}\text{U} = 0.000\ 010\ 08(11)$), whereas the dotted lines indicate the certified range. Spot sizes of $10\ \mu\text{m}$ (white symbols) and $15\ \mu\text{m}$ (black symbols) were applied. Error bars are indicating the expanded uncertainty of $^{236}\text{U}/^{238}\text{U}$ isotope ratios ($k=2$).99
- Fig. 2.2-2: LA-MC-ICPMS transients signal recorded during raster scanning of a NUSIMEP-7 interlaboratory comparison test sample.....119
- Fig. 2.2-3. Use of the 'PBP' method for the evaluation of the NUSIMEP-7 'double' deposition measurement data. $^{235}\text{U}/^{238}\text{U}$ isotope ratios are plotted in ascending order. The dotted lines are indicating the lower and the upper ends of the standard deviations (2σ).120
- Fig. 2.2-4: Determination of two different $^{235}\text{U}/^{238}\text{U}$ isotope ratios by means of the slopes of linear regression lines applying the 'finite mixture model'. A) Scatter plot of a data set of 9073-01-B and CRM U010 particle measurements that were combined to one test data set. B) Application of the 'finite mixture model' to the test data set: the circles and the triangles are representing the two clusters (i.e. two isotopic signatures) that are distinguishable. The isotopic signatures are determined by means of the slope of the linear regression lines. The in the legend stated slopes are not externally corrected. Outliers are marked by grey colored rectangles.....121
- Fig. 2.2-5: Application of the finite mixture model to the blank corrected ^{235}U and ^{238}U measurement data of the NUSIMEP-7 inter-laboratory comparison test samples (A: NUSIMEP 7 single deposition; B: NUSIMEP 7 double deposition). A contamination during sample handling with a ^{235}U enrichment of about 21 % was detected on both planchets.....123
- Fig. 2.3-2: Pu isotopic composition of micro-samples ($n=35$) collected in the vicinity of the ChNPP-4. The Pu isotope ratios were calculated as weighted means of $^{242}\text{Pu}/^{239}\text{Pu}$ and $^{240}\text{Pu}/^{239}\text{Pu}$, respectively, isotope ratios measured per micro-sample. The distribution of the Pu isotopic compositions is shown for smaller (A) and larger (B) clusters; the micro-sample size is expressed as size of the ablation area that was applied for Pu analysis. The error bars are indicating the expanded ($k=2$) combined standard measurement uncertainties.....137
- Fig. 2.3-3: Heterogeneous distribution of $^{242}\text{Pu}/^{239}\text{Pu}$ and $^{240}\text{Pu}/^{239}\text{Pu}$ isotope ratios measured in two micro-samples, Px and Py, collected in the vicinity of Chernobyl. The error bars are indicating the expanded ($k=2$) combined standard measurement uncertainties U_c ($k=2$).138
- Fig. 5.1-1: Particle transfer onto a cellulose acetate membrane.....161
- Fig. 5.1-2: Non-linear behavior of ion counting multipliers (i.e. IC0, IC1, IC2).....166
- Fig. 5.1-3: Correlation of ion counter yield with increasing ^{235}U count rate167

5.4 List of Abbreviations

Ac	actinium
Ag	silver
Al	aluminum
AMS	accelerator mass spectrometry
AP	additional protocol
Ar	argon
Ar	argon
ArF	argon fluoride
As	arsenic
Au	gold
Ba	barium
Ba	barium
Bi	bismuth
BOG	Board of Governors
Bq	becquerel
Ca	calcium
Ca	calcium
Cd	cadmium
Cd	cadmium
CDD	Compact discrete dynode
Ce	cerium
CEM	continuous dynode or channel electron multiplier
ChNPP	Chernobyl nuclear power plant
CL	clean Laboratory for Safeguards
Cl	chlorine
Co	cobalt
cps	counts per second
Cr	chromium
CRM	certified reference material
CRM	certified reference material
CSAs	comprehensive safeguards agreements
Cu	copper
DNAA	Delayed neutron activation analysis
DPRK	Democratic People's Republic of Korea
DU	depleted uranium
EDX	energy-dispersive x-ray

ELPI	electrical low-pressure impactor
ELPI	electrical low-pressure impactor
EMPA	electron microprobe
ES	environmental sampling
Fe	iron
Fr	francium
fs	femtosecond
FT	fission track
Ga	gallium
Ga	gallium
GC	gas chromatography
Gd	gadolinium
Ge	germanium
GSR	gunshot residue
He	helium
HEU	highly enriched uranium
Hg	mercury
HPLC	high performance liquid chromatography
HR	high resolution
HRGS	high-resolution gamma spectrometry
IAEA	International atomic energy agency
IC	ion counter
ICP	inductively coupled plasma
IDA	inter-digitated electrode array
INAA	instrumental neutron activation analysis
IR	infrared
IRMM	Institute for Reference Materials and Measurements
ITWG	International Technical Working Group Combating Illicit Trafficking
JRC	Joint research center
K	potassium
keV	kilo electron volt
LA	laser ablation
LEU	low enriched uranium
LG	large geometry
LIBS	laser induced breakdown spectroscopy
LRS	linear regression slope
MC	multi collector
MeV	mega electron volt
Mg	magnesium
MIC	multi ion counting
Mn	manganese

Mo	molybdenum
MS	mass spectrometry
Na	sodium
Nd	neodymium
Nd:YAG	neodymium-doped yttrium aluminum garnet
Ni	nickel
NIST	National Institute of Standards and Technology
NNWS	non-nuclear weapon States
NPP	nuclear power plant
NPT	Treaty on the Non-Proliferation of Nuclear Weapons
ns	nanosecond
NU	natural uranium
NUSIMEP	Nuclear signatures interlaboratory measurement evaluation programme
NWAL	Network Analytical Laboratories
NWR	New Wave Research
P	phosphorus
Pa	protactinium
Pb	lead
PBP	point by point
Pd	palladium
PGE	platinum group elements
Po	polonium
POI	person of interest
Pt	platinum
PTFE	polytetrafluoroethylene
PTFE	polytetrafluoroethylene
Pu	plutonium
Q	quadrupole
Ra	radium
Re	rhenium
Rh	rhodium
Rn	radon
RPQ	retarding potential quadrupole
RSD	relative standard deviation
RU	relative expanded uncertainty (k=2)
Ru	ruthenium
S	sulphur
Sb	antimony
Se	selenium
SEM	scanning electron microscopy or discrete dynode secondary electron multiplier

SF	sector field
SG	small geometry
Si	silicon
SIMS	secondary ion mass spectrometry
Sn	tin
Sr	strontium
SRM	standard reference material
SSNTD	solid state nuclear track detector
STEM	scanning transmission electron microscopy
Ta	tantalum
Ta	tantalum
Tc	technetium
Th	thorium
Ti	titanium
TIMS	thermal ionization mass spectrometry
Tl	thallium
Tl	thallium
TOF	time of flight
U	uranium
UV	ultraviolet
V	vanadium
VUV	vacuum ultraviolet
W	tungsten
WARP	wide-angle energy retarding filter
WDX	wavelength-dispersive x-ray
XRF	x-ray fluorescence spectrometry
Yb:KGW	ytterbium doped potassium gadolinium tungstate
Zn	zinc

5.5 Curriculum Vitae

Name: Stefanie Kappel
Date of birth: 15/03/1984
Place of birth: Oberwart / Austria
Gender: Female
Marital status: Unmarried
Nationality: Austrian



Contact

Linzer Straße 303/12
 1140 Vienna
 Austria

Mobile: +43 664 4336746
 E-mail: steffi.kappel@gmail.com

Education

03/2009 - present **University of Natural Resources and Life Sciences, Vienna (BOKU)/International Atomic Energy Agency (IAEA)**

- PhD thesis '*Uranium and Plutonium Isotopic Fingerprinting of Single Particles by Laser Ablation – Multi Collector – Inductively Coupled Plasma Mass Spectrometry*' at the Department of Chemistry, Division of Analytical Chemistry, VIRIS Laboratory
- Collaboration with the International Atomic Energy Agency (IAEA) – Safeguards Analytical Laboratory as a consultant

10/2006 – 01/2009 **Vienna University of Technology**

- Study of Technical Chemistry – Materials Technology and Materials Analytics (Master degree programme)
- Degree of Dipl.-Ing. (i.e. MSc)
 Master thesis '*Radionuclide Fingerprinting of Hot Particles by Laser Ablation – Multiple Collector – Inductively Coupled Plasma*

Mass Spectrometry'

(Supervision: Ao. Prof. DI Dr. Thomas Prohaska)

10/2002 – 05/2006 University of Natural Resources and Life Sciences, Vienna (BOKU)

- Study of Food Science and Biotechnology
(Bachelor degree programme)
- Degree of Bachelor of Technical Sciences (i.e. Bakk. techn.)
Baccalaureate thesis '*Determination of heavy metals in human tissues*'
(Supervision: Ao. Prof. DI Dr. Thomas Prohaska)

09/1994 – 06/2002 BG/BRG/BORG Oberschützen (Grammar school)

- Bilingual education (German – English, 1994-1998)
- School leaving examination with distinction

Work experience

2004 – 2007 University of Natural Resources and Life Sciences, Vienna (BOKU)

(Department of Chemistry, Division of Analytical Chemistry)

- Student teaching assistant
- Supervision of students in undergraduate laboratories

2004 – 2006 Boehringer Ingelheim Austria GmbH

- Summer internships (2 months each summer)
- Product quality control within the Biopharmaceuticals /
Operations section

2003 University of Natural Resources and Life Sciences, Vienna (BOKU)**- Christian Doppler Laboratory of Pulp Reactivity**

(Department of Chemistry, Division of Organic Chemistry)

- Summer internship (1 month)
- Training in liquid chromatography and NMR

Grants

Merit scholarships

University of Natural Resources and Life Sciences, Vienna (2003)

Vienna University of Technology (2007)

Research grant for promising master thesis

Vienna University of Technology (2008)

Scholarship for short-term scientific research work abroad

University of Natural Resources and Life Sciences, Vienna (2011):

Scholarship for a scientific research work at the Swiss Federal Institute of Technology Zurich (ETH Zürich)

Language skills

German	mother tongue
English	fluently in writing and speaking
French	basic knowledge

Contributions to conferences and meetings

Poster Presentations

Data Evaluation Strategies for U Isotope Ratio Measurements of Single Particles by Laser Ablation – Multi Collector – Inductively Coupled Plasma Mass Spectrometry

S. Kappel, D. Koffler, G. Laaha and T. Prohaska

European Geosciences Union General Assembly 2012, 23/04/2012 – 27/04/2012, Vienna/Austria

Application of mass spectrometric techniques for the determination of n(U-235)/n(U-238) isotope ratios in depleted to low enriched U material

S. Kappel, S.F. Boulyga, S. Bürger and T. Prohaska

European Geosciences Union General Assembly 2011, 03/04/2011 – 08/04/2011, Vienna/Austria

The preparation and calibration of calcium synthetic isotope mixtures

M. Berglund, C. Hennessy, S. Richter, G. Fortunato, S. Wunderli, S. Kappel and T. Prohaska

2010 AGU Fall Meeting, 13/12/2010 – 17/12/2010, San Francisco/USA

Radionuclide fingerprinting of μm -sized hot particles by LA-MC-ICPMS

S. Kappel, S. F. Boulyga and T. Prohaska

9th European Workshop on Laser Ablation in Elemental and Isotopic Analysis, 07/07/2008 – 09/07/2008, Prague/Czech Republic

Uranium isotopic analysis in particles by LA-MC-ICP-MS

S. F. Boulyga, J. Poths, D. Donohue, K. König, S. Kappel and T. Prohaska

Nordic Conference on Plasma Spectrochemistry, 15/06/2008 – 18/06/2008, Loen/Norway

Isotope Analysis of Actinides in Micro – Samples Using LA-ICP-MS with Multiple Ion Counters

S. F. Boulyga, S. Kappel and T. Prohaska

Winter Conference on Plasma Spectrochemistry, 07/01/2008 – 12/01/2008, Temecula/USA

Oral presentations

U isotopic fingerprinting of single particles by LA-MC-ICPMS

S. Kappel

Pumpaya Workshop, 13/09/2012 to 14/09/2012, Podersdorf am See/Austria

Räumlich aufgelöste Plutonium-Analyse von Mikro-Proben aus dem Tschernobyl-Fallout

S. Kappel, Sergei F. Boulyga and T. Prohaska

23. ICPMS-Anwendertreffen, 10/09/2010 to 12/09/2010, Tulln/Austria

Temporal resolution of LA-ICPMS analyses of fish hard parts

A. Zitek, J. Irrgeher, S. Kappel, F. Kendlbacher and T. Prohaska

22nd V.M. Goldschmidt Conference, 24/06/2012 to 29/06/2012, Montreal/Canada

Data evaluation strategy for the determination of multiple U isotopic signatures of adjacent single particles

S. Kappel, D. Koffler, G. Laaha and T. Prohaska

European Geosciences Union General Assembly 2012, 23/04/2012 to 27/04/2012, Vienna/Austria

Uncertainty calculation for U isotope ratio analyses of single particles by LA-MC-ICP-MS - Data reduction, evaluation of total combined uncertainties and assessment of main contributors

S. Kappel, S.F. Boulyga and Thomas Prohaska

ESARDA Working Group on Standards and Techniques for Destructive Analysis -Workshop on Uncertainties in Nuclear Measurements, 08/11/2011 to 09/11/2011, International Atomic Energy Agency – Safeguards Analytical Services (IAEA-SGAS), Seibersdorf/ Austria

Performance evaluation of LA-ICP-MS for U isotope ratio measurements in single particle

S. Kappel, S.F. Boulyga and Thomas Prohaska

Technical Meeting on Particle Analysis of Environmental Samples for Safeguards, 04/10/2011 to 06/10/2011, IAEA, Vienna/Austria

Single particle measurements using laser ablation and multicollector ICP-MS

S. Kappel and Thomas Prohaska

ESARDA Working Group on Standards and Techniques for Destructive Analysis -Workshop on Direct Analysis of Solid Samples Using Laser Ablation-Inductively Coupled Plasma-Mass Spectrometry (LA-ICP-MS), 16/05/2011, Budapest/ Hungary

Direkte Uranisotopenanalytik von Einzelpartikeln mittels LA-MC-ICP-MS

S. Kappel and T. Prohaska

22. ICPMS-Anwendertreffen, 06-09-2010 to 08-09-2010, Berlin/Germany

Optimisation and application of multicollector ICP-MS (MC-ICP-MS) in combination with laser ablation (LA) and conventional sample introduction system for precise isotope ratio analysis of uranium in glass particles and liquid samples

S. Kappel, S.F. Boulyga and Thomas Prohaska

MS Seminar (International Atomic Energy Agency), 26/01/2010, Seibersdorf/Austria

LA-MC-ICP-MS - application for U isotope ratio measurements of single particles

S. Kappel, S.F. Boulyga and Thomas Prohaska

Technical Meeting on Particle Analysis (International Atomic Energy Agency), 28/09/2009 – 29/09/2009, Vienna/Austria

LA-MC-ICP-MS - A valuable tool for the determination of the U isotopic signature of single, μm -sized particles

S. Kappel, S. F. Boulyga and T. Prohaska

Junganalytikerforum ASAC 2009, 05/09/2009 – 06/09/2009, Innsbruck/Austria

Environmental monitoring

S. Kappel, S.F. Boulyga and T. Prohaska

Workshop: The Game of Isotopes, Isotopes in Ecology and Forensic Chemistry, 15/06/2009, Lisbon/Portugal

Direct U isotope analysis in μm -sized particles by LA-MC-ICP-MS

S. Kappel S, S. F. Boulyga and T. Prohaska

European Winter Conference on Plasma Spectrochemistry, 15/02/2009 to 20/02/2009, Graz/Austria

ICPMS for nuclear applications: Merits, limitations and prospective developments

Boulyga S. F., J. Poths, S. Balsley, D. Donohue, S. Kappel and T. Prohaska

European Winter Conference on Plasma Spectrochemistry, 15/02/2009 to 20/02/2009, Graz/Austria

Uranisotopenanalytik mittels LA-MC-ICP-MS

S. Kappel, S. F. Boulyga and T. Prohaska

Österreichischer Wasser und Abfallwirtschaftsverband (ÖWAV), Analytikplattform, Umweltbundesamt, 18/09/2008, Vienna/Austria

Radionuclide fingerprinting of μm -sized hot particles

S. Kappel, S. F. Boulyga and T. Prohaska

5th Pumpaya Workshop, 31/07/2008 to 02/08/2008, Drosendorf/Austria

Performance of laser ablation inductively coupled plasma mass spectrometry (LA-ICP-MS) for actinide isotopic analysis in particles

S. F. Boulyga, K. König, S. Kappel and Thomas Prohaska

Technical Meeting on Particle Analysis (International Atomic Energy Agency), 12/11/2007 to 16/11/2007, Vienna/Austria

Publications**Direct uranium isotope ratio analysis of single micrometer-sized glass particles**

S. Kappel, S. F. Boulyga and T. Prohaska

Journal of Environmental Radioactivity 113 (2012) 8-15

Uranium and plutonium analysis of nuclear material samples by multi-collector thermal ionisation mass spectrometry: Quality control, measurement uncertainty, and metrological traceability

S. Bürger, S. D. Balsley, S. Baumann, J. Berger, S. F. Boulyga, J. A. Cunningham, S. Kappel, A. Koepf and J. Poths

International Journal of Mass Spectrometry 311 (2012) 40-50